AD-A047 740 ENVIRONMENTAL RESEARCH AND TECHNOLOGY INC CONCORD MASS F/G 4/2
STRATOSPHERIC TURBULENCE ANALYSIS.(U)
SEP 77 R K CRANE F19628-77-C-0059
UNCLASSIFIED AFGL-TR-77-0207 NL



AD A047740

AFGL-TR-77-0207

STRATOSPHERIC TURBULENCE ANALYSIS

Robert K. Crane
Environmental Research & Technology, Inc.
696 Virginia Road
Concord, Massachusetts 01742

September 1977

Final Report for Period
1 January 1977 to 31 August 1977

Approved for Public Release
Distribution Unlimited

AIR FORCE GEOPHYSICS LABORATORY
AIR FORCE SYSTEMS COMMAND
UNITED STATES AIR FORCE
HANSCOM AFB, MASSACHUSETTS 01731

AD No.
DDC FILE COPY

Qualified requestors may obtain additional copies from the Defense Documentation Center. All others should apply to the National Technical Information Service.

Unclassified

SECURITY CLASSIFICATION OF THIS PAGE (When Data Entered)

REPORT DOCUMENTATION PAGE		READ INSTRUCTIONS BEFORE COMPLETING FORM
1. REPORT NUMBER AFGL-TR-77-0207	2. GOVT ACCESSION NO.	3. RECIPIENT'S CATALOG NUMBER
4. TITLE (and Subtitle) STRATOSPHERIC TURBULENCE ANALYSIS.		5. TYPE OF REPORT & PERIOD COVERED Final rept. 1 Jan 19[illegible] - 31 Aug 1977
		6. PERFORMING ORG. REPORT NUMBER
7. AUTHOR(s) Robert K. Crane		8. CONTRACT OR GRANT NUMBER(s) F19628-77-C-0059
9. PERFORMING ORGANIZATION NAME AND ADDRESS Environmental Research & Technology, Inc. 696 Virginia Road Concord, Massachusetts 01742		10. PROGRAM ELEMENT, PROJECT, TASK AREA & WORK UNIT NUMBERS 62101F 668705AL
11. CONTROLLING OFFICE NAME AND ADDRESS Air Force Geophysics Laboratory Hanscom AFB, Massachusetts 01731 Monitor/E.M. Dewan/LKC		12. REPORT DATE September 1977 13. NUMBER OF PAGES 150
14. MONITORING AGENCY NAME & ADDRESS (if different from Controlling Office) 148p.		15. SECURITY CLASS. (of this report) Unclassified 15a. DECLASSIFICATION/DOWNGRADING SCHEDULE

16. DISTRIBUTION STATEMENT (of this Report)

Approved for public release; distribution unlimited.

17. DISTRIBUTION STATEMENT (of the abstract entered in Block 20, if different from Report)

18. SUPPLEMENTARY NOTES

19. KEY WORDS (Continue on reverse side if necessary and identify by block number)

Stratosphere
Eddy diffusion coefficients
Radar measurements
Turbulence

20. ABSTRACT (Continue on reverse side if necessary and identify by block number)

A model was developed to combine radiosonde observations with ultrasensitive well-calibrated radar measurements of clear air turbulence to provide estimates of two eddy parameters, the eddy dissipation rate and the eddy heat diffusion coefficient. The eddy parameters were obtained as volume averages over 1 km thick layers and time averages over several hours. The model was tested using simultaneously obtained radar measurements and pilot reports of turbulence intensity from a U-2 aircraft. The model was also shown to be consistant with other reported radar and aircraft measurements.

DD FORM 1 JAN 73 1473 EDITION OF 1 NOV 65 IS OBSOLETE

Unclassified

SECURITY CLASSIFICATION OF THIS PAGE (When Data Entered)

391 776

20. Abstract (continued)

Simultaneous radar and radiosonde measurements were obtained on 24 different days spanning all seasons. The median eddy heat diffusion coefficient for all the observations and the 13 to 16 km height region was 0.02 m^2/sec (200 cm^2/s). This value did not change from season to season.

ACCESSION for
NTIS White Section
DDC Buff Section
UNANNOUNCED
JUSTIFICATION
BY
DISTRIBUTION/AVAILABILITY CODES
Dist. SPECIAL
A

TABLE OF CONTENTS

	Page
ABSTRACT	5
1. INTRODUCTION	7
1.1 Objectives	7
1.2 Summary of Results	7
2. BACKGROUND	10
2.1 The Roles of Stratospheric Turbulence	10
2.2 Radar as a Tool for the Measurement of Stratospheric Turbulence	11
3. RADAR MEASUREMENTS OF STRATOSPHERIC TURBULENCE	13
3.1 Radar Estimation of the Refractive Index Structure Function	13
3.2 A Model to Estimate the Intensity of Turbulence Using Radar Data	14
3.2.1 The Temperature Structure Parameter, C_T^2	14
3.2.2 Eddy Parameters $\bar{\varepsilon}_m$ and $\bar{K}_H$	15
4. THE RADAR OBSERVATIONS	23
4.1 The Millstone Hill L-band Radar System	23
4.2 Data Processing	25
4.2.1 Radar Data	25
4.2.2 Radiosonde Data	32
5. APPLICATION OF THE TURBULENCE MODEL	40
5.1 Comparison with U-2 Pilot Reports	40
5.2 Eddy Dissipation Rate Estimates	48
5.3 Eddy Diffusion Coefficient Estimates	48
5.4 Active Layer Thickness Estimates	63
5.5 Temporal Variation of Turbulent Layer Intensity	63
6. CONCLUSIONS	67
ACKNOWLEDGEMENTS	68
REFERENCES	69
APPENDIX A: Median $\bar{C}_T^2$, d, $\bar{\varepsilon}_m$ and $\bar{K}_H$ Profiles	A-1
APPENDIX B: Median C_n^2 Profiles	B-1

Preceding Page BLANK - NOT FILMED

ABSTRACT

A model was developed to combine radiosonde observations with ultrasensitive well-calibrated radar measurements of clear air turbulence to provide estimates of two eddy parameters, the eddy dissipation rate and the eddy heat diffusion coefficient. The eddy parameters were obtained as volume averages over 1 km thick layers and time averages over several hours. The model was tested using simultaneously obtained radar measurements and pilot reports of turbulence intensity from a U-2 aircraft. The model was also shown to be consistant with other reported radar and aircraft measurements.

Simultaneous radar and radiosonde measurements were obtained on 24 different days spanning all seasons. The median eddy heat diffusion coefficient for all the observations and the 13 to 16 km height region was 0.02 m^2/sec (200 cm^2/s). This value did not change from season to season.

Preceding Page BLANK - FILMED

1. INTRODUCTION

1.1 Objectives

The objective of this contract is the estimation of turbulent eddy diffusion coefficients for the lower stratosphere using a collection of simultaneous radar and radiosonde observations. An important aspect of the study reported herein is the use of a unique set of radar data obtained by MIT Lincoln Laboratory at the Millstone Hill Radar Facility during the 1968-1970 time period.

1.2 Summary of Results

The simultaneously acquired radar and radiosonde data were processed to provide estimates of the turbulent eddy dissipation rate and eddy heat diffusion coefficient. Median profiles of these eddy parameters are given in Table I. The profiles represent the median values of the medians for each observation set. Thirty-two sets of observations were obtained on 24 different days: 3 days between 11 January and 10 February 1968; 4 between 28 May and 27 June 1968; 4 between 29 July and 2 August 1968; 7 between 20 July and 31 July 1970; and 6 between 26 October and 12 November 1970.

The data processing started with profiles of the refractive index structure parameter C_n^2, produced by the well calibrated Millstone Hill L-band radar (Crane, 1970; Crane, 1974). The C_n^2 profiles were transformed into profiles of the temperature structure parameter, C_T^2, using the radiosonde data. A model was developed to use the C_T^2 estimates and radiosonde data to provide the required eddy parameter estimates plus estimates of the volume filled by turbulence. The model was verified using pilot reports of turbulence obtained during U-2 aircraft flights made in conjunction with 5 of the observation sets.

The radar derived eddy parameters represent one of the most extensive data sets available to date on the intensity of small scale lower stratospheric turbulence at a single geographical location. The eddy heat diffusion coefficient estimates presented in Table I for the 13-16 km height interval are identical to the mean value computed by Lilly et al (1974) based upon Project HICAT data for the 13.7 - 15.2 km height interval

TABLE I

MEDIAN EDDY PARAMETERS

Height Interval (km)	Eddy Heat Diffusion Coefficient $\overline{K}_H$ (m^2/s)	Eddy Dissipation Rate $\overline{\epsilon}_m$ (m^2/s^3)	No. of Observation Sets
12-13	3×10^{-2}	3×10^{-5}	32
13-14	2×10^{-2}	3×10^{-5}	32
14-15	2×10^{-2}	3×10^{-5}	32
15-16	2×10^{-2}	2×10^{-5}	32
16-17	3×10^{-2}	4×10^{-5}	31

and similar underlying terrain. The 12-13 km values in Table I are also consistant with the estimates of mean eddy parameters reported by Cadet (1977) although his data are for a single set of observations over mountainous terrain. The eddy diffusion coefficients are an order of magnitude smaller than the estimates provided by Rosenberg and Dewan (1974). Their estimation procedure employed however, a free parameter, the time step, which must be adjusted to match the eddy dissipation rate.

The results presented herein are consistant with the available data on transport by small scale turbulence in the lower stratosphere. They are one-to-two orders of magnitude smaller than the coefficients used to adjust the output of one-dimensional modeling analyses to match observations of trace constituent distributions. This large discrepancy arises because the one-dimensional models are generally formulated to use the turbulent diffusion model to account for larger scale non-diffusive transport (see for example, Reiter, 1975).

2. BACKGROUND

2.1 The Roles of Stratospheric Turbulence

Initially, interest in clear air turbulence (CAT) in the lower stratosphere and upper troposphere arose because of its potential hazard to aircraft. Project HICAT (Crooks et al, 1967) was conducted by the U.S. Air Force to establish structural design criteria for aircraft. The single U-2 aircraft used for project HICAT was equipped to obtain true gust velocity data on scale sizes ranging from 20 meters (m) to 20 kilometers (km). The HICAT U-2 flew over 6.6×10^5 km sampling turbulence in the 13 to 20 km height range. These data are the most extensive available for the study of CAT in the lower stratosphere. Lilly et al (1974) analyzed these data to provide eddy heat diffusion coefficient estimates for several height regions and different underlying terrain conditions. The HICAT instrumentation was designed to obtain true gust velocities - velocity variance data on the 100-300 m scale size of importance to aircraft design. The instrumentation was not designed however, to obtain the data at the much smaller scale sizes within the inertial subrange of the turbulence spectrum required for the direct estimation of eddy parameters.

Currently, interest in CAT in the lower stratosphere is centered on the estimation of vertical eddy diffusion coefficients for use in modeling the effects of stratospheric pollutants. The stable region between 13 and 16 km height acts as a barrier to the vertical transport of fluorocarborns from the lower atmosphere into the stratosphere where they participate in catalytic reactions to reduce ozone concentrations (Molina and Rowland, 1974). The lower stratosphere also acts as a barrier to the vertical transport of long lived foreign gasses. This latter problem has been actively studied under the sponsorship of the U.S. Dept. of Transport to assess the effects of supersonic transport (SST) aircraft (see the CIAP monographs, 1975).

Models generated for the analysis of the effects of possible stratospheric pollutants depend critically on the values assumed for the eddy diffusion coefficient . These models must parameterize the role of subgrid scale transport processes. One-dimensional models must combine the effects of small scale turbulence, larger scale transport by convective

elements, transport by larger scale folds or breaks in the tropopause (Danielson, 1968) and perhaps other larger scale processes. Of these, only transport by small scale turbulence is truly diffusive and amenable to analysis using the gradient diffusion equation. The selection of a diffusion coefficient for a one-dimensional model is usually an exercise in curve fitting using observations of a tracer (see for example, Reiter and Bauer, 1975). The same may also be true of three-dimensional models if the larger scale processes are not included explicitly.

A study of small scale turbulence is important to the understanding of the possible deficiencies of a model and to provide estimates of the minimum values to be expected if the other larger scale processes are not operative. Unfortunately, the intensity of turbulence is not a parameter of the medium but a parameter of the larger scale atmospheric motions. The eddy diffusion coefficients are not constant but depend upon the larger scale processes. The studies of small scale turbulence therefore must be morphological - they must establish both the magnitude of the small scale transport and its variation and their dependences on the large scale flow.

2.2 Radar as a Tool for the Measurement of Stratospheric Turbulence

Studies of small scale turbulence in the lower stratosphere can be performed using insitu observations from aircraft or balloon borne platforms or remotely using monostatic or bistatic radar systems. The aircraft measurements (Crooks et al, 1967) or balloon measurements (Cadet, 1977) currently available, however, do not sense fluctuations at small enough scales to provide direct observations of the eddy parameters. Monostatic radar systems can directly observe the intensity of the turbulent refractive index fluctuations at scale sizes equal to one-half the radar wavelength. These observations must also be interpreted, however, to provide eddy parameter estimates.

Radar observations of CAT have been available for over a decade. Hardy and Katz (1969) reviewed the observations of CAT and showed that high powered radar systems were useful for morphological studies of the occurrence of thin turbulent layers in the troposphere. Occasionally, radar detections of the tropopause were possible (Atlas et al, 1966). Using the high powered Millstone Hill L-band radar, Crane (1970) reported

the regular detection of thin turbulent layers at the tropopause and at heights up through 20 km. On one occasion a layer was detected at a height of 25 km.

In the early radar observations, the main interest was to demonstrate that the echo structure observed by the radar was indeed CAT and was correlated with CAT as observed by aircraft. As the association between CAT and the observed radar echoes became better established, the interest changed to obtaining a better picture of the production mechanism. The observations of the marine inversion layer reported by Atlas et al (1970) and by Metcalf and Atlas (1973) using the extremely high resolution FM-CW radar and observations of large-amplitude Kelvin-Helmholtz billows reported by Browning (1971) showed that the thin turbulent layers occur in stably stratified shear flow when the gradient Richardson number is less than 0.25. The structure of the resultant turbulence traced the classical pattern for the initial stages of roll-up by Kelvin-Helmholtz instability. The association between the thin layer radar echoes and turbulence was complete; the mechanism for CAT in stably stratified shear flow revealed.

Currently, radar observations of lower stratospheric CAT are used to obtain wind profiles (Green et al, 1975; Balsley and Farley, 1976). The turbulent fluctuations of refractive index are used as tracers for the measurement of the mean wind profile. Radar data have not been used to provide eddy parameter estimates because most of the radars are not adequately calibrated and an adequate analysis model was not available. Crane used the high powered Millstone Hill L-band radar to obtain well calibrated radar measurements of CAT in the upper troposphere and lower stratosphere as an element of a larger propagation measurement program conducted for NASA (Crane, 1973) and for the U.S. Air Force (Crane, 1970). The object of this contract for the Air Force Geophysics Laboratory is to develop a model for the interpretation of the radar data and to reprocess the data acquired between 1968 and 1970 to obtain eddy diffusion coefficient estimates.

3. RADAR MEASUREMENTS OF STRATOSPHERIC TURBULENCE

3.1 Radar Estimation of the Refractive Index Structure Function

Fluctuations of the index of refraction within a turbulent region can produce scattering of electromagnetic waves propagating through the region. Sensitive radars can detect the scattering to remotely sense the intensity of the refractive index fluctuations. The theory of scattering of electromagnetic waves by a turbulent medium is well established (Tatarskii, 1967). The bistatic radar cross section per unit volume of a turbulent medium is related to the three-dimensional (3-d) power spectral density of refractive index fluctuations, by (Crane, 1968; Crane, 1973):

$$\beta = 8\pi^2 k^4 m \Phi_n(\underset{\sim}{k}-k\hat{\rho}) \tag{1}$$

where β = bistatic scattering cross section per unit volume

k = $2\pi/\lambda$ = wavenumber; λ = wavelength

m = polarization mismatch factor

Φ_n = 3-d power spectral density of refractive index fluctuations

$\underset{\sim}{k}$ = $k\hat{x}$ where $\hat{x}$ is a unit vector from the transmitter to the scatterer

$\hat{\rho}$ = unit vector from the scatterer to the receiver.

Bistatic refers to a radar system with the transmitting antenna physically separated from the receiving antenna. When the same antenna is used for both transmission and reception, the system is called a monostatic radar or, more commonly, a radar.

For clear air turbulence sampled at a wavenumber $|\underset{\sim}{k}-k\hat{\rho}|$ in the inertial subrange (Tatarskii, 1967):

$$\Phi_n(\underset{\sim}{s}) = \Phi_n(s) = 0.033\ C_n^2\ s^{-11/3} \tag{2}$$

where C_n^2 is the refractive index structure parameter and $\underset{\sim}{s} = \underset{\sim}{k}-k\hat{\rho} = k(\hat{x}-\hat{\rho})$. The radar observable, the scattering cross section per unit volume therefore is related to the refractive index structure parameter by:

$$\beta = 8\pi^2 k^4 \Phi_n(2\underset{\sim}{k}) = \frac{0.378\ C_n^2}{\lambda^{1/3}} \tag{3}$$

where, for the monostatic radar case, $\hat{\rho} = -\hat{x}$, and m = 1.

A radar observes the total scattering cross section obtained by integrating the scattering cross section per unit volume over the resolution volume of the radar. The radar equation for a distributed target such as turbulence is given by

$$\frac{P_r}{P_t} = \frac{G_1 G_2 \ell_1 \ell_2 \lambda^2}{(4\pi)^3} \int g_1(\underset{\sim}{x}) g_2(\underset{\sim}{x}) \beta(\underset{\sim}{x}) H(\underset{\sim}{x}) \frac{d\underset{\sim}{x}}{x^4} \tag{4}$$

where P_r is the measured received power

P_t is the transmitted power

ℓ_1, ℓ_2 are receiver and transmitter line losses

g_1, g_2 are normalized radiation patterns for the receiver and transmitter antennas (directivity)

G_1, G_2 are the receiver and transmitter antenna gains

and $H(x)$ is the range weighting function.

Assuming that the turbulence uniformly fills the resolution volume, equation (4) may be reduced to

$$\frac{P_r}{P_t} = \frac{G_1 G_2 \ell_1 \ell_2 \lambda^2}{(4\pi)^3 X^4} \beta(\underset{\sim}{X}) V(\underset{\sim}{X}) \tag{5}$$

where $V(\underset{\sim}{X}) = \int g_1 g_2 H \, d\underset{\sim}{x}$ is the resolution volume for a radar return at $\underset{\sim}{X}$.

Using the equations (3) and (5), the radar observables P_r and $\underset{\sim}{X}$ may be converted into a measurement of C_n^2:

$$C_n^2 = K \cdot P_r \cdot X^2 \tag{6}$$

where X is the range to target and K is the radar calibration constant.

3.2 A Model to Estimate the Intensity of Turbulence Using Radar Data

3.2.1 The Temperature Structure Parameter, C_T^2

The radar system provides an estimate of C_n^2 averaged over the radar resolution volume. The estimate is derived from an observation made at a spatial wavenumber of 2k or a scale size equal to one half the

radar wavelength, a scale size that generally lies in the inertial subrange for the radars used for turbulence analysis. The parameters of interest are the eddy parameters, the eddy dissipation rate and eddy heat diffusion coefficient, not C_n^2.

At microwave frequencies, the index of refraction is related to the meteorological properties of the medium by (Crane, 1976):

$$n = 1 + \left(\frac{77.6P}{T} + \frac{3.73 \times 10^5 e}{T^2}\right) \times 10^{-6} \qquad (7)$$

where n is index of refraction

P is pressure (in millibars, mb)

T is temperature (in degrees Kelvin, °K)

and e is water vapor pressure (in mb).

The refractive index fluctuations are caused by turbulent variations in temperature (or density) and water vapor concentration. At the heights of interest in the lower stratosphere and upper troposphere, the effects of water vapor are negligible. The relevant equation for refractive index variation about the mean value reduces to

$$\Delta n = \left(\frac{77.6P\Delta\Theta}{T^2}\right) \times 10^{-6} \qquad (8)$$

where Δ denotes change and Θ is the potential temperature. The expression for C_n^2 therefore may be simply related to the temperature structure parameter, C_T^2 by

$$C_T^2 = \left(\frac{T^2}{77.6P} \times 10^6\right)^2 C_n^2 \qquad (9)$$

hence, C_T^2 may be obtained directly from the radar observations of P_r and X when the pressure and temperature in the scattering volume are known.

3.2.2 Eddy Parameters $\overline{\epsilon}_m$ and $\overline{K}_H$

The radar may be used to obtain an estimate for the temperature structure parameter averaged over the radar resolution volume. The large number of available radar observations of CAT show that the actively turbulent regions are very thin, and may in general be thinner than the resolution volume of the radar (Hardy and Katz, 1969; Atlas et al, 1970). Let the actively turbulent region occupy a thin layer of height increment

d within a radar resolution volume, of height increment h. Noting that the layers are generally large in horizontal extent, assume that the radar resolution volume is smaller in the horizontal than the actively turbulent region. Assume also that the turbulence is of uniform intensity throughout its active region. Then,

$$C_T^2 = (\frac{h}{d})C_{Te}^2 \tag{10}$$

where C_{Te}^2 is the value measured by the radar and C_T^2 is the actual value for the turbulent region.

Similarly, assume that only turbulence within the active region contributes to the eddy dissipation rate.

$$\overline{\varepsilon}_m = \frac{d\varepsilon_{mm} + (h-d)\varepsilon_{mo}}{h}$$

where $\overline{\varepsilon}_m$ is the mean (in time and space) eddy dissipation rate for the layer of thickness h and within the horizontal dimensions of the radar resolution volume, ε_{mm} is the dissipation rate within the active region, ε_{mo} is the dissipation rate outside the active region and $\varepsilon_{mm} >> \varepsilon_{mo}$. Then,

$$\overline{\varepsilon}_m = (\frac{d}{h})\varepsilon_{mm}. \tag{11}$$

Similarly, the mean eddy diffusion rate may be expressed as

$$\overline{\varepsilon}_q = (\frac{d}{h})\varepsilon_{qm}. \tag{12}$$

The region of the atmosphere of interest, the lower stratosphere and upper troposphere, are statically stable. In such a region, the eddy diffusion parameters for momentum and heat may be defined by (Monin and Yaglom, 1975; Dutton, 1969)

$$\overline{\varepsilon}_m = \overline{K}_m(\frac{\Delta V}{h})^2(1-\overline{R_f}) \tag{13}$$

and

$$\overline{\varepsilon}_q = \overline{K}_H(\frac{\Delta\Theta}{h})^2 \tag{14}$$

where $\overline{\varepsilon}_m, \overline{\varepsilon}_q$ are the mean eddy dissipation rate and eddy heat diffusion rate values respectively,

$\overline{K}_m, \overline{K}_H$ are the eddy diffusion coefficients for momentum and heat respectively,

ΔV is the mean vector velocity change (difference) across the layer of thickness h,

$\Delta\Theta$ is the mean potential temperature across the layer

and
$$\bar{R}_f = \frac{g}{\Theta_o} \cdot \frac{\langle w\phi \rangle}{\sum_{i=1}^{2} \langle wv_i \rangle \left(\frac{\Delta V_i}{h}\right)} = \frac{g}{\Theta_o} \frac{\bar{K}_H}{\bar{K}_m} \frac{\Delta\Theta/h}{(\Delta\chi)^2/h^2} \tag{15}$$

g is the acceleration due to gravity,

Θ_o is the mean potential temperature of the layer,

$\langle w\phi \rangle$ is the turbulent heat, vertical velocity covariance,

$c_p \rho_o \langle w\phi \rangle$ is the vertical turbulent heat flux and

$\langle wv_i \rangle$ are the turbulent velocity covariances with i = 1,2 horizontal directions; $\rho_o \sum_{i=1} \langle wv_i \rangle$ is the vertical momentum transport.

The turbulent kinetic energy balance equation (13) was derived using the standard assumptions of steady state turbulence, horizontal homogeneity, vertical volume boundaries not within the actively turbulent region. The last two assumptions are required to eliminate terms including the divergence of the turbulent transport of turbulent kinetic energy and the divergence of the turbulent velocity, pressure covariance. It is noted that in most measurements of turbulence, these assumptions are often violated when the turbulence is not homogeneous but in radar measurements of apparently steady state, homogeneous thin horizontal turbulent layers thinner than a resolution element, the assumptions are not. Similar assumptions are required for the simplification of the turbulent heat diffusion rate equation (14). Both equations express the steady state balance between larger scale production and small scale dissipation assumed for the existence of an inertial subrange.

The turbulent momentum and heat diffusion rate equations (13) and (14) do not require the existence of eddy diffusion coefficients since they were initially derived using turbulent heat and momentum fluxes. They describe volume averaged turbulence production and dissipation. Similarly, the flux Richardson number is a ratio of volume averaged covariances divided by the mean wind shear across the layer. The average intensity of the turbulence within the volume may be characterized by the eddy parameter $\bar{\varepsilon}_m$; the average vertical transport through the layer by

the eddy heat diffusion coefficient $\overline{K}_H$. The flux Richardson number is related to the gradient Richardson number by

$$\overline{R}_f = \frac{\overline{K}_H}{\overline{K}_m} \overline{R}_i = \frac{\overline{R}_i}{\overline{P}_\varepsilon} \tag{16}$$

where $\overline{R}_i = \frac{g}{\overline{\Theta}_o} \frac{\Delta\Theta/h}{(\Delta\underset{\sim}{V})^2/h^2} = \frac{g}{\overline{\Theta}_o} \frac{\Delta\Theta h}{(\Delta\underset{\sim}{V})^2}$ is the gradient Richardson number and $P_\varepsilon = \overline{K}_m/\overline{K}_H$ is the eddy Prandtl number.

The parameters defined by equations (13) and (14) are for a layer of thickness h. For the actively turbulent layer of thickness d, a new set of parameters are required each of which apply only to the active region:

$$\varepsilon_{mm} = K_m \left(\frac{\Delta\underset{\sim}{V}}{d}\right)^2 (1-R_f) \tag{17}$$

$$\varepsilon_{qm} = K_H \left(\frac{\Delta\phi}{d}\right)^2 \tag{18}$$

where $\Delta\underset{\sim}{V}$ expresses the mean vector velocity change across the thickness d and $\Delta\phi$ the potential temperature difference across the layer. The quantities K_m, K_H and R_f will in general be different from the h-layer quantities $\overline{K}_m$, $\overline{K}_H$ and $\overline{R}_f$. Equations (10) through (18) are consistant with current ideas of intermittant turbulence (Monin and Yaglom, 1975). They do not provide a complete set of equations for the computation of d or any of the d-layer or h-layer eddy parameters. The h-layer gradient values may be obtained from radiosonde observations; the d-layer values cannot.

An additional equation relating ε_{qm}, ε_{mm}, and C_T^2 can be obtained from the classical dimensional analysis of inertial subrange turbulence (Monin and Yaglom, 1975)

$$C_T^2 = \alpha_\Theta \varepsilon_{mm}^{-1/3} \varepsilon_{qm} \tag{19}$$

where α_Θ is an empirical constant currently estimated at 3.3. Further progress in the reduction of these equations requires new assumptions.

The first new assumption is that every volume in the atmosphere is on average (in time) always turbulent. This assumption is consistant with recent observations such as those reported by Goodman and Miller (1977) which provide evidence for turbulent mass transport across a stably stratified layer with a gradient Richardson number near 24. For turbulent transport across a stable layer, the time averaged flux Richardson number for the layer must lie in the range between 0 and 1. If this layer is turbulent but with different magnitudes of turbulence in sublayers within the layer, the time averaged R_f should be within this range for each of the sublayers. This model agrees with the accepted model for turbulence production in a stable region with shear flow and is consistant with available radar observations and laboratory measurements. A cascade of Kelvin-Helmholtz instabilities occur at random in time within each layer. The stably stratified shear flow becomes locally unstable when the local gradient Richardson number is less than 1/4. Theoretical estimates reviewed by Howard and Maslowe (1973) shows that stability (no turbulence) may be assumed only if the local R_i is greater than 1/4 for all d. Experimental data reported by Thorpe (1973) showed the local R_i < 0.2 across the active region at the onset of turbulence and the local R_i = 0.3 at the cessation of turbulence. A model consistant with these observations is that the flux Richardson number is everywhere constant throughout the layer at a value between 0.2 and 0.3. The flux Richardson number may be taken to equal the gradient Richardson number within the actively turbulent region; the h-layer gradient Richardson number, $\overline{R}_i$ is given by the radiosonde derived value for a thickness h. For an actively turbulent layer, the local R_i is taken as equal to the critical value, R_i = 1/4.

Using the concept of a flux Richardson number defined for a layer,

$$\overline{K}_m = \overline{K}_H \, \overline{R}_i / \overline{R}_f$$

and

$$\overline{\varepsilon}_m = \overline{K}_H \, \overline{R}_i \, \frac{(\Delta V)^2}{h^2} \, \frac{(1-\overline{R}_f)}{\overline{R}_f} \qquad (21)$$

$$= \overline{K}_H \, \frac{g}{\Theta_o} \, \frac{\Delta\Theta}{h} \, \frac{(1-\overline{R}_f)}{\overline{R}_f}$$

For $\bar{R}_f = 1/4 = \text{constant}$, $(1-\bar{R}_f)/\bar{R}_f = 3$ and

$$\bar{\varepsilon}_m = 3\bar{K}_H \frac{g}{\theta_o} \frac{\Delta\theta}{h} = 3\bar{N}^2\bar{K}_H \tag{22}$$

where $\bar{N} = (\frac{g}{\theta_o} \frac{\Delta\theta}{h})^{1/2}$, the Brunt Väisälä frequency. The result, equation (22) is the relationship Lilly et al (1974) used to reduce the Project HICAT data and Cadet (1977) used to reduce his balloon data. Using equations (21) and (11) and the assumed constancy of R_f over layers of thicknesses d and h, $R_f = \bar{R}_f$ and

$$\bar{\varepsilon}_m = \bar{K}_H \frac{\Delta\theta}{h} \frac{g}{\theta_o} \frac{1-R_f}{R_f} = \frac{d}{h} K_H \frac{\Delta\phi}{d} \frac{g}{\theta_o} \frac{1-R_f}{R_f}$$

$$\text{or} \qquad \bar{K}_H \Delta\theta = K_H \Delta\phi \tag{23}$$

and, since $$\bar{\varepsilon}_q = \bar{K}_H (\frac{\Delta\theta}{h})^2 = \frac{d}{h} K_H (\frac{\Delta\phi}{d})^2$$

$$\frac{\Delta\theta}{h} = \frac{\Delta\phi}{d}$$

This result shows that the potential temperature gradient is maintained across the turbulent layer, a result experimentally obtained in the laboratory by Long (1973) and evident in the aircraft data presented by Metcalf and Atlas (1973).

By the definition of R_i and the assumed equality of R_i and R_f with the actively turbulent layer ($P_\varepsilon = 1$ in the actively turbulent layer),

$$(\frac{\Delta V}{d})^2 = \frac{g}{\theta_o} \frac{\Delta\phi}{d} \cdot \frac{1}{R_f} = \frac{\bar{R}_i}{R_f} (\frac{\Delta V}{h})^2 \tag{24}$$

where $\bar{R}_i$ is defined over the layer of thickness h. Equation (24) expresses the relationship between the velocity gradients across the actively turbulent layer and the layer of thickness h. To close the full set of equations, an additional relaltionship between $\Delta\chi$ and ΔV is required. Noting the tendency for stably stratified fluids to form horizontal

internal boundary layers, the second new assumption that $(\Delta\underset{\sim}{V})^2 = (\Delta\underset{\sim}{V})^2$ is made. Using this assumption and equation (24),

$$d = h\sqrt{\frac{R_f}{R_i}} = \frac{h}{\sqrt{P_\varepsilon}} = \frac{h}{\sqrt{R_i}} \tag{25}$$

Equation (25) matches the equation Long (1973) obtained to fit his experimental data for the thickness of the actively-turbulent steady state shear layer.

The two new assumptions required to close the equations were argued on physical grounds and shown to match the experimental results obtained by Long. Using these assumptions and equations (10) through (25), the final results for the analysis of the radar data are obtained:

$$\bar{K}_H = (C_{Te}^2)^{3/2} \left[\left(\frac{1-\bar{R}_f}{\bar{R}_f}\right) \frac{g}{\bar{\theta}_o} \frac{h}{d}\right]^{1/2} \left(\frac{\Delta\theta}{h}\right)^{5/2} \alpha_\theta^{-3/2} \tag{26}$$

$$\bar{\varepsilon}_m = (C_{Te}^2)^{3/2} \left(\frac{g}{\bar{\theta}_o}\right)^{3/2} \left(\frac{1-\bar{R}_f}{\bar{R}_f}\right)^{3/2} \left(\frac{h}{d}\right)^{1/2} \left(\frac{\Delta\theta}{h}\right)^{-3/2} \alpha_\theta^{-3/2} \tag{27}$$

These results are similar to those recently presented by Van Zandt et al (1977) and have definite advantages over previous analyses (see Hardy and Katz, 1969; Metcalf and Atlas, 1973) in that an outer scale for turbulence does not have to be assumed. The results still are an approximation in that the h-layer contains many active sublayers, not one - each turbulent region is intermittent. If the eddy dissipation rate values for each sublayer of intermittent turbulence were identical, the empirical coefficient α_θ would account for the non-linear averaging of the randomly intermittent patches within the layer of thickness d (or h) (see Monin and Yaglom, 1975, section 25). Since ε_{mm} can vary from sublayer to sublayer, α_θ may differ from the assumed value. Noting that the larger scale motions responsible for generating the turbulence will not selectively pick the same sublayers when h is the order of 1 km, it is expected that the differences are small when long time averages are used.

The final equations (26) and (27) follow directly from the definitions of K_m and K_H and the inertial subrange expression for C_T^2 - equation (19) when h = d and the entire layer is turbulent. In this case, the new assumptions used to find d are not required. The impact of the new assumptions is to provide a derivation of the correction factor for layer thickness, the factor including h/d which adjusts the radar data because the thin turbulent layers do not normally fill the radar resolution volume. If a radar with a sufficiently small resolution volume is used, such as the FM-CW radar of Richter (1969), with a resolution volume entirely filled by the active region, then the new assumptions are not required. In this case, the application of equations (26) and (27), however, may be more difficult to justify because a small active region that completely fills a small resolution volume may be only one of the many intermittent patches within the larger turbulent region and the steady state and spatially homogeneous assumptions used to derive the turbulent energy balance equation (13) may be violated.

4. THE RADAR OBSERVATIONS

4.1 The Millstone Hill L-band Radar System

The radar system and its calibration for use in observing meteorological targets has been described by Crane (1971; 1973). The characteristics of the radar as configured in 1968 and 1970 are given in Table II. The radar used an 84-foot antenna that was computer controlled. The antenna gain was measured using radio star flux measurements. The antenna pattern information required to compute the radar resolution volume was obtained both for the transmission and reception patterns (which were different due to the use of circular polarization which required orthogonally polarized transmitter and receiver).

The radar system used a Klystron transmitter and low-noise parametric receivers which could be cooled. A coherent linear receiver system was used with matched filters on both the sine and cosine output channels. The output from each filter was sampled and stored in real time in a SDS 9300 computer. The data were square law detected and incoherently integrated in the computer. An estimate of the receiver noise power was subtracted from the detected signal plus noise to obtain a signal power estimate. Fifty independent samples were processed resulting in a statistical uncertainty of 0.7 dB rms in a back scatter cross section per unit volume estimate. To obtain independent pulses, a sampling rate of 20 pulses per second was used taking 2.5 seconds to obtain an observation.

Radar system performance was continuously monitored. The receiver system was continuously monitored using a pulsed noise tube of known temperature. The average transmitter power was continuously recorded. During 1970 an additional calibration pulse was used to provide a second receiver calibration. The two independent receiver calibrations differed by less than ±0.2 dB.

The absolute radar system calibration was made by combining the values for each factor in the radar equation. The maximum error in the calibration constant was estimated at ±1.4 dB (at 3 standard deviations). An overall calibration check was made by tracking orbiting spheres of known cross section. The measured cross sections were within 0.5 dB of the known (true) cross sections. Recent observations made by the author in 1974 using an improved computer aided satellite tracking system and

TABLE II

MILLSTONE HILL L-BAND RADAR

	Summer 1968	Summer and Fall 1970
Frequency	1.295 GHZ (23.2-cm wavelength)	1.295 GHz
Antenna	84-foot paraboloid with Cassegrainian feed	
Antenna Gain	47.2±0.3 dB	46.7±0.3 dB
Beamwidth	0.7°	0.7°
Polarization	Right-hand circular transit, left-hand circular receive	
Transmitted Power	3.3 MW peak	3.3 MW peak
Pulse Length	10.0 μsec	12.4 μsec
Pulse Repetition Rate	120 per second	120 per second
Receiver Bandwidth	80.5 kHz	80.5 kHz
Data Processing	Analog-to-digital conversion of the IF sine and cosine channels every 10 μsec	
Computer Sampling Rate	20 per second	20 per second
Detection	Square law by computer operations	
Dynamic Range	40 dB*	80 dB
System Noise Temperature	280°K	280°K
System Line Losses (transmit and receive)	2.2 dB	2.8 dB
Matched Filter Processing Loss	1.4 dB	1.1 dB
Single Pulse C_n^2 Value for Unity Signal-to-Noise Ratio	10^{-16} $m^{-2/3}$ at 100 km	10^{-16} $m^{-2/3}$ at 100 km

*Increased to 80 dB by a manually adjusted variable attenuator in the transmission line between the antenna and receiver.

the Millstone radar produced cross sections within 0.25 dB of the true value. Intercomparisons between Millstone Hill L-band radar measurements of rain and simultaneous measurements with the independently calibrated Avon-to-Westford Bistatic Radar System of the same rain volume produced differences of less than 1 dB when corrected for known rain drop shape effects. These results show that the most likely absolute calibration error for the radar system is in the ±0.4 - ±0.5 dB range.

4.2 Data Processing

4.2.1 Radar Data

The radar observations were recorded on magnetic tape for post test analysis. The data were processed to obtain vertical surface distance, height (RHI) maps of C_n^2 estimates. These values were further integrated over a 22.5 km surface distance and 1 km height interval at a constant height to further improve the signal to noise ratio of a C_n^2 profile estimate. The calculated minimum single pulse C_n^2 value detectable for a non-fluctuation target at a range of 100 km with a unity signal-to-noise ratio is 1×10^{-16} $m^{-2/3}$ as indicated in Table II. Using both noise power subtraction in the process of signal detection and the additional 15 range cell integration implied in the processing to obtain a C_n^2 profile improved the signal-to-noise ratio by 14 dB yielding a minimum detectable C_n^2 value of 4×10^{-18} $m^{-2/3}$. In practice, the minimum detectable value ranged between 8×10^{-18} and 2×10^{-17} at heights below 20 km depending upon the system configuration and the extent to which the system was bothered by man-made interference.

The radar system was bothered by sidelobe detection of ground clutter, aircraft, and heavy rain. To circumvent the effect of ground clutter, data were processed only for ranges in excess of 60 km. CAT detection was not attempted during periods of heavy rain; radar operations, however, were conducted during such periods because the investigation of rain scatter was the principal motivation for the measurement program (Crane, 1974). The effects of aircraft and ground clutter at long ranges during periods with ducting were more difficult to combat.

Figures 1 and 2 depict the raw radar measurements and a computer generated surface distance, height map (RHI). In figure 2, the intensity

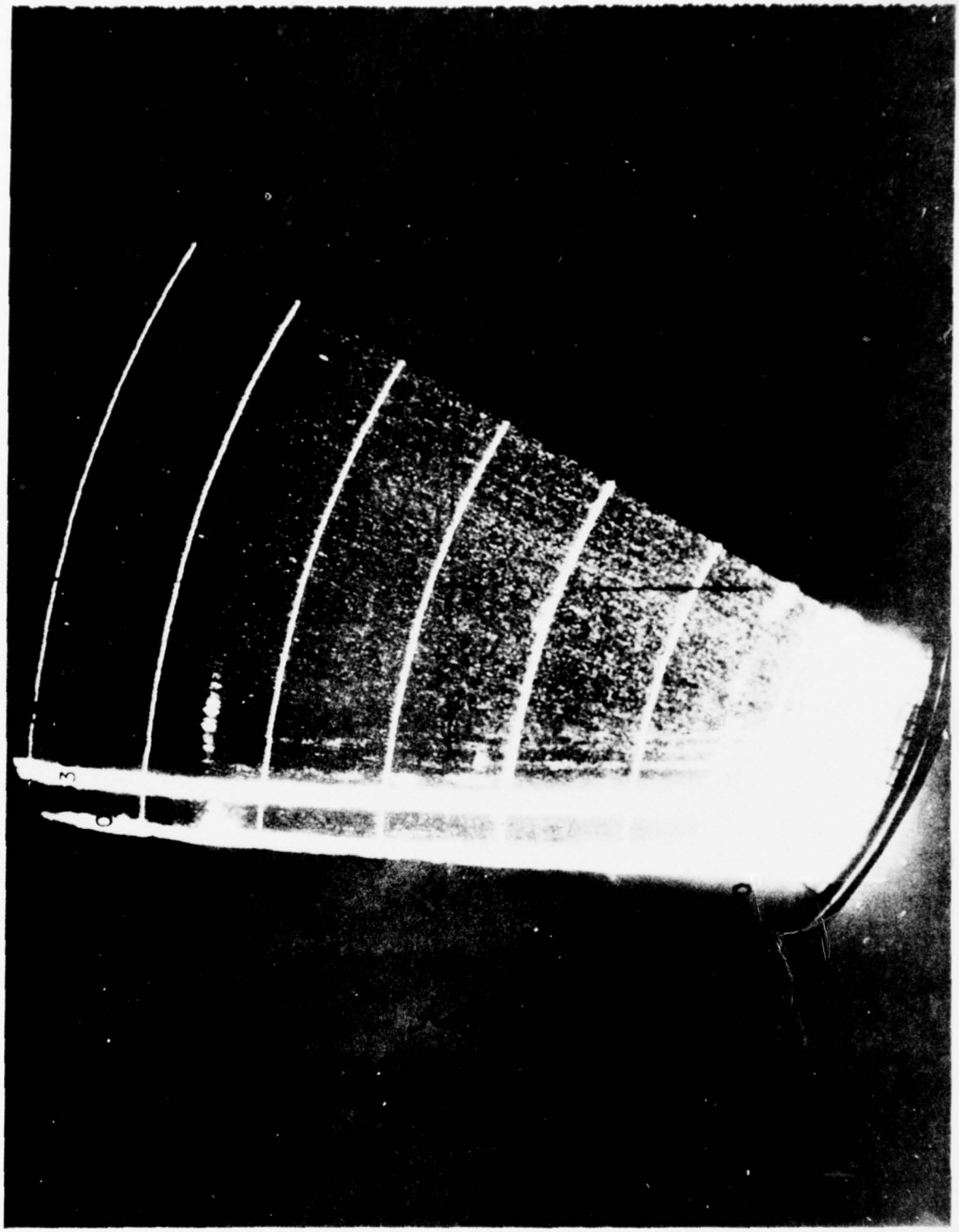


Figure 1 Elevation Scan, Millstone Hill Radar 1439 UT, May 28, 1968

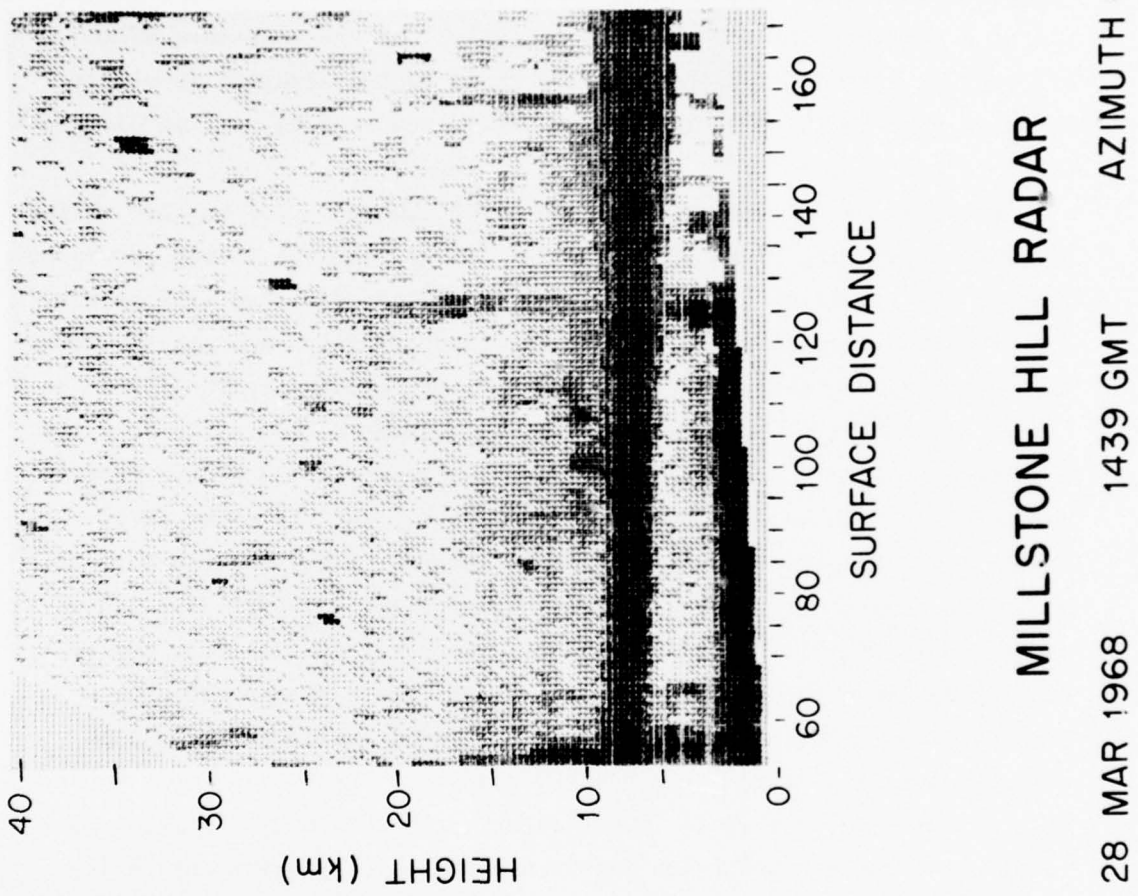


Figure 2 Computer generated RHI (note the correct date is May 28, 1968)

changes represent 5 dB steps in C_n^2. The raw radar data show strong echoes from turbulence in the planetary boundary layer (height less than 3 km), an intermediate layer of weak turbulence ($C_n^2 \sim 10^{-17}$, see figure 4), solid cirrus overcast in the 7 to 9 km height region and 4 turbulent layers above. The layer at 10 km height reveals a billow-like structure (at the resolution of this radar) with strong intensity variations at an 8 km spacing. Also evident in the data are enhanced ground clutter. The strong, constant range return at 125 km corresponds to the location of Cape Code as viewed from the Millstone radar. The intermittent arc starting at a surface distance of 65 km is typical of the signature of an aircraft in a radar sidelobe when the range to the aircraft is slowly changing over the 5 to 6 minute time period required to make an elevation scan.

Profiles of C_n^2 were constructed for 3 separate 22.5 km wide surface distance intervals, 77 to 99 km, 100 to 123 km, and 124 to 146 km respectively. The profiles obtained for the radar data depicted in figures 1 and 2 are presented in figure 3. The three profiles are combined to make one best estimate profile depicted by the curve labeled 1439 UT on figure 4. The three profiles were intercompared to remove the spurious effects of aircraft and isolated ground clutter. In the height interval between 20 and 30 km, the profile for 123.6 to 146.1 km shows large variations in C_n^2 due to the strong ground clutter. Similar variation, but of smaller magnitude is seen in the curve for 100.2 to 122.7 km and no variation is seen in the third profile. Spurious effects were removed by picking the minimum value from the three curves at each height. The resultant profile is displayed in figure 4. Guidance in profile estimation is also taken from the RHI display. The 76.8 to 99.3 km profile was used for the 11 to 16 km height region because it showed equivalent apparent contamination to the minimum value profile and better reproduced the structure evident in the 65 to 80 km surface distance interval at those heights. As seen from the profile data in figure 3, the differences between the two possible profiles in the 11 to 16 km height region are less than 1 dB.

The apparent spread in the width of the cirrus cloud layer in the computer generated RHI is due in part to the method used to construct the RHI. Radar data from each range, elevation interval was assumed to uniformly fill the radar resolution volume. The radar beamwidth is 0.7°

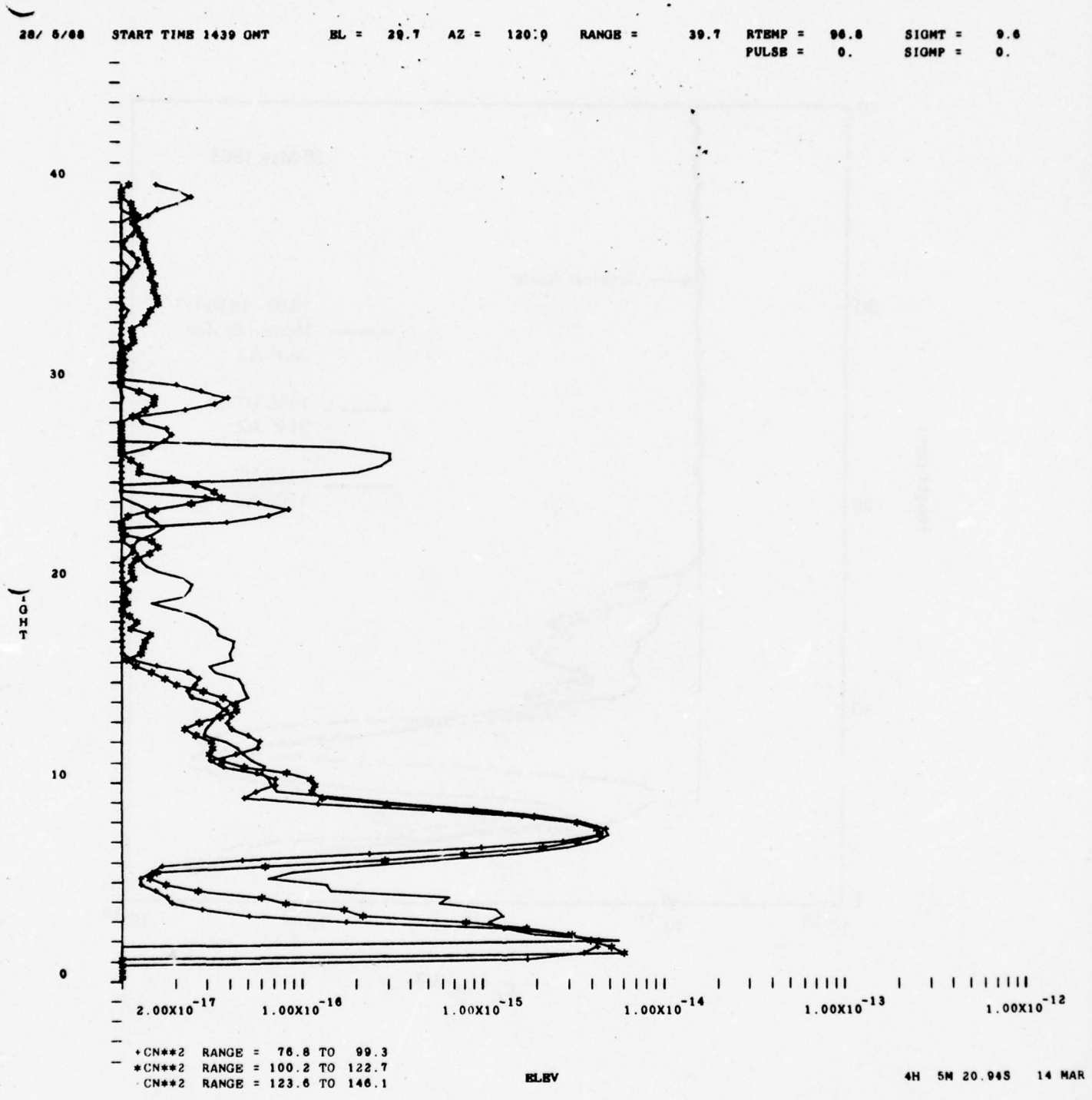


Figure 3 Computer generated C_n^2 profiles, 1439 UT, May 28, 1968

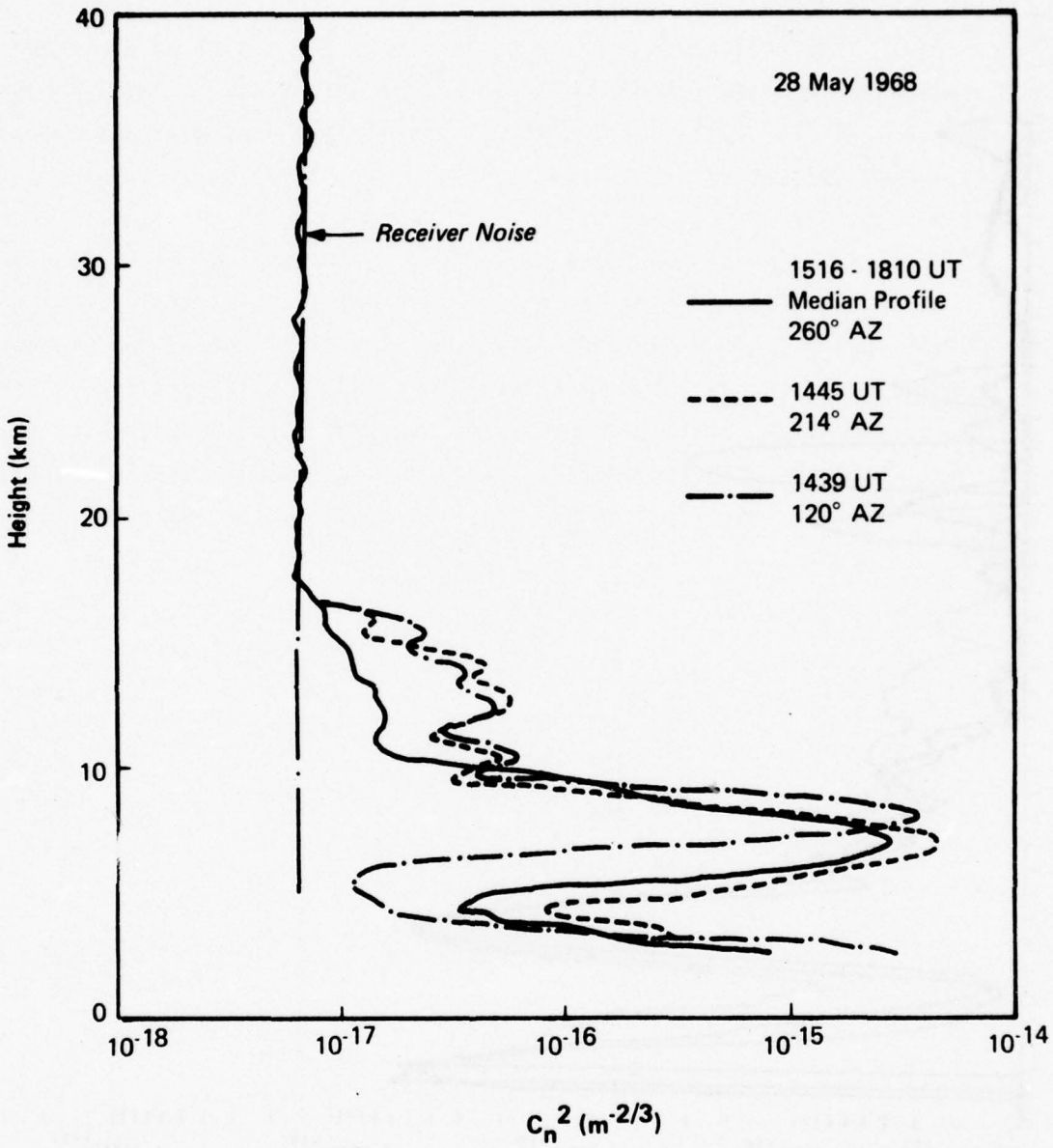


Figure 4 Best estimate C_n^2 profiles, May 28, 1968

spanning a 1.2 km height interval at 100 km range. When the layer is thinner than the beamwidth, the amplitude of the layer changes with difference to the profile. When the layer is thicker than a beamwidth, as in this case, the magnitude is constant but the width appears to increase with distance to the layer. When the profiles are nearly identical as in the case considered above for the 11 to 16 km height region, the profile for the smallest surface distance is used because of its better height resolution.

The computer processing used to produce the C_n^2 profiles presented in figure 3 was accomplished at Lincoln Laboratory between 1970 and 1972. The data tapes used to generate the plots were released during the 1974-1975 time period when support for further processing was not available. For this contract further processing was accomplished manually using the computer generated C_n^2 profiles. A computer profile was generated for each RHI scan. The median profile for 5 successive RHI scans was obtained as a best estimate of the mean C_n^2 profile for a 20 to 30 minute period. The median of these profiles was then constructed as a best estimate for the mean of an observation set. The median of the medians is used to characterize the C_n^2 profile for one set of observations. It is used to provide the representation of the time average of the profile required for use in estimating the eddy parameters as described in section 2. The median and two sample profiles taken 6 minutes apart are shown in figure 4. Although the data for 1439 and 1445 UT are obtained from spatial locations nearly 140 km apart, the profiles in the region of turbulence above a height of 10 km are nearly identical. The height of the cirrus cloud layer does change over that spatial distance.

The median for the observation set is roughly a factor of 4 lower at 12-14 km height. The receiver noise line displayed on the figure represents the expected median profile if receiver noise alone were present. The variation of the median curve about this line at heights above about 17 km may be used as an indication of the statistical uncertainty in the median estimate. Where possible, median estimates were obtained only for observations in a narrow azimuth sector of less than 40° to remove any possible large scale spatial changes. For the data on figure 4, neither single observation profile was used in the construction of the median. This selection process did not appear to change the resultant median suggesting that the steady state, horizontally homogeneous assumptions are valid on the time scale used for analysis.

The median profiles for each observation set are given in Appendix B.

4.2.2 Radiosonde Data

Standard radiosonde observations were specially made by the Air Force Cambridge Research Laboratory (now Air Force Geophsyics Laboratory) in support of the radar measurement program. These data were computer processed at MIT Lincoln Laboratory using raw data samples at 30 second intervals in addition to the significant level values. On several ocassions, Loran C wind sensors were flown on the balloons to provide improved wind velocity profiles. The data were processed to provide potential temperature, refractive index, and windspeed and direction profiles. Sample profiles for the data presented in figures 1 to 4 are presented in figures 5 to 9. Two sets of soundings were available on many of the days. Although the water vapor contribution to the refractive index was not explicitly treated in Section 2, the data were available for analysis as shown in figure 8. Figure 9 presents the radio reflectivity profile where refractivity is $(n-1) \times 10^6$ (see equation (7)).

The radiosonde data were processed in 1 km height intervals. The layer thickness h was taken to be 1 km to approximate the vertical resolution of the radar system at the 70 to 140 km ranges and the low elevation angles used for the measurements. The data required to calculate $\overline{\varepsilon}_m$, $\overline{K}_H$, and d were selected from the radiosonde data computer output (print out) and used to manually calculate the parameters (using a desk calculator). Intermediate profiles of $\overline{C}_T^2$ were generated and are separately displayed as shown in figure 10. Profiles of $\overline{K}_H$ and $\overline{\varepsilon}_m$ were then calculated as displayed in figure 11. A complete set of $\overline{C}_T^2$, d, $\overline{\varepsilon}_m$ and $\overline{K}_H$ profiles are given in Appendix A.

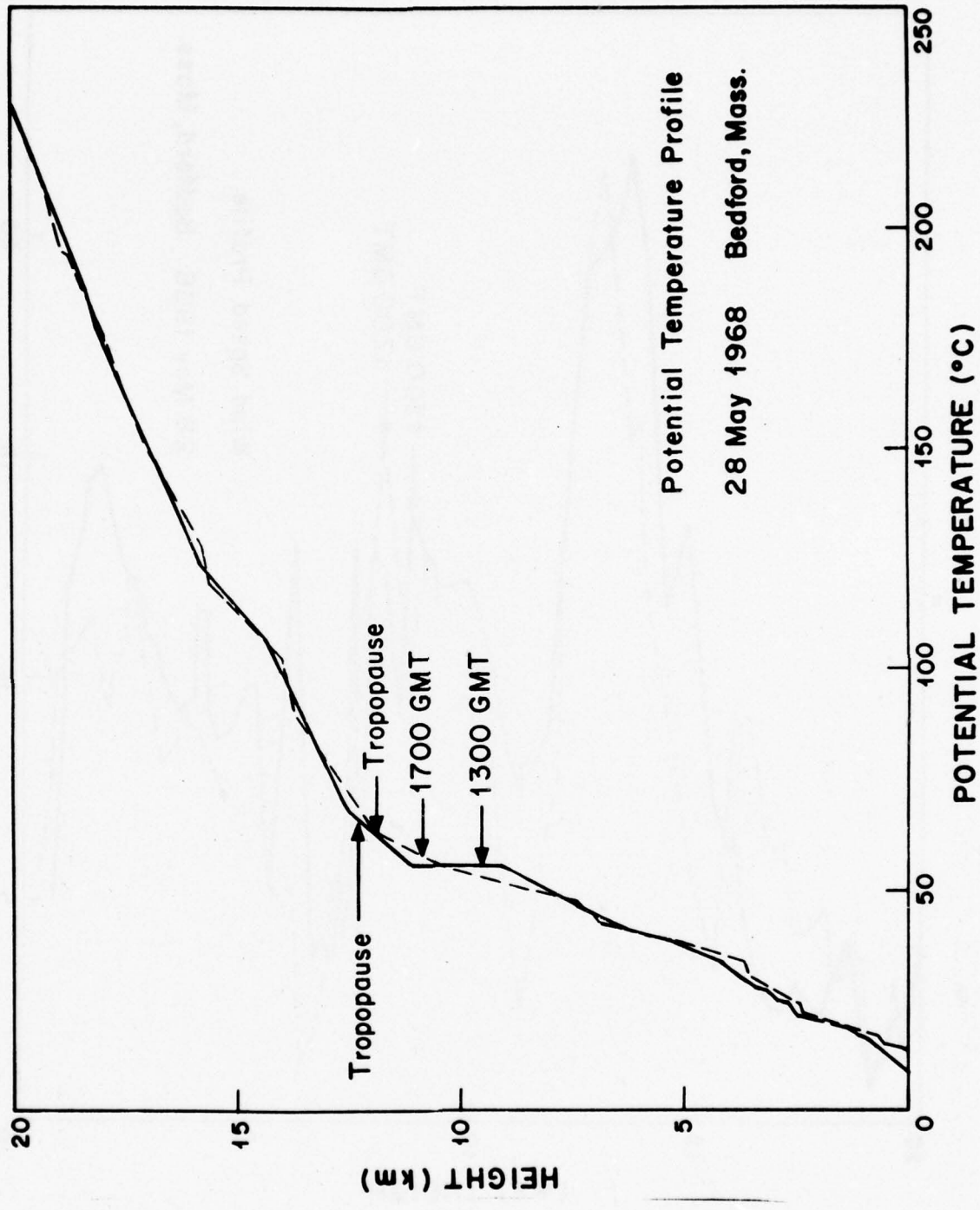


Figure 5 Potential temperature profile, May 28, 1968

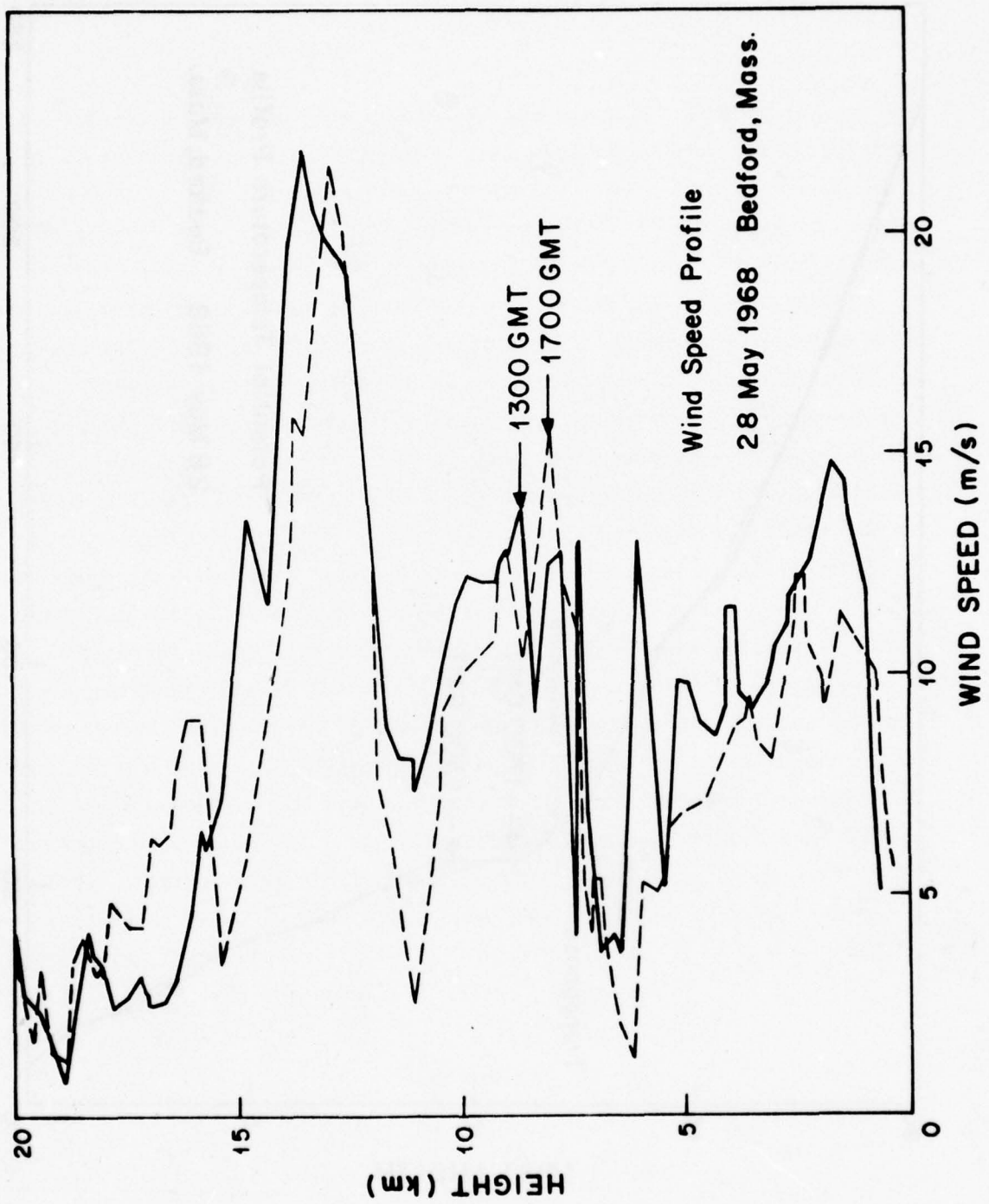


Figure 6 Wind Speed profile, May 28, 1968

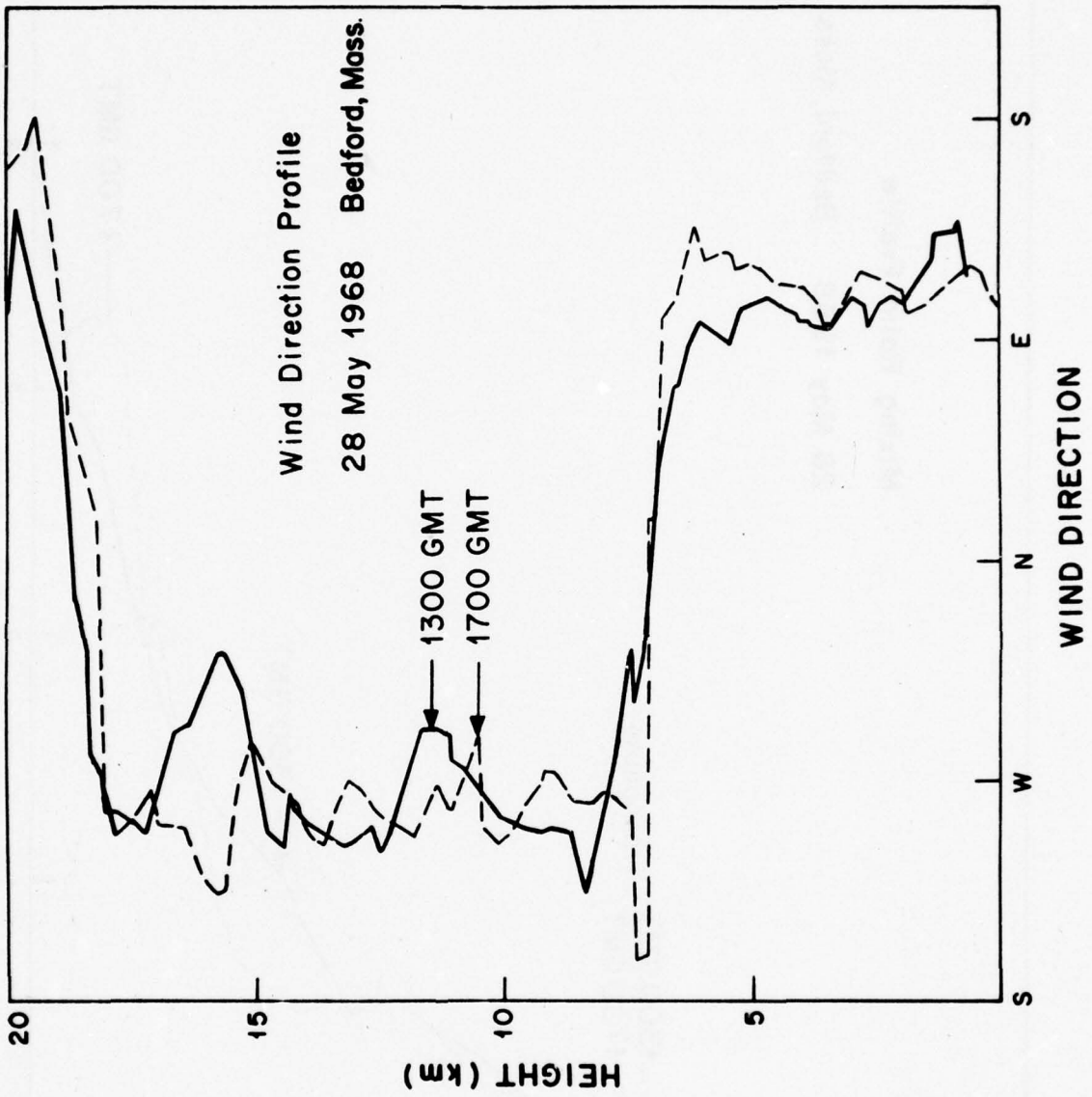


Figure 7 Wind Direction profile, May 28, 1968

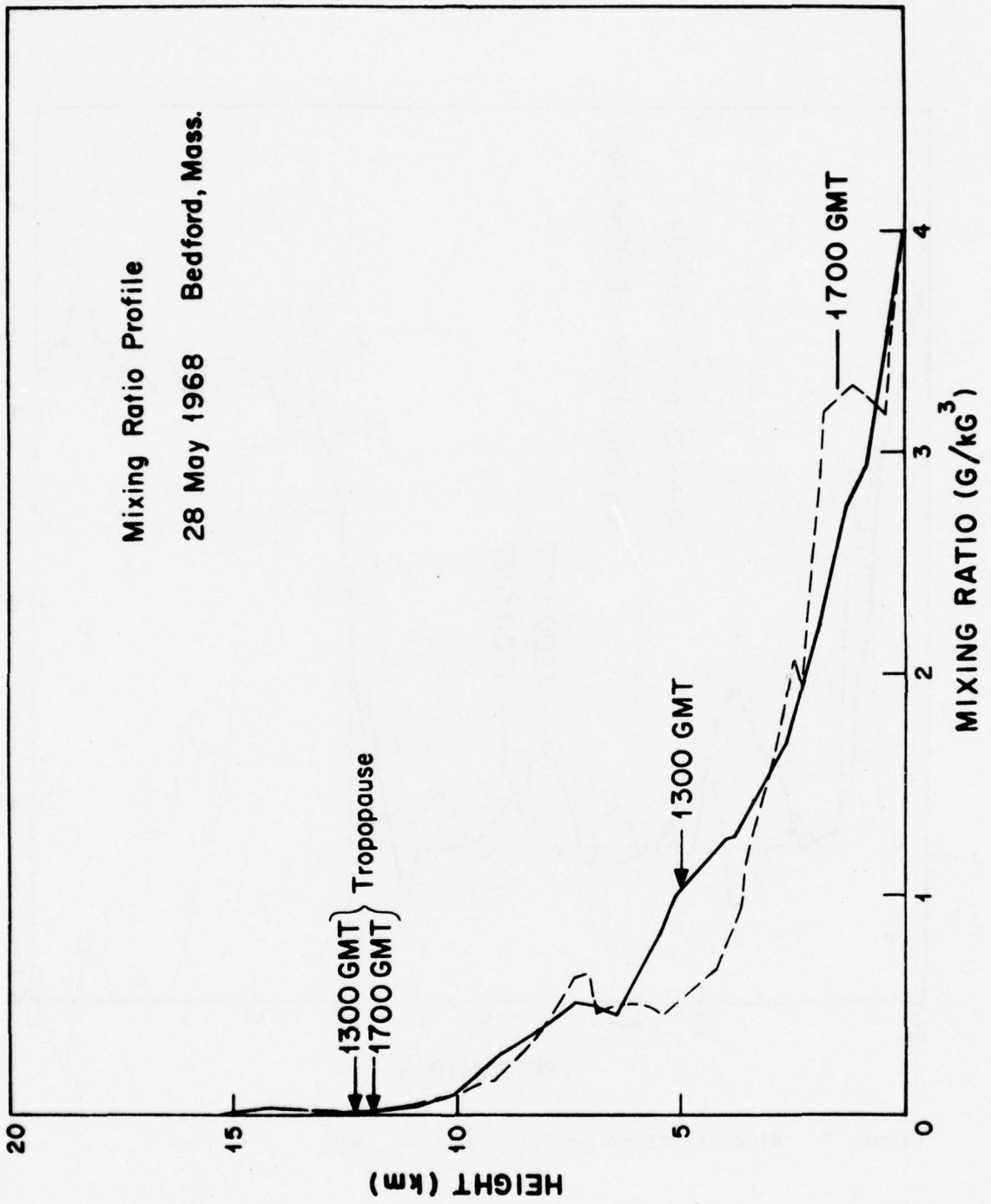


Figure 8 Water Vapor Mixing Ratio profile, May 28, 1968

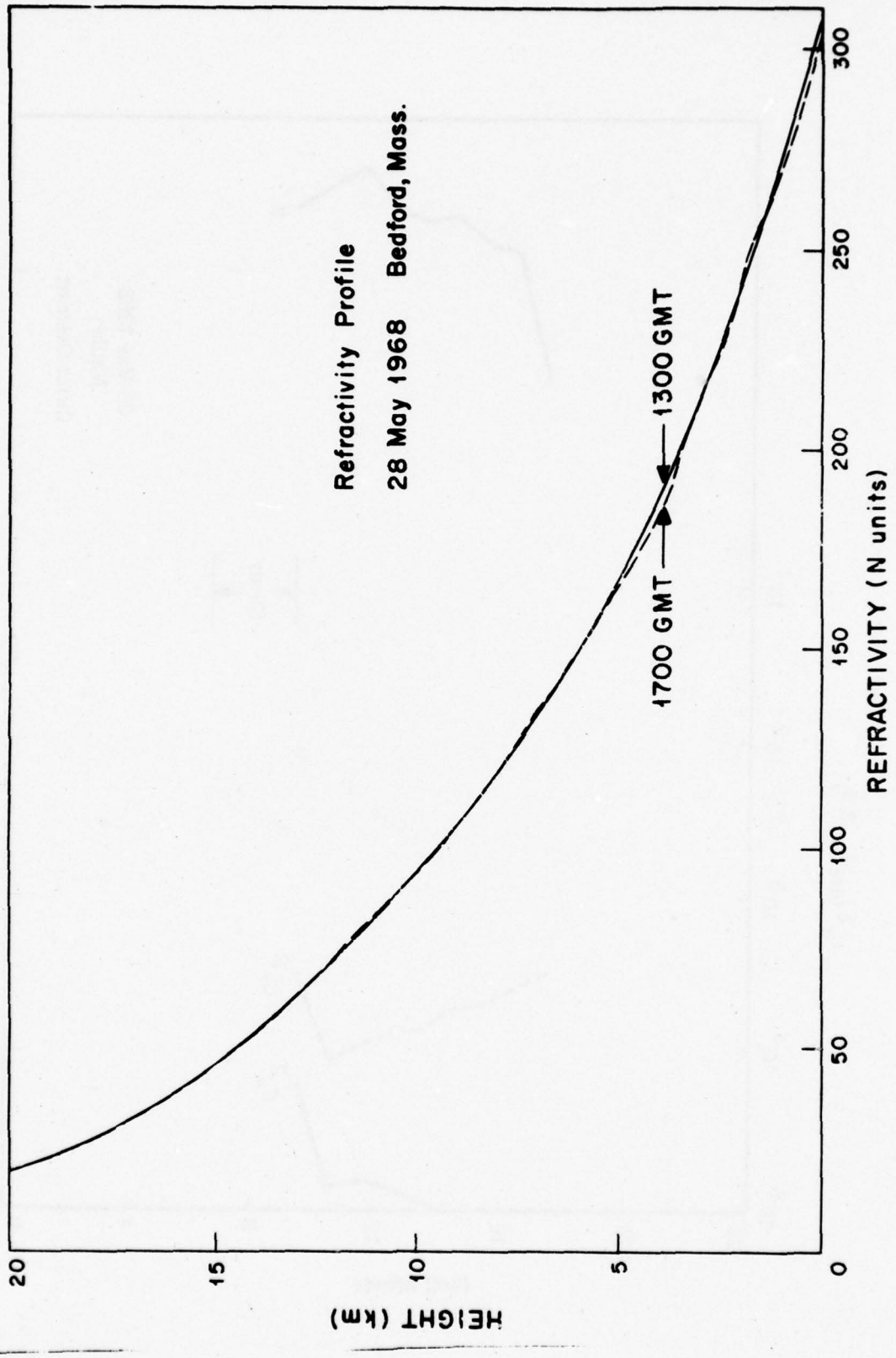


Figure 9 Refractivity profile, May 28, 1968

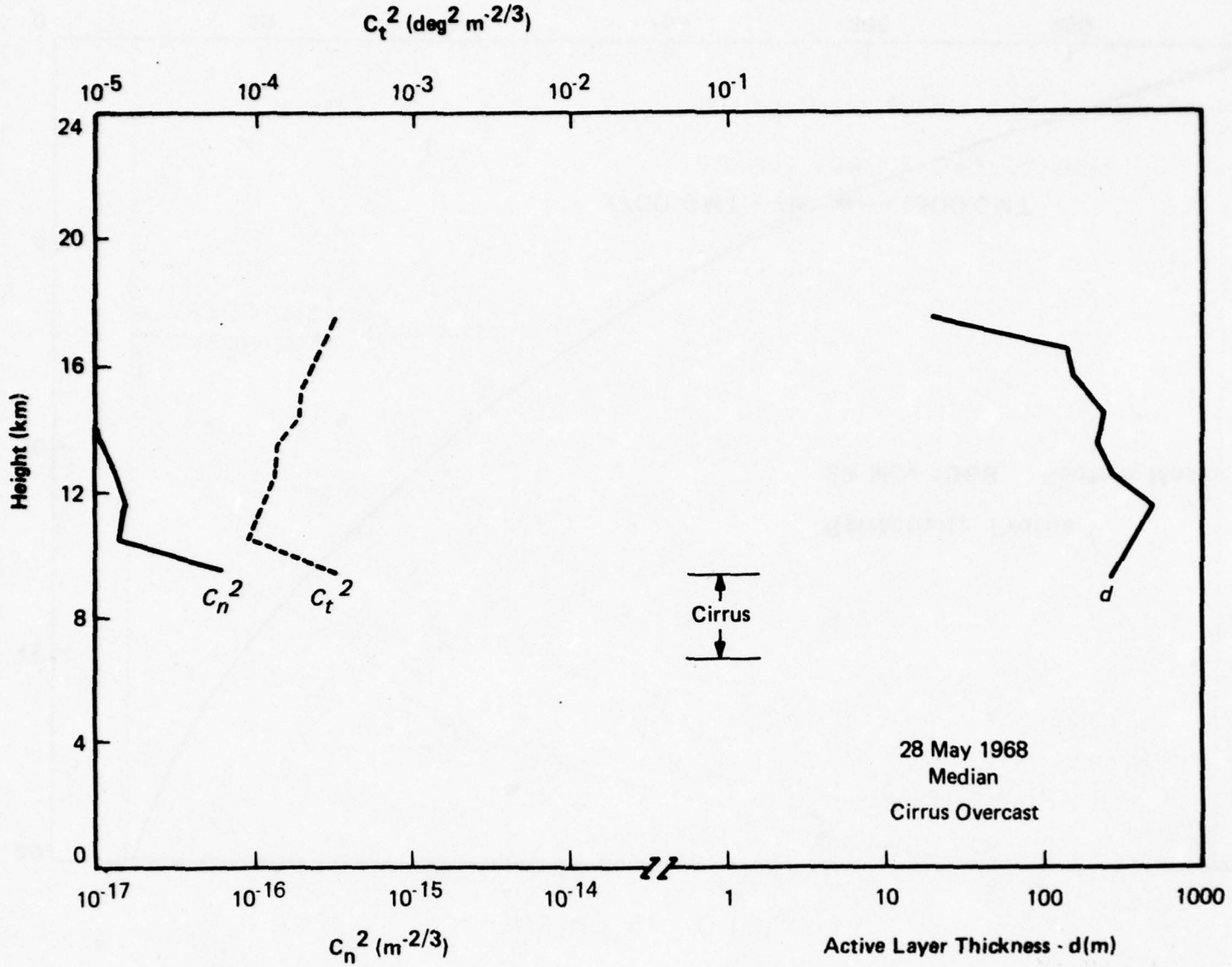


Figure 10 C_n^2, C_t^2 and active layer thickness profiles, May 28, 1968

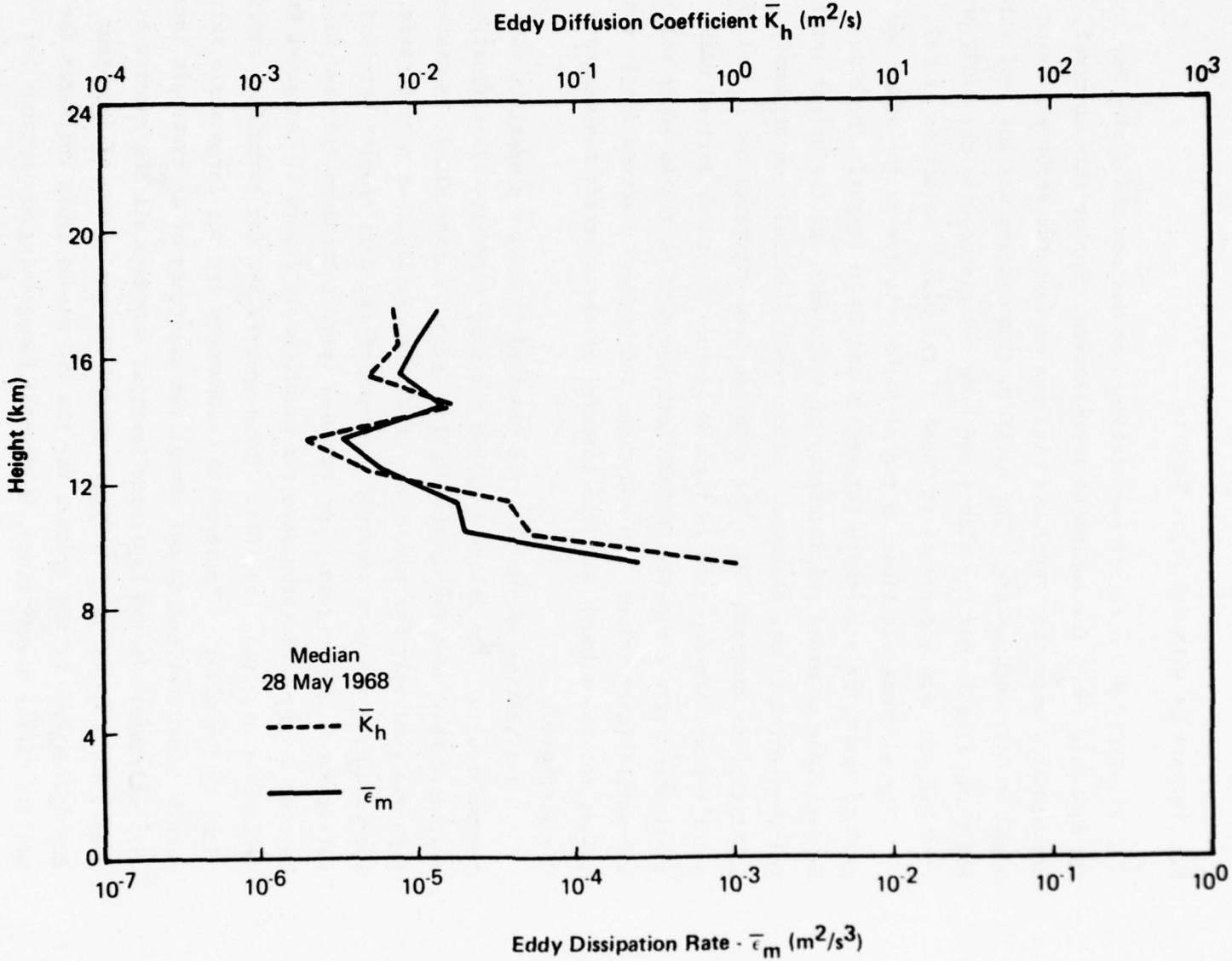


Figure 11 $\overline{K}_H$ and $\overline{\epsilon}_m$ profiles, May 28, 1968

5. APPLICATION OF THE TURBULENCE MODEL

5.1 Comparison with U-2 Pilot Reports

The HICAT U-2 aircraft was stationed at Hanscom AFB during May through July 1968, for equipment installation. During this interval, arrangements were made for 7 U-2 missions on days the radar was being used for CAT measurements. The HICAT instrumentation was not available for these flights but the pilots had been associated with the HICAT program and had some experience in "seat of the pants" detection of CAT.

The aircraft was flown on radial paths relative to the radar and used to sound the atmosphere between 10 and 20 km height. The pilot subjectively recorded the intensity of turbulence and the height interval over which it was observed. Pilot reports ranged from extremely light (EL) to moderate (M). The radar derived estimates for $\bar{\epsilon}_m$ and the pilot reports are depicted in figures 12-16. The radar derived eddy dissipation rate estimates include both the mean estimated layer values and active layer values. In addition, the highest observed single scan values for the azimuth and time interval of the aircraft measurements are displayed.

A calibration of the pilot is required to make a comparison with the radar data. The pilots employed the same intensity classification procedure they used during the HICAT program. During HICAT, instrumentation was used only for turbulence catalogued as light or more intense. The pilot reports were recorded for each of the data samples obtained during the HICAT program. For example, spectra obtained from two passes through a region of turbulence are displayed in figure 17 (obtained from Crooks, et al, 1967, Vol.III). These spectra are for turbulence reported as light by the pilot. The reported wavenumbers are for large scale anisotropic turbulence and do not reveal the existence of an isotropic inertial subrange. In the isotropic inertial subrange all the spectra as scaled for display on this figure should lie one on top of the other. The equivalence of the spectra for the two passes again indicates the utility of the steady state, horizontal homogeneity assumptions for stratospheric turbulence. The short straight line superimposed on the figure is an attempt to estimate the behavior of the spectra in the isotropic inertial subrange. The eddy dissipation rate value for these

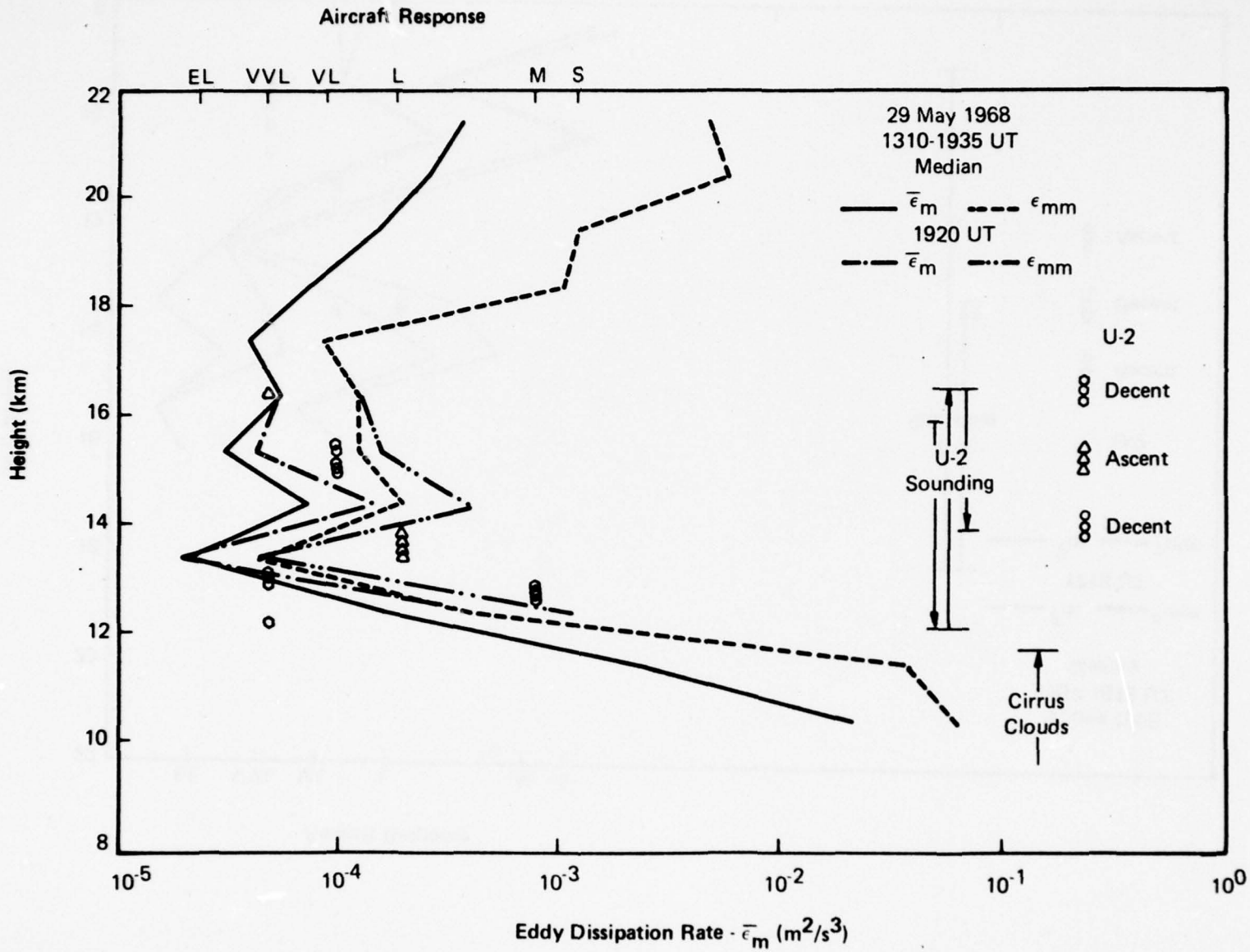


Figure 12 Radar and Aircraft comparison; ε_m profiles, May 29, 1968

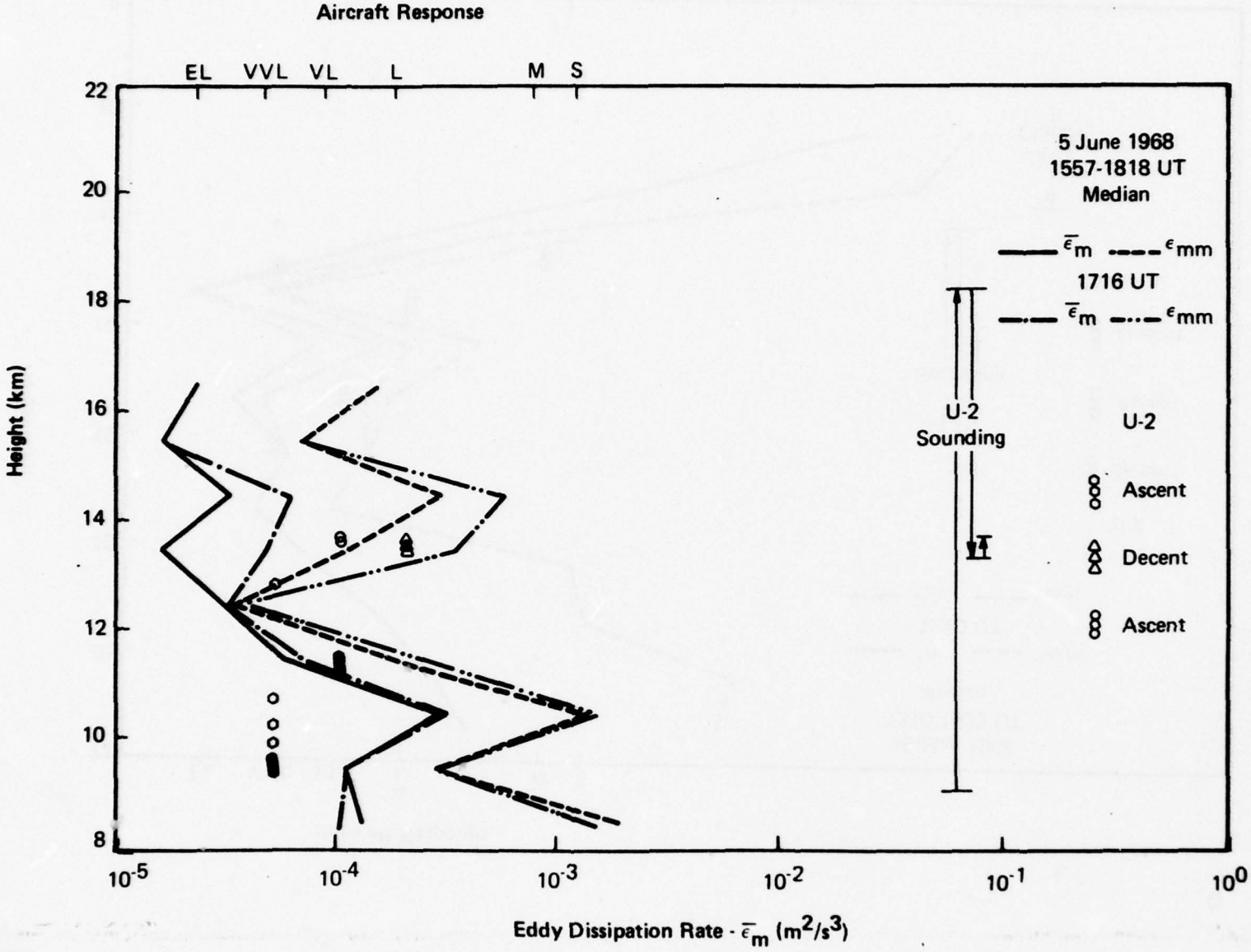


Figure 13 Radar and Aircraft comparison; ϵ_m profiles, June 5, 1968

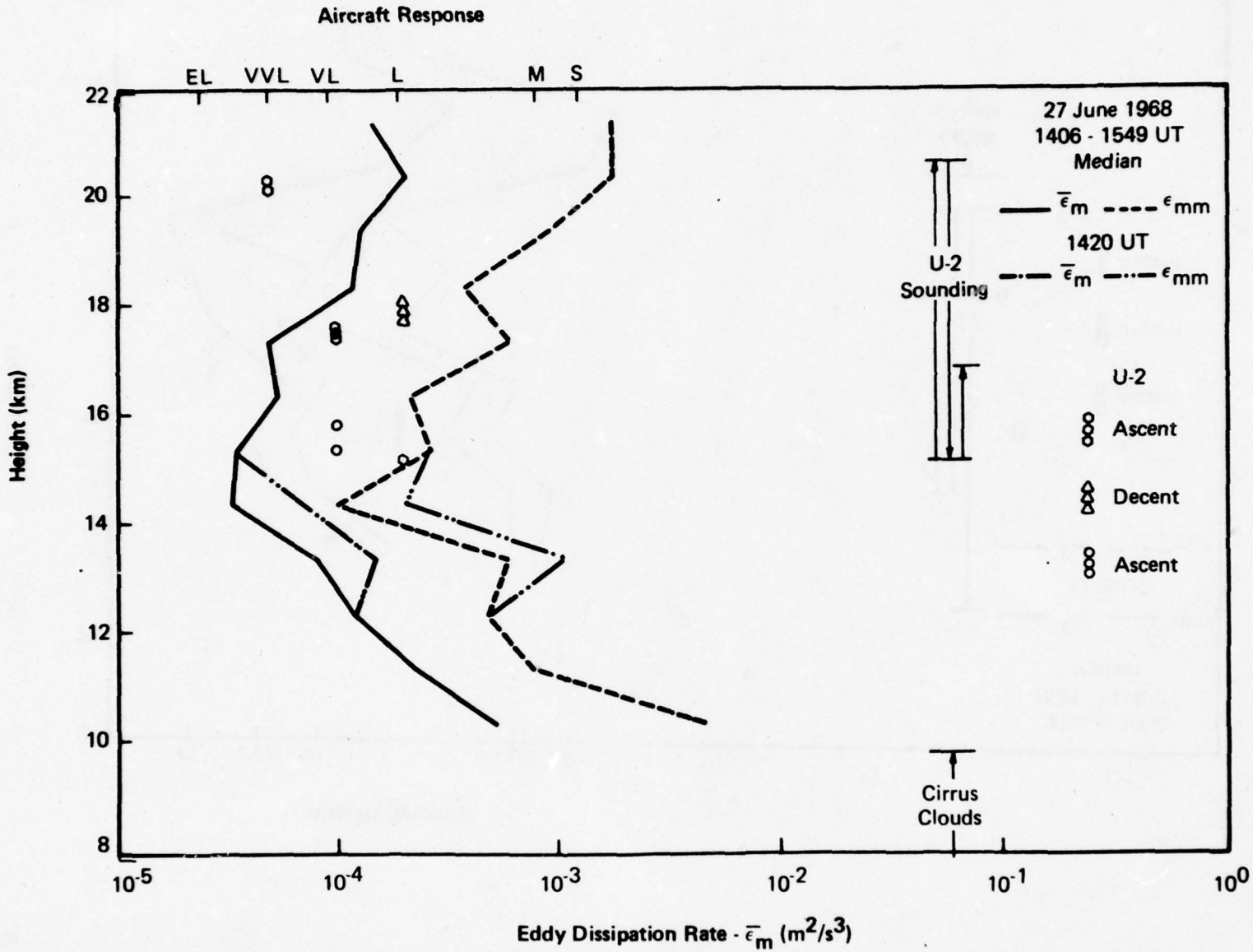


Figure 14 Radar and Aircraft comparison; ϵ_m profiles, June 27, 1968

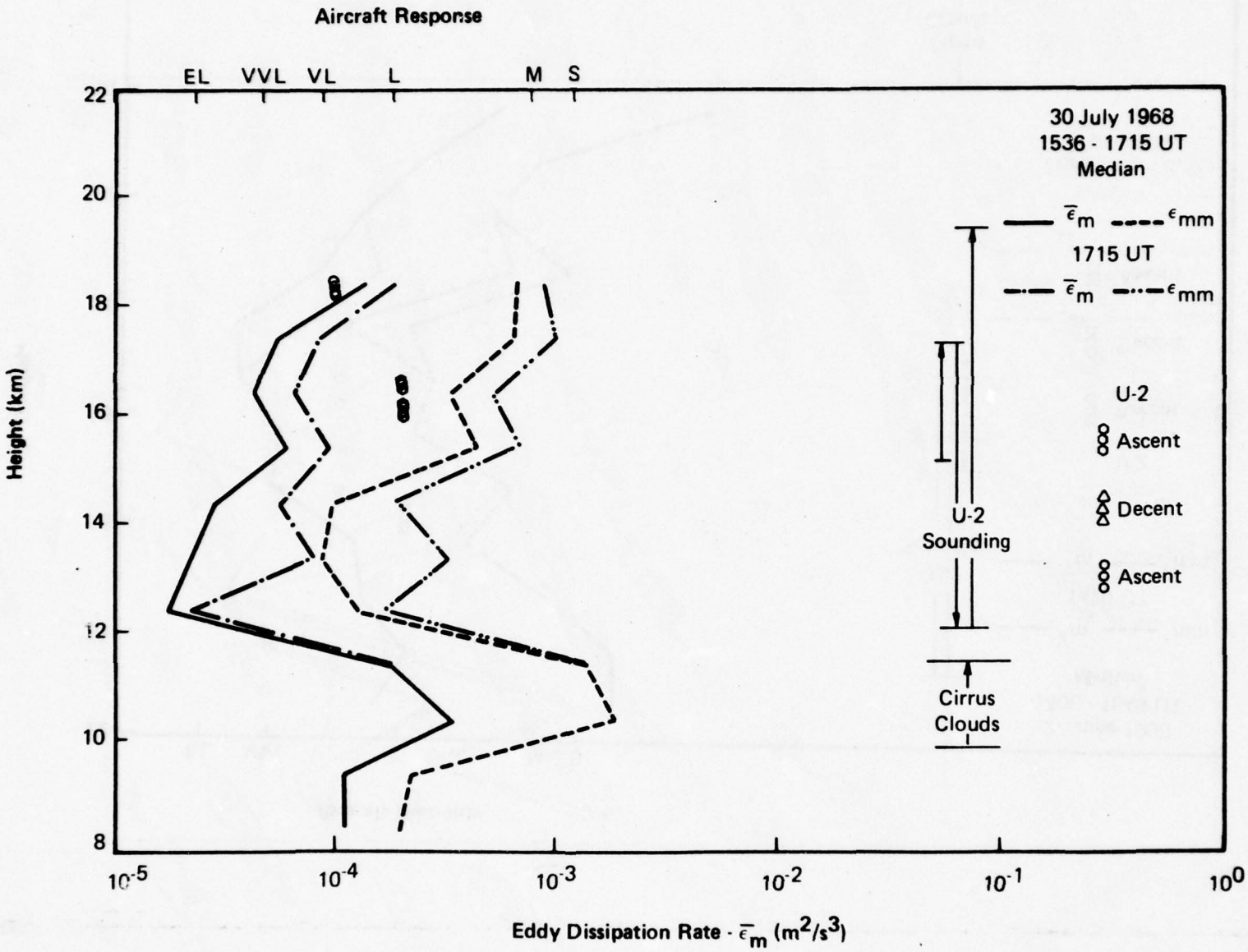


Figure 15 Radar and Aircraft comparison; ε_m profiles, July 30, 1968

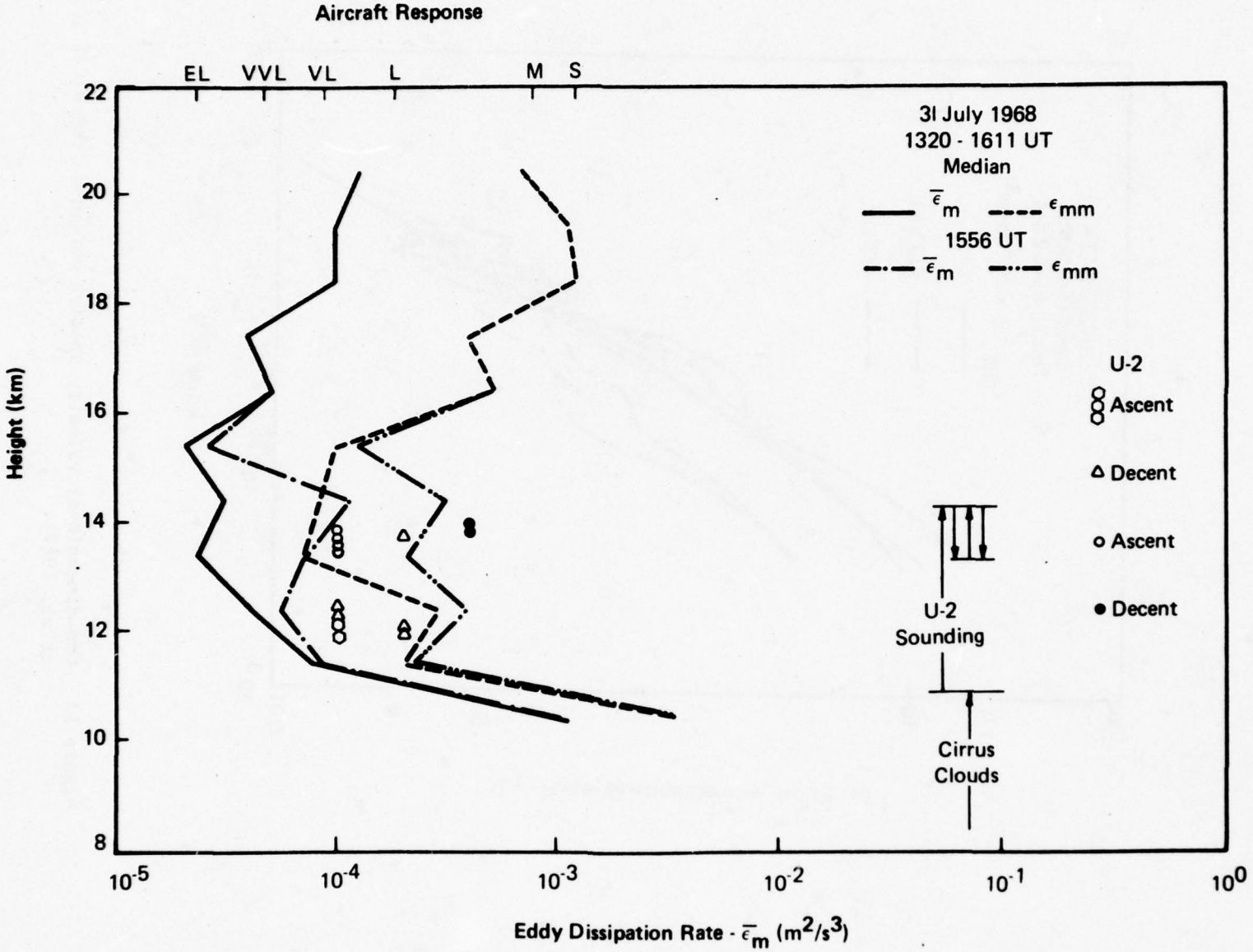


Figure 16 Radar and Aircraft comparison; ϵ_m profiles, July 31, 1968

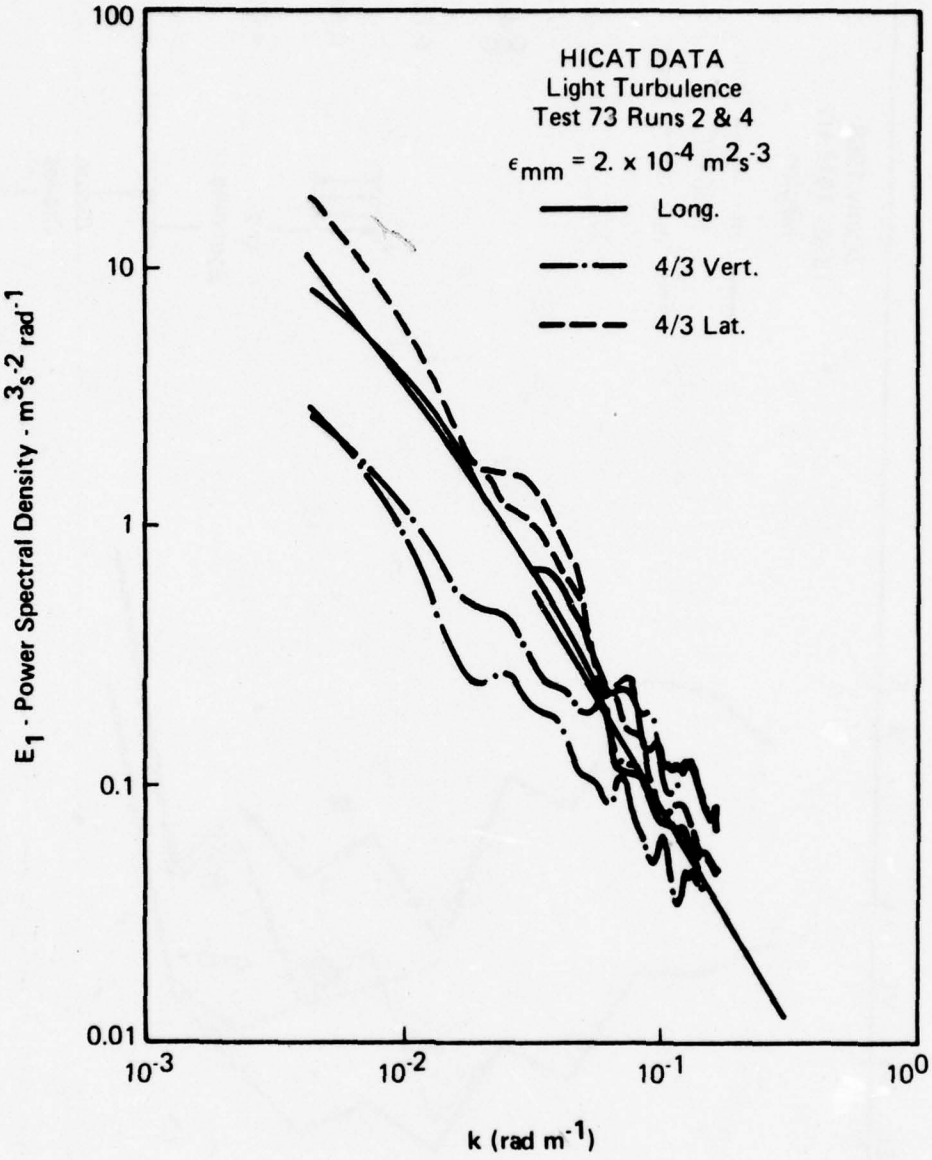


Figure 17 One-dimensional velocity spectra obtained from HICAT (Crooks, *et al, 1967*)

spectra was calculated using the location of this approximate line on the plot (using a power spectral density value at a given wavenumber). A value of 2×10^{-4} m^2/s^3 was obtained as reported on the figure. This process was repeated for a number of spectra catalogued as corresponding to light or moderate turbulence. The resultant ε_{mm} values were used to position the L (light) and M (moderate) values on figures 12-16. The calibration of EL (extremely light) through VL (very light) could not be made using reported spectra since they correspond to turbulence of insufficient intensity to produce reliable estimates of the spectra. These levels were approximated using information reported by Crooks et al (1967) and supplied by the pilots.

The U-2 reports are for single passes through active regions of turbulence exceeding the intensity - layer thickness threshold needed to trigger a pilot response. Since the maximum to median ratios for C_n^2 typically varied by less than a factor of 4, it is expected that the maximum to median ε_m values should vary by less than a factor of 8. Agreement between the pilot reports (uncertain by a factor of 4 perhaps) and the radar derived estimates is obtained when the pilot reports are within a factor of 10 of $\bar{\varepsilon}_m$ and a factor of 4 of ε_{mm} for the single scan. The U-2 reports should indicate more intense turbulence than the radar. This behavior is apparent for all the U-2/radar comparisons with the exception of observations made below 11 km on 29 May and 5 June (figs. 12 and 13). The radar data for 29 May are probably contaminated by cirrus clouds. This possibility also exists for 5 June although no visual reports of cirrus were received. The results of this comparison indicate that within the uncertainties associated with the use of pilot reports, excellent agreement was obtained.

The U-2/radar comparisons are the most extensive collection of data available for the validation of the model, equations (26) and (27). The only other available data useful for model verification were reported by Metcalf and Atlas (1973). They reported maximum radar cross section values obtained using a radar resolution volume smaller than the region of active turbulence. They also reported aircraft observations made through the turbulent region. Their turbulent energy balance however, was calculated based upon data from a region thicker than the peak of the turbulent layer. Based upon their data and equation (27), the eddy

dissipation rate at the peak of their layer should be in the 10-40 cm^2/s^3 range. They report estimated eddy dissipation rates in the 4-26 cm^2/s^3 range, the value depending upon the procedure they used for estimation. Considering the uncertainties in their data particularly with respect to the relative effects of the potential temperature and absolute humidity gradients and the discrepancy associated with using the maximum radar return with a 1 meter (height) resolution volume to compare against aircraft data with a 20 m (height) resolution volume, excellent agreement is apparent.

5.2 Eddy Dissipation Rate Estimates

Median profiles of eddy dissipation rate were obtained for each observation set. The individual profiles are presented in Appendix A. Composite profiles organized by observing period are presented in figures 18 through 24. These figures show rather large variations from one observation set to another at heights below about 12 km and little variation above. In the region between 12 and 16 km most of the observed median $\bar{\varepsilon}_m$ values are within an order of magnitude range. These results indicate that although a rather large variation in turbulent energy dissipation may occur in the lower troposphere, the average dissipation rate within the barrier between the troposphere and stratosphere is remarkably consistant from day-to-day.

Data that were obviously contaminated by scattering from cirrus clouds were not included in these figures. Some contamination still may be present at heights below 12 km. The minimum on average at the barrier is real. The median of all the medians was used to obtain the values given in Table I. To reduce possible biasing affects caused by cirrus clouds at heights below 12 km and by radar sensitivity at heights above 16 km, values at these heights were not entered in Table I.

5.3 Eddy Diffusion Coefficient Estimates

The median eddy diffusion parameters are presented in figures 25 through 31. The general shapes of the curves are identical to the eddy dissipation rate curves. These data demonstrate the existence of a barrier in the lower stratosphere to vertical transport by small scale turbulent processes. The increase of $\bar{K}_H$ above the barrier is in agreement

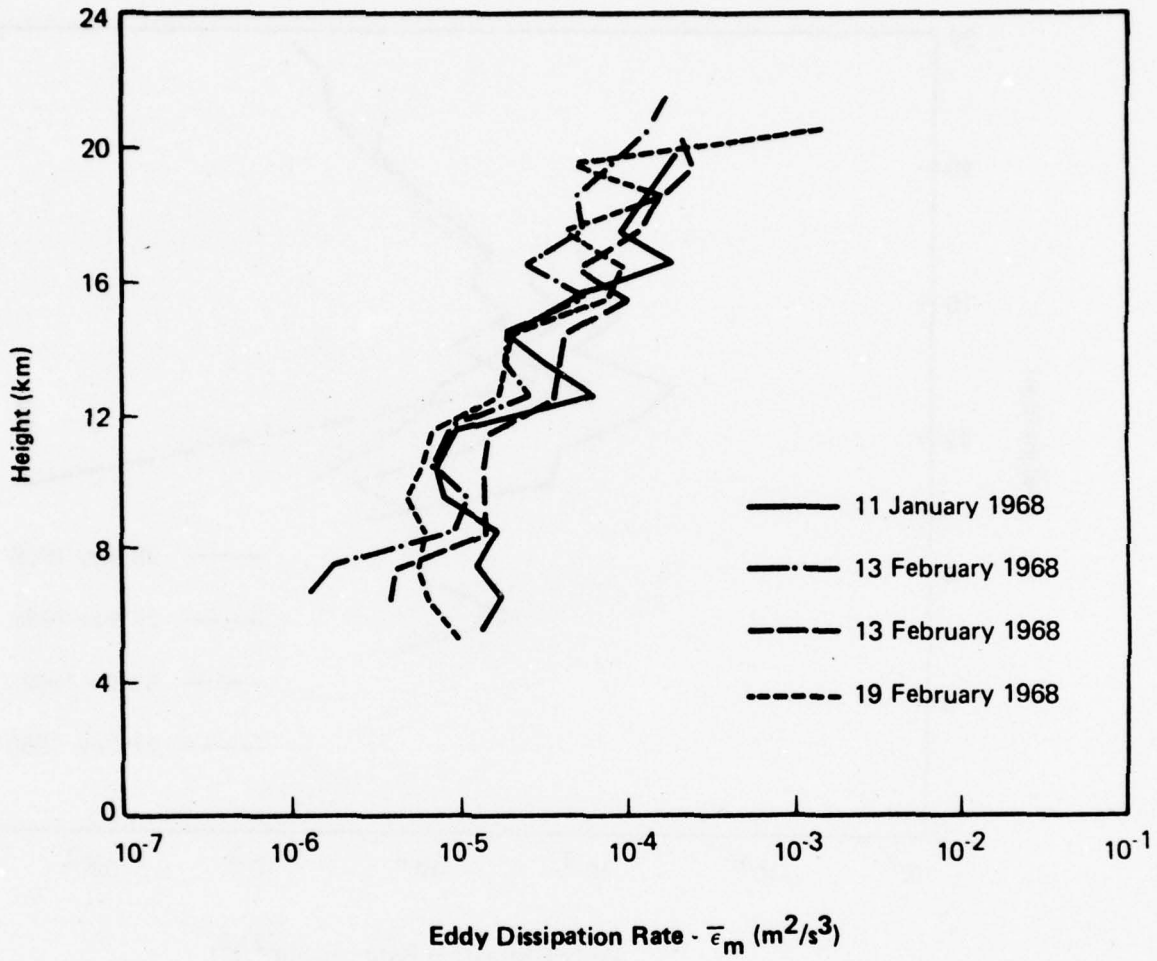


Figure 18 Eddy dissipation rate profiles, winter 1968

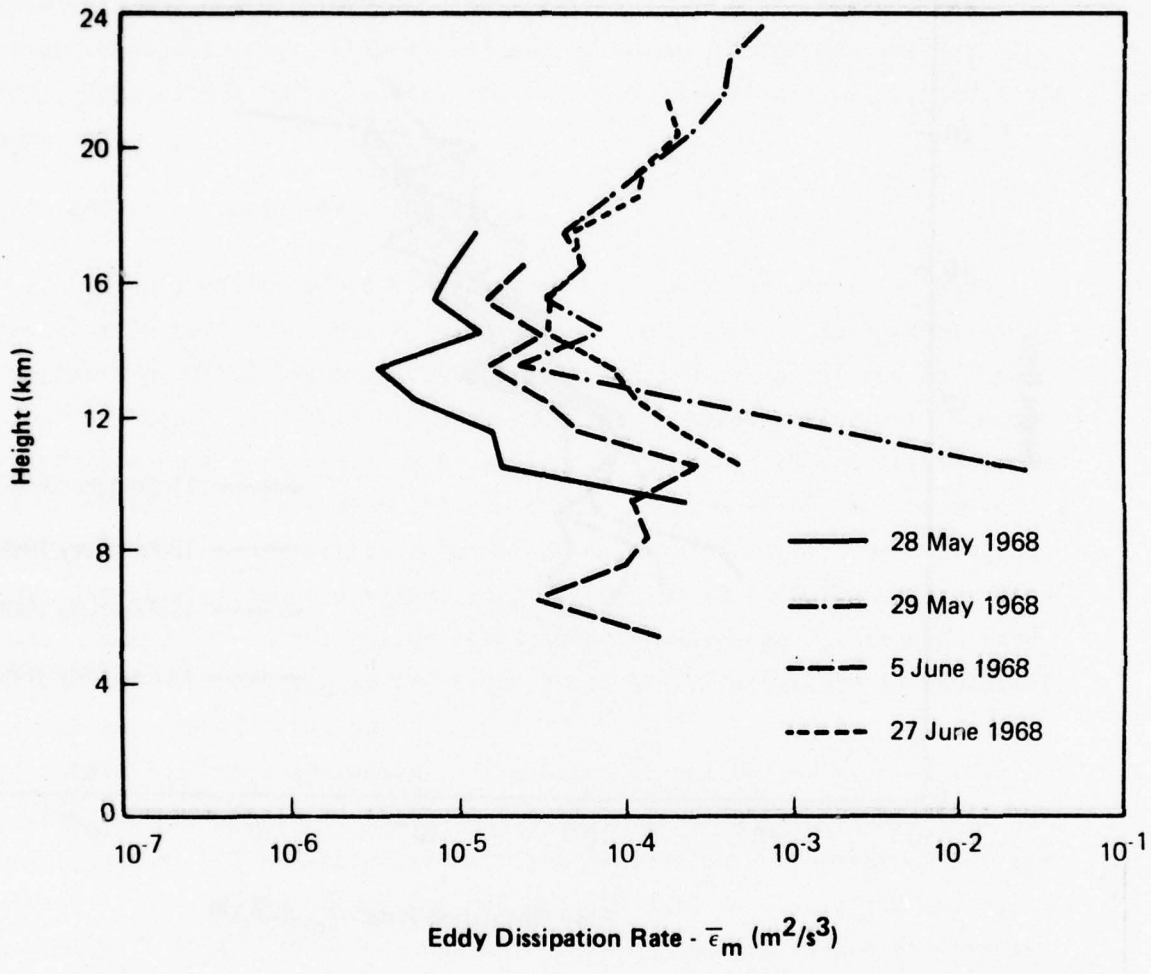


Figure 19 Eddy dissipation rate profiles, spring 1968

08156

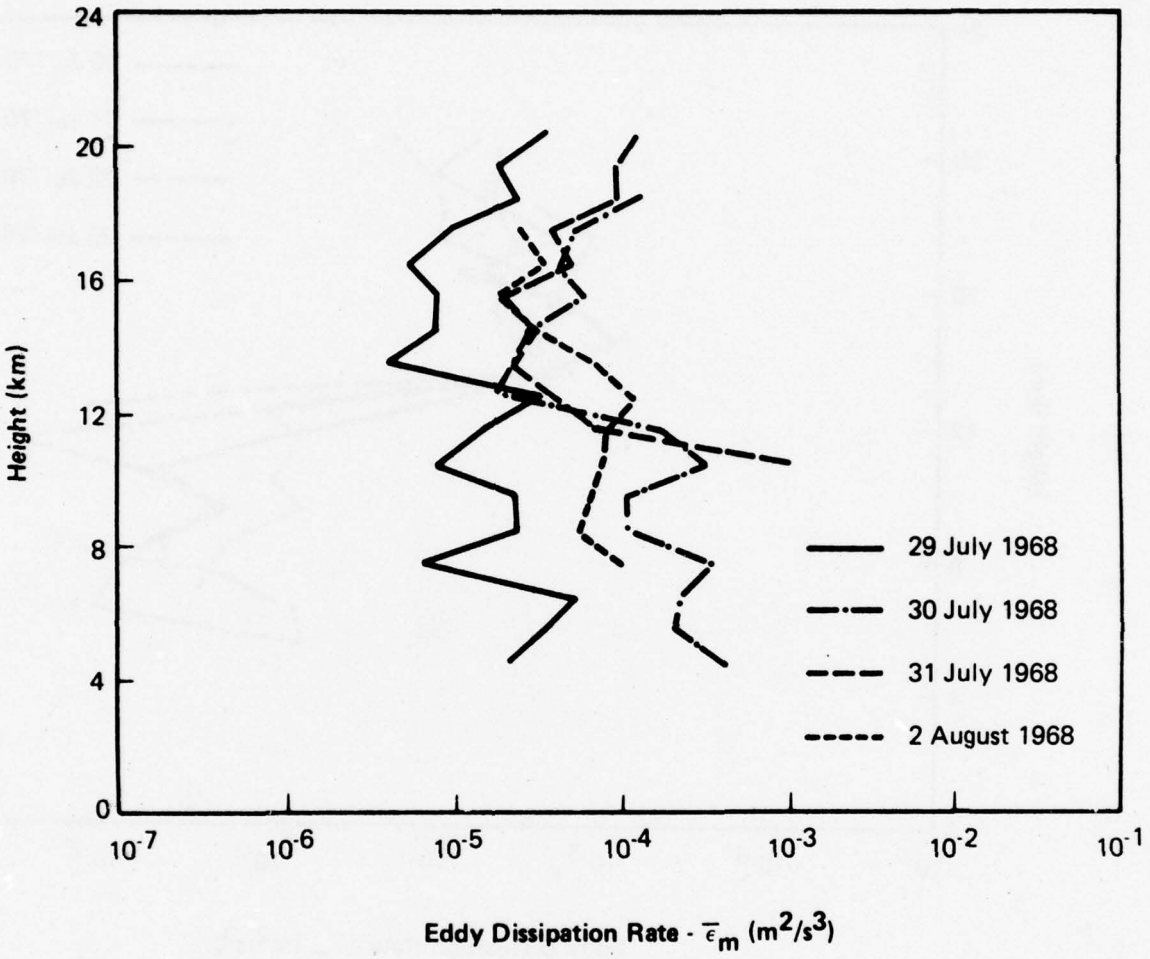


Figure 20 Eddy dissipation rate profiles, summer 1968

708187

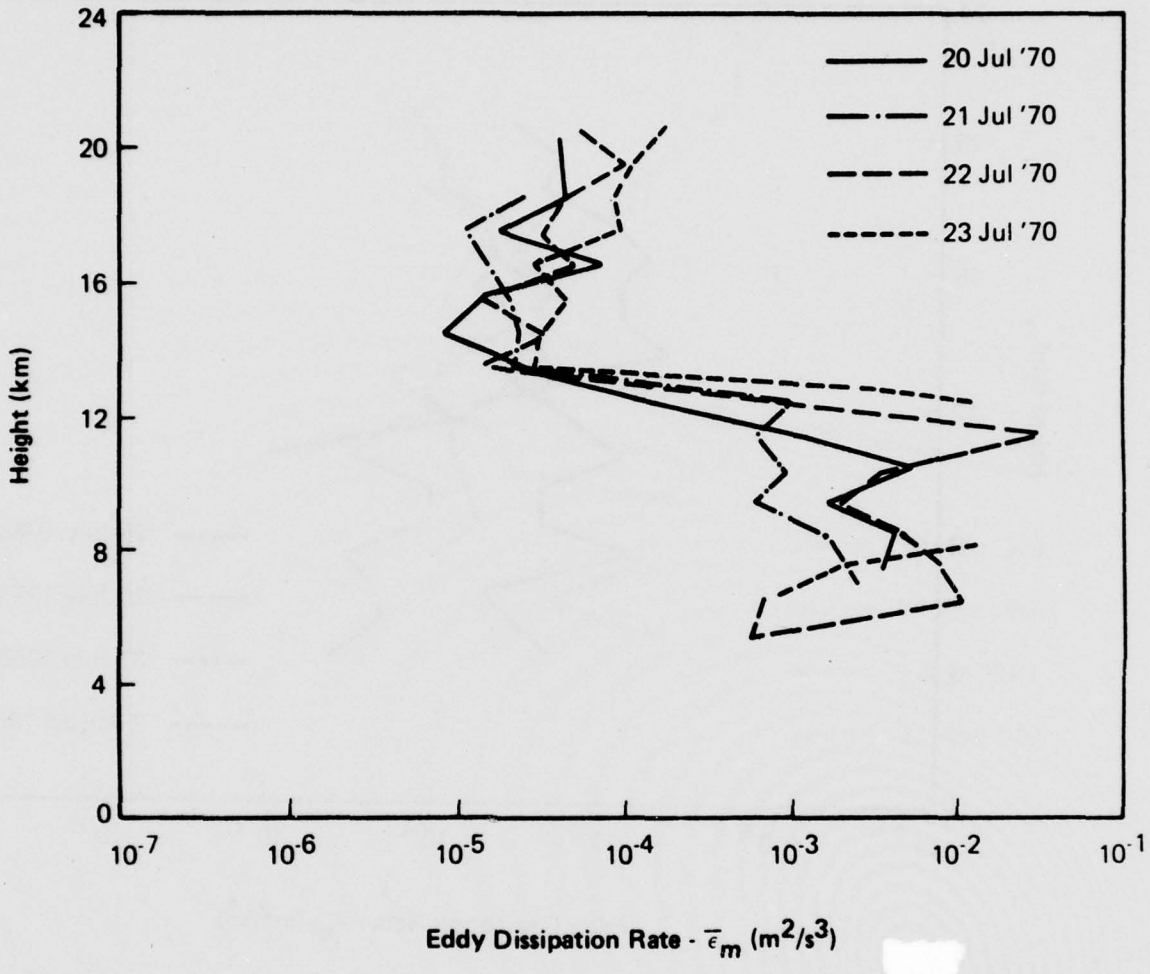


Figure 21 Eddy dissipation rate profiles, summer 1970

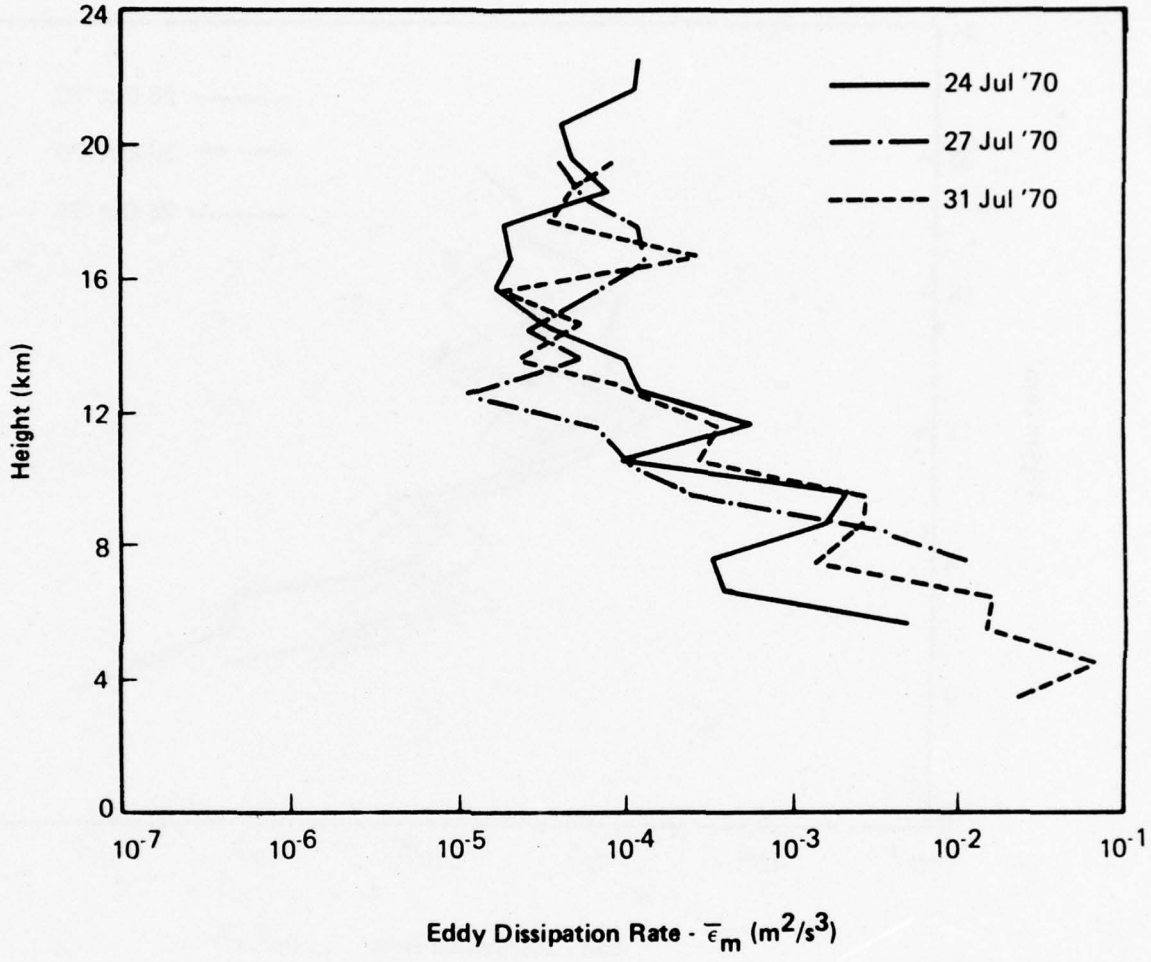


Figure 22 Eddy dissipation rate profiles, summer 1970

709001

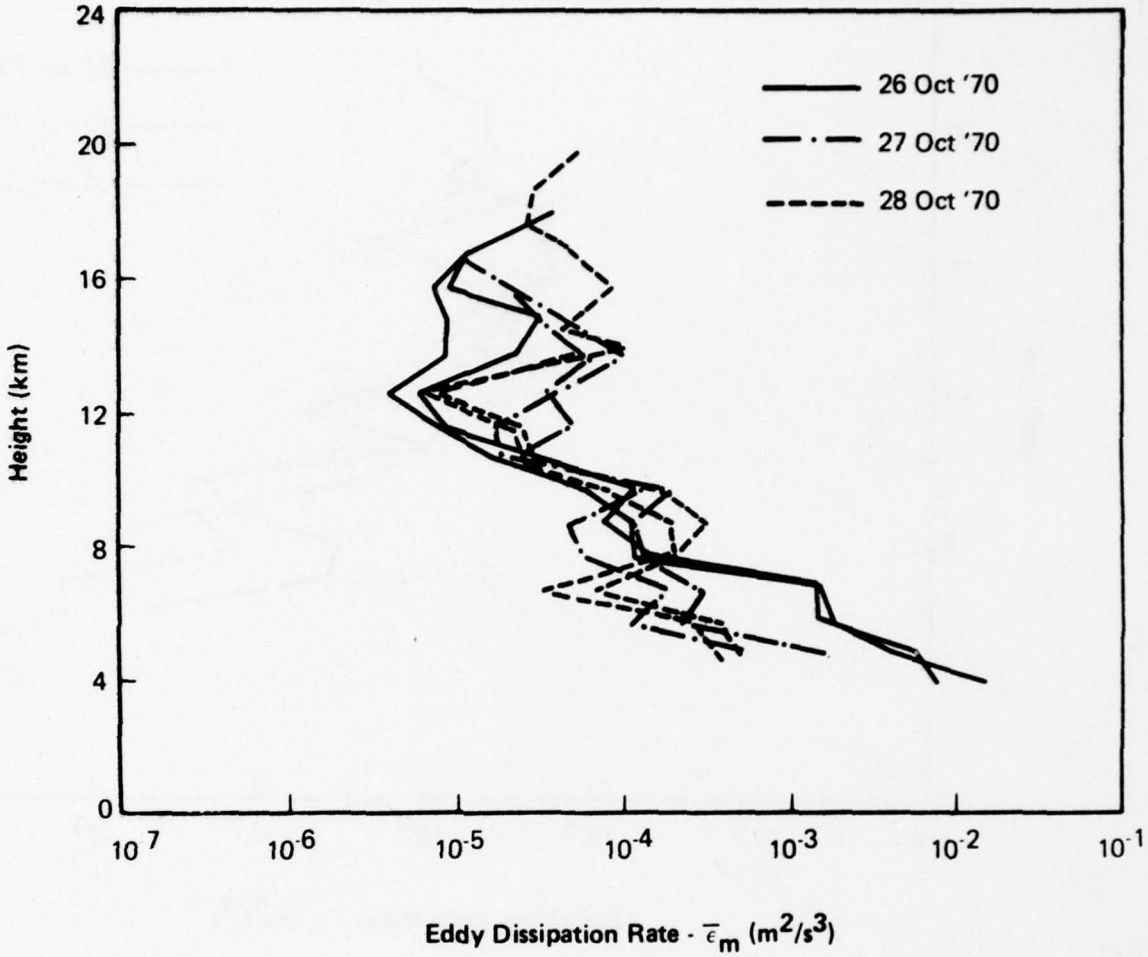


Figure 23 Eddy dissipation rate profiles, fall 1970

708200

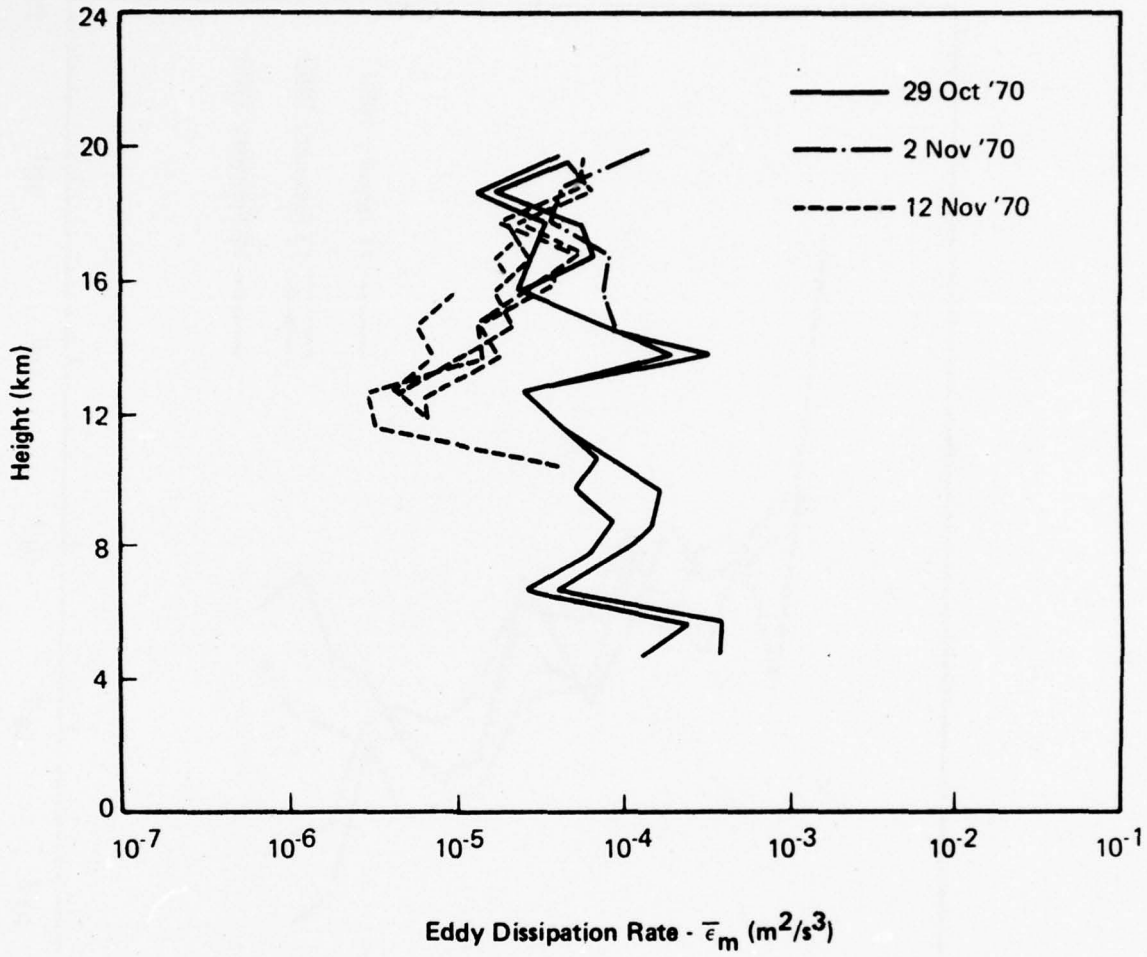


Figure 24 . Eddy dissipation rate profiles, fall 1970

708201

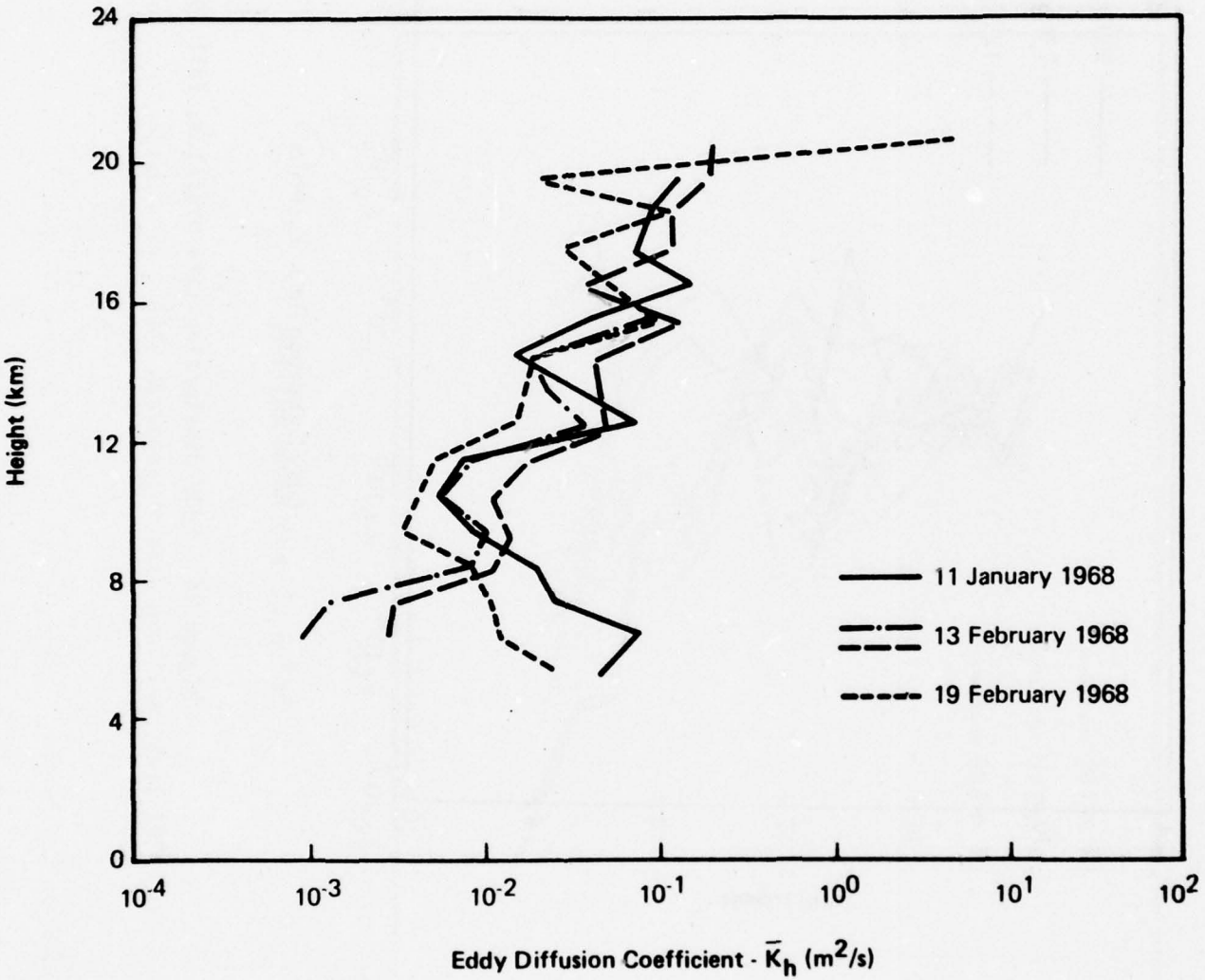


Figure 25 Eddy heat diffusion coefficients, winter 1968

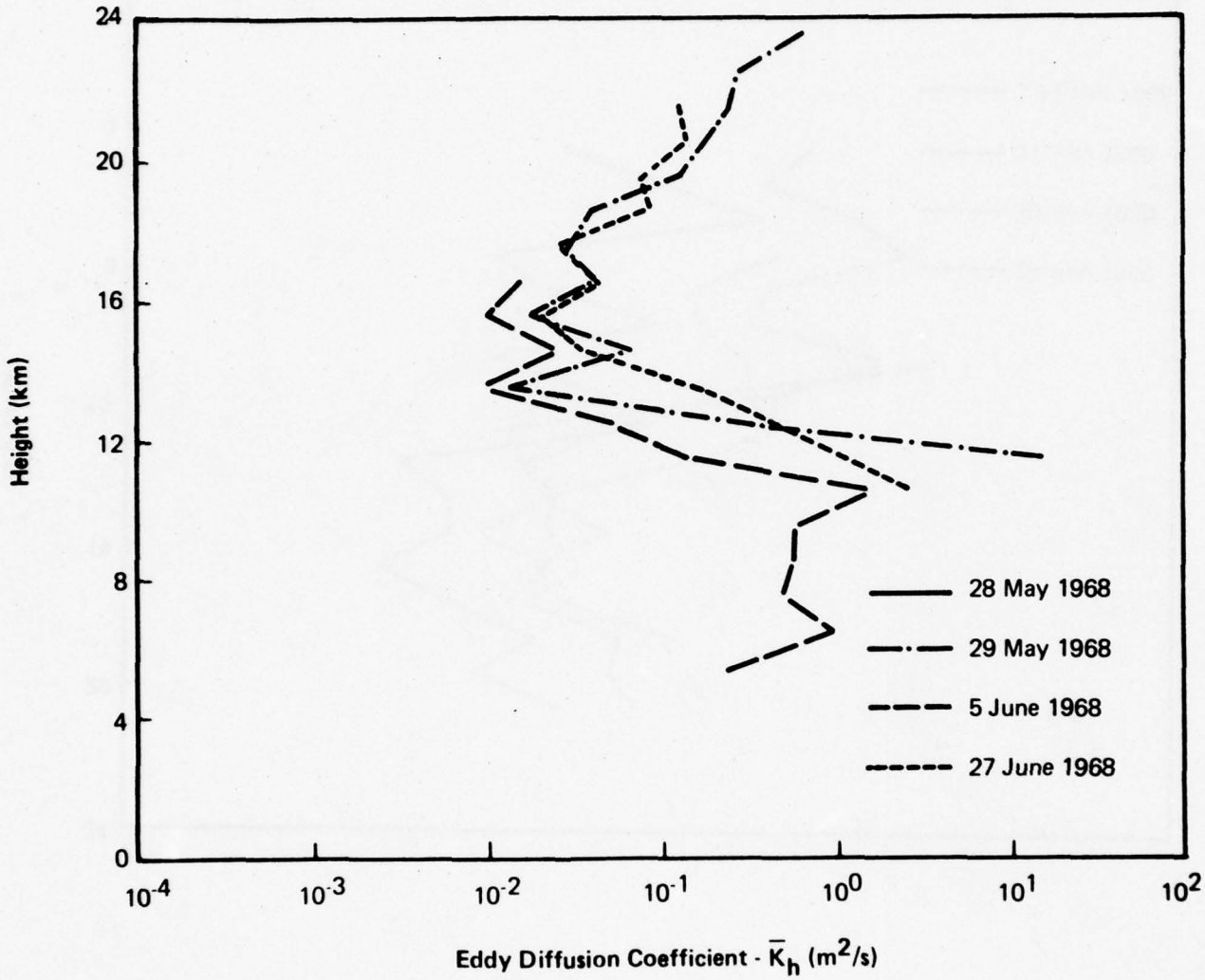


Figure 26 Eddy heat diffusion coefficients, spring 1968

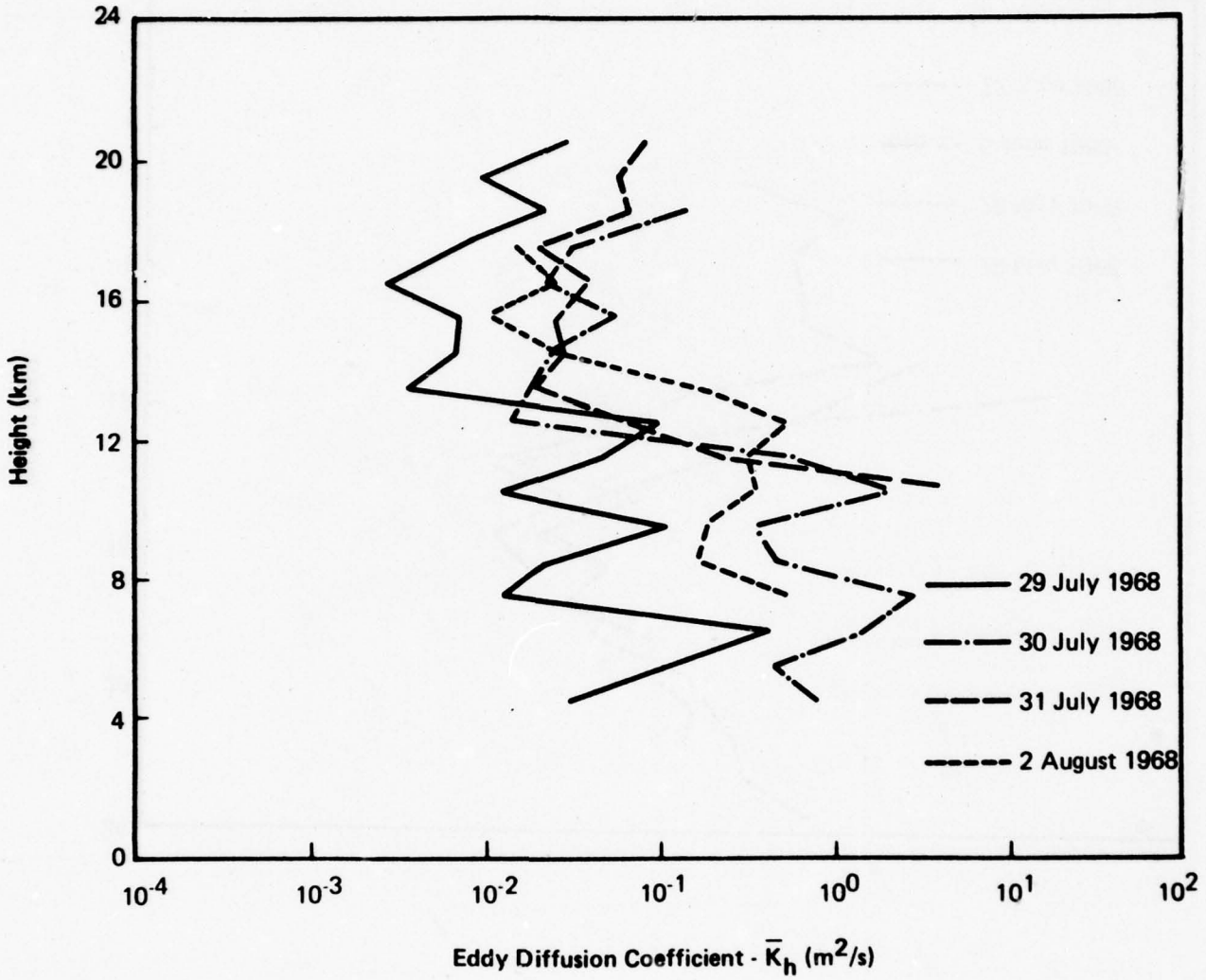


Figure 27 Eddy heat diffusion coefficients, summer 1968

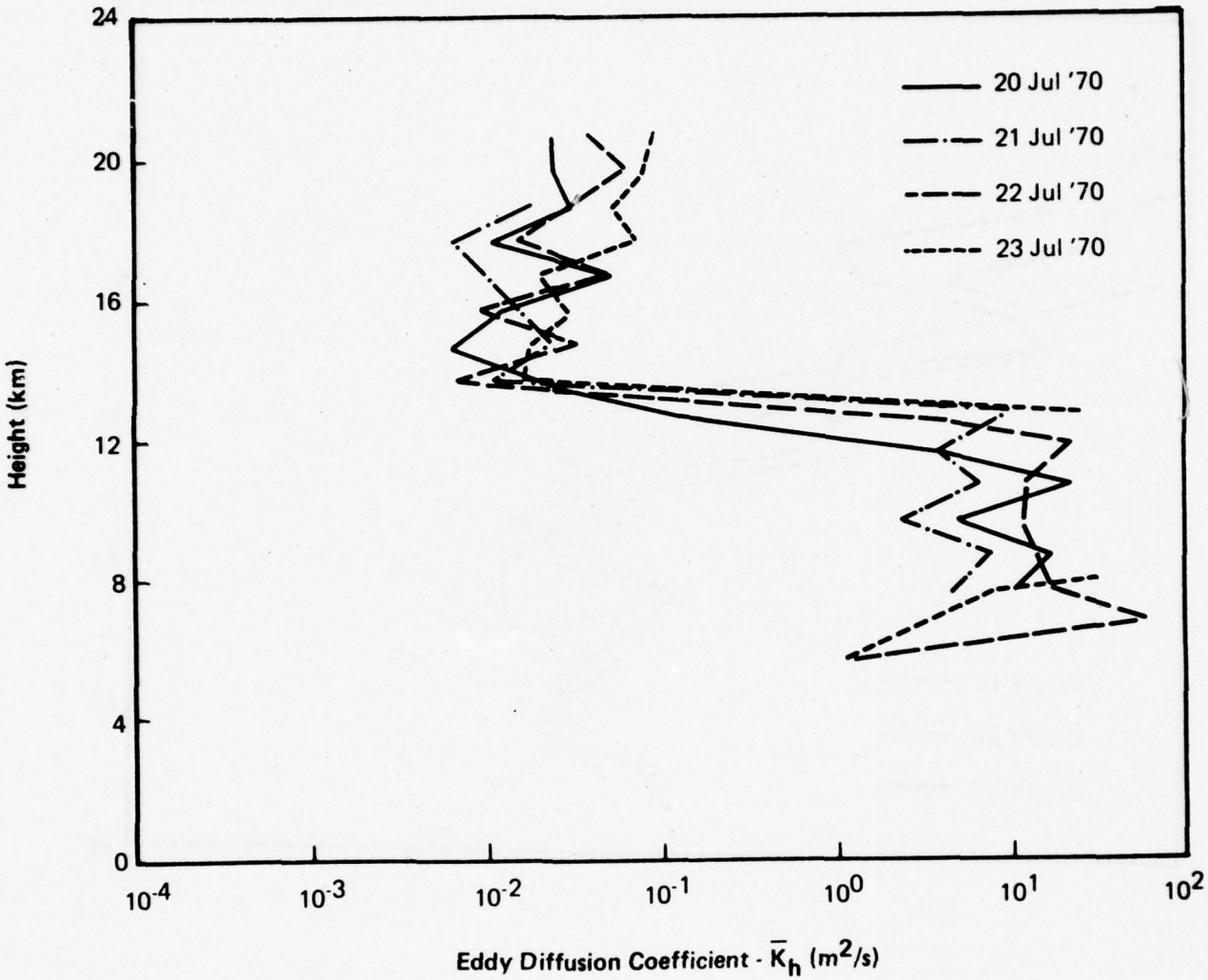


Figure 28 Eddy heat diffusion coefficients, summer 1970

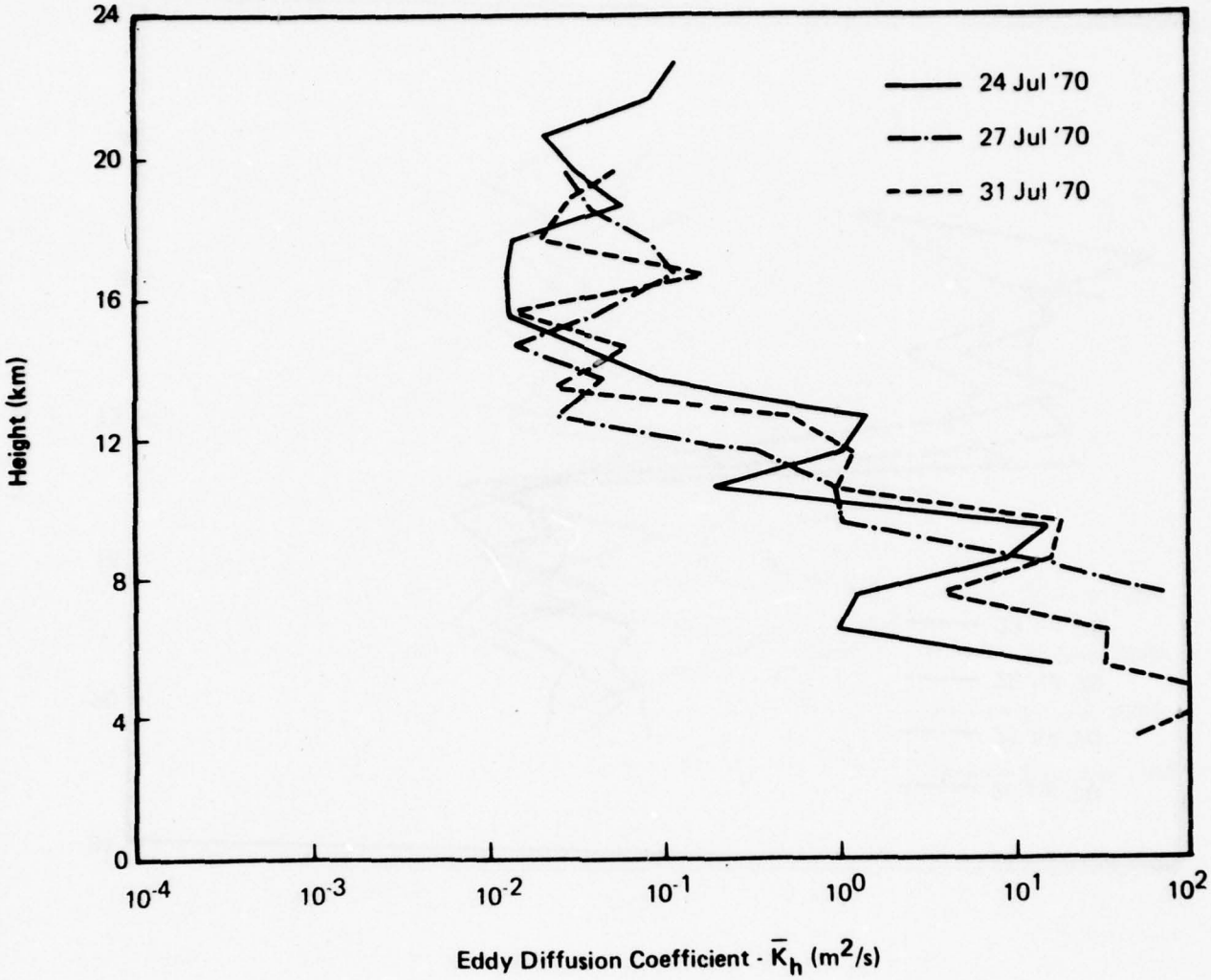


Figure 29 Eddy heat diffusion coefficients, summer 1970

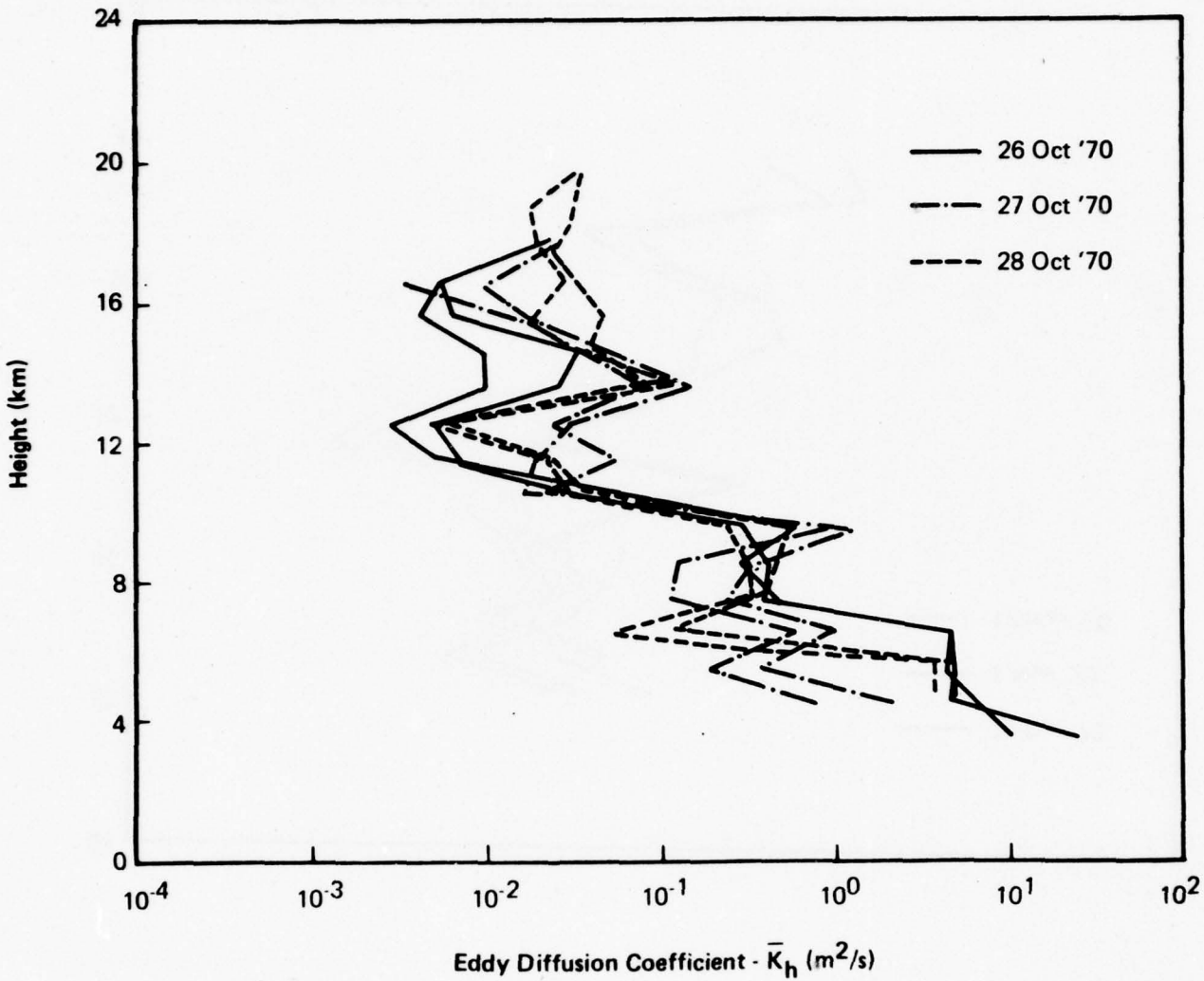


Figure 30 Eddy heat diffusion coefficients, fall 1970

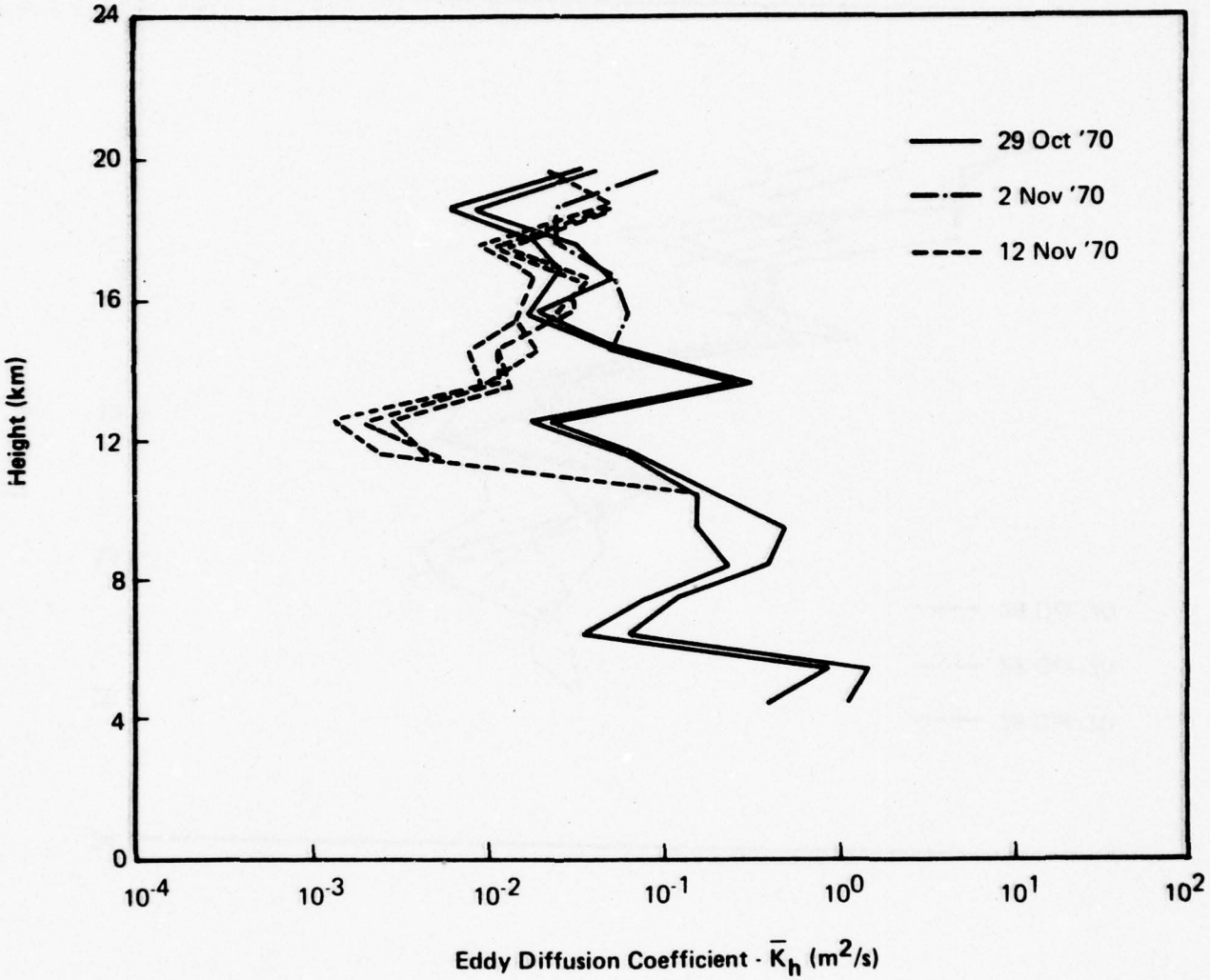


Figure 31 Eddy heat diffusion coefficients, fall 1970

with the shape of the eddy diffusion curves used in large scale transport models (see Reiter, 1975). Radar observations of vertical transport coefficients in the mesosphere indicate that the $\bar{K}_H$ values continue to increase in height eventually merging with the values assumed by larger scale modelers (Cunnold, 1975) indicating that the small scale turbulent processes are the most important processes at the higher altitudes well above the lower stratosphere barrier.

5.4 Active Layer Thickness Estimates

The model developed for the estimation of $\bar{K}_H$ and $\bar{\varepsilon}_m$ using the radar data required an estimate of d since the dominant region of active turbulence is thinner than the resolution volume of the radar. If this analysis were not performed, the $\bar{K}_H$ and $\bar{\varepsilon}_m$ values would be underestimated since the turbulence did not "fill the beam". The active layer thickness estimates were obtained directly from radiosonde data assuming only that the atmosphere was everywhere turbulent but with no knowledge of the intensity of the turbulence. Only the aircraft or radar can provide estimates of the intensity of turbulence.

The median layer thickness for all heights in the 12 through 16 km region was estimated using the radiosonde data (all ε_{mm} values), all the available U-2 observations (ε_{mm} above 2×10^{-5} m^2/s^3 or *all pilot reports*), and for all U-2 observations that would have been processed using the Project HICAT criterion (ε_{mm} above 2×10^{-4} m^2/sec^3 or all light and moderate turbulence). The results are shown in Table III together with the number of samples used. These data show that the median turbulent layer size is thin and the stronger layers are very thin. It is interesting to note that these observations are at variance with the results reported by Crooks et al (1967) which showed a median layer thickness of 750 m for 13 samples, a factor of 15 times thicker than our results. Our data were obtained over flat terrain but no indication was given about the conditions under which the HICAT data were obtained.

5.5 Temporal Variation of Turbulent Layer Intensity

The raw elevation scan data - the RHI's such as Figure 1 - always depict CAT as occurring in thin layers. The weaker layers are sometimes evident only in a single RHI observation; the stronger layers may persist

TABLE III

ACTIVE LAYER THICKNESS ESTIMATES

	d(m)	# of samples
All Layers from Radiosonde Data	200	236
All U-2 Observations	100	49
All U-2 Data in the Light to Moderate Category	50	12

for one-to-two hours. The layer at the tropopause may persist throughout an entire measurement period. The temporal variation of the layer structure for 28 May 1968 is revealed in Figure 4 and Figure 32. The median C_n^2 profile in Figure 4 shows a general decrease in C_n^2 with height above the tropopause (∿12 km). The two "instantaneous" profiles - RHI's taken 6 minutes apart - show a definite layer structure. The time history of the layer structure is revealed in Figure 32. The data used to generate this figure were obtained from the raw RHI photographs and the layer intensities coded on the figure are only approximate.

The time history reveals a persistant layer at the tropopause. The height of this layer varies over the observing period producing a smearing of the structure as revealed by the median profile. The layers above the tropopause persist for one-to-two hours. The layers in this region seem to occur at different heights. The general decrease in C_n^2 with height depicted by the median profile reflects the variation in height of the persistant layer at the tropopause and the random occurrence of the layers at higher altitudes.

The median C_n^2 profiles depicted in the figures in Appendix B reveal the same behavior. Median profiles for one-to-two hour time durations sometimes show a layer structure as evident at a height of 19 km on the 13 February '68 profile but at other times show little structure indicative of weak, randomly occuring layers (see the 19 February '68 profile).

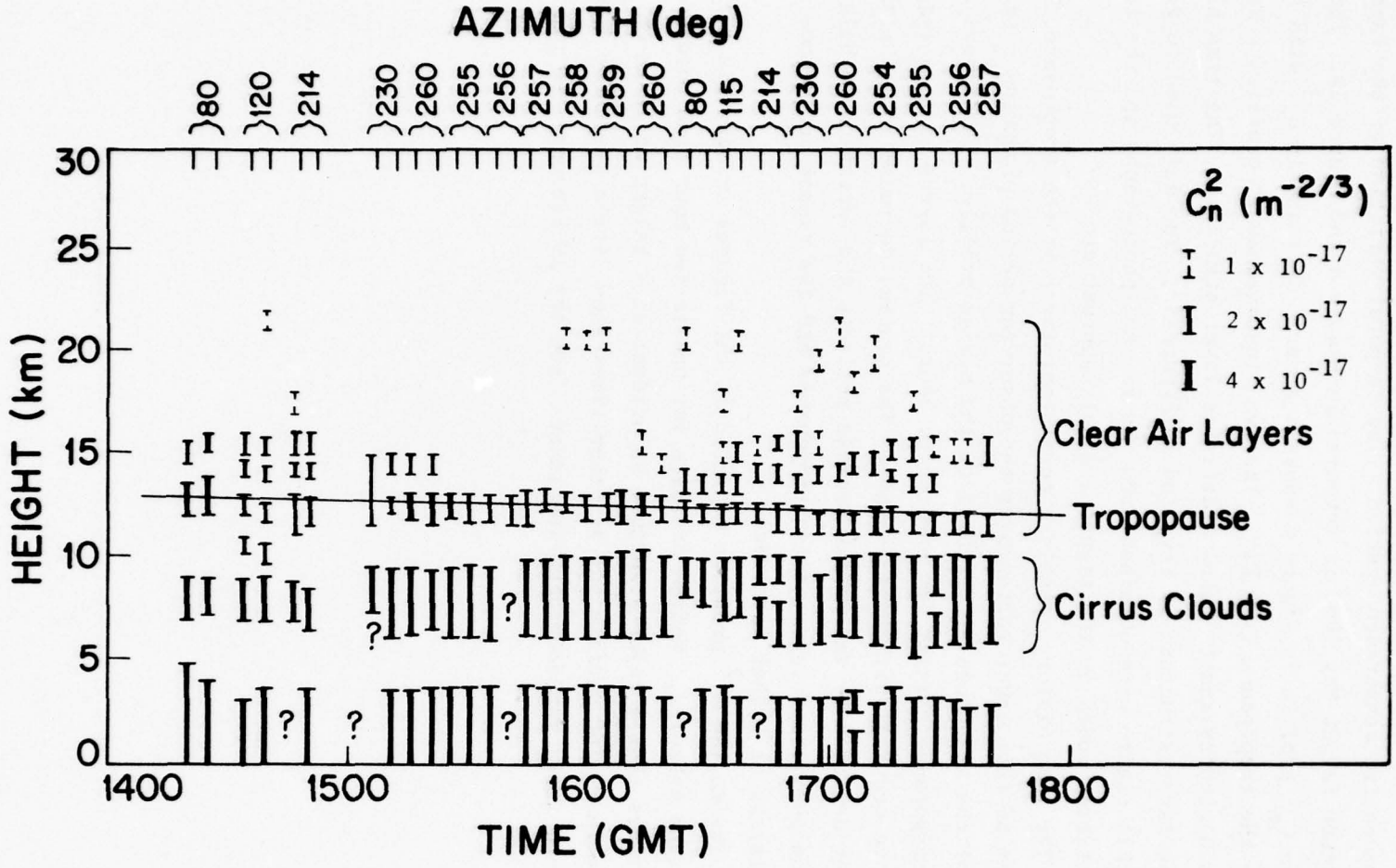


Figure 32 Turbulent Layer Time History - 28 May 1968

6. CONCLUSIONS

A model was developed for the combination of radar and radiosonde data. The basic premise used for the development of the model was that the atmosphere and all its sublayers is always turbulent. The intensity of the turbulence may vary by orders of magnitude from layer to layer. The mean profiles provided by radiosonde measurements cannot be used to estimate the intensity of turbulence - the eddy dissipation rate - but can only be used to characterize the stability of the layers. Additional data must be provided to estimate the intensity of turbulence. These data may be obtained from well calibrated radars or from instrumented aircraft. In the analysis performed by VanZandt et al (1977) the required additional data were assumed. In the analysis performed by Rosenberg and Dewan (1974), the additional data were also assumed, this time by picking a value for the time step.

The model developed for the analysis of radar and radiosonde data was shown to be consistant with all the available measurements. The results match closely results obtained by Lilly et al (1974) for similar conditions of underlying terrain. The data show the existence of a barrier to vertical transport by small scale turbulence between the troposphere and stratosphere. The small scale turbulent transport process over flat land at a midlatitude location is an order of magnitude smaller than required to explain the observed distributions of trace constituents using one-dimensional models. This discrepancy may be caused either by the neglect of larger scale transport processes or by strong geographical variations in the intensity of turbulence within the barrier. The results presented above show that seasonal variations cannot explain the discrepancies.

ACKNOWLEDGEMENTS

The author wishes to acknowledge the effort of the staff of the Millstone Hill Radar Facility in obtaining the high quality radar data during the 1968-1970 time period and to thank MIT Lincoln Laboratory for making the data available. The radar observations were made by Lincoln Laboratory under sponsorship from the U.S. Air Force and the National Aeronautics and Space Administration (NASA). The radiosonde observations were made at Hanscom AFB by staff members of the Air Force Cambridge Research Laboratory (now Air Force Geophysics Laboratory-AFGL). The U-2 flights were piloted by Maj. K. Mason and Maj. T. Smith, then of Edwards AFB. Finally, the author wishes to thank the technical contract monitor, Dr. E. Dewan of AFGL for the opportunity to process the data acquired back in 1968-1970 and for the many discussions on the fine points of small scale stratospheric turbulence.

REFERENCES

CIAP (1975): CIAP Monographs, U.S. Dept. of Transport., Washington, D.C.

R.K. Crane (1970): "Measurements of Clear Air Turbulence in the Lower Stratosphere using the Millstone Hill L-band Radar", Preprints 14th Radar Meteorol. Conf., Amer. Meteorol. Soc., Boston, MA, pp. 101-106.

R.K. Crane (1974): "Bistatic Scatter from Rain", IEEE Trans. Antennas and Propagation, AP-22, 312-320.

D.K. Lilly, D.E. Waco, and S.I. Adelfang (1974): "Stratospheric Mixing Estimated from High-Altitude Turbulence Measurements", Jour. Appl. Meteorol., 13, 488-493.

M.J. Molina, and F.S. Rowland (1974): "Stratospheric Sink for Chlorofluoromethanes: Chlorine Atom Catalysed Destruction of Ozone", Nature, 249, 810-812.

D. Cadet (1977): "Energy Dissipation Within Intermittent Clear Air Turbulence Patches", Jour. Atmosph. Sci., 34, 137-142.

N.W. Rosenberg and E.M. Dewan (1974): "Stratospheric Turbulence and Vertical Effective Diffusion Coefficients", Third Conf. on CIAP, U.S. Dept. of Transportation.

E.R. Reiter and E. Bauer (1975): "Residence Times of Atmospheric Pollutants", Appendix A to Section II, The Natural Stratosphere 1974 CIAP Monograph 1, U.S. Dept. of Transport., Washington, D.C., pp. 2-125 to 2-147.

W.M. Crooks, R.M. Hoblet, D.T. Prophet, et al (1967): "Project HICAT, An Investigation of High Altitude Clear Air Turbulence", Tech. Rept. AFFDL-TR-67-123, Air Force Flight Dynamics Lab, WPAFB.

E.F. Danielson (1968): "Stratospheric-Tropospheric Exchange Based on Radioactivity, Ozone, and Potential Vorticity", Jour. Atmosph. Sci., 25, 502-518.

K.R. Hardy and I. Katz (1969): "Probing the Clear Atmosphere with High Power, High Resolution Radars", Proc. IEEE, 57, 468-480.

D. Atlas, K.R. Hardy and T.G. Konrad (1966): "Radar Detection of the Tropopause and Clear Air Turbulence", Preprints 12th Weather Radar Conf., Amer. Meteorol. Soc., Boston, MA, pp. 279-284.

D. Atlas, J.I. Metcalf, J.H. Richter and E.E. Gossard (1970): "The Birth of 'CAT' and Microscale Turbulence", Jour. Atmosph. Sci., 27, 903-913.

K.A. Browning (1971): "Structure of the Atmosphere in the Vicinity of Large-Amplitude Kelvin-Helmholtz Billows", Quart. J. Roy. Meteorol. Soc., 97, 283-299.

R.K. Crane (1973): "Analysis of Data from the Avon-to-Westford Experiment", Tech. Rept. 498, MIT Lincoln Laboratory, Lexington, MA.

J.L. Green, J.M. Warnock, R.H. Winkler, and T.E. VanZandt (1975): "Studies of Winds in the Upper Troposphere with a Sensitive VHF Radar", Geophys. Res. Letters, 2, 19-21.

B.B. Balsley and D.T. Farley (1976): "Auroral Zone Winds Detected Near the Tropopause with the Chatanika UHF Doppler Radar", Geophys. Res. Letters, 3, 525-528.

V.I. Tatarskii (1967): Wave Propagation in a Turbulent Atmosphere, Nauka, Moskow (Translation: The Effects of the Turbulent Atmosphere on Wave Propagation, available from U.S. Dept. of Commerce, National Technical Information Service, Springhill, VA, 1971).

R.K. Crane (1968): "Monostatic and Bistatic Scattering from Thin Turbulent Layers in the Atmosphere", Tech. Note 1968-34, MIT Lincoln Laboratory, Lexington, MA.

R.K. Crane (1976): "Refraction Effects in the Neutral Atmosphere" in Methods of Experimental Physics, Vol. 12, Astrophysics, Part B, Radio Telescopes, ed. by M.L. Meeks, Academic Press, New York.

A.S. Monin and A.M. Yaglom (1975): Statistical Fluid Mechanics: Mechanics of Turbulence, Vol. 2, English Edition ed by J.L. Lumley, MIT Press, Cambridge, MA.

J.A. Dutton (1969): "An Energy Budget for a Layer of Stratospheric CAT", Radio Sci., 4, 1137-1142.

J.K. Goodman and A. Miller (1977): "Mass Transport Across a Temperature Inversion", Jour. Geophys. Res., 82, 3463-3471.

L.N. Howard and S.A. Maslowe (1973): "Stability of Stratified Shear Flows", Bound. Layer Meteorol., 4, 511-523.

S.A. Thorpe (1973): "Turbulence in Stably Stratified Fluids: A Review of Laboratory Experiments", Bound. Layer Meteorol., 5, 95-119.

R.R. Long (1973): "Some Properties of Horizontally Homogeneous, Statistically Steady Turbulence in a Stratified Fluid", Bound. Layer Meteorol., 5, 139-157.

E.R. Reiter (1975): "Stratospheric-Tropospheric Exchange Processes", Rev. Geophys. and Space Phys. 13, 459-474.

J.I. Metcalf and D. Atlas (1973): "Microscale Ordered Motions and Atmospheric Structure Associated with Thin Echo Layers in Stably Stratified Zones", Bound. Layer Meteorol., 4, 7-35.

R.K. Crane (1971): "Description of the Avon-to-Westford Experiment", Tech. Rept. 483, MIT Lincoln Laboratory, Lexington, MA.

J.H. Richter (1969): "High Resolution Tropospheric Radar Sounding", Radio Sci., 4, 1261-1268.

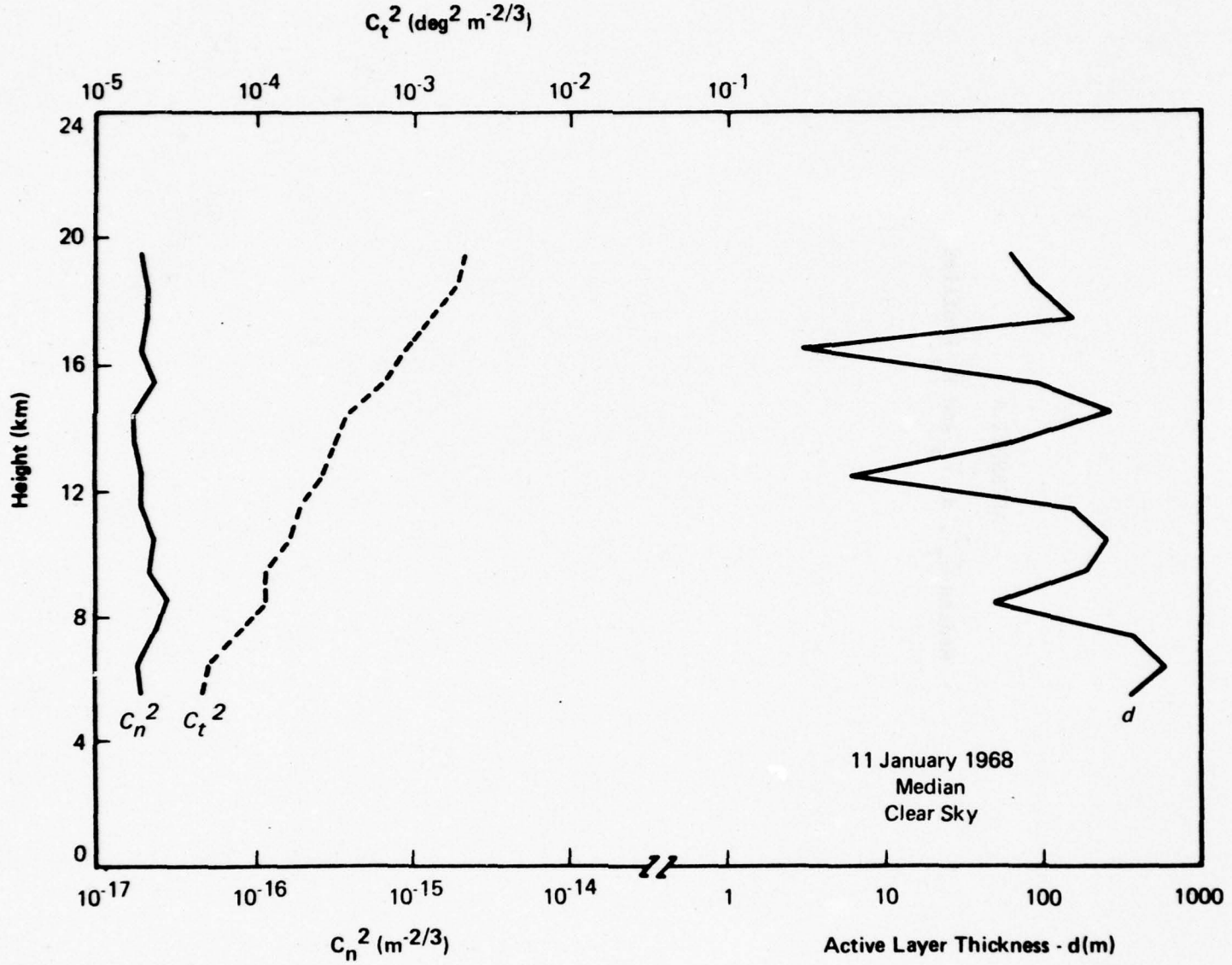
D.M. Cunnold (1975): "Vertical Transport Coefficients in the Mesosphere Obtained from Radar Observations", Jour. Atmos. Sci., 32, 2191-2200.

T.E. VanZandt, J.L. Green, K.S. Gage, W.L. Clark (1977): "Reflectivity Studies with the Sunset VHF Pulsed Doppler Radar", Proc. URSI Comm. F. Open Symposium at La Baule, France, Center National d'Etudes des Telecommunications, pp. 519-524.

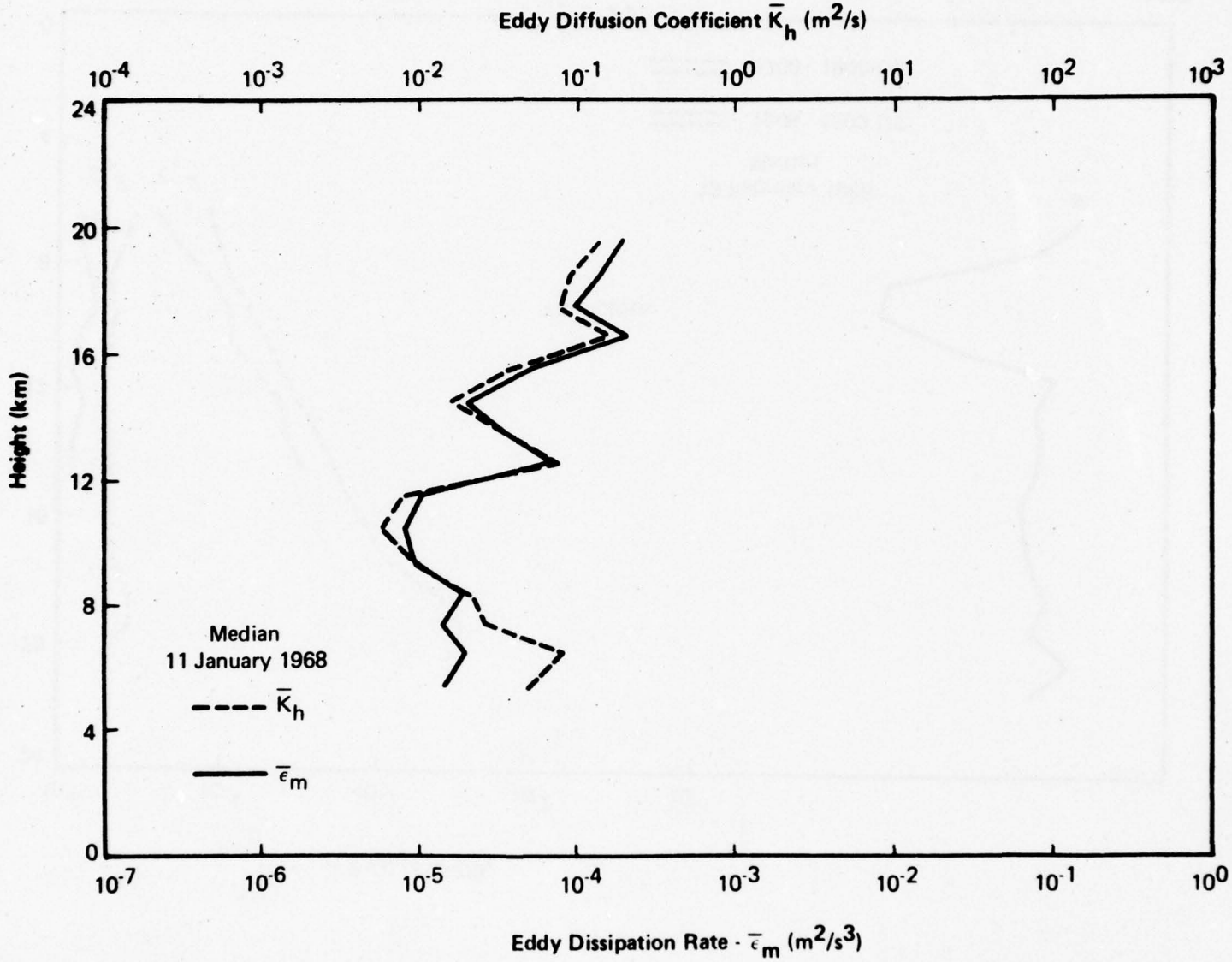
APPENDIX A

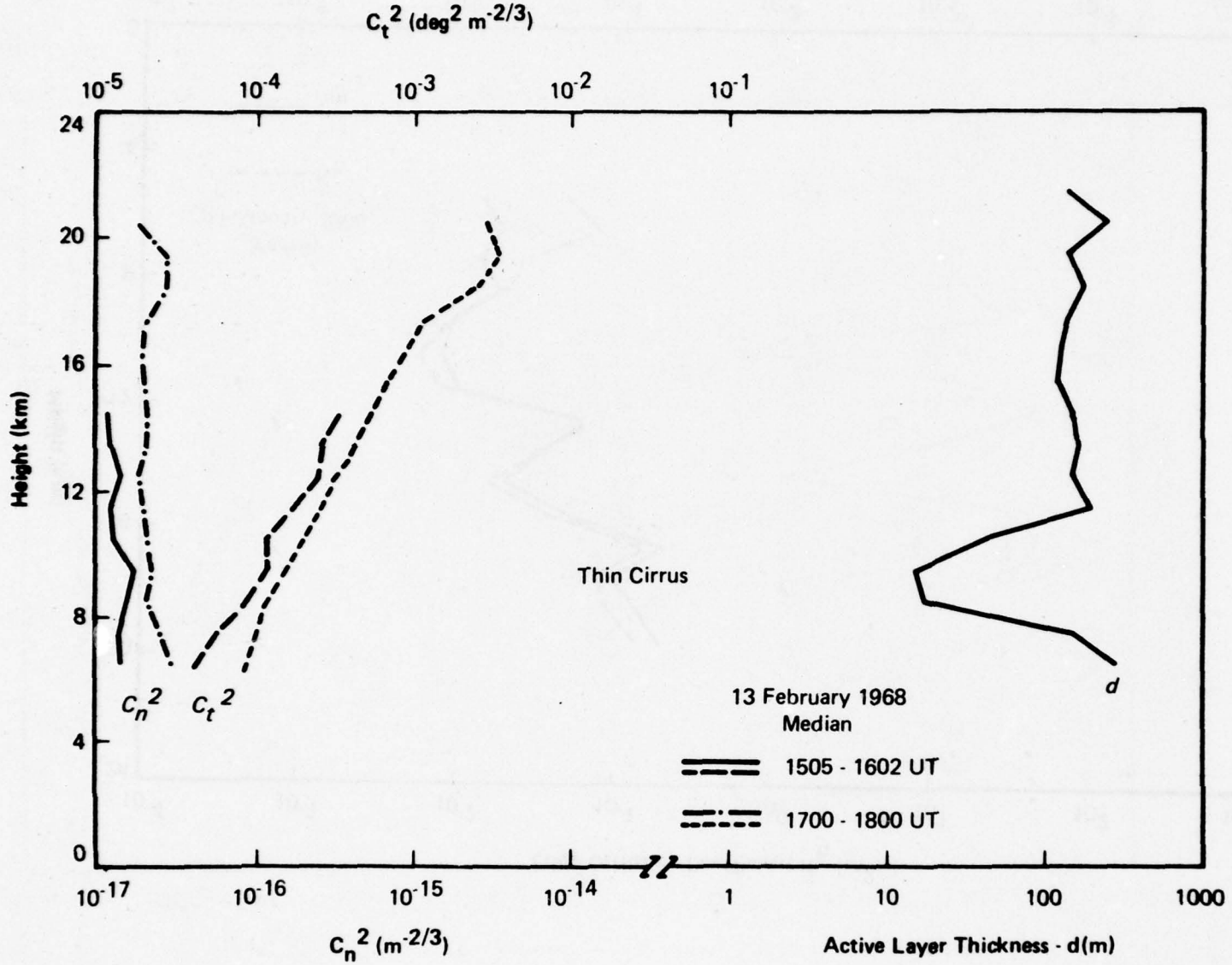
Median $\overline{C}_T^2$, d, $\overline{\varepsilon}_m$ and $\overline{K}_H$ Profiles

708069
708045

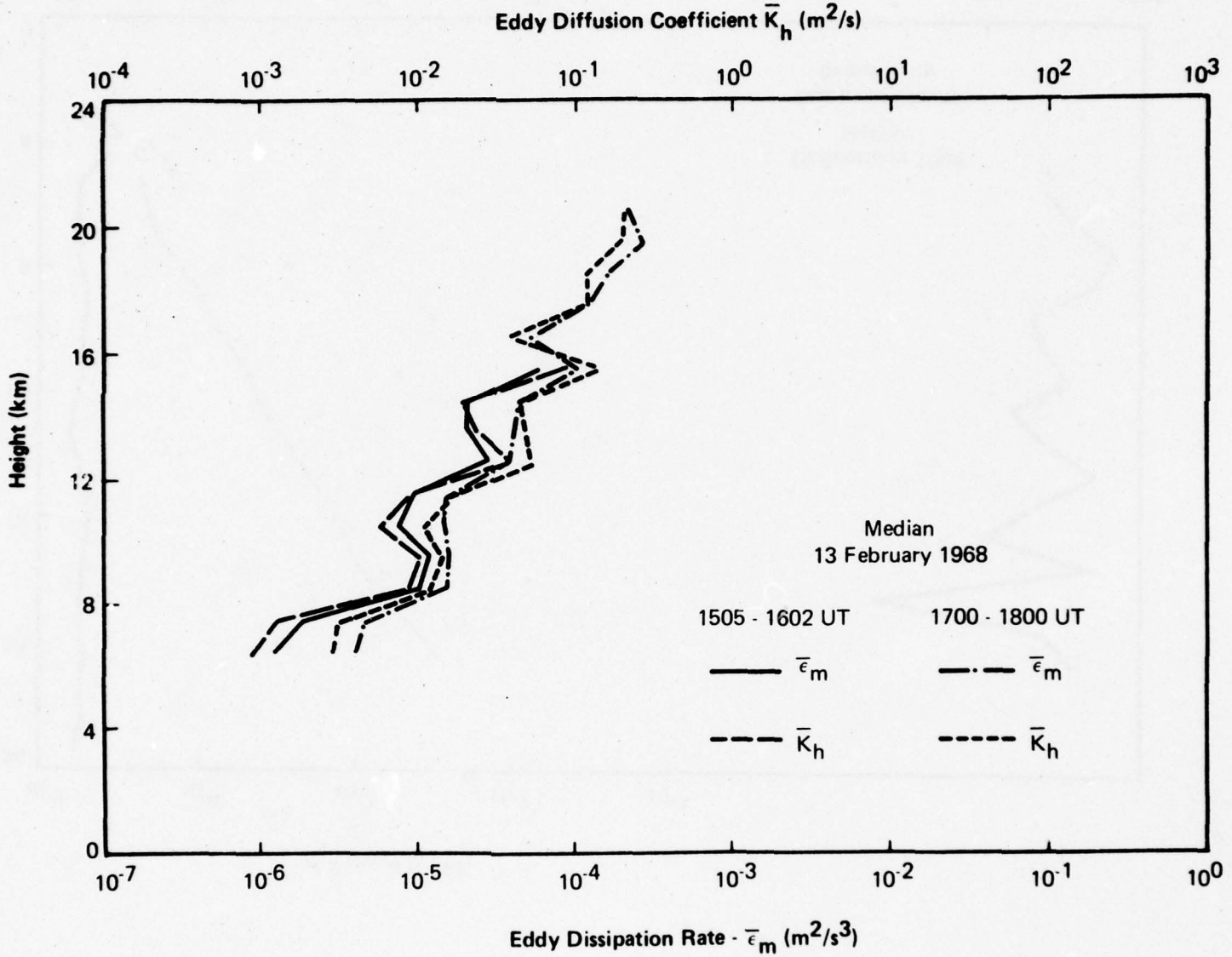


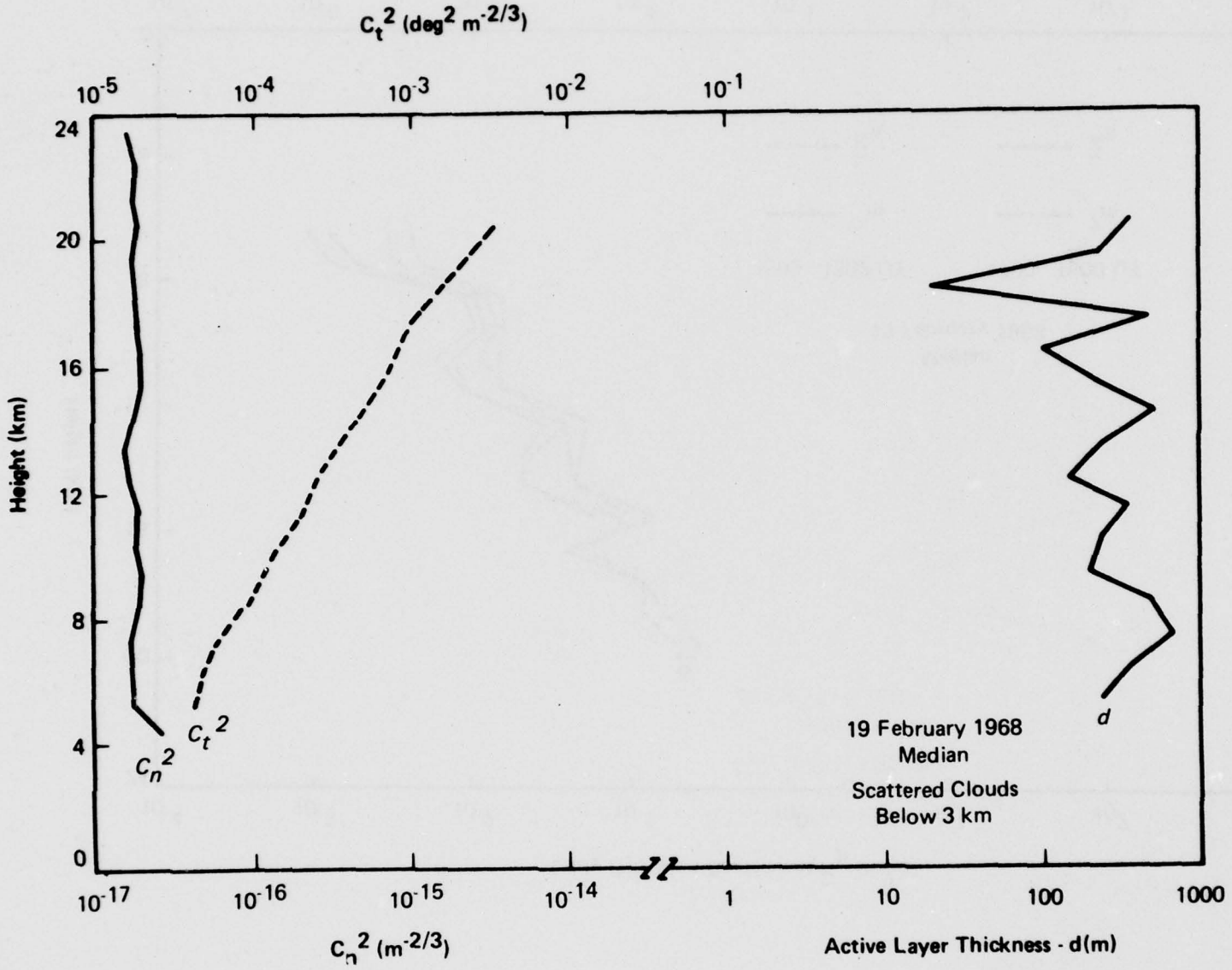
708150
708137



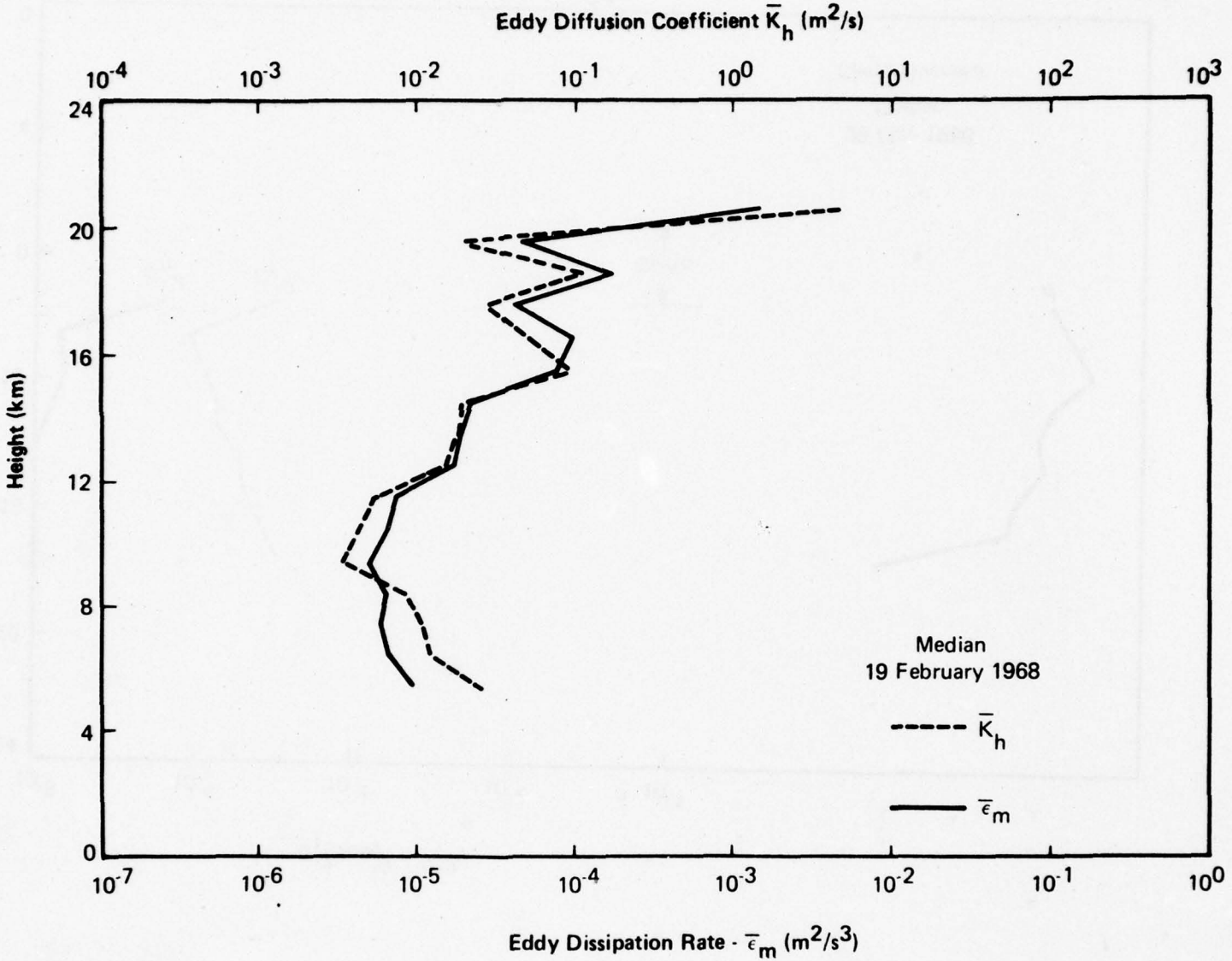

C_t^2 (deg^2 m$^{-2/3}$)
10^{-5}
10^{-4}
10^{-3}
10^{-2}
10^{-1}
24
20
16
12
8
4
0
Height (km)
Thin Cirrus
C_n^2
C_t^2
d
13 February 1968
Median
1505 - 1602 UT
1700 - 1800 UT
10^{-17}
10^{-16}
10^{-15}
10^{-14}
1
10
100
1000
C_n^2 (m$^{-2/3}$)
Active Layer Thickness - d(m)

708151
708137




C_t^2 (deg^2 m$^{-2/3}$)
10^{-5}
10^{-4}
10^{-3}
10^{-2}
10^{-1}
24
20
16
12
8
4
0
Height (km)
C_n^2
C_t^2
d
19 February 1968
Median
Scattered Clouds
Below 3 km
10^{-17}
10^{-16}
10^{-15}
10^{-14}
1
10
100
1000
C_n^2 (m$^{-2/3}$)
Active Layer Thickness - d(m)

708152
708137



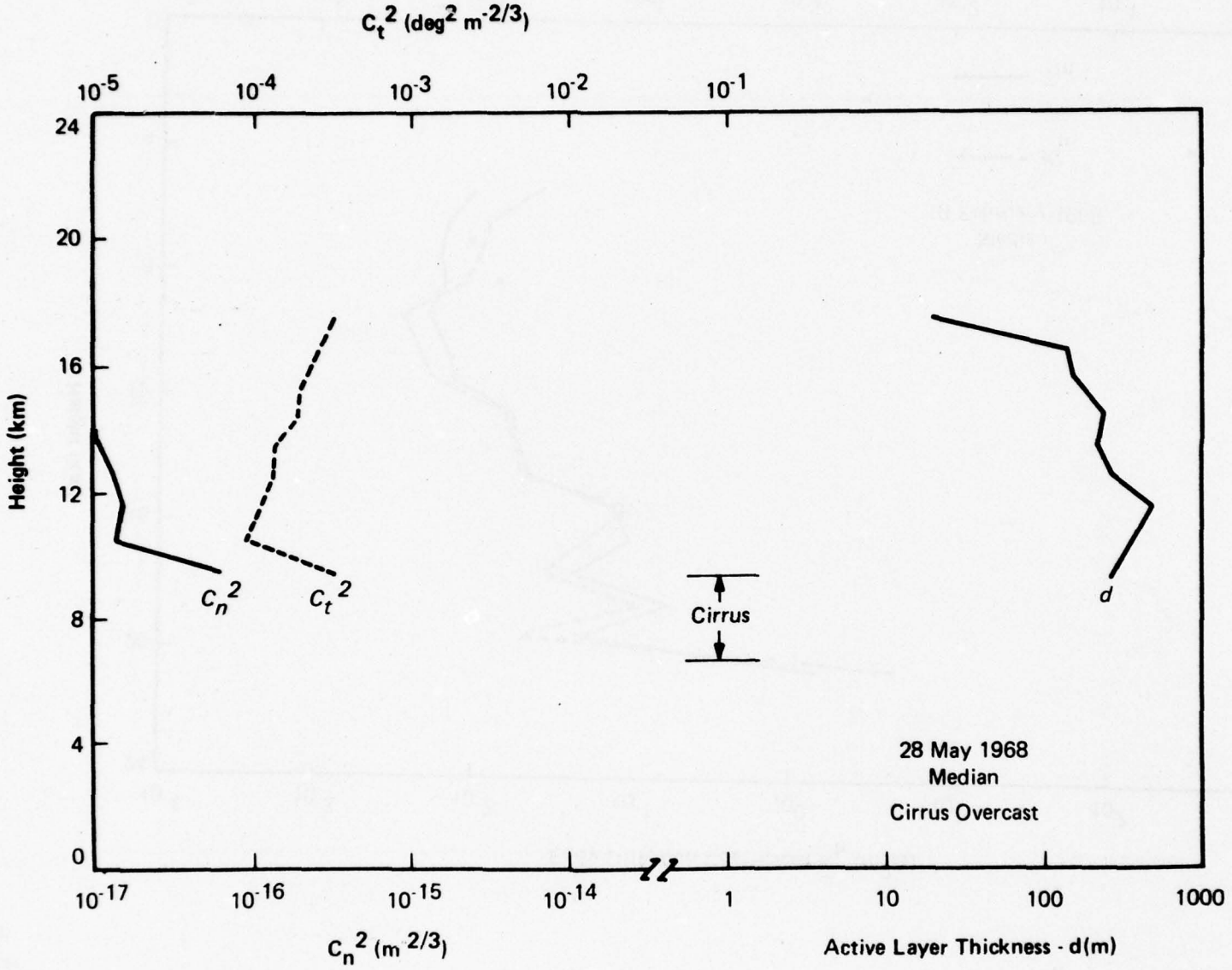


Figure 10 C_n^2, C_t^2 and active layer thickness profiles, May 28, 1968

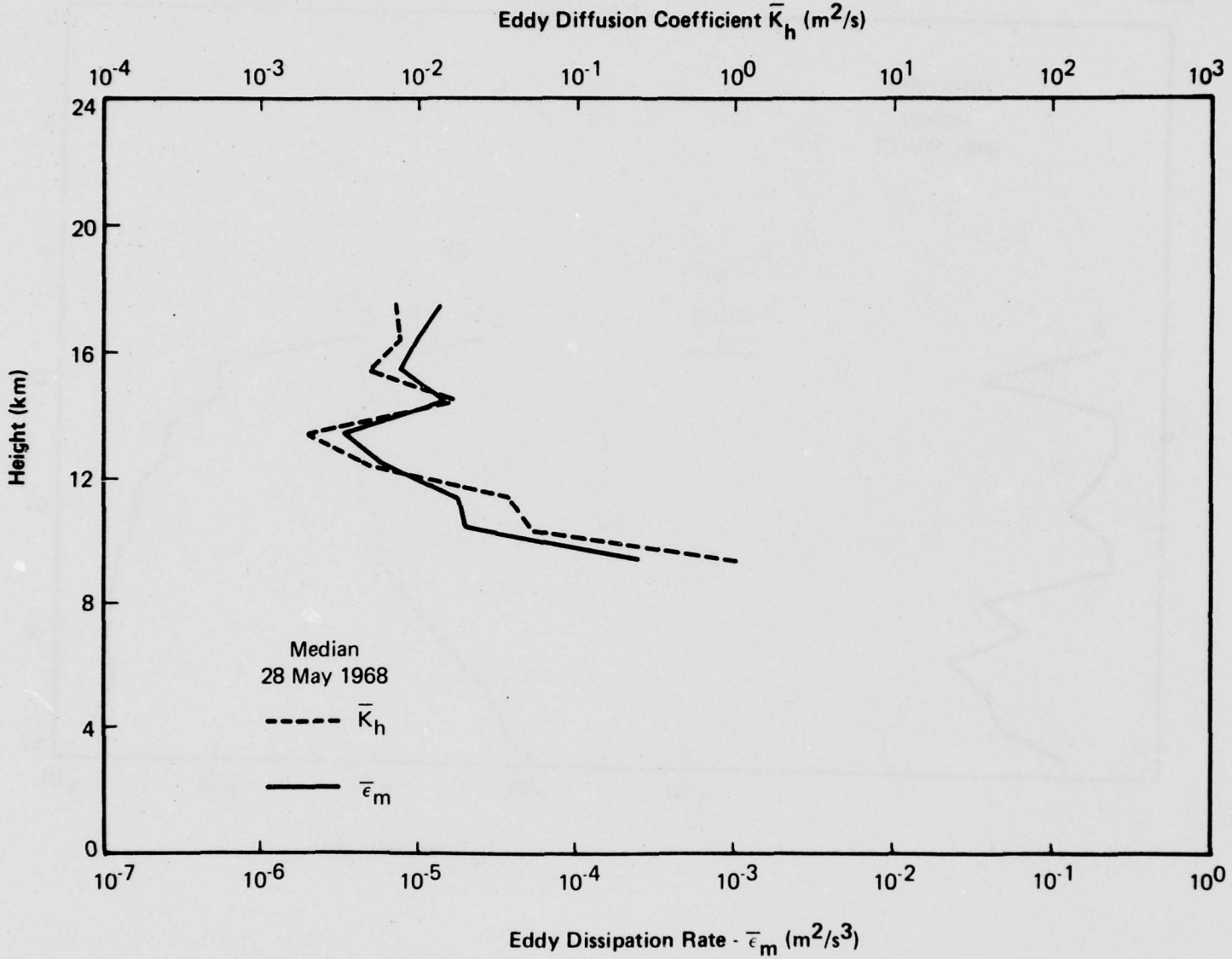
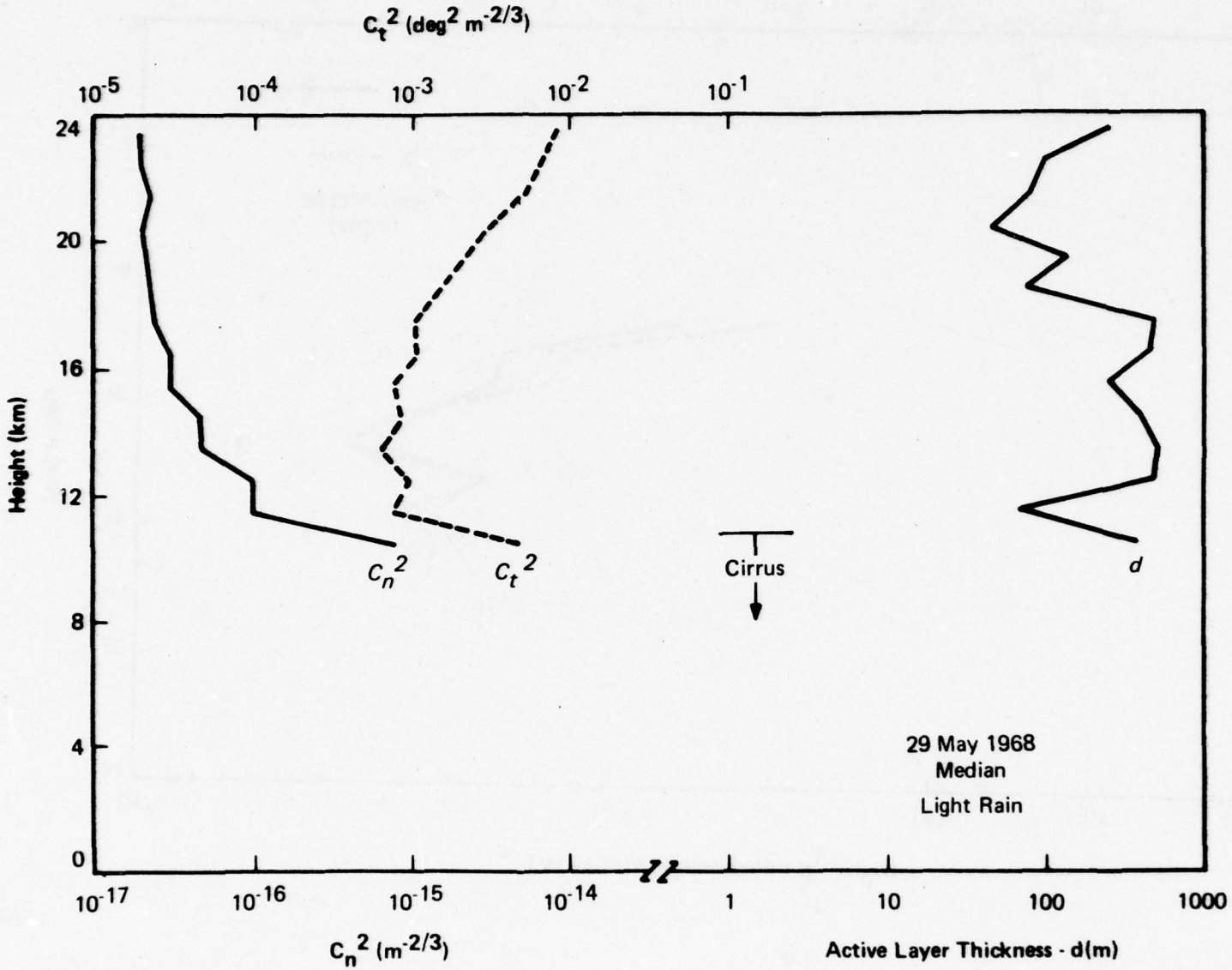
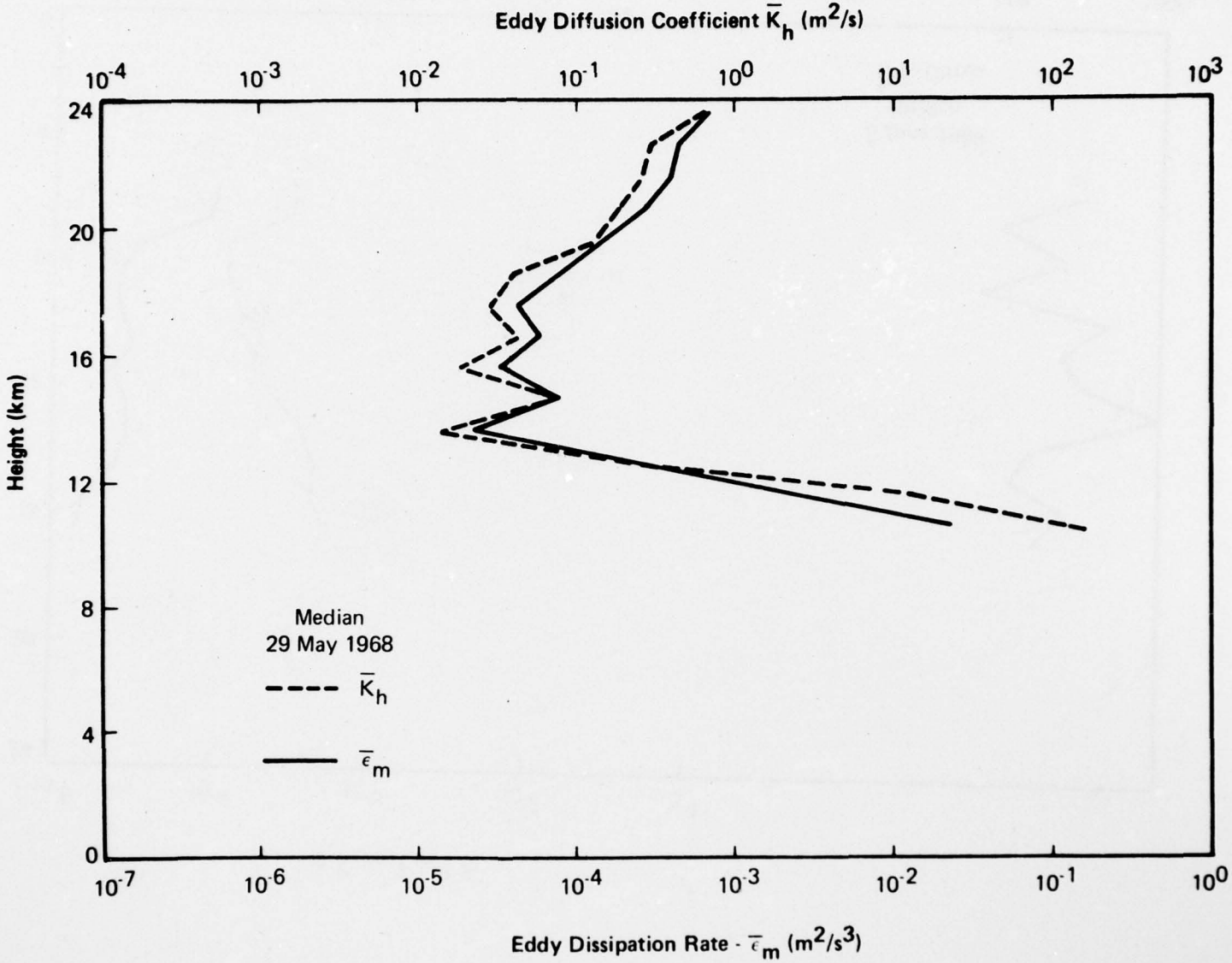
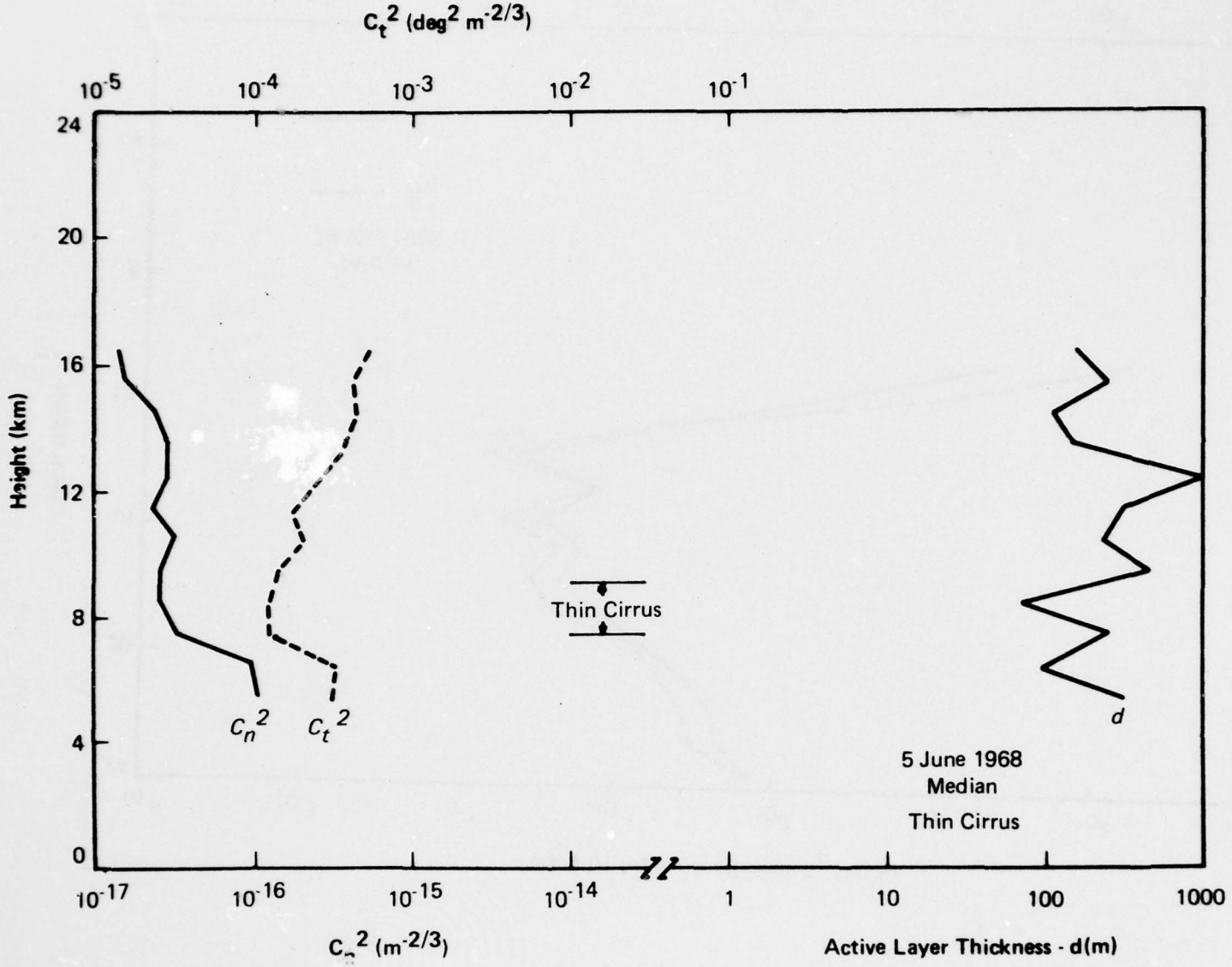


Figure 11 $\bar{K}_H$ and $\bar{\epsilon}_m$ profiles, May 28, 1968

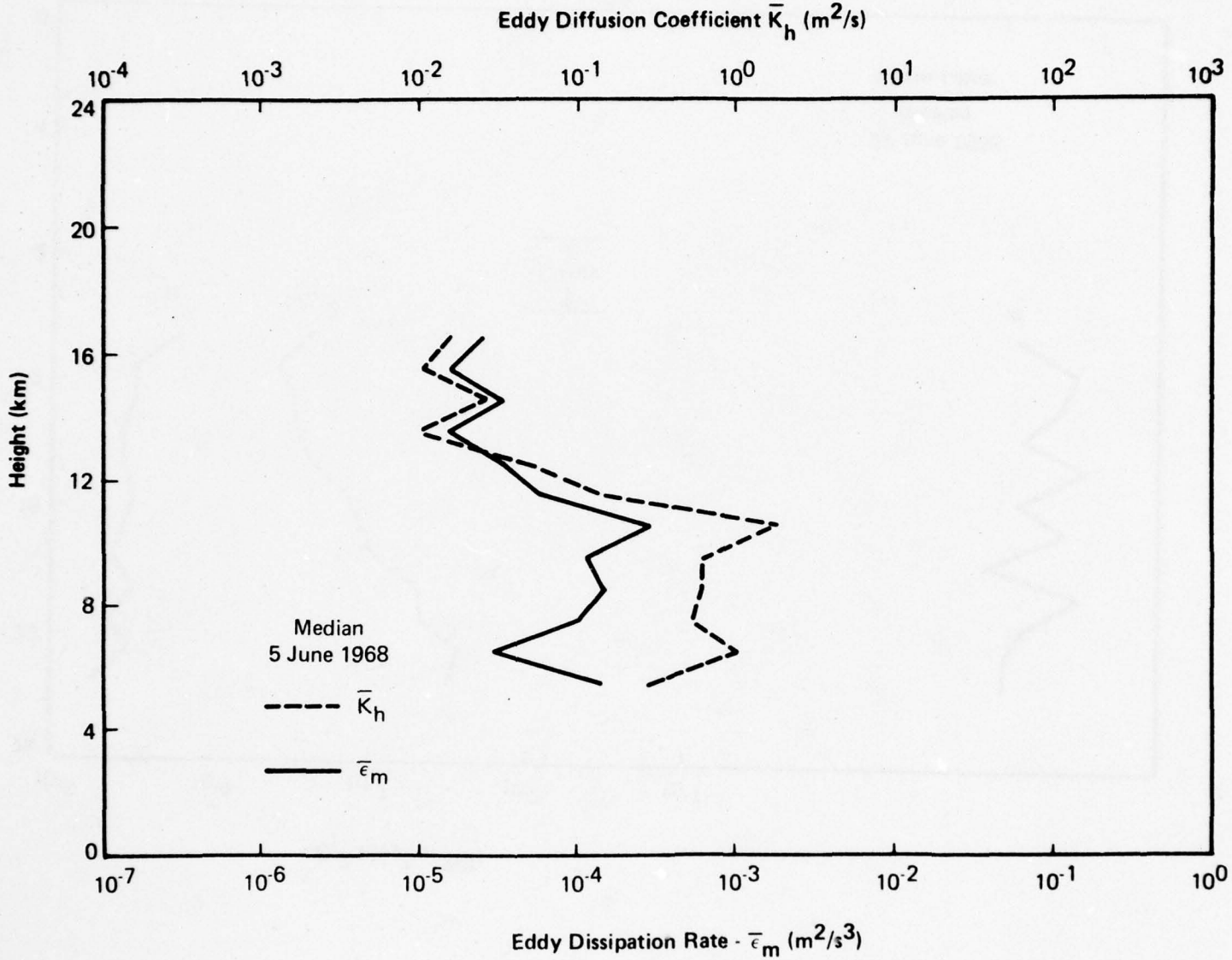

C_t^2 (deg^2 m$^{-2/3}$)
10^{-5}
10^{-4}
10^{-3}
10^{-2}
10^{-1}
24
20
16
12
8
4
0
Height (km)
C_n^2
C_t^2
Cirrus
d
29 May 1968
Median
Light Rain
10^{-17}
10^{-16}
10^{-15}
10^{-14}
1
10
100
1000
C_n^2 (m$^{-2/3}$)
Active Layer Thickness - d(m)

708154
708137

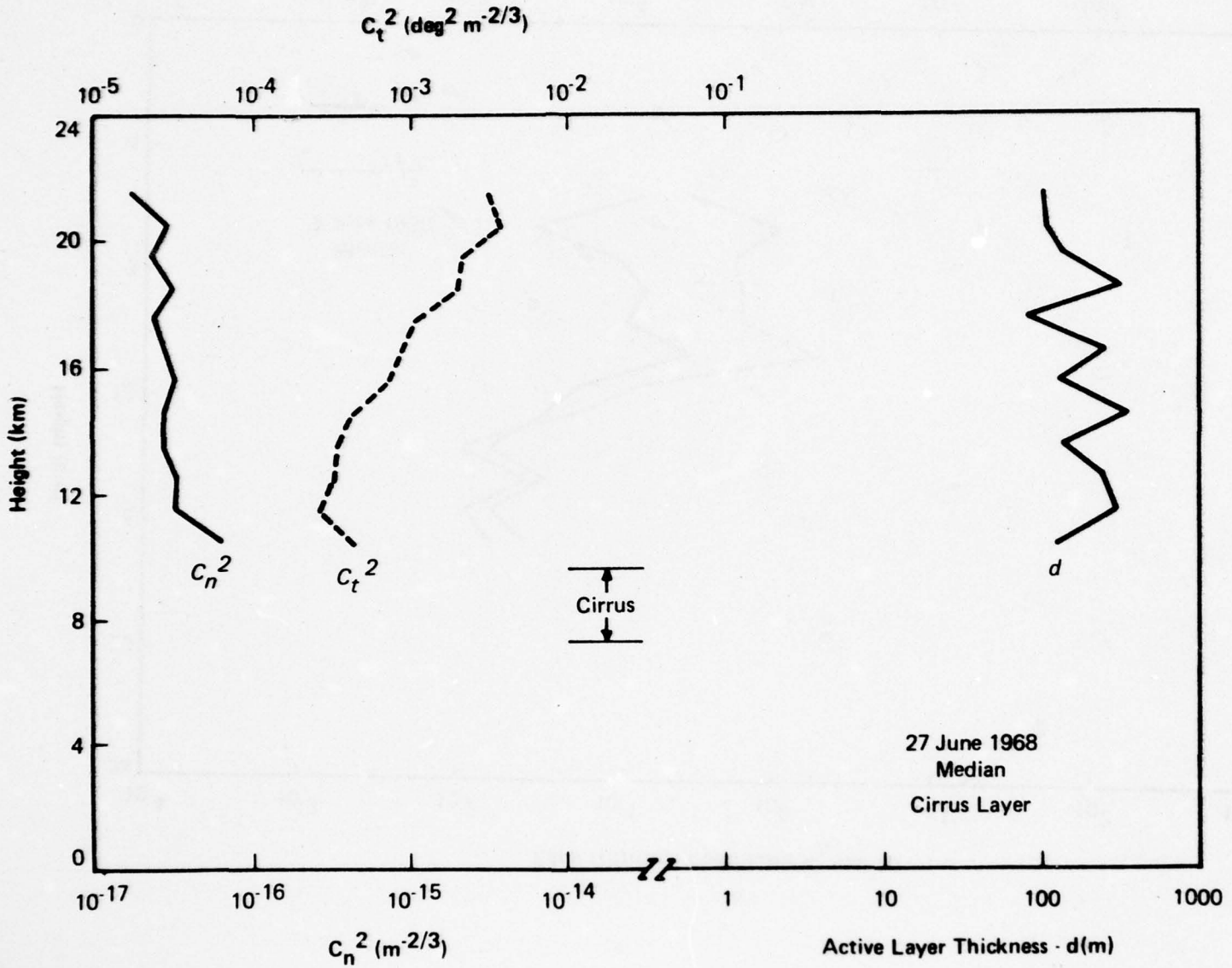



C_t^2 (deg^2 m$^{-2/3}$)
10^{-5}
10^{-4}
10^{-3}
10^{-2}
10^{-1}
24
20
16
12
8
4
0
Height (km)
C_n^2
C_t^2
Thin Cirrus
d
5 June 1968
Median
Thin Cirrus
10^{-17}
10^{-16}
10^{-15}
10^{-14}
1
10
100
1000
C_n^2 (m$^{-2/3}$)
Active Layer Thickness - d(m)

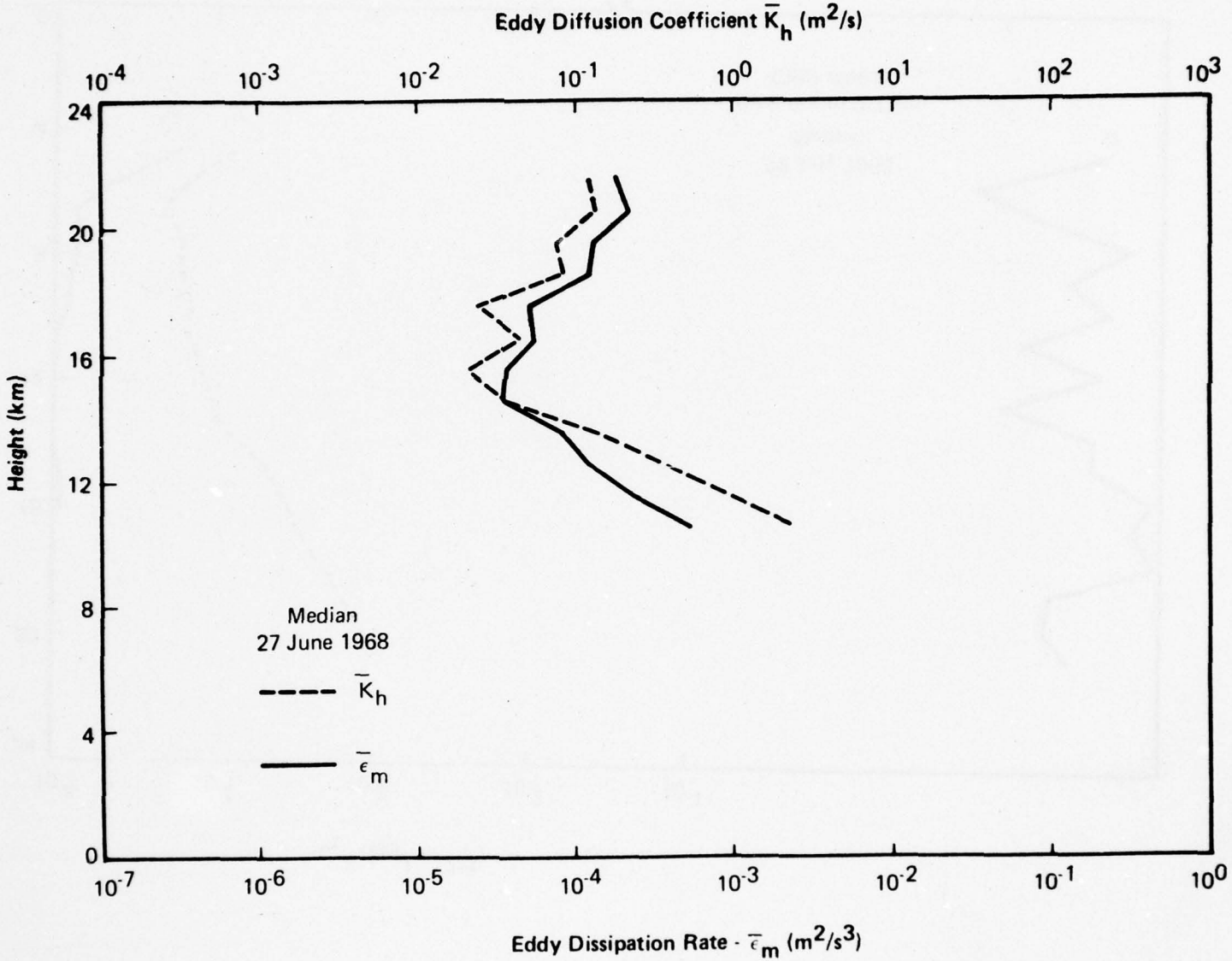
708149
708137



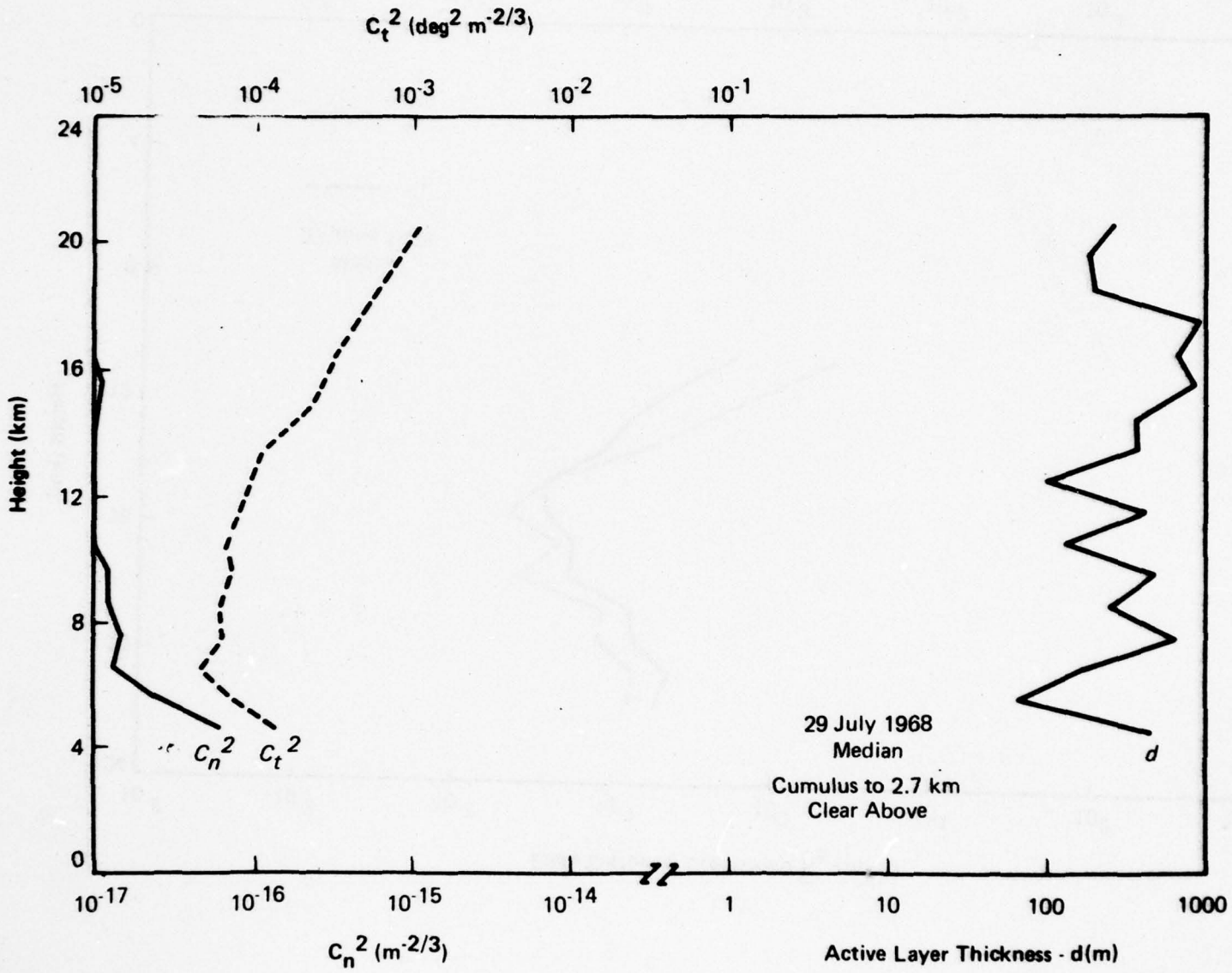
708071
708045



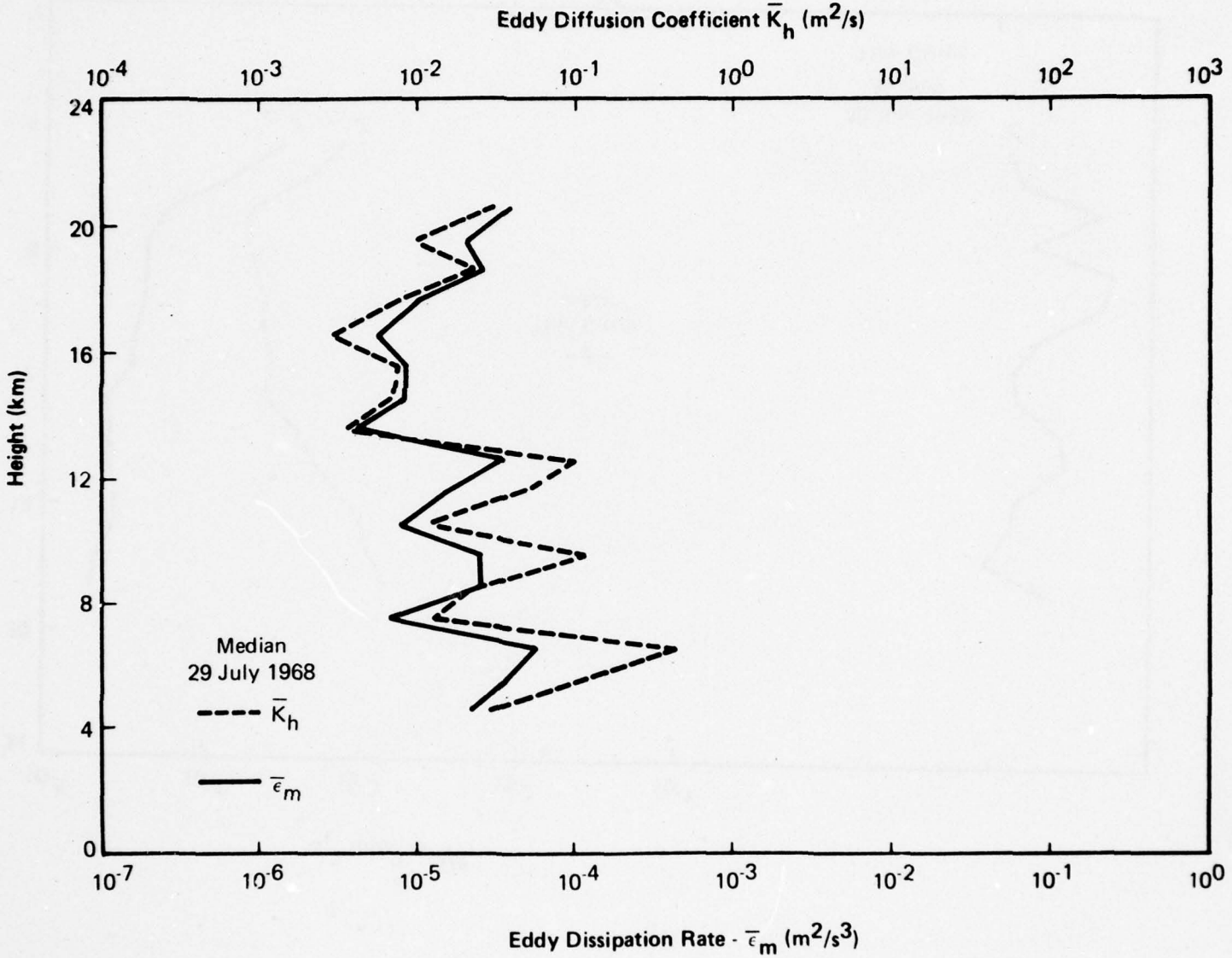
708148
708137



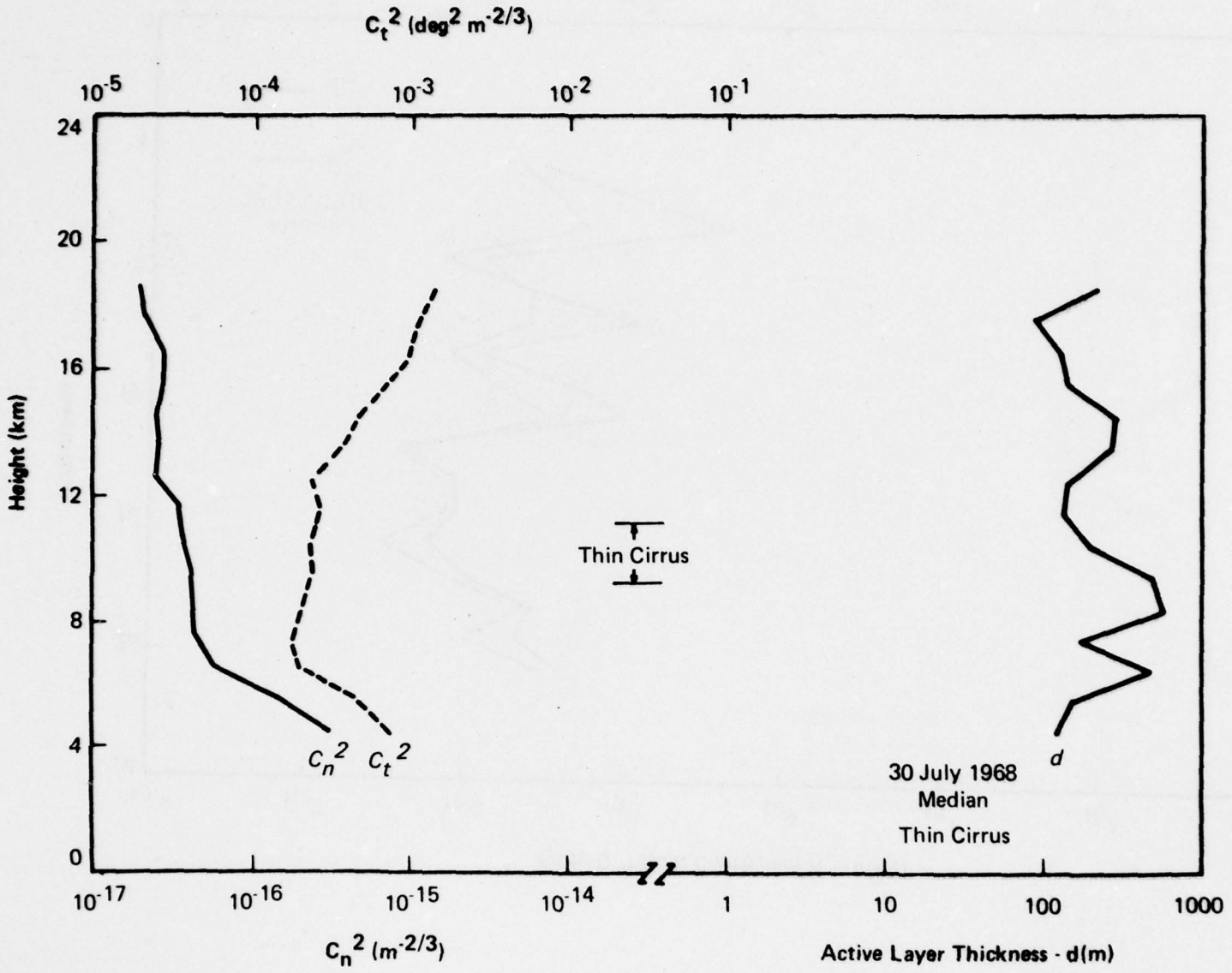
708066
708045



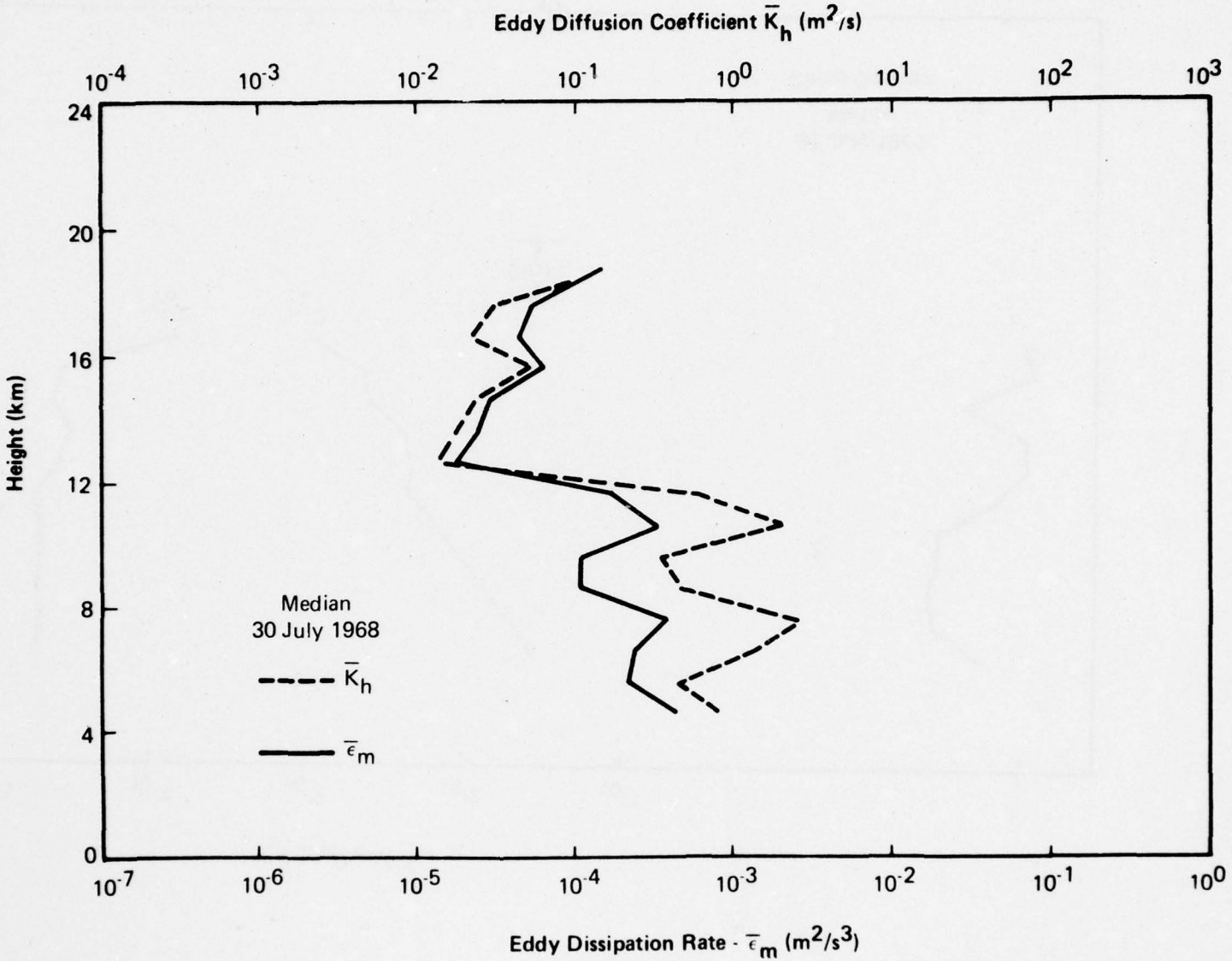
708147
708137



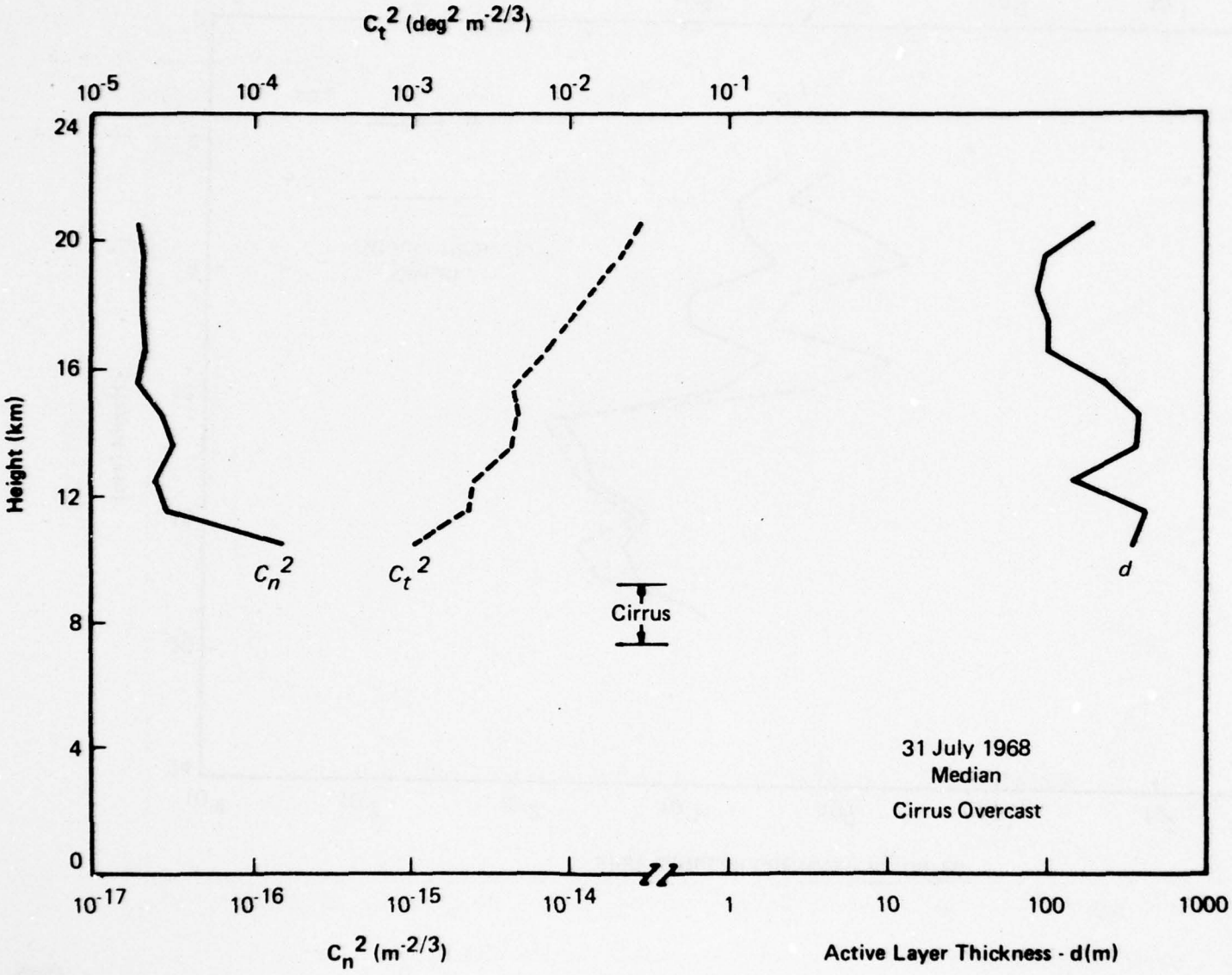
708067
708045



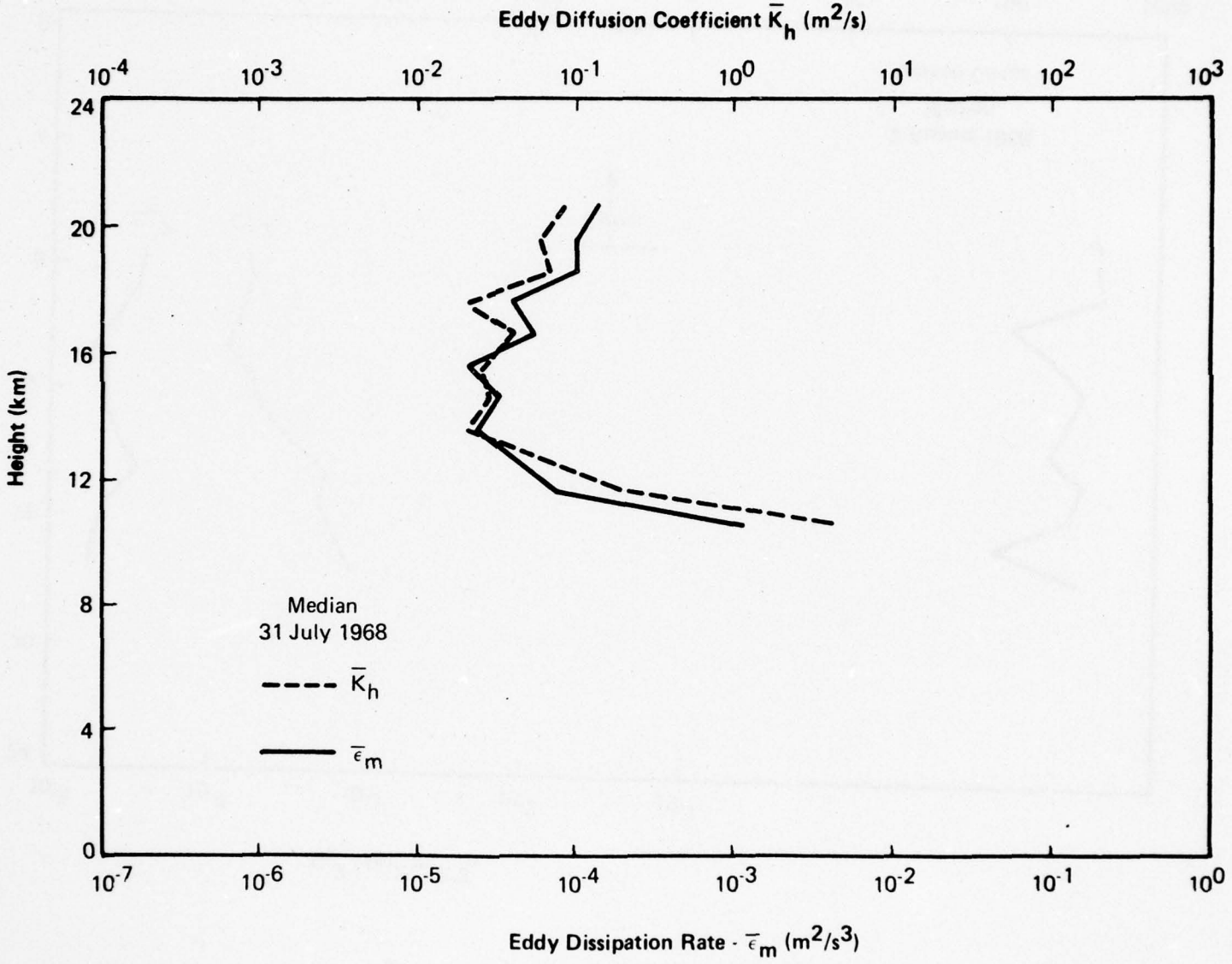
708146
708137



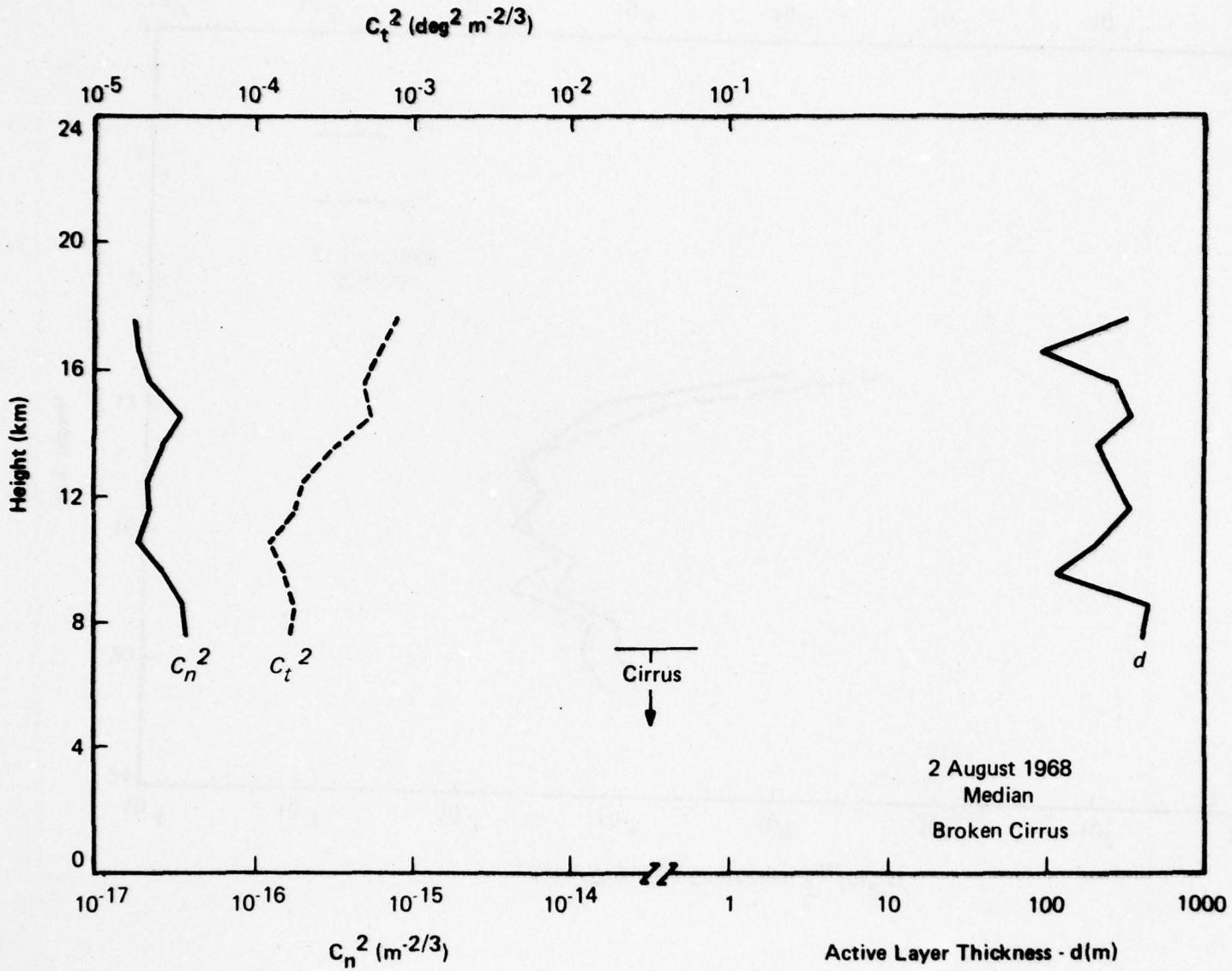
708068
708045



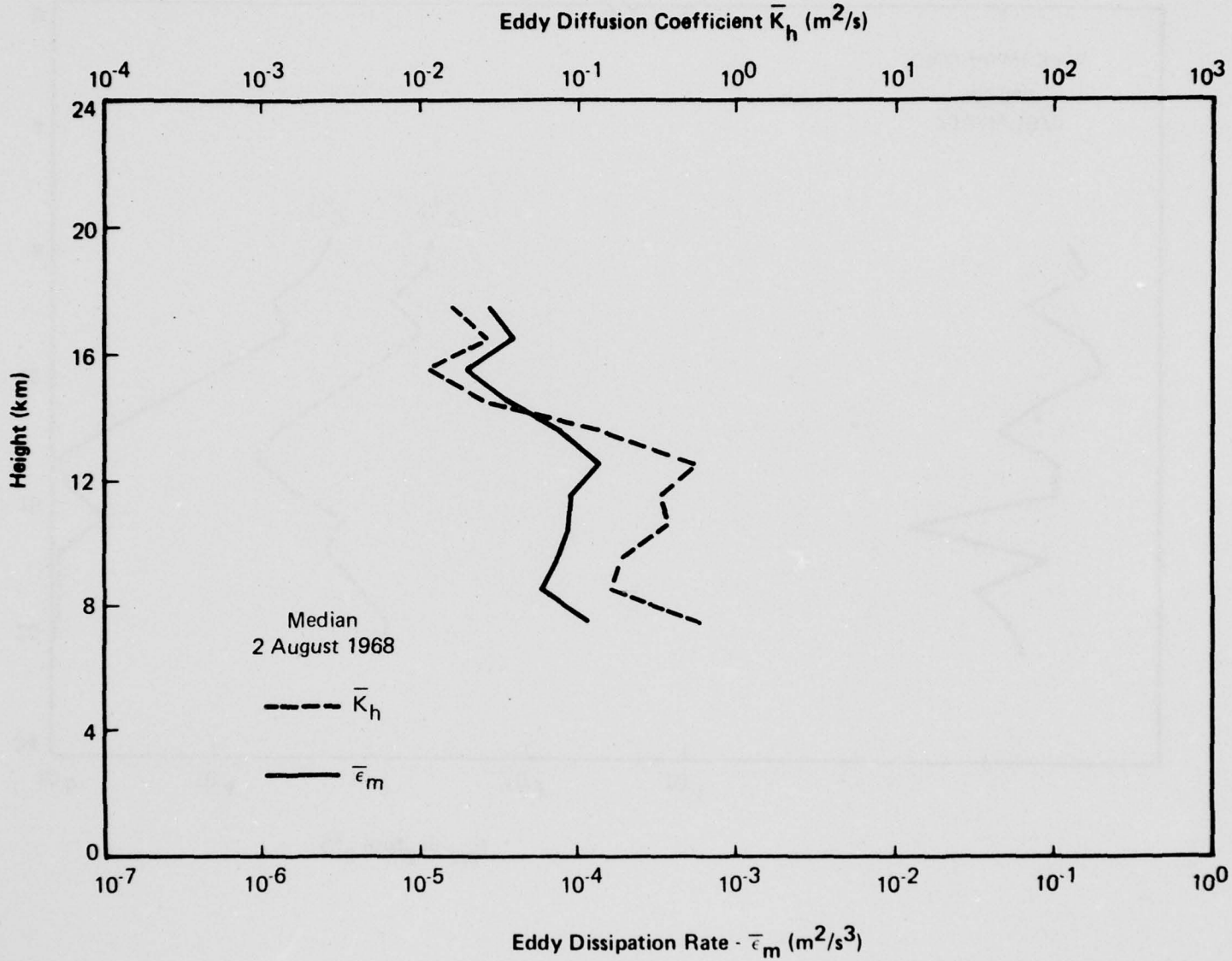
708144
708137



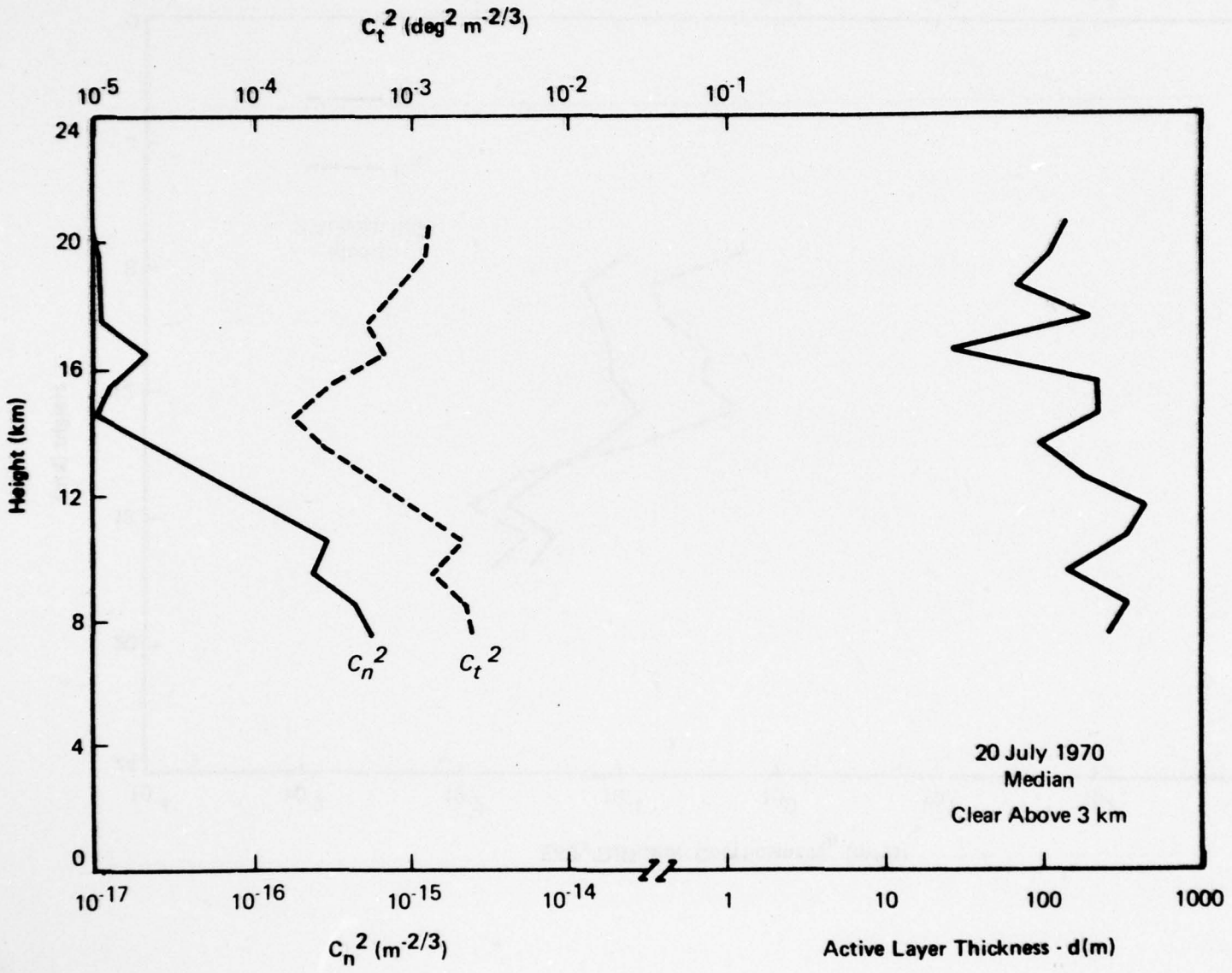
708065
708045



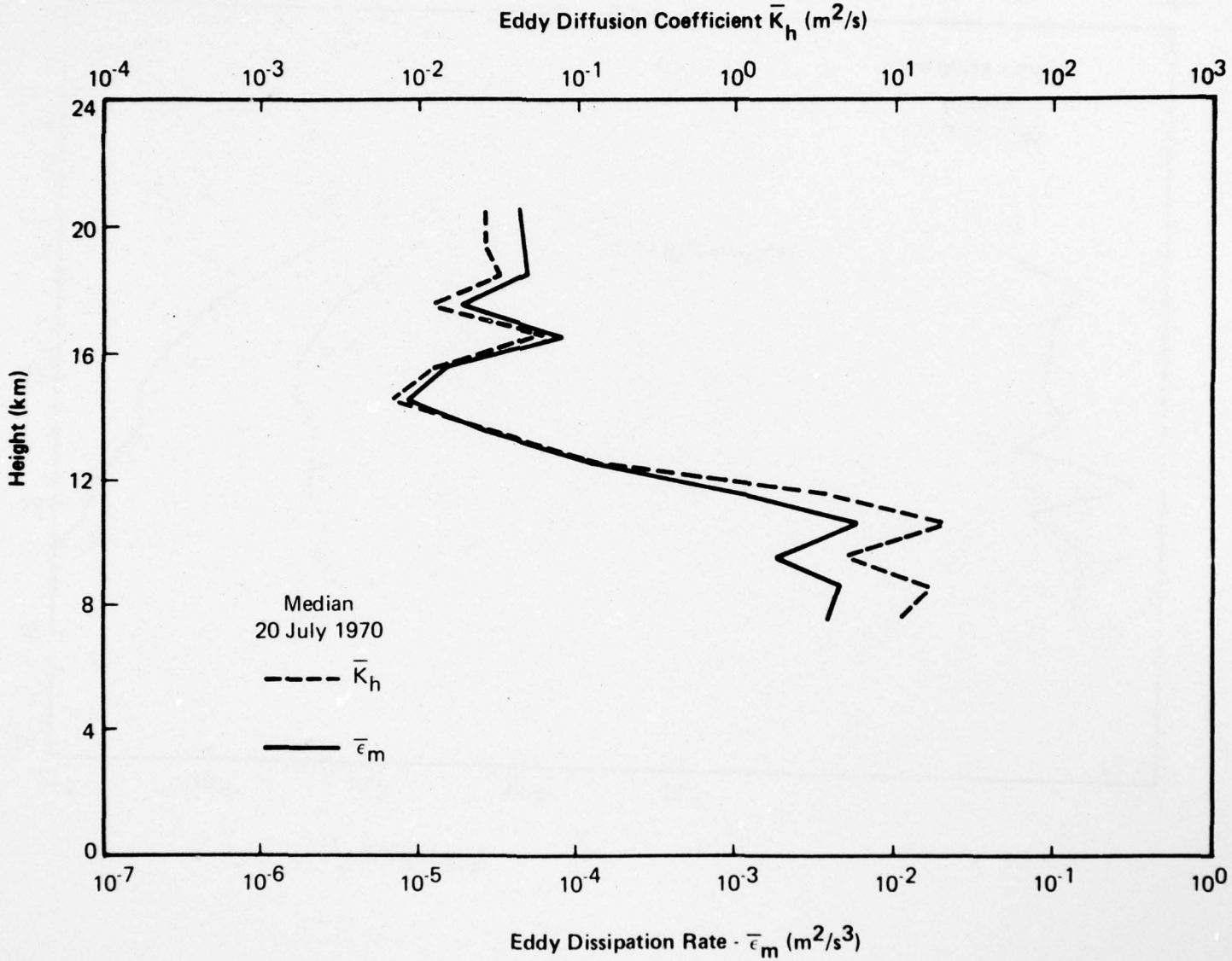
708143
708137



708046
708045



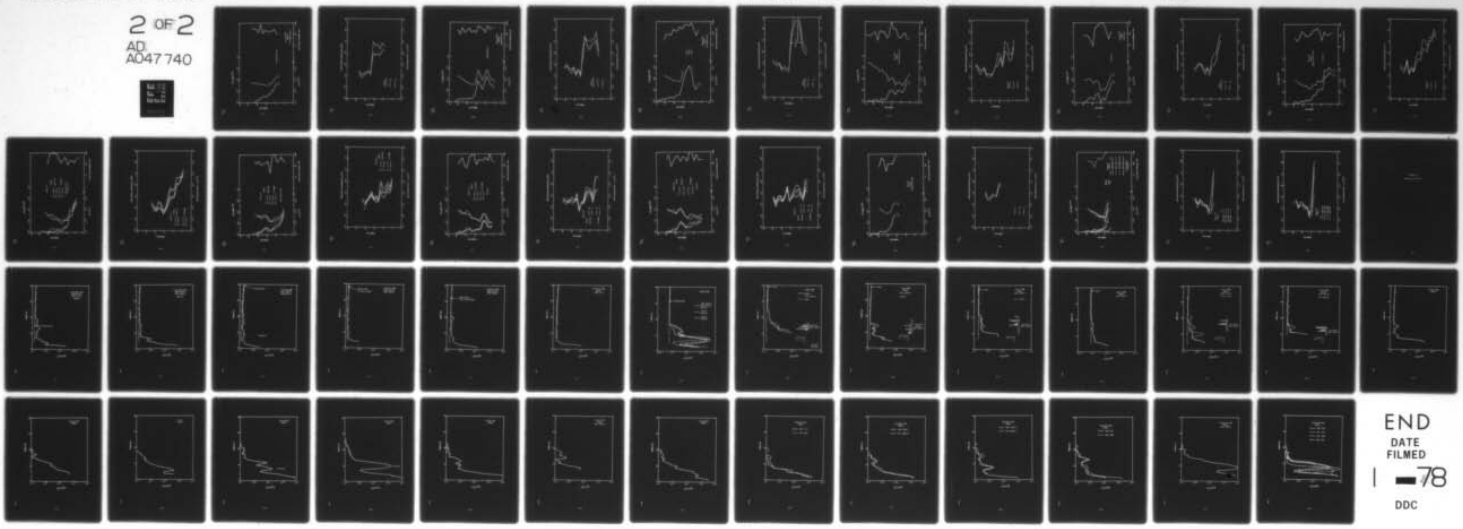
708142
708137



AD-A047 740 ENVIRONMENTAL RESEARCH AND TECHNOLOGY INC CONCORD MASS F/G 4/2
STRATOSPHERIC TURBULENCE ANALYSIS.(U)
SEP 77 R K CRANE F19628-77-C-0059

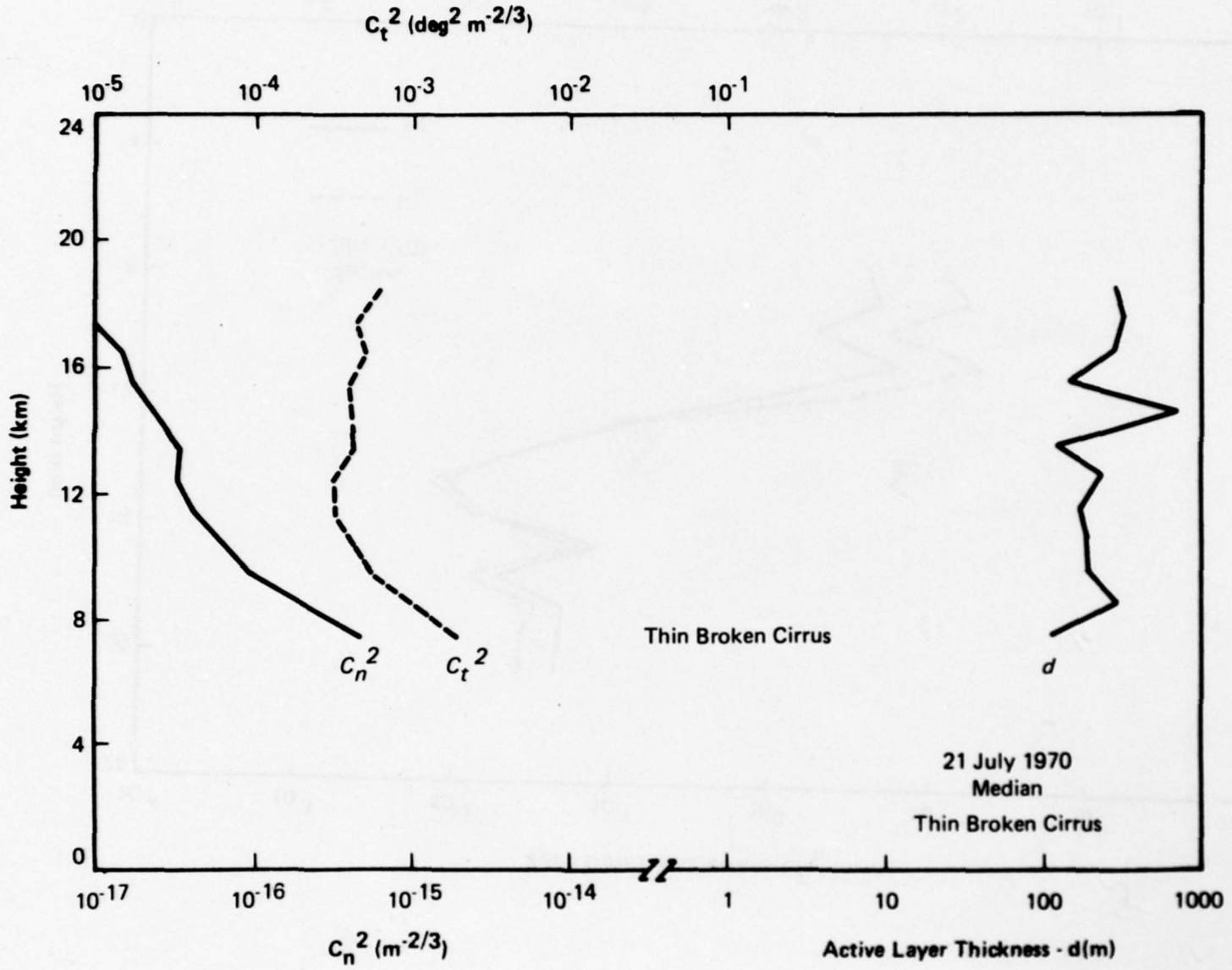
UNCLASSIFIED AFGL-TR-77-0207 NL

2 OF 2
AD
A047740

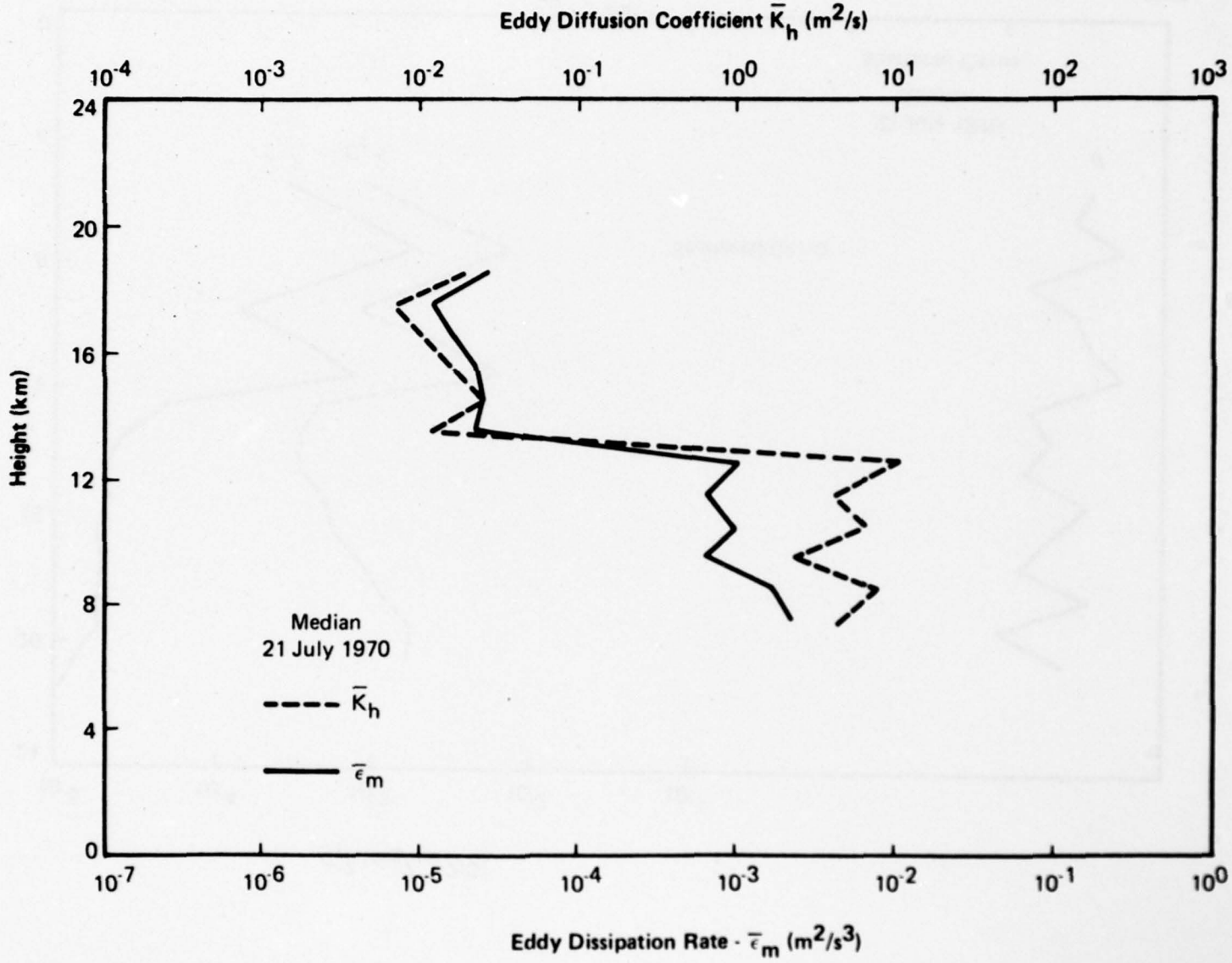


END
DATE
FILMED
1 -78
DDC

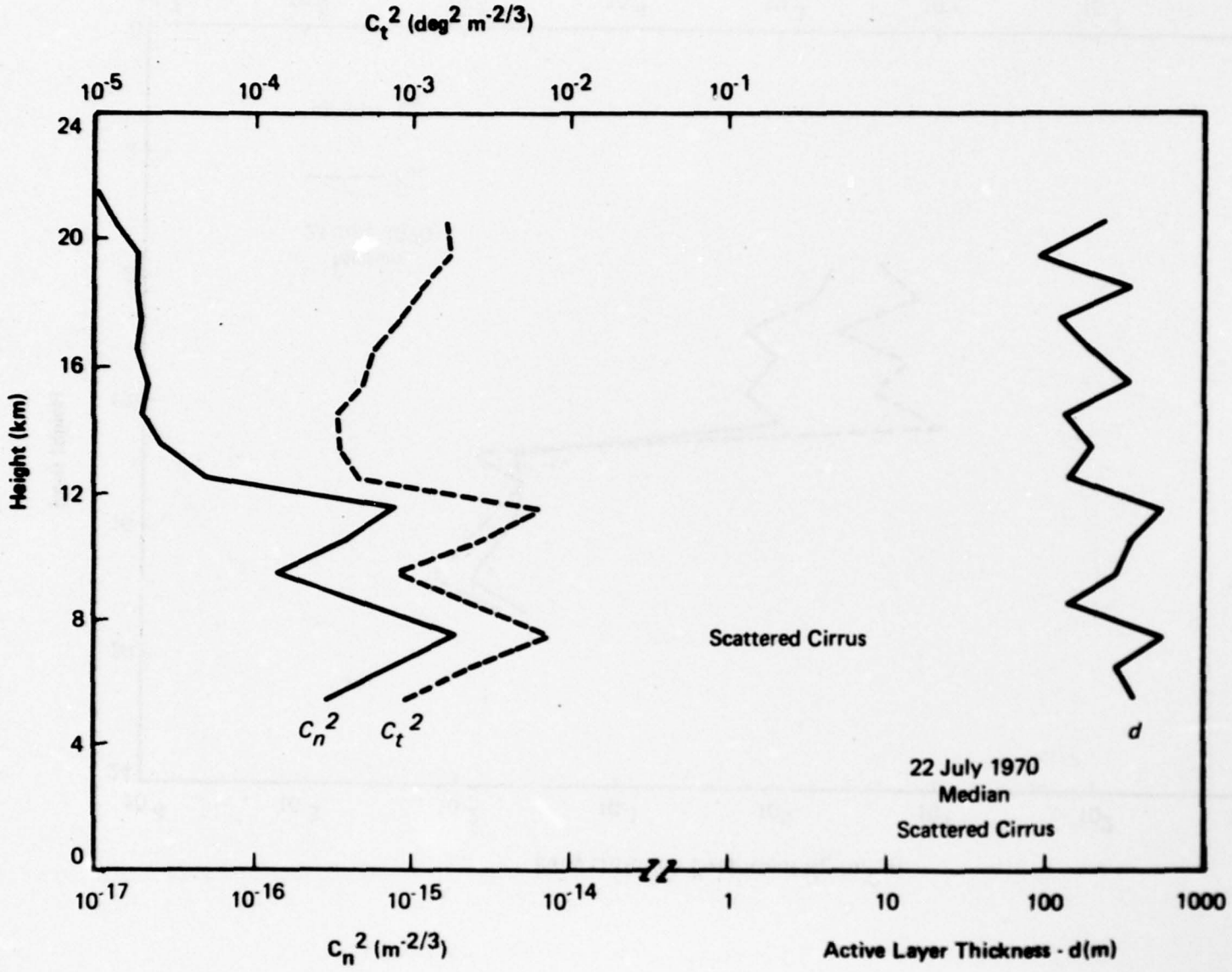
708047
708045



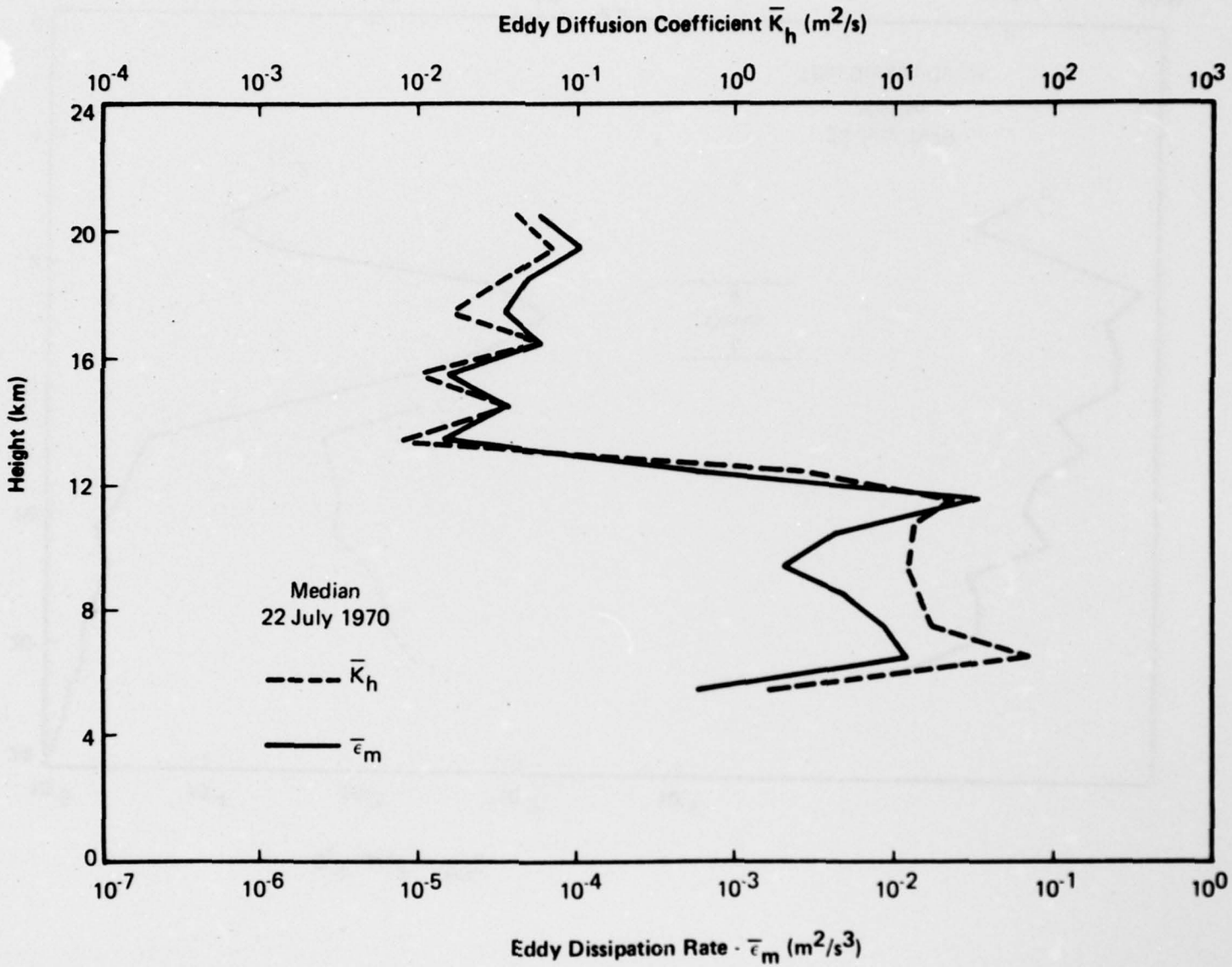
708141
708137



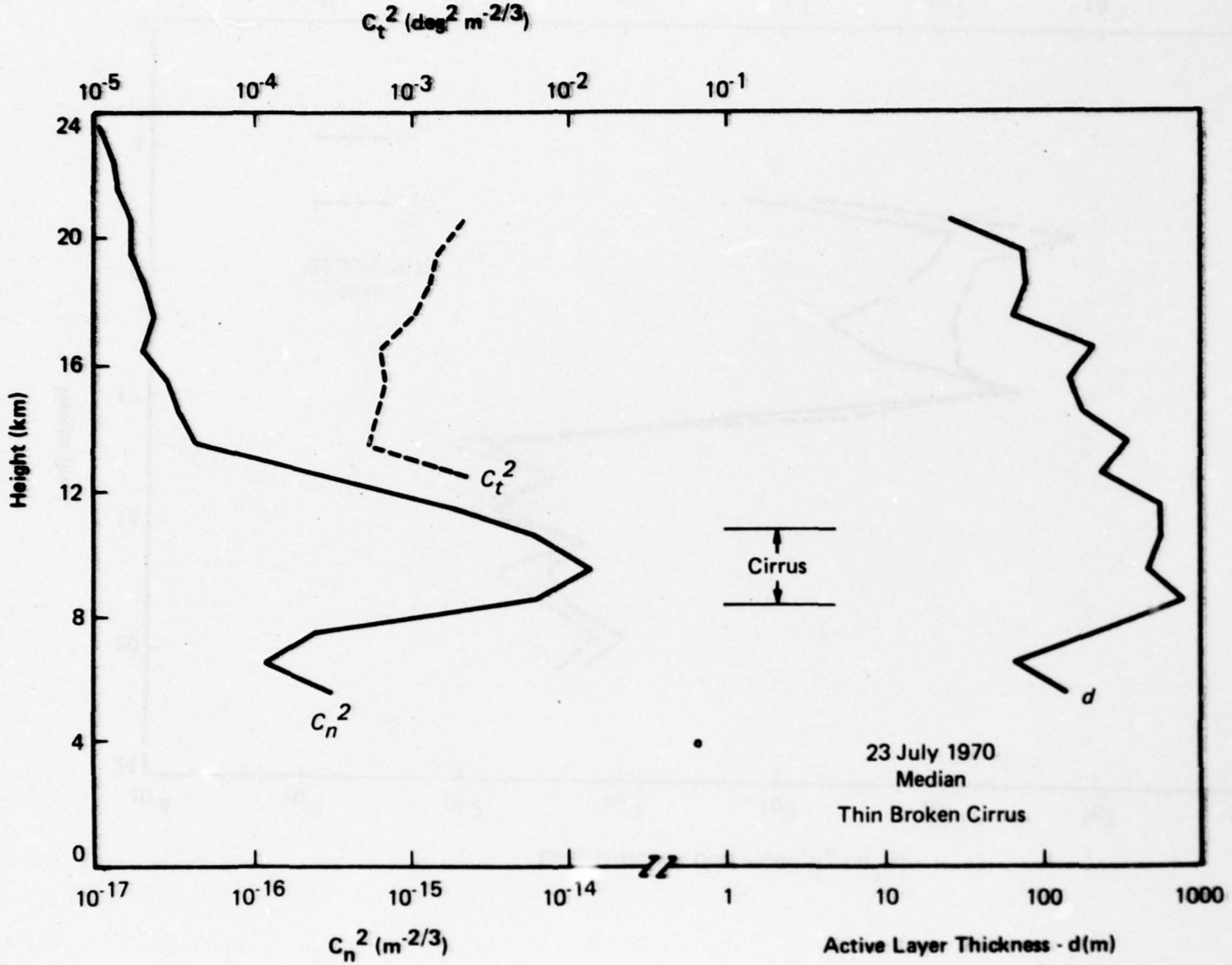
708062
708045



708140
708137

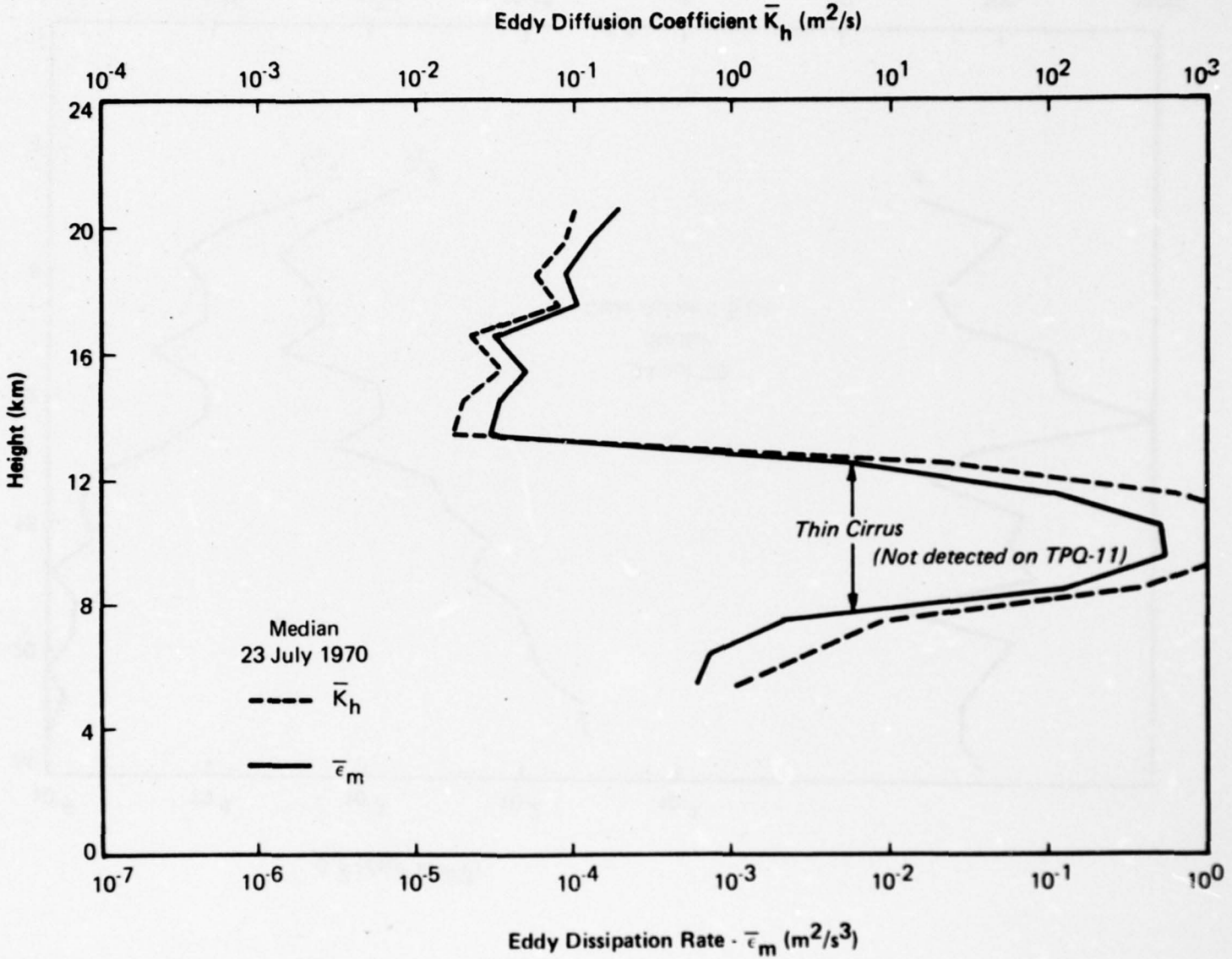


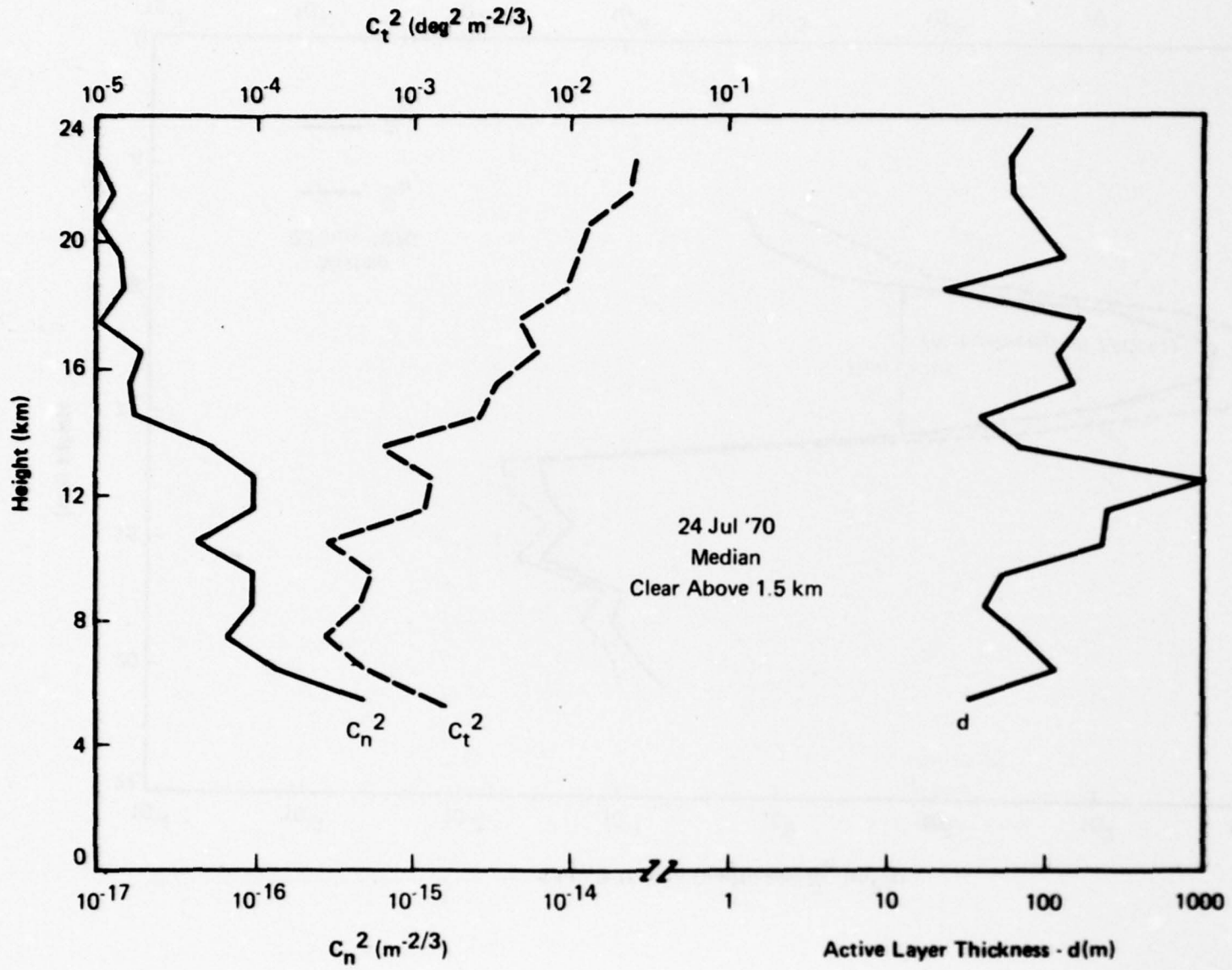
708063
708045



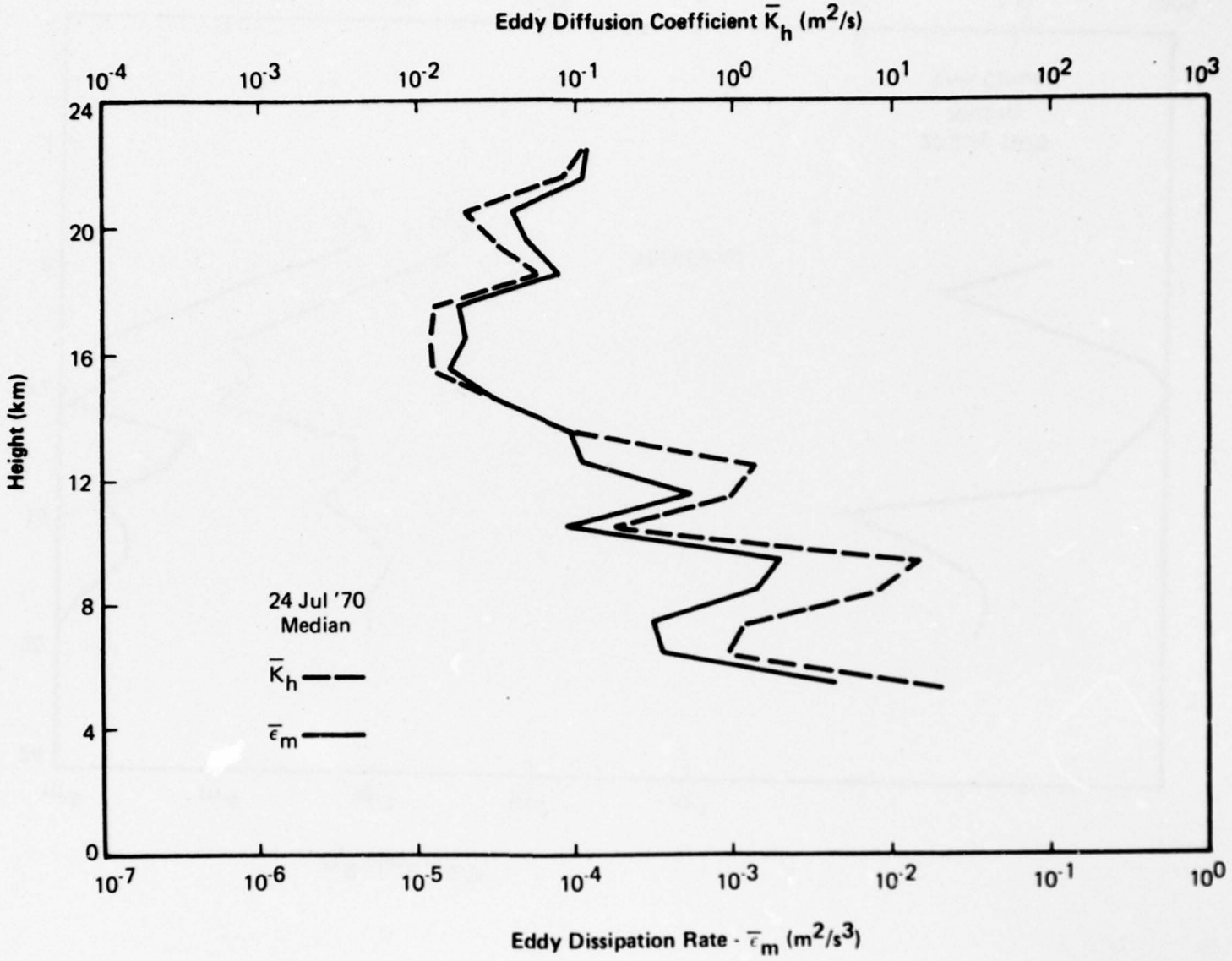
708139

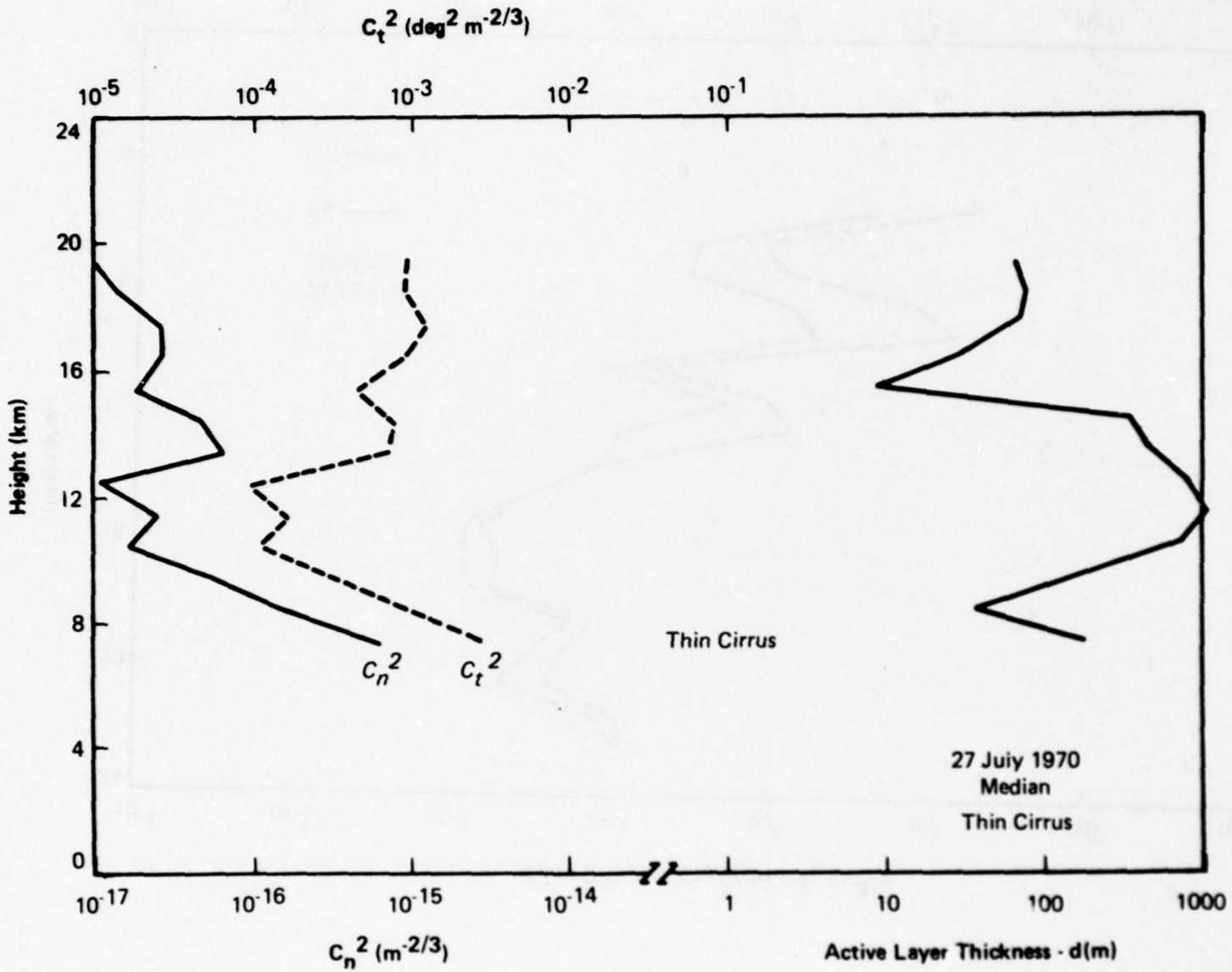
708137



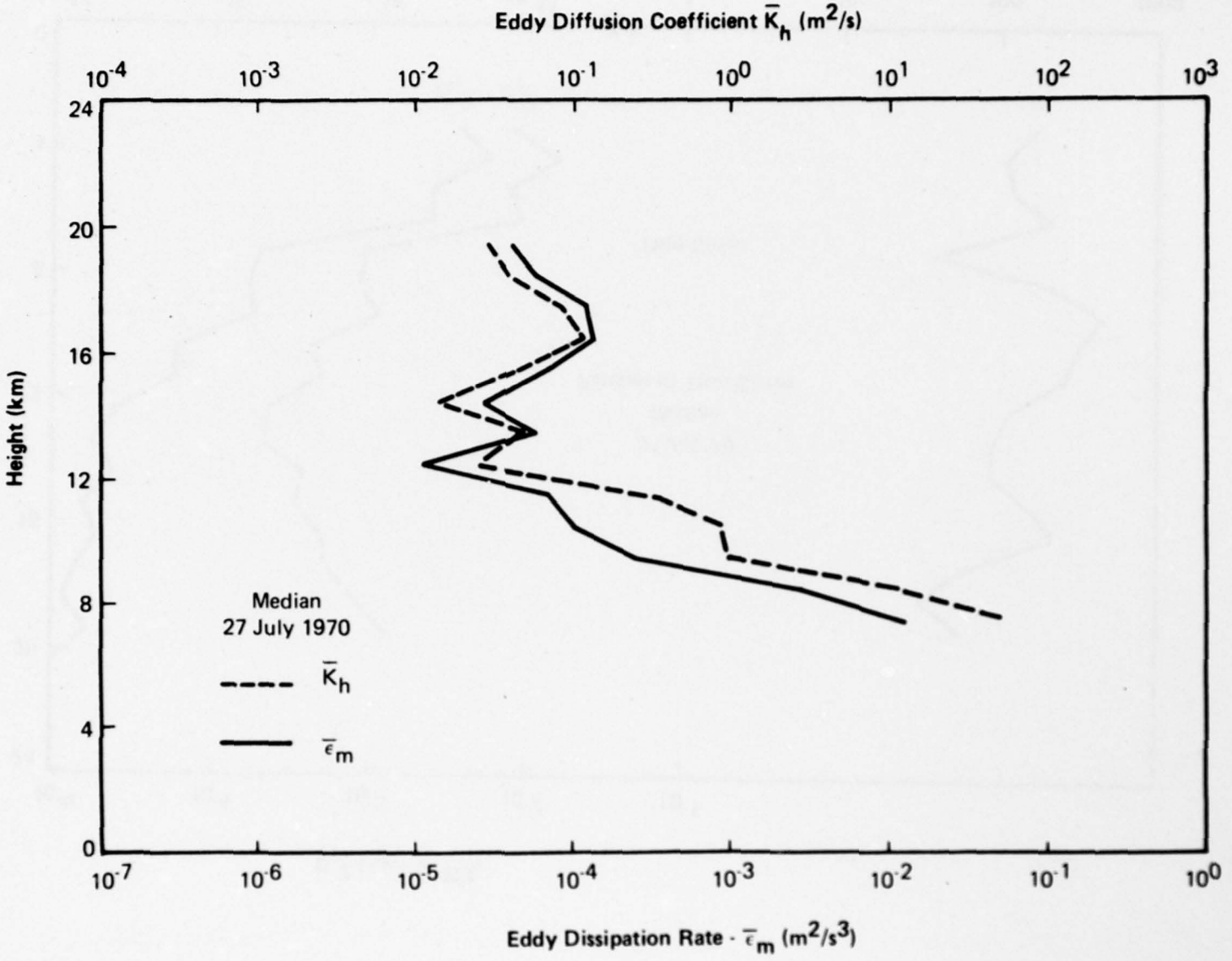

C_t^2 (deg^2 m$^{-2/3}$)
10^{-5}
10^{-4}
10^{-3}
10^{-2}
10^{-1}
24
20
16
12
8
4
0
Height (km)
24 Jul '70
Median
Clear Above 1.5 km
C_n^2
C_t^2
d
10^{-17}
10^{-16}
10^{-15}
10^{-14}
1
10
100
1000
C_n^2 (m$^{-2/3}$)
Active Layer Thickness - d(m)

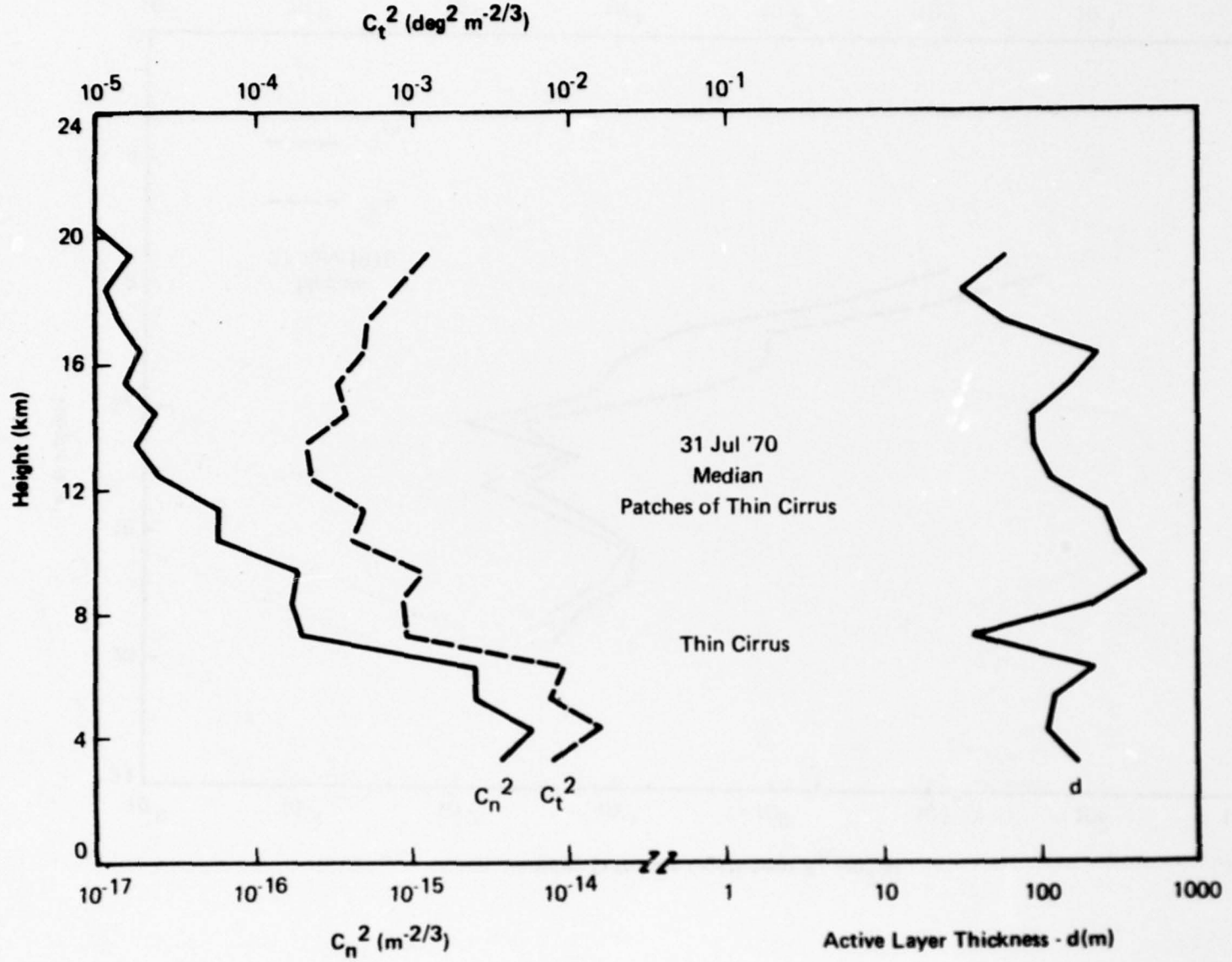
709008
708137




C_t^2 (deg^2 m$^{-2/3}$)
10^{-5}
10^{-4}
10^{-3}
10^{-2}
10^{-1}
24
20
16
12
8
4
0
Height (km)
C_n^2
C_t^2
Thin Cirrus
27 July 1970
Median
Thin Cirrus
10^{-17}
10^{-16}
10^{-15}
10^{-14}
1
10
100
1000
C_n^2 (m$^{-2/3}$)
Active Layer Thickness - d(m)

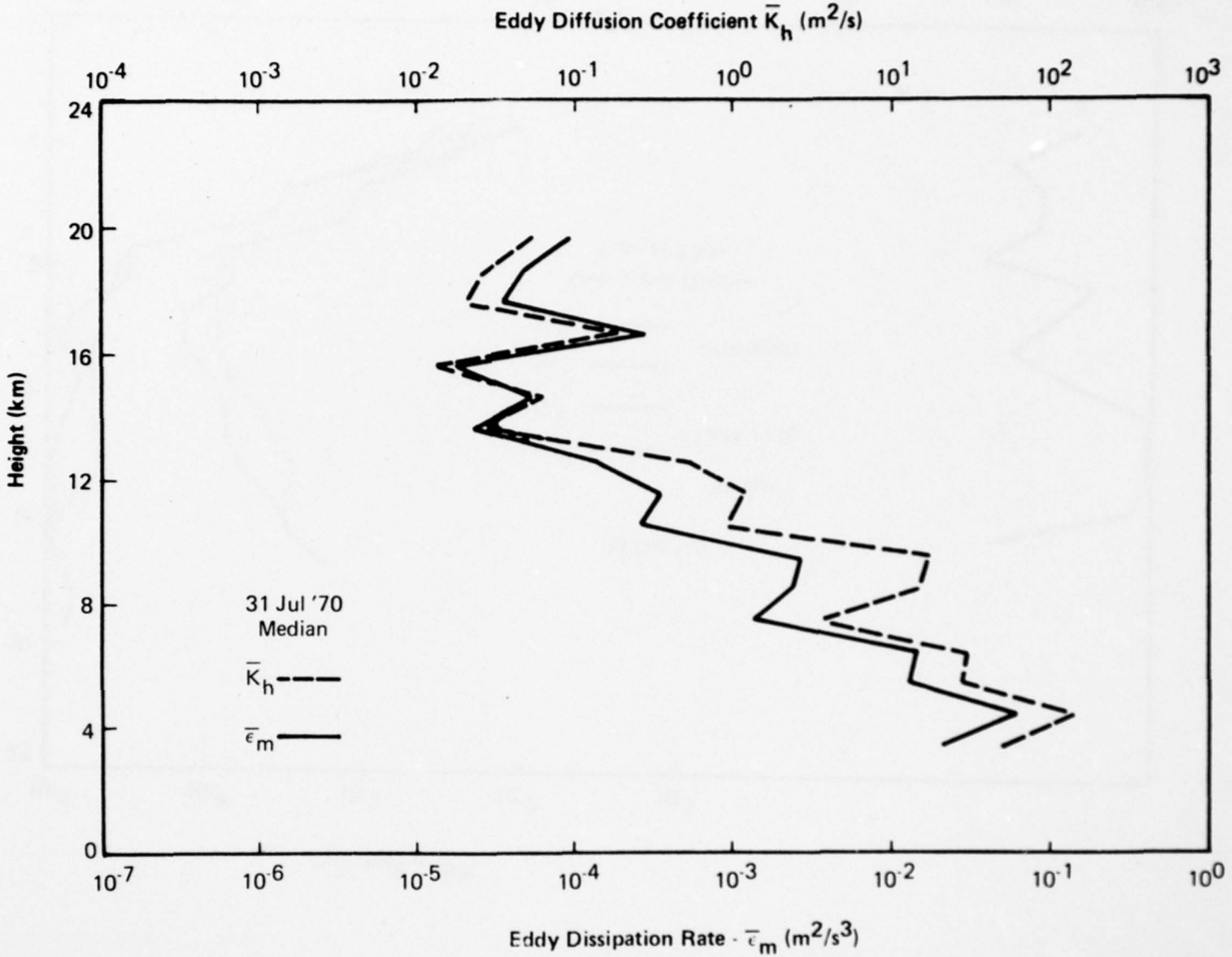
708138
708137

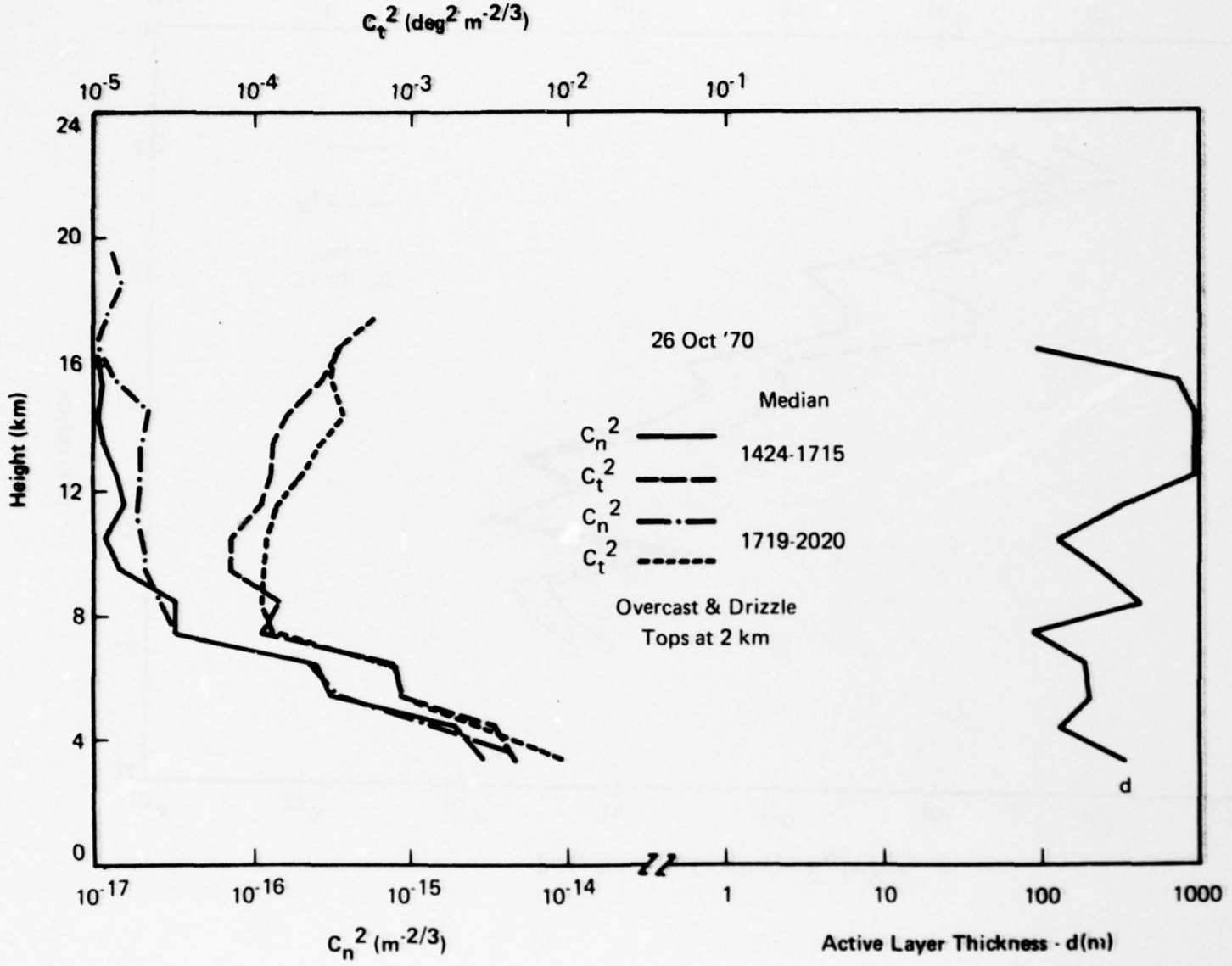



C_t^2 (deg^2 m$^{-2/3}$)
10^{-5}
10^{-4}
10^{-3}
10^{-2}
10^{-1}
24
20
16
12
8
4
0
Height (km)
31 Jul '70
Median
Patches of Thin Cirrus
Thin Cirrus
C_n^2
C_t^2
d
10^{-17}
10^{-16}
10^{-15}
10^{-14}
1
10
100
1000
C_n^2 (m$^{-2/3}$)
Active Layer Thickness - d(m)

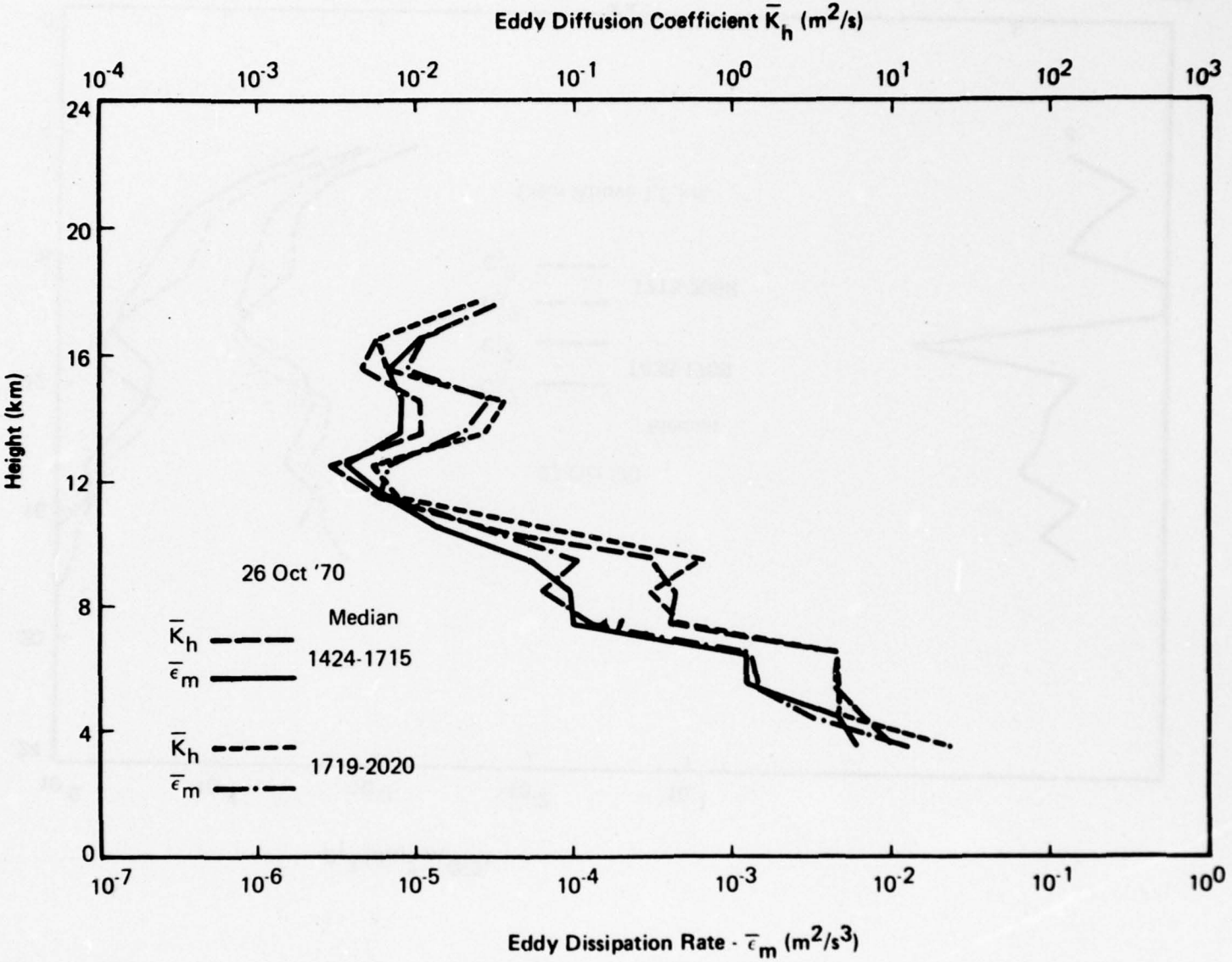
709007

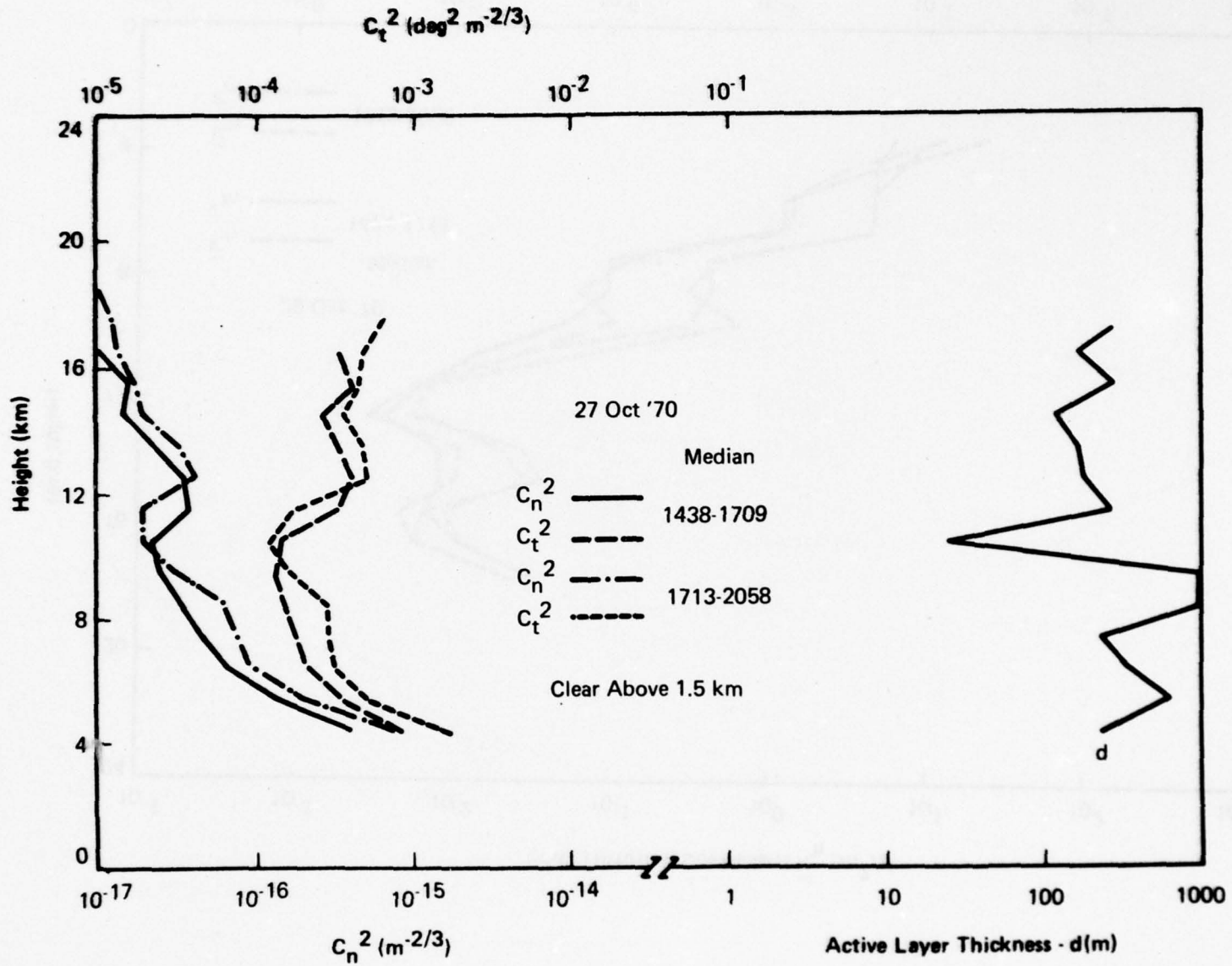
708137




C_t^2 (deg^2 m$^{-2/3}$)
10^{-5}
10^{-4}
10^{-3}
10^{-2}
10^{-1}
24
20
16
12
8
4
0
Height (km)
26 Oct '70
Median
C_n^2
1424-1715
C_t^2
C_n^2
1719-2020
C_t^2
Overcast & Drizzle
Tops at 2 km
d
10^{-17}
10^{-16}
10^{-15}
10^{-14}
1
10
100
1000
C_n^2 (m$^{-2/3}$)
Active Layer Thickness - d(m)

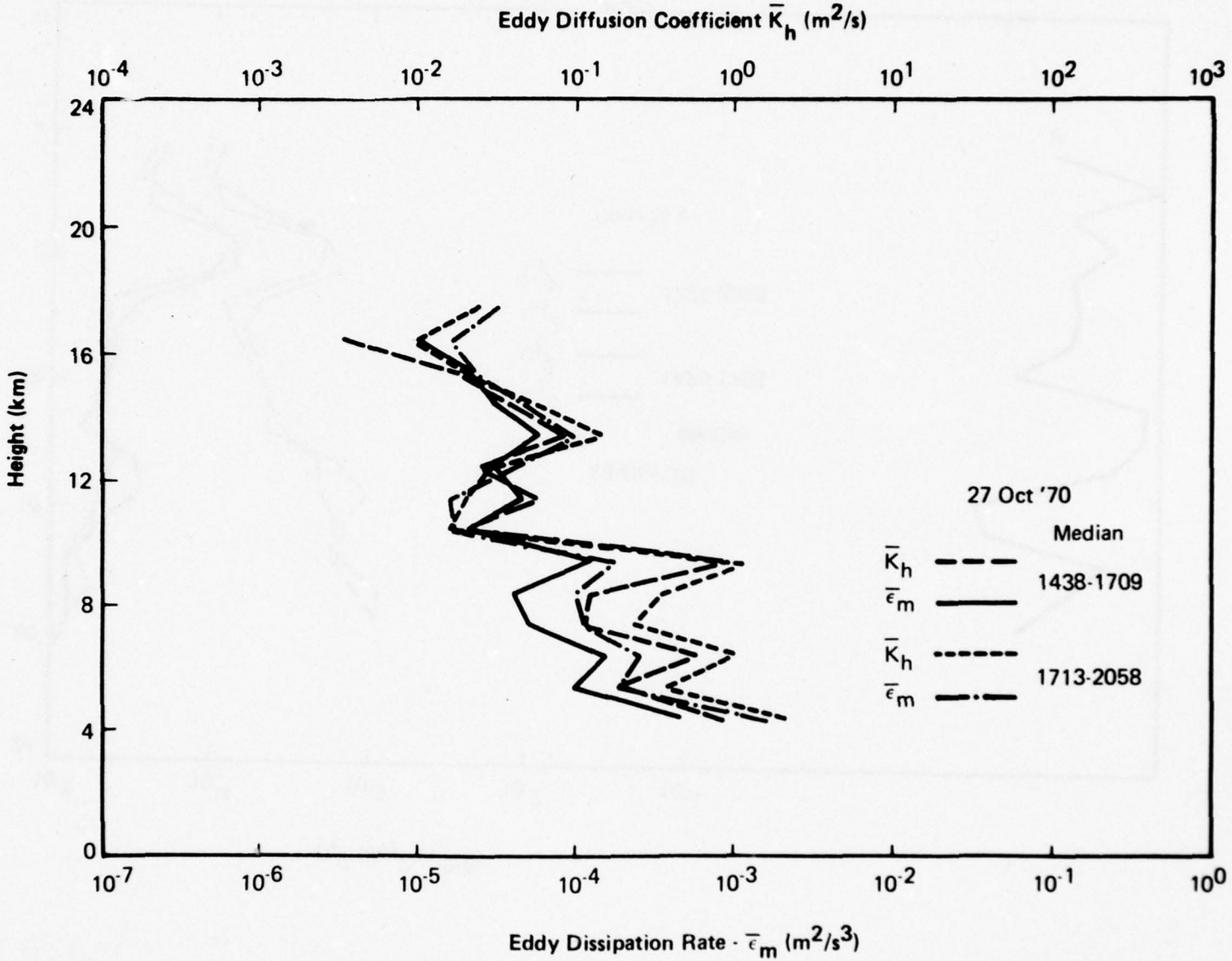
709006
708137

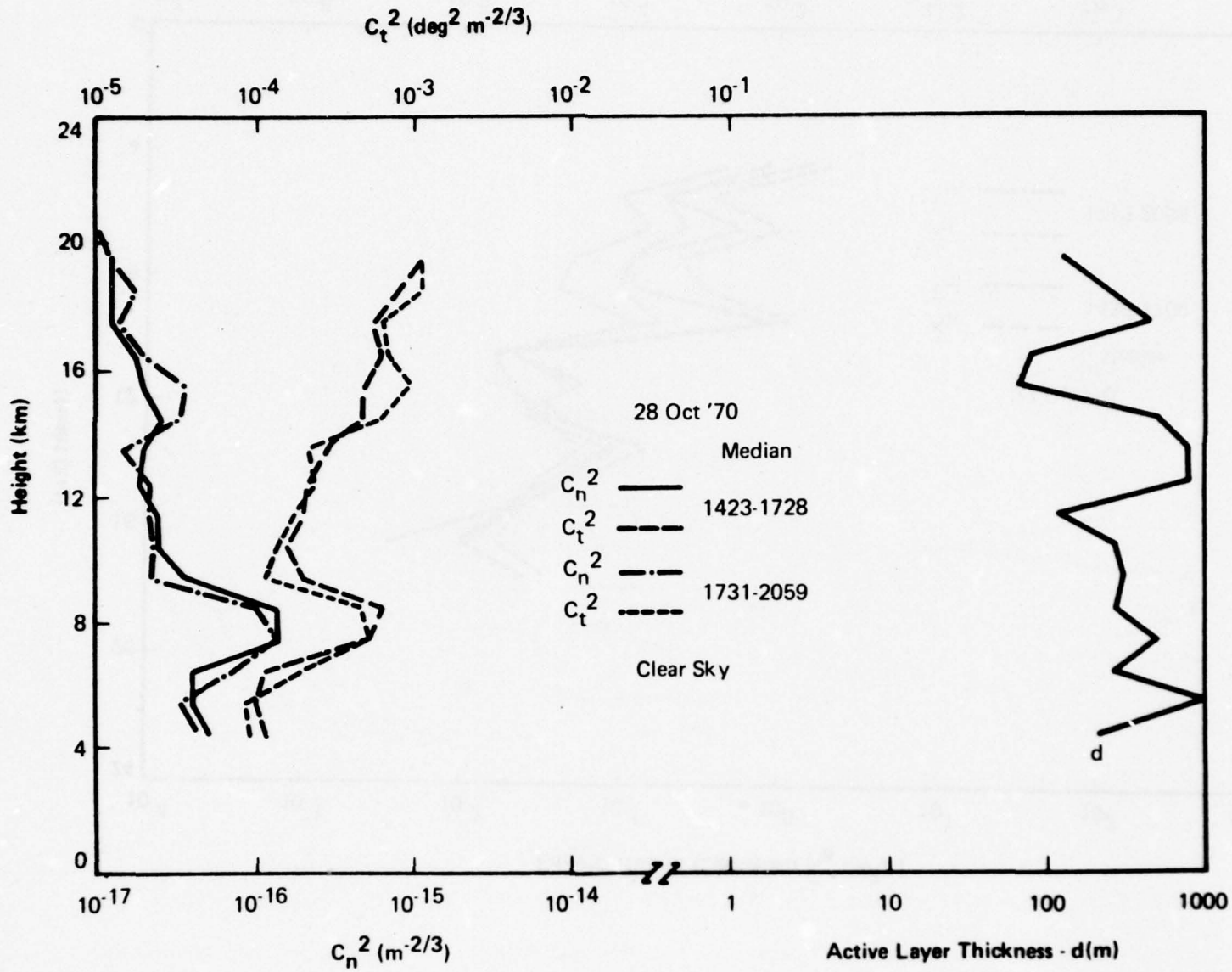



C_t^2 (deg^2 m$^{-2/3}$)
10^{-5}
10^{-4}
10^{-3}
10^{-2}
10^{-1}
24
20
16
12
8
4
0
Height (km)
27 Oct '70
Median
C_n^2
C_t^2
1438-1709
C_n^2
C_t^2
1713-2058
Clear Above 1.5 km
d
10^{-17}
10^{-16}
10^{-15}
10^{-14}
1
10
100
1000
C_n^2 (m$^{-2/3}$)
Active Layer Thickness - d(m)

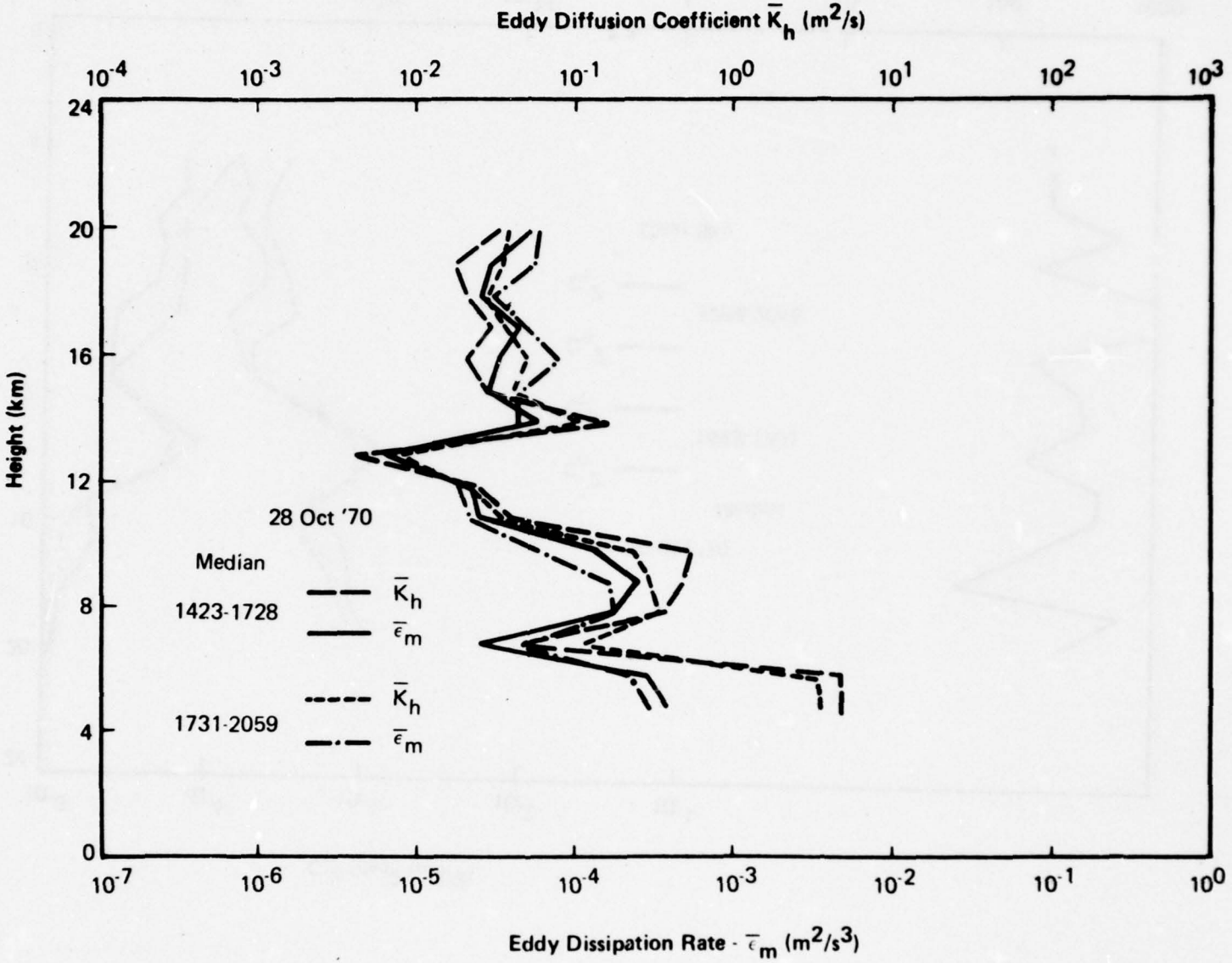
709005

708137

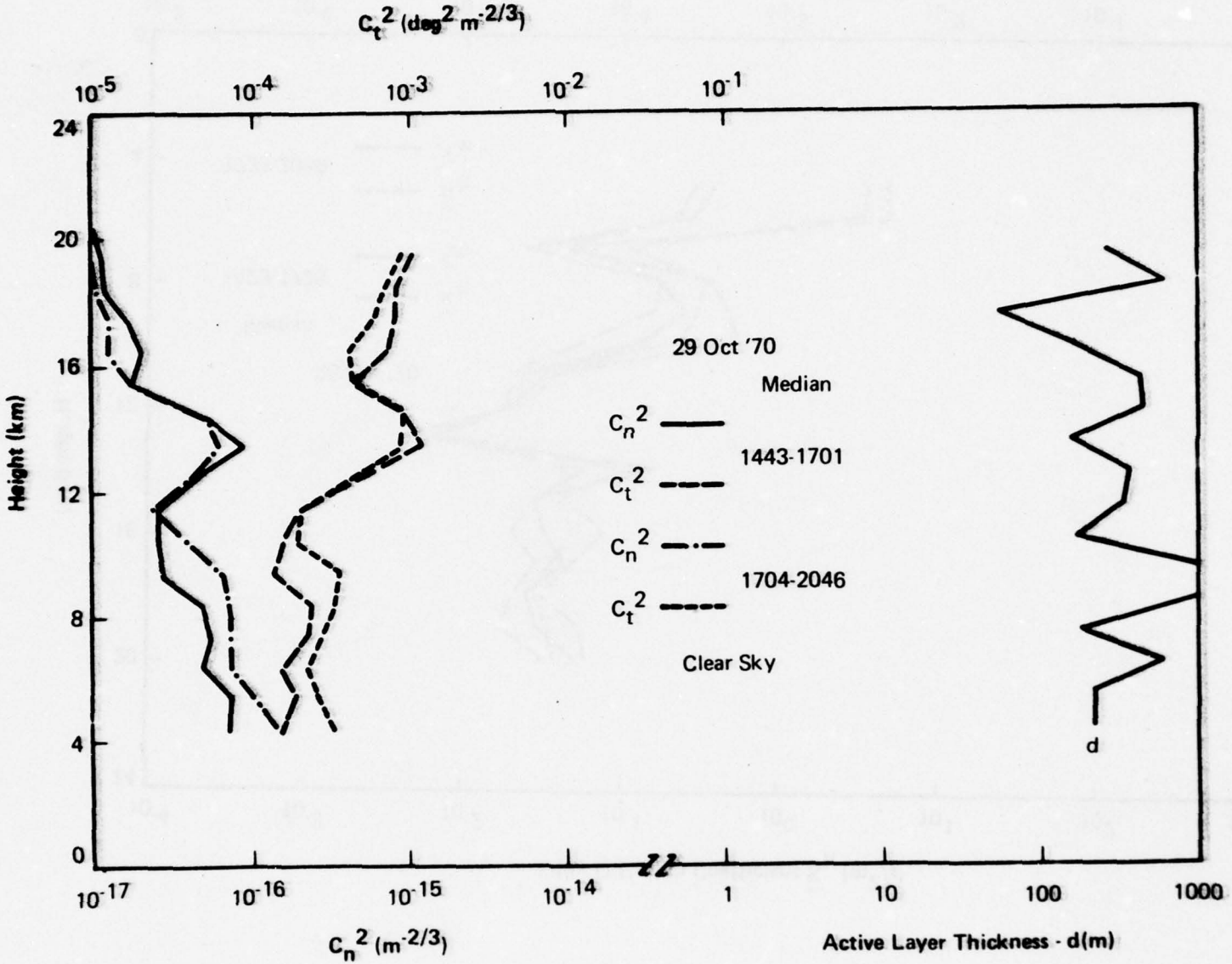



C_t^2 (deg^2 m$^{-2/3}$)
10^{-5}
10^{-4}
10^{-3}
10^{-2}
10^{-1}
24
20
16
12
8
4
0
Height (km)
28 Oct '70
Median
C_n^2
C_t^2
1423-1728
C_n^2
C_t^2
1731-2059
Clear Sky
d
10^{-17}
10^{-16}
10^{-15}
10^{-14}
1
10
100
1000
C_n^2 (m$^{-2/3}$)
Active Layer Thickness - d(m)

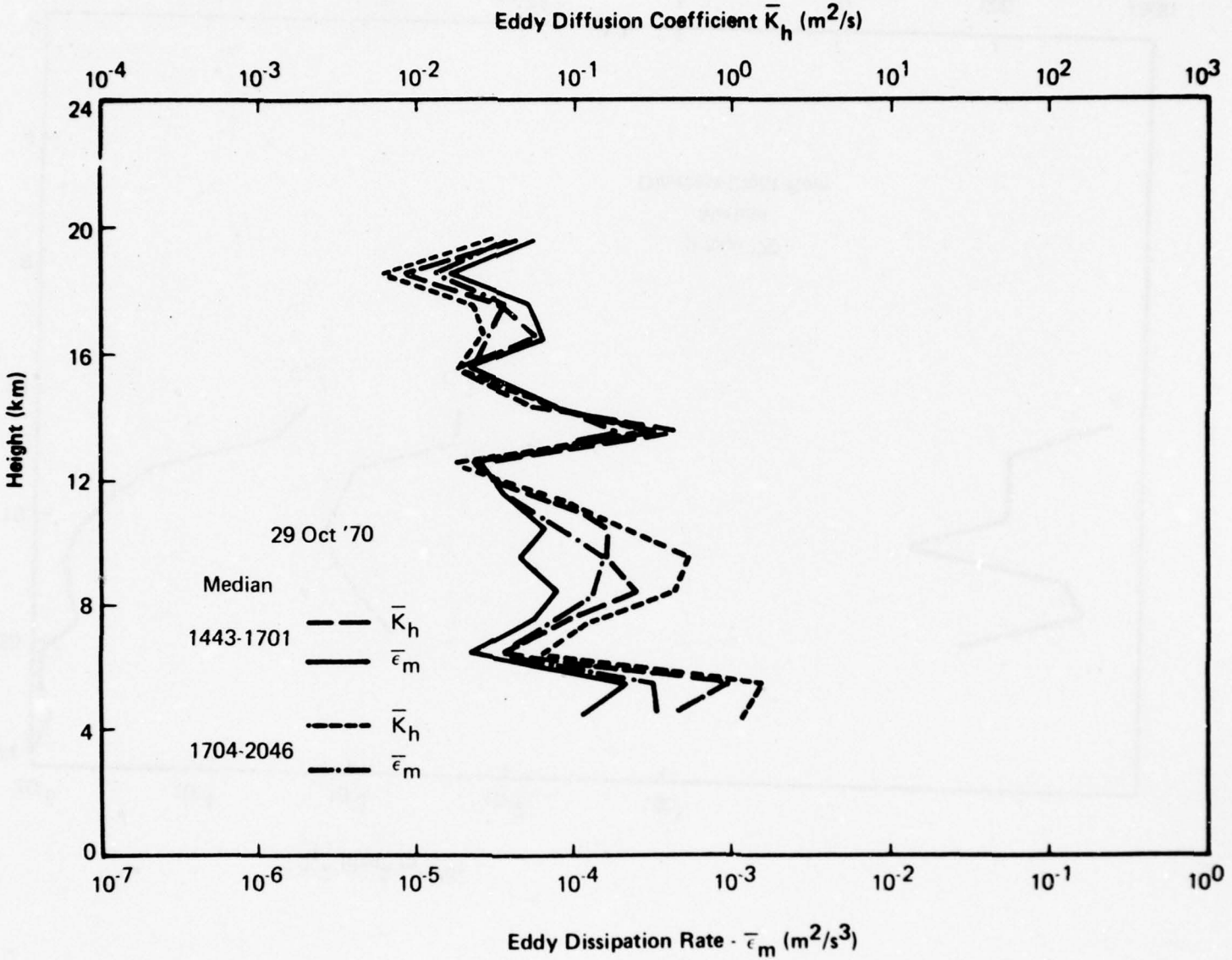
709004
708137



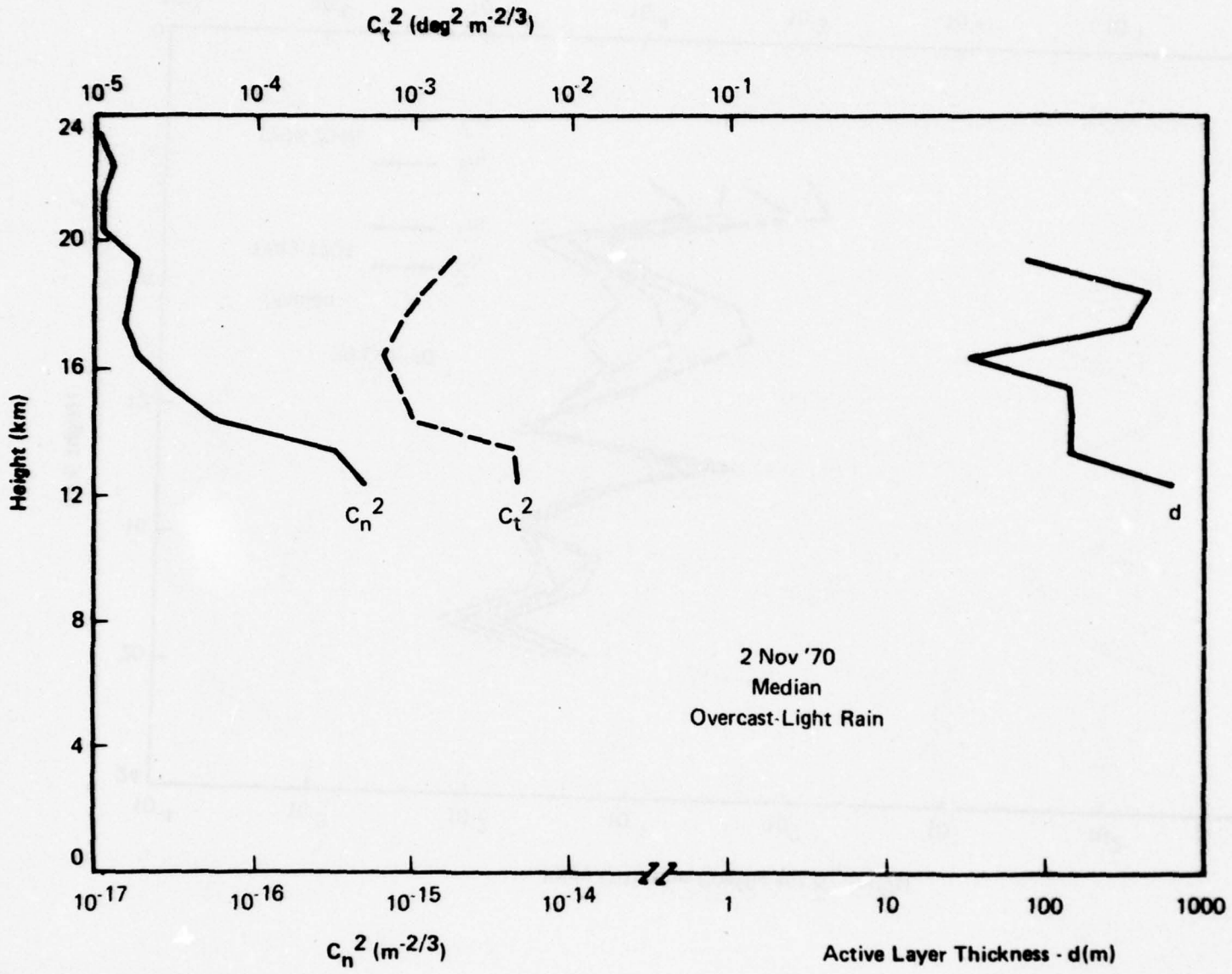
709013
708045



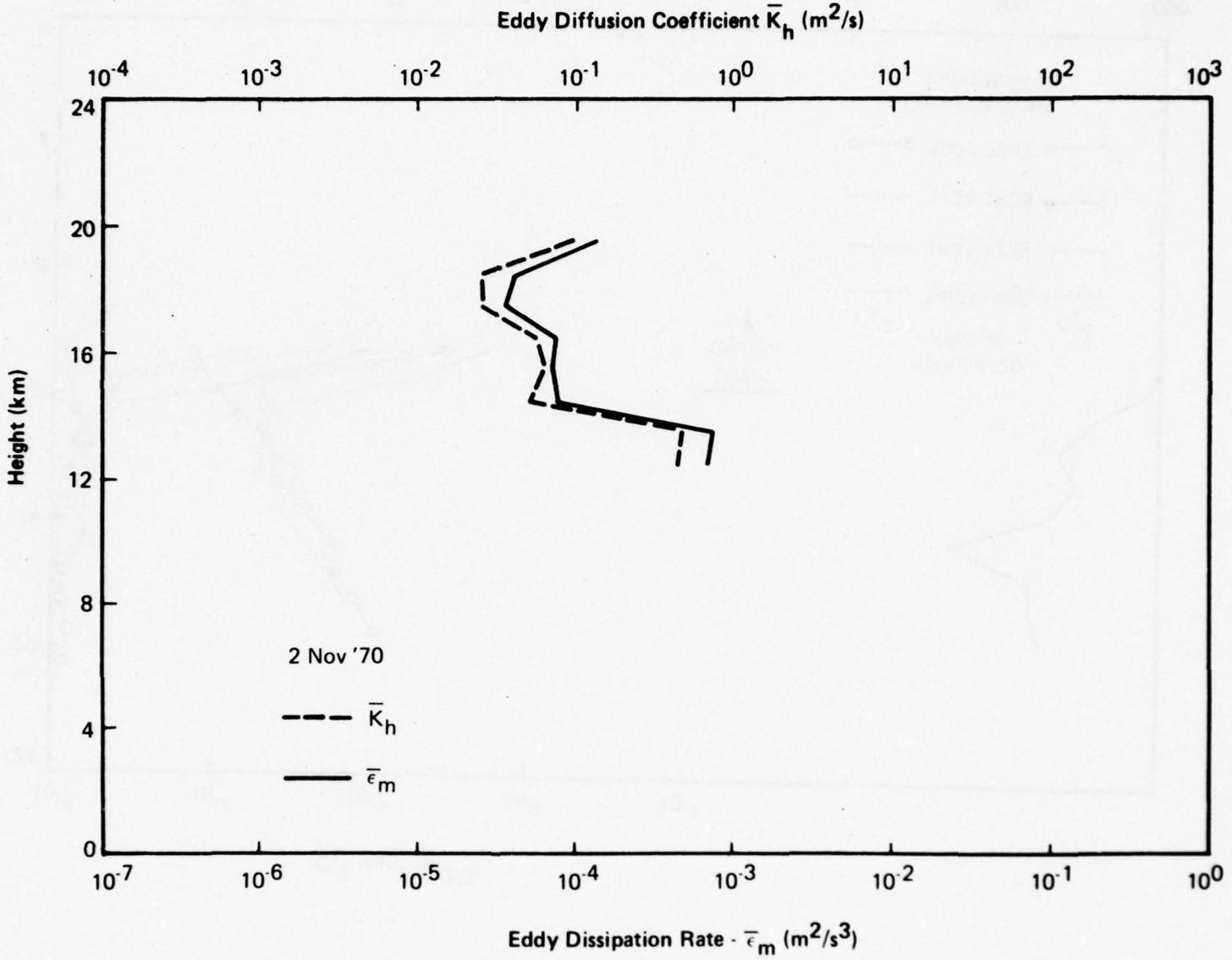
709003
708137

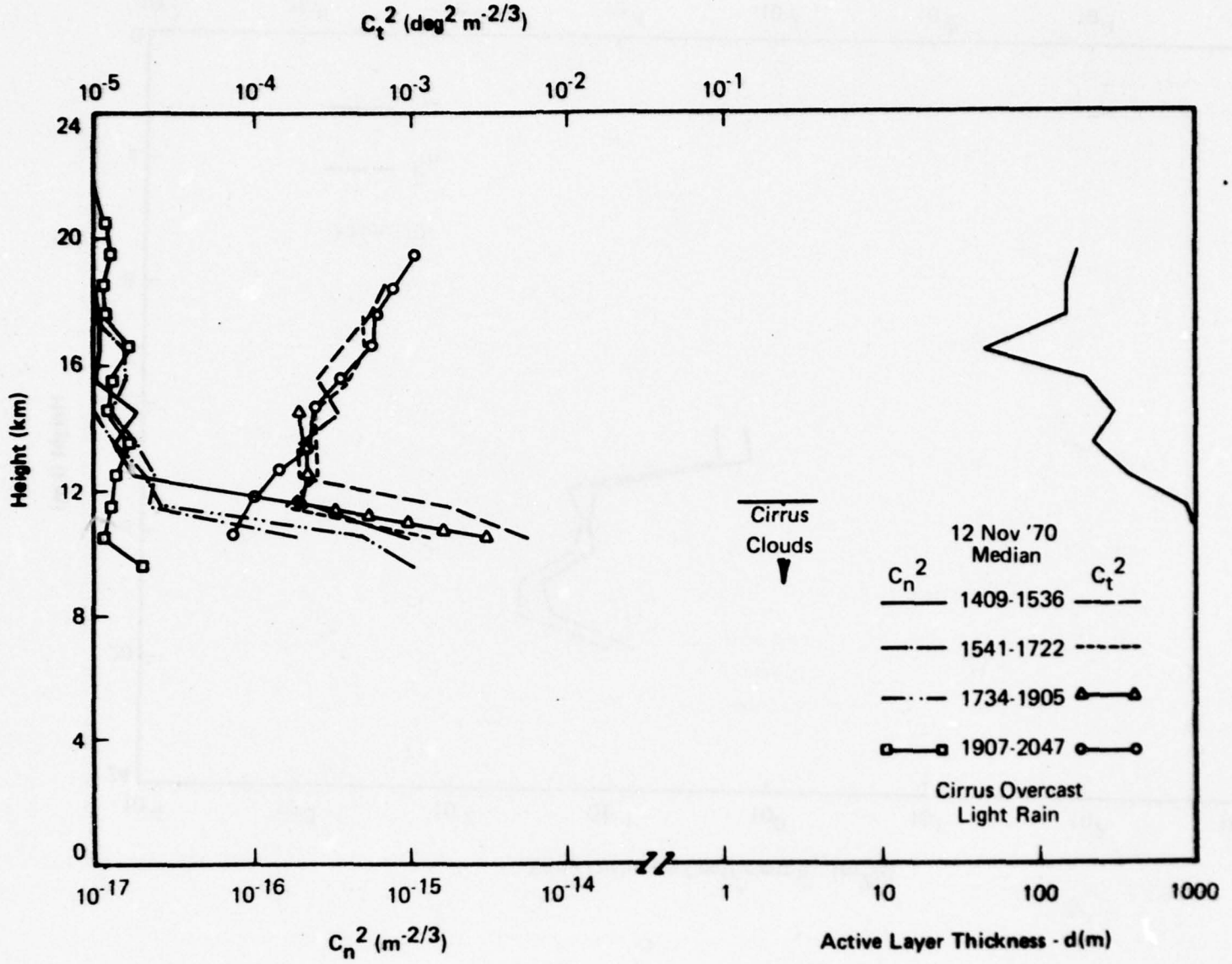


709012
708045

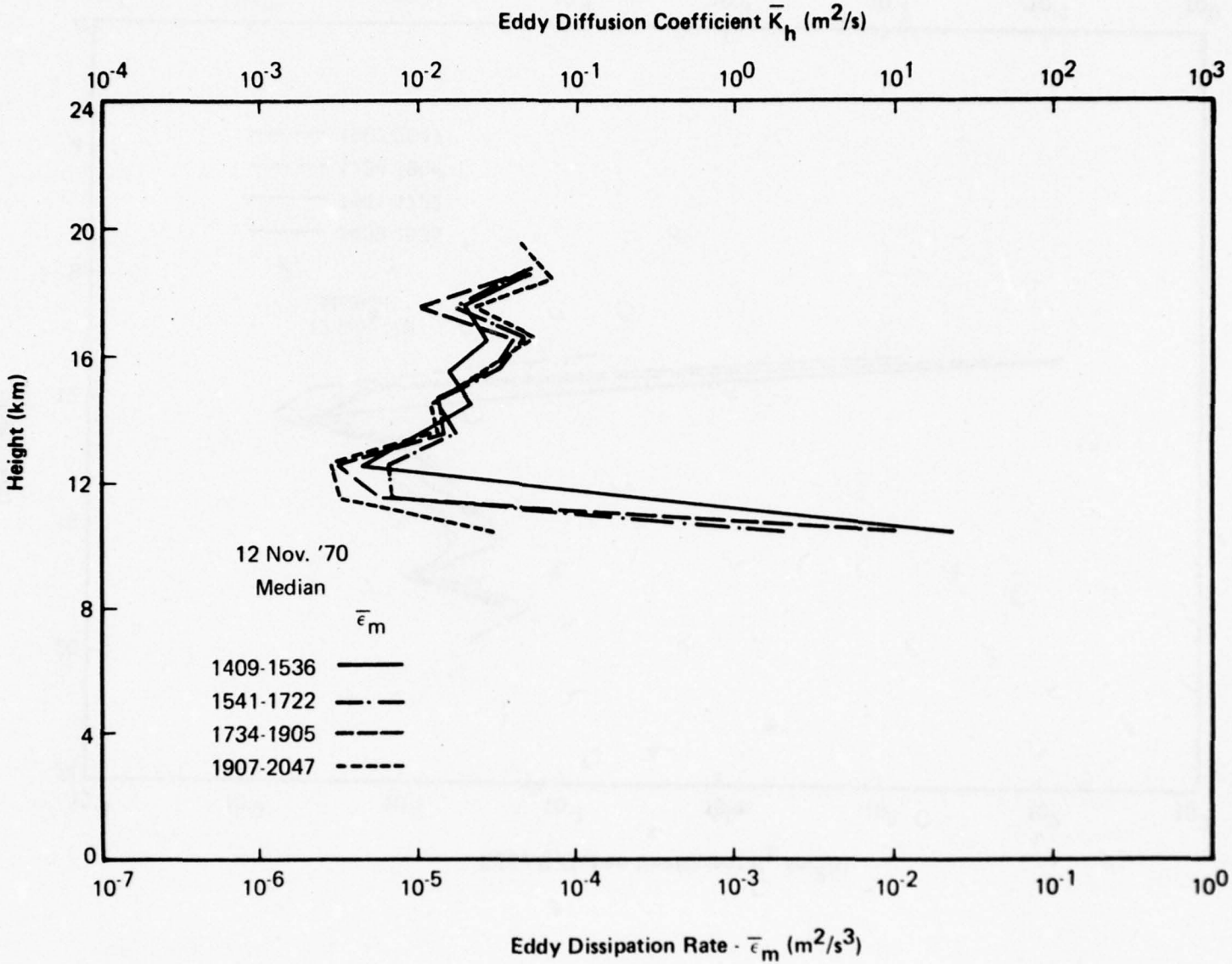


709002
708137



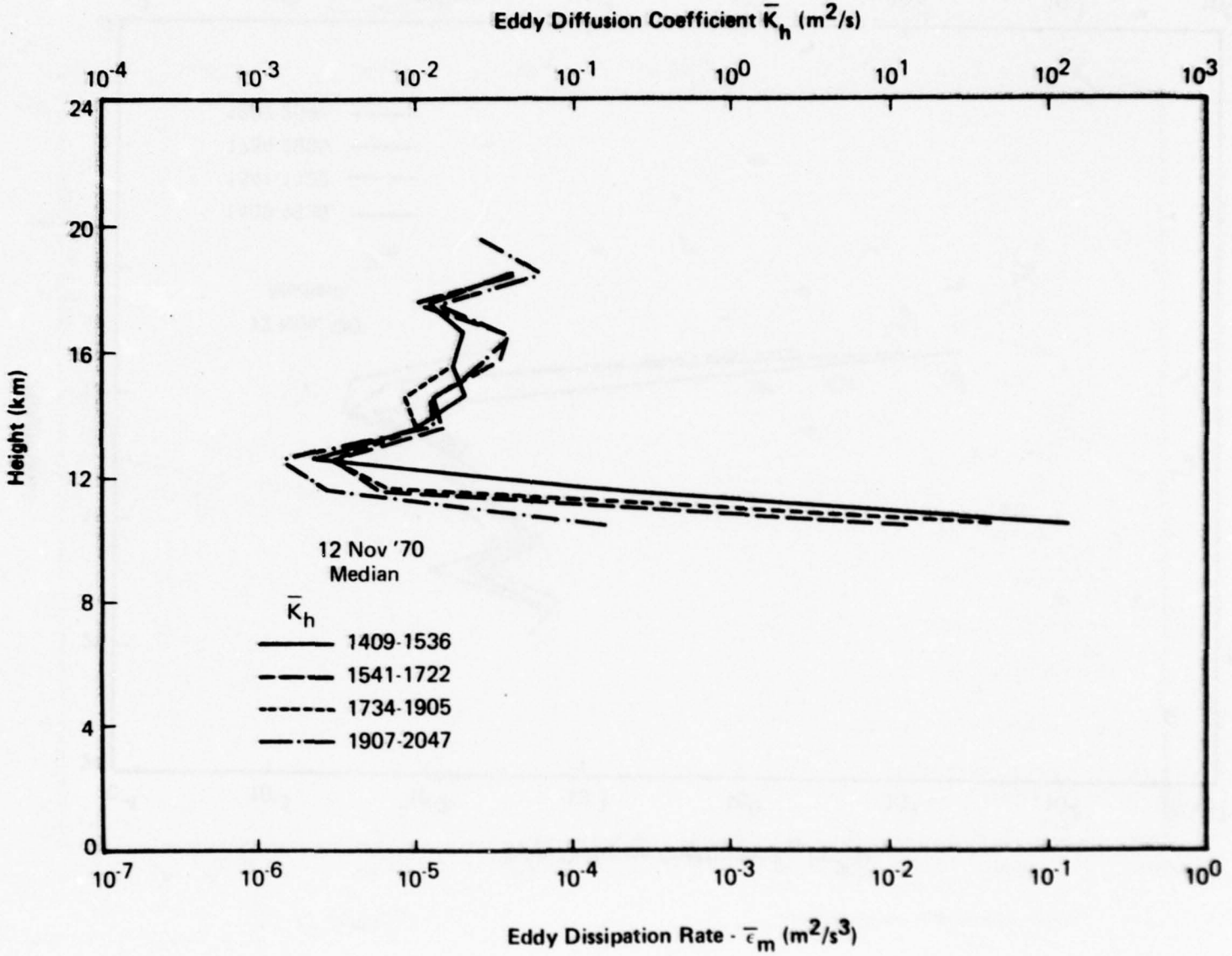

C_t^2 (deg^2 m$^{-2/3}$)
10^{-5}
10^{-4}
10^{-3}
10^{-2}
10^{-1}
24
20
16
12
8
4
0
Height (km)
Cirrus
Clouds
12 Nov '70
Median
C_n^2
C_t^2
1409-1536
1541-1722
1734-1905
1907-2047
Cirrus Overcast
Light Rain
10^{-17}
10^{-16}
10^{-15}
10^{-14}
1
10
100
1000
C_n^2 (m$^{-2/3}$)
Active Layer Thickness - d(m)

709010
708137



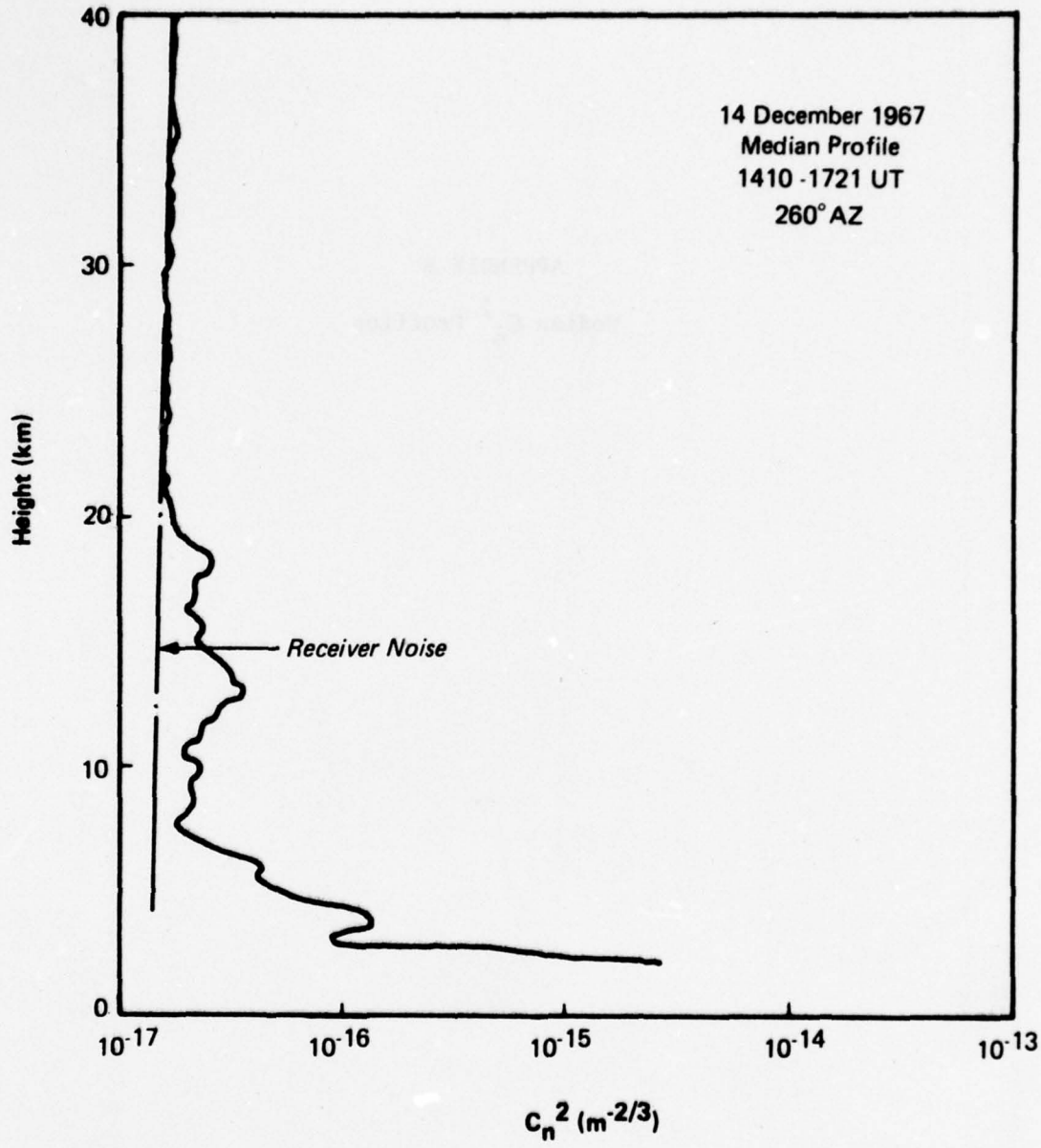
709009

708137

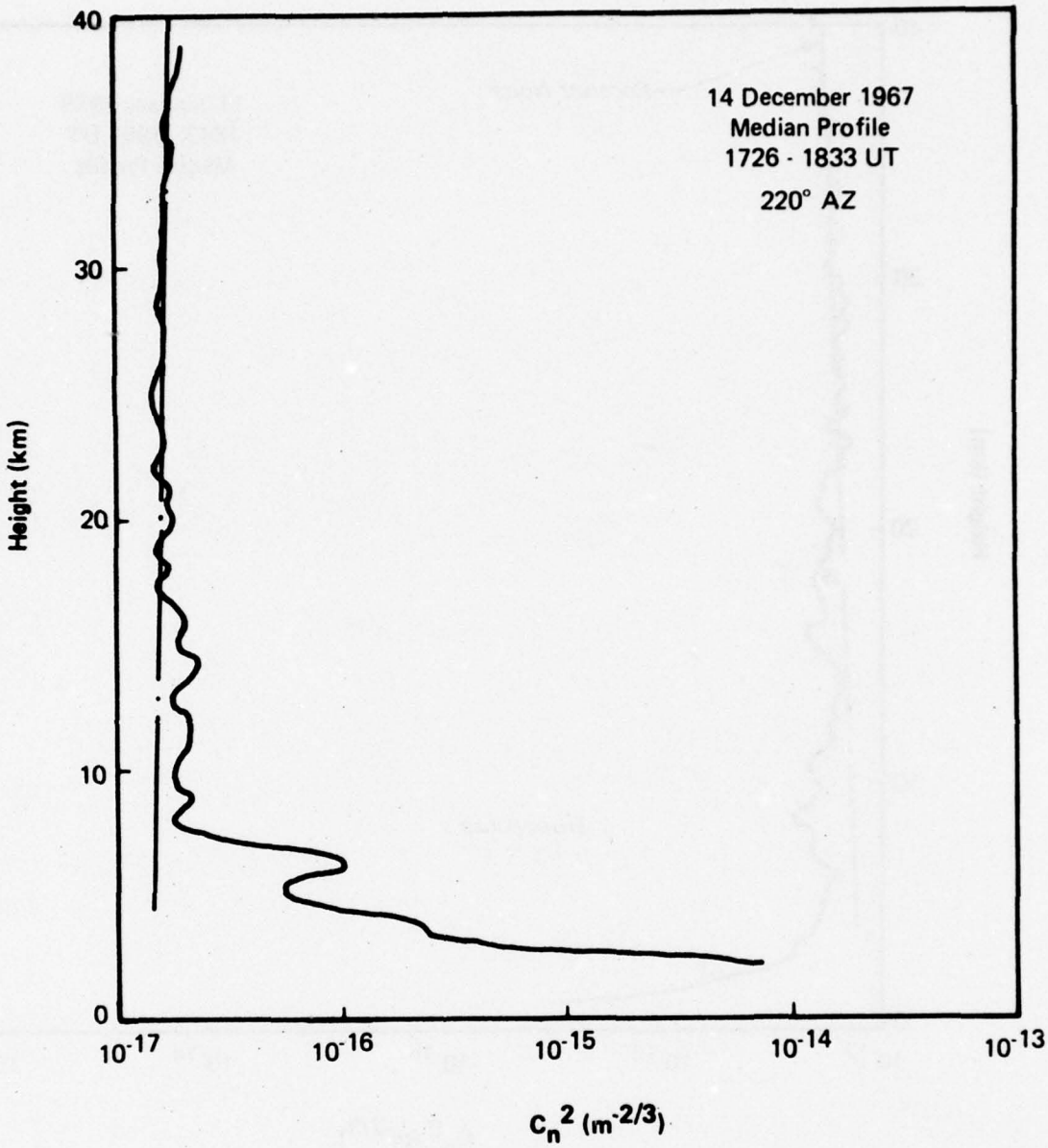


APPENDIX B

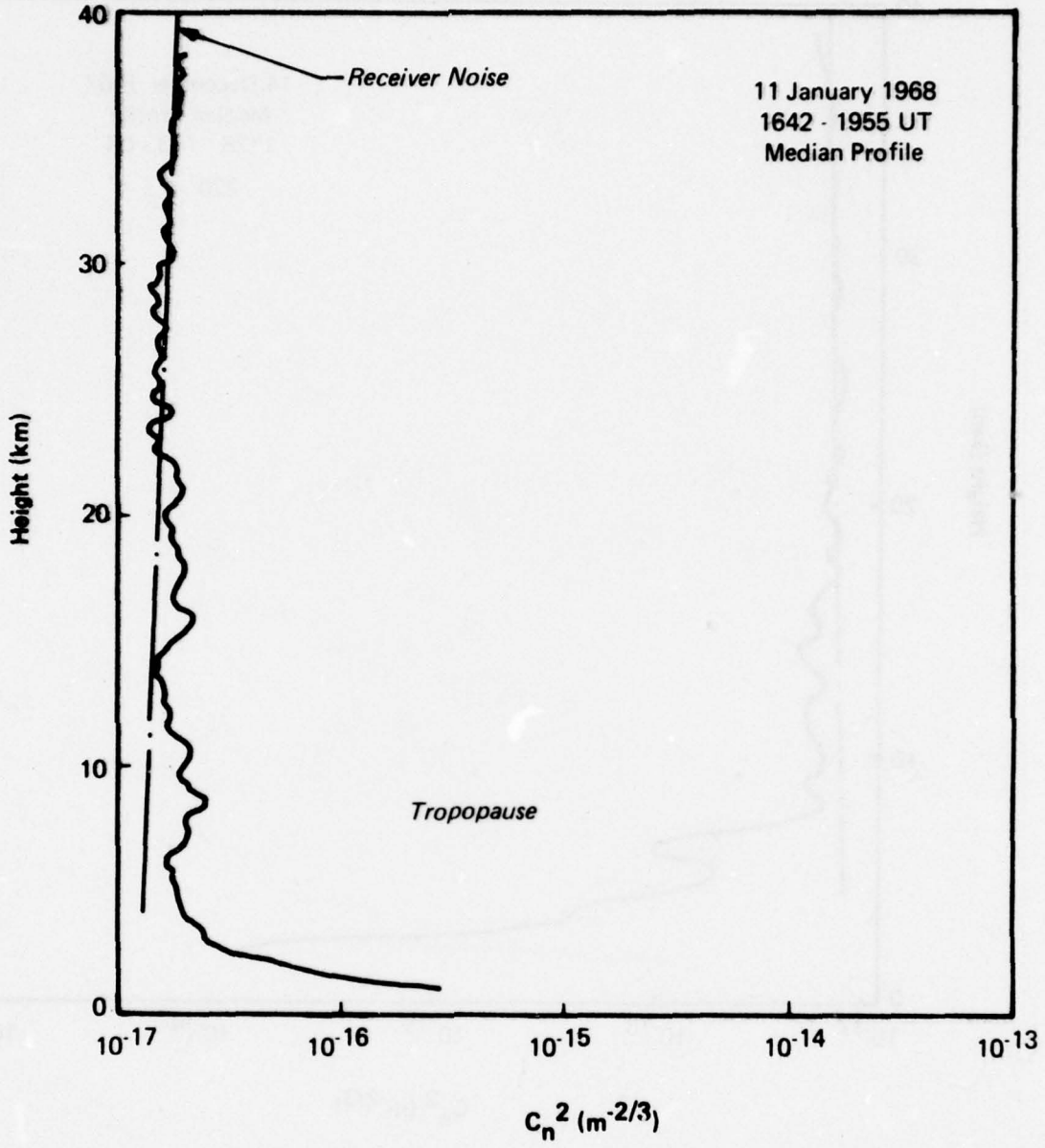
Median C_n^2 Profiles


14 December 1967
Median Profile
1410 -1721 UT
260° AZ
Height (km)
40
30
20
10
0
Receiver Noise
10^{-17}
10^{-16}
10^{-15}
10^{-14}
10^{-13}
C_n^2 ($m^{-2/3}$)

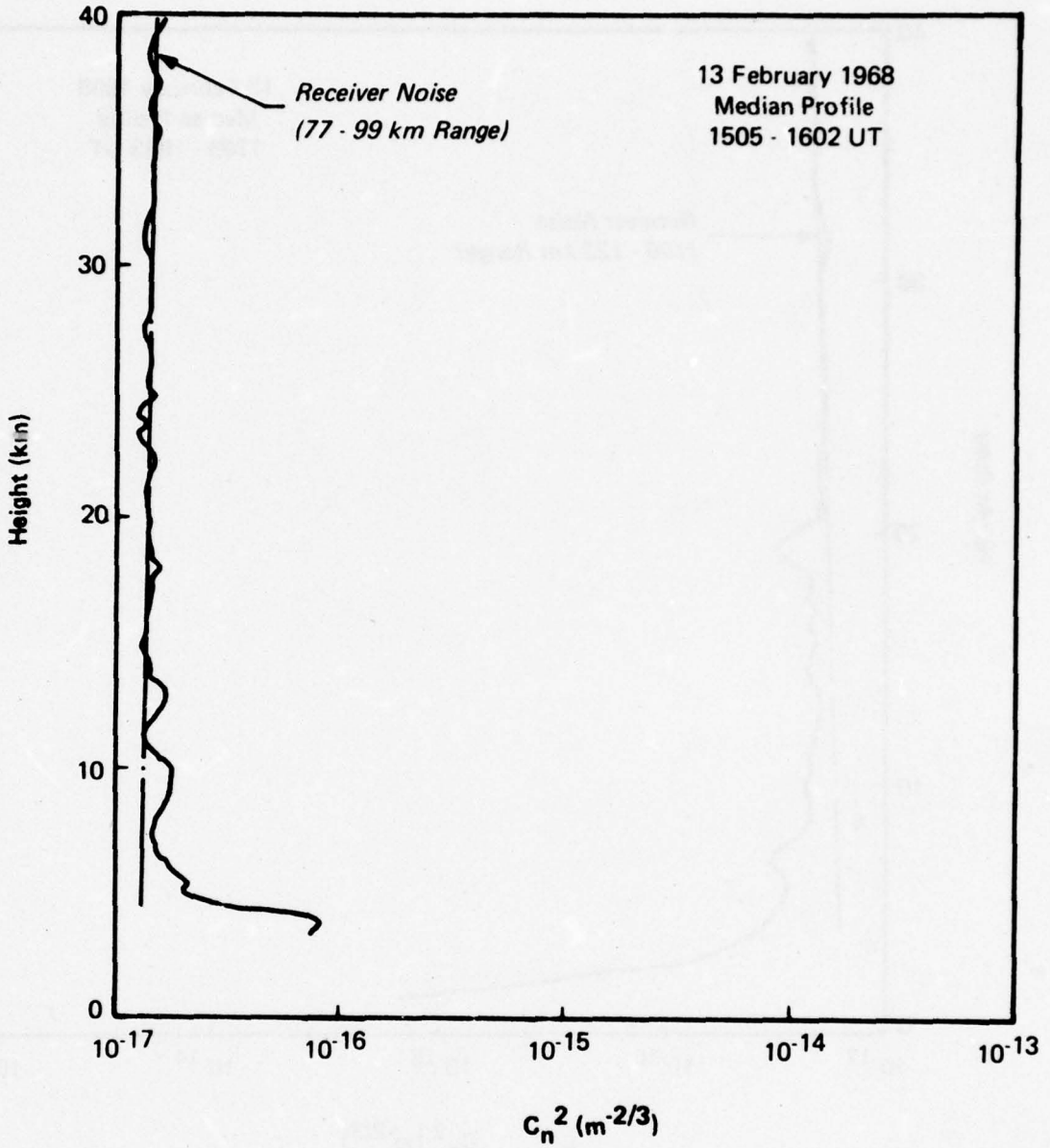
708106


14 December 1967
Median Profile
1726 - 1833 UT
220° AZ
Height (km)
40
30
20
10
0
10^{-17}
10^{-16}
10^{-15}
10^{-14}
10^{-13}
C_n^2 ($m^{-2/3}$)

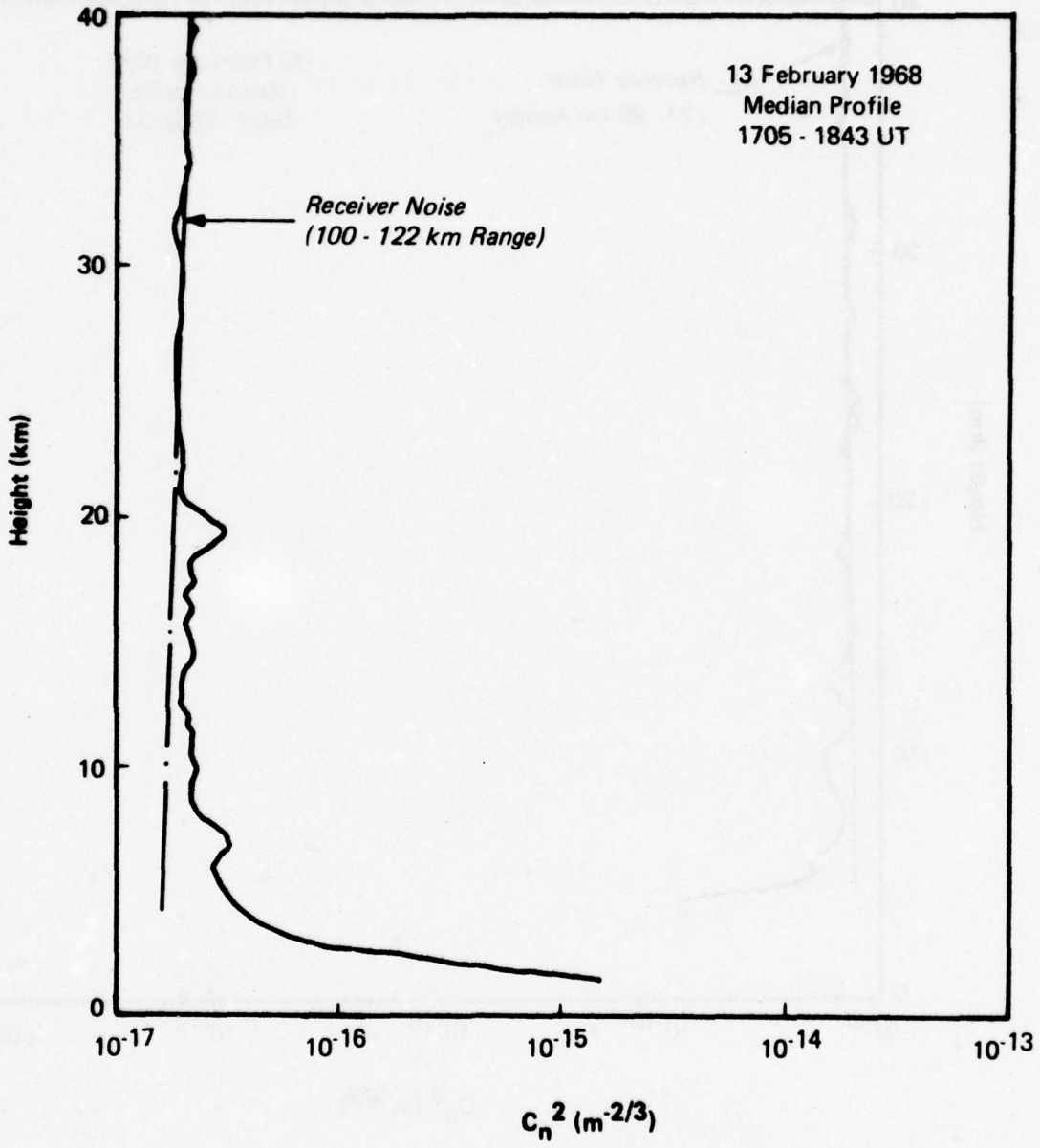
708109

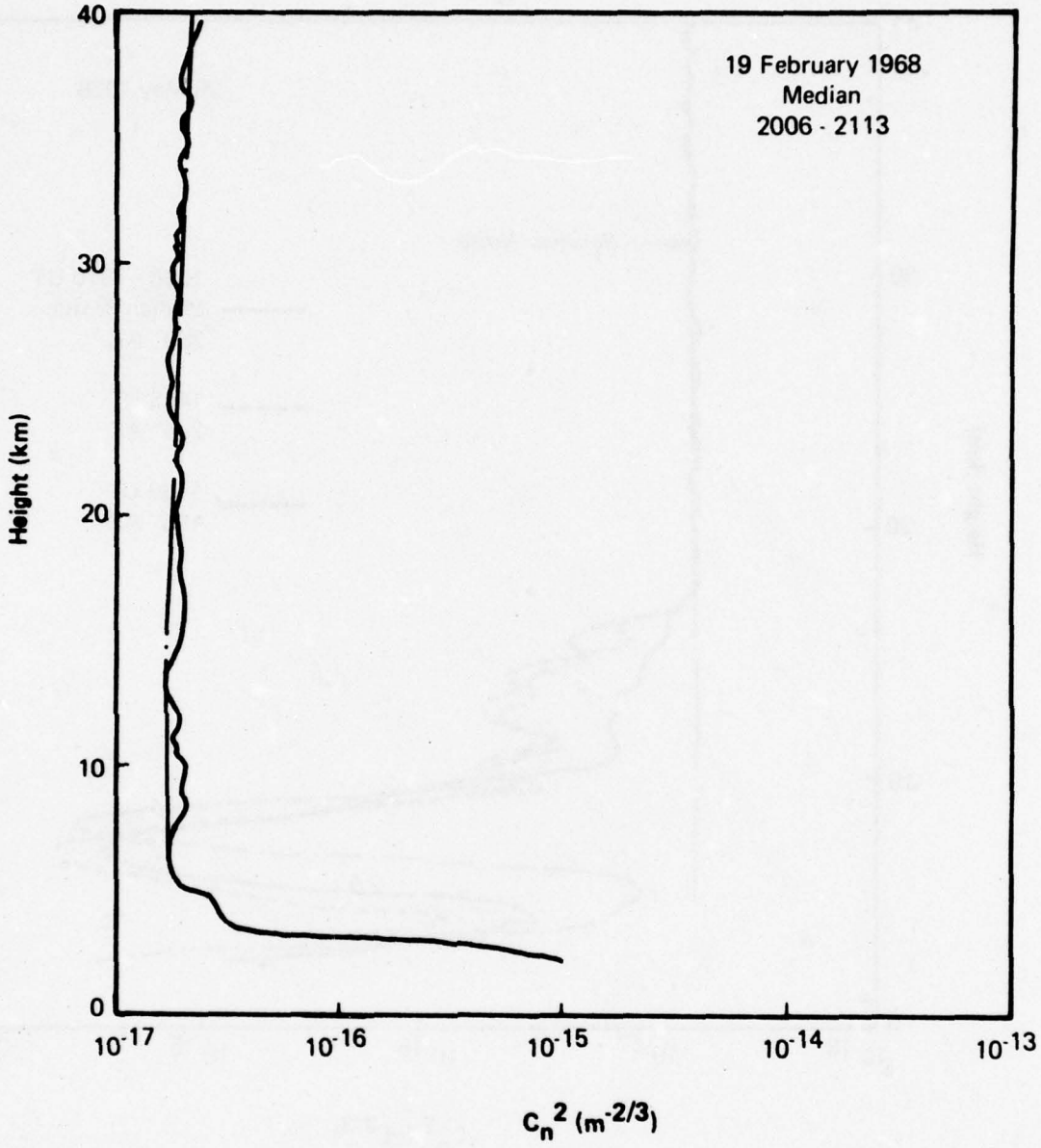

40
30
20
10
0
Height (km)
Receiver Noise
11 January 1968
1642 - 1955 UT
Median Profile
Tropopause
10^{-17}
10^{-16}
10^{-15}
10^{-14}
10^{-13}
C_n^2 ($m^{-2/3}$)

708110

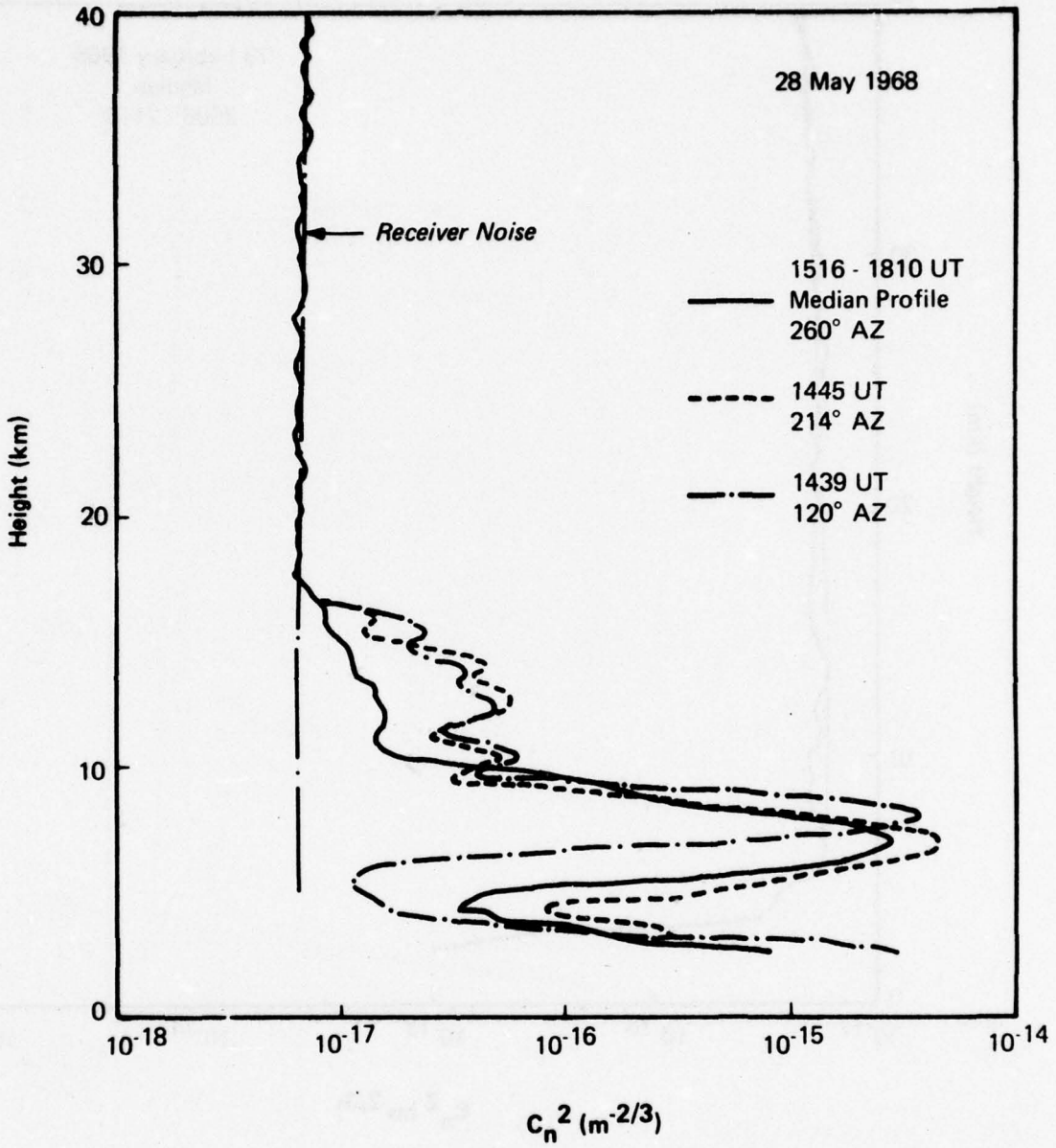

40
30
20
10
0
Height (km)
Receiver Noise
(77 - 99 km Range)
13 February 1968
Median Profile
1505 - 1602 UT
10^{-17}
10^{-16}
10^{-15}
10^{-14}
10^{-13}
C_n^2 ($m^{-2/3}$)

708111

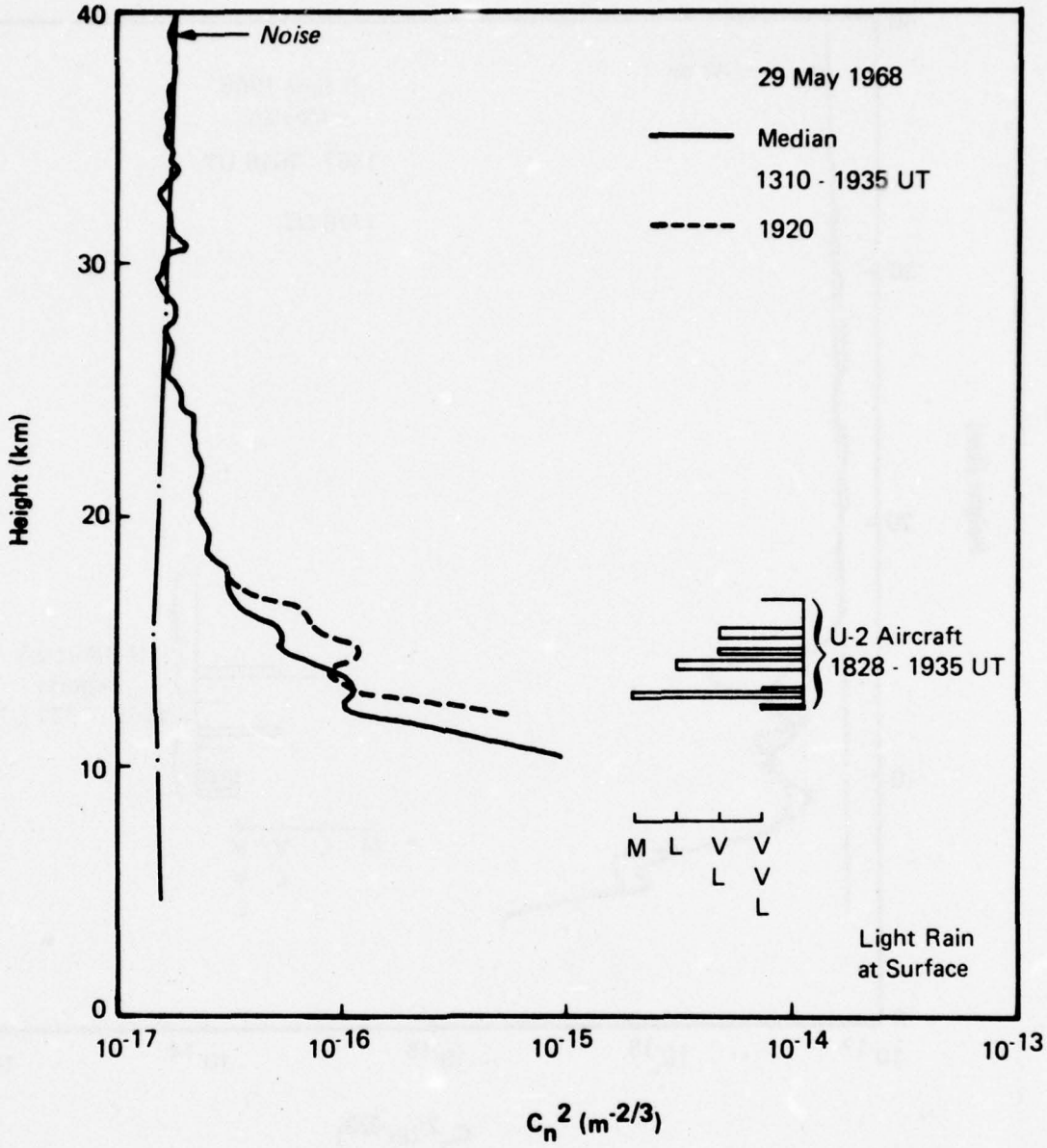

13 February 1968
Median Profile
1705 - 1843 UT
Receiver Noise
(100 - 122 km Range)
Height (km)
40
30
20
10
0
10-17
10-16
10-15
10-14
10-13
Cn2 (m-2/3)


19 February 1968
Median
2006 - 2113
Height (km)
40
30
20
10
0
10^{-17}
10^{-16}
10^{-15}
10^{-14}
10^{-13}
C_n^2 ($m^{-2/3}$)

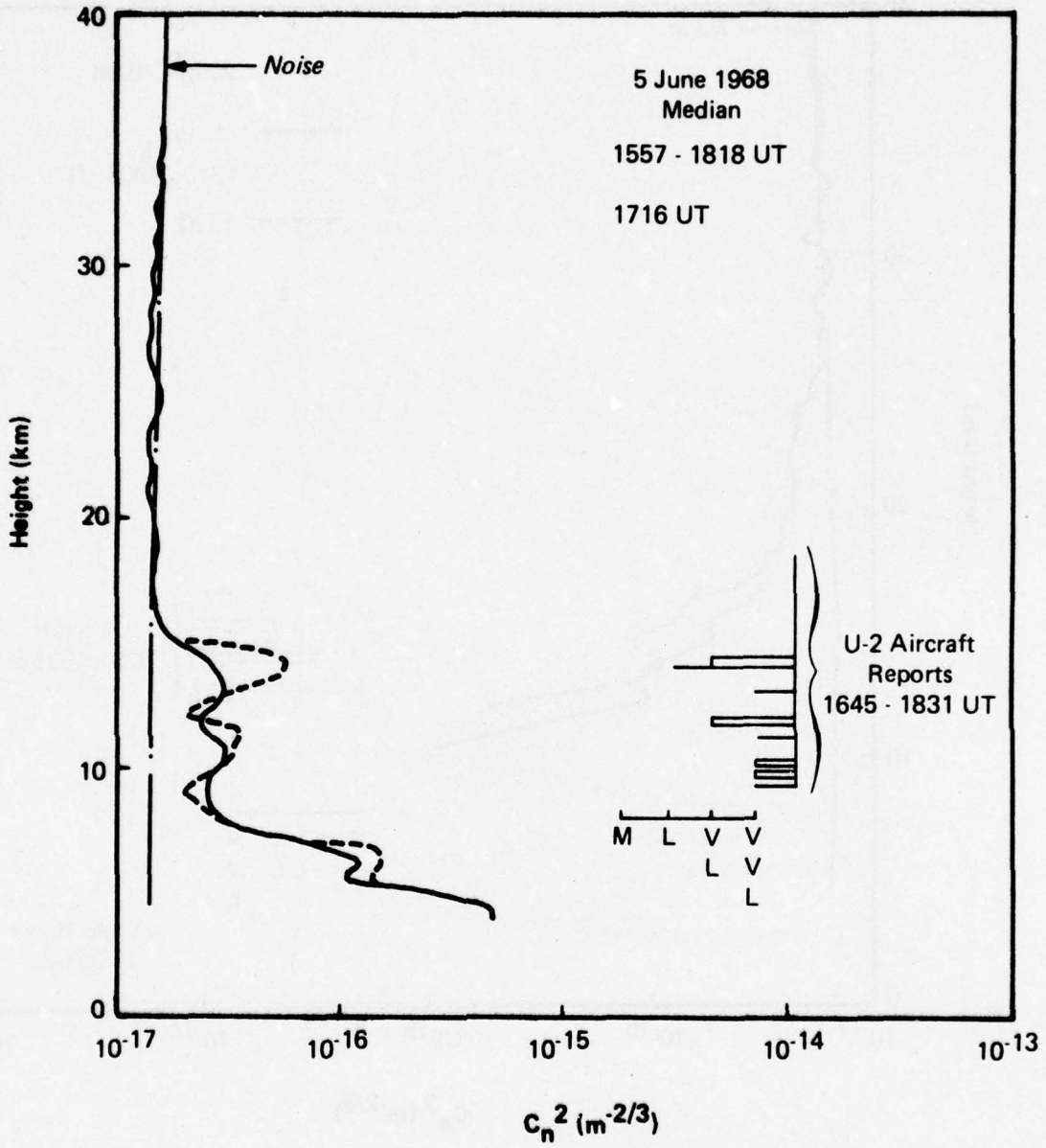
708113


28 May 1968
Receiver Noise
1516 - 1810 UT
Median Profile
260° AZ
1445 UT
214° AZ
1439 UT
120° AZ
Height (km)
40
30
20
10
0
10-18
10-17
10-16
10-15
10-14
Cn2 (m-2/3)

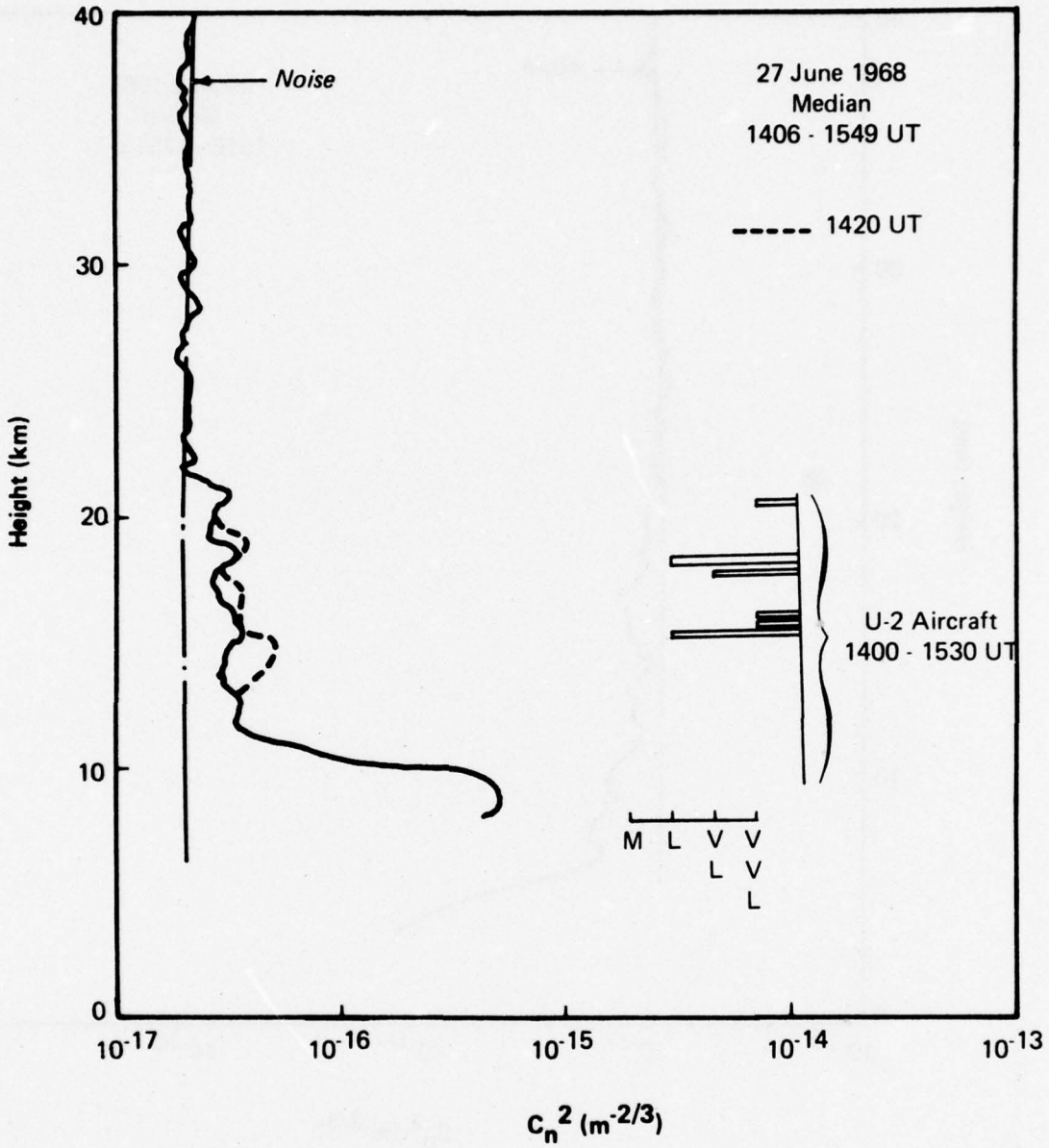
708114


40
30
20
10
0
Height (km)
Noise
29 May 1968
Median
1310 - 1935 UT
1920
U-2 Aircraft
1828 - 1935 UT
M L V L V V L
Light Rain
at Surface
10^{-17}
10^{-16}
10^{-15}
10^{-14}
10^{-13}
C_n^2 ($m^{-2/3}$)

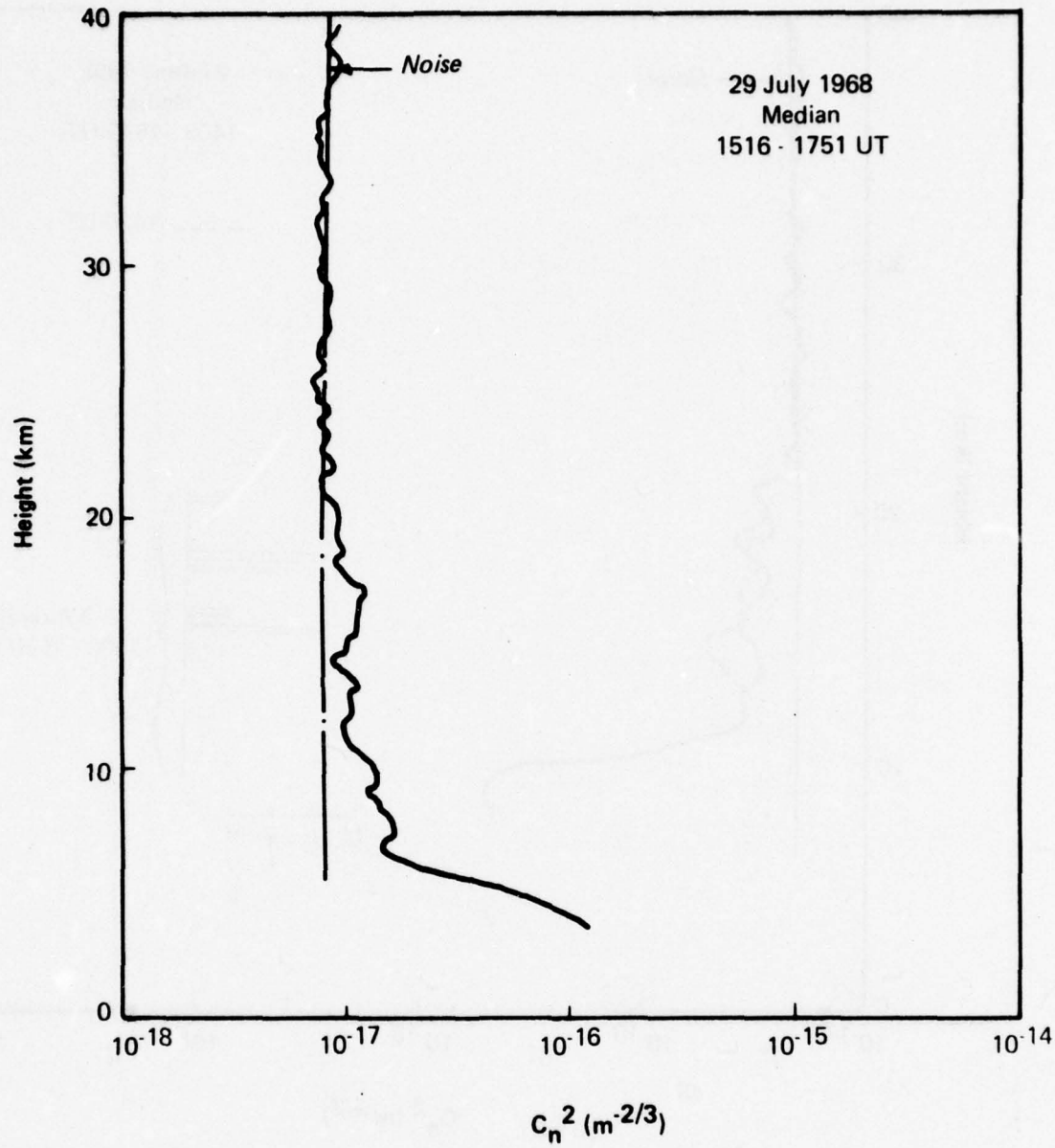
708115


40
30
20
10
0
Height (km)
Noise
5 June 1968
Median
1557 - 1818 UT
1716 UT
U-2 Aircraft
Reports
1645 - 1831 UT
M L V V
L V
L
10^{-17}
10^{-16}
10^{-15}
10^{-14}
10^{-13}
C_n^2 ($m^{-2/3}$)

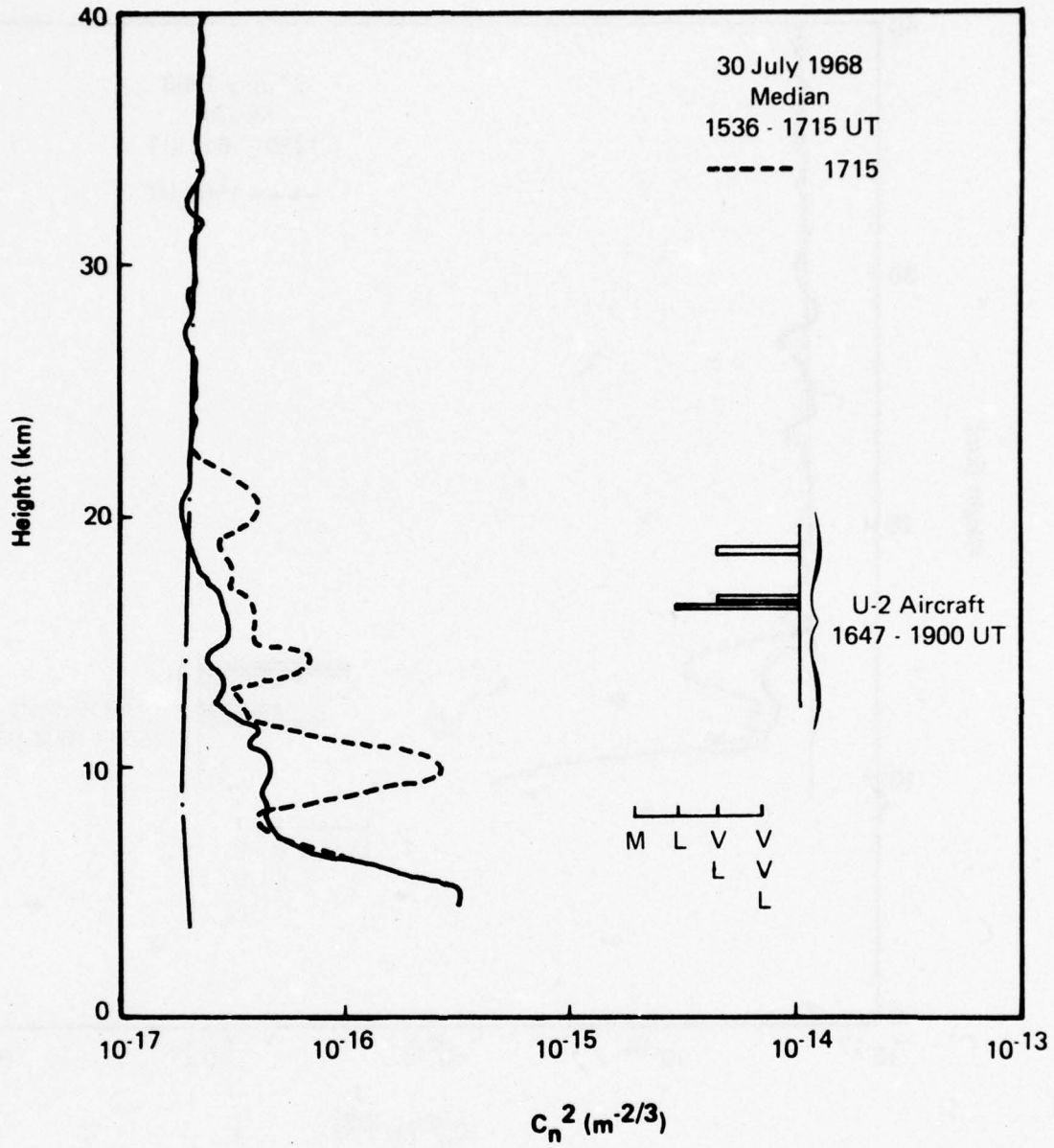
708116


40
30
20
10
0
Height (km)
Noise
27 June 1968
Median
1406 - 1549 UT
----- 1420 UT
U-2 Aircraft
1400 - 1530 UT
M L V L V V L
10^{-17}
10^{-16}
10^{-15}
10^{-14}
10^{-13}
C_n^2 ($m^{-2/3}$)

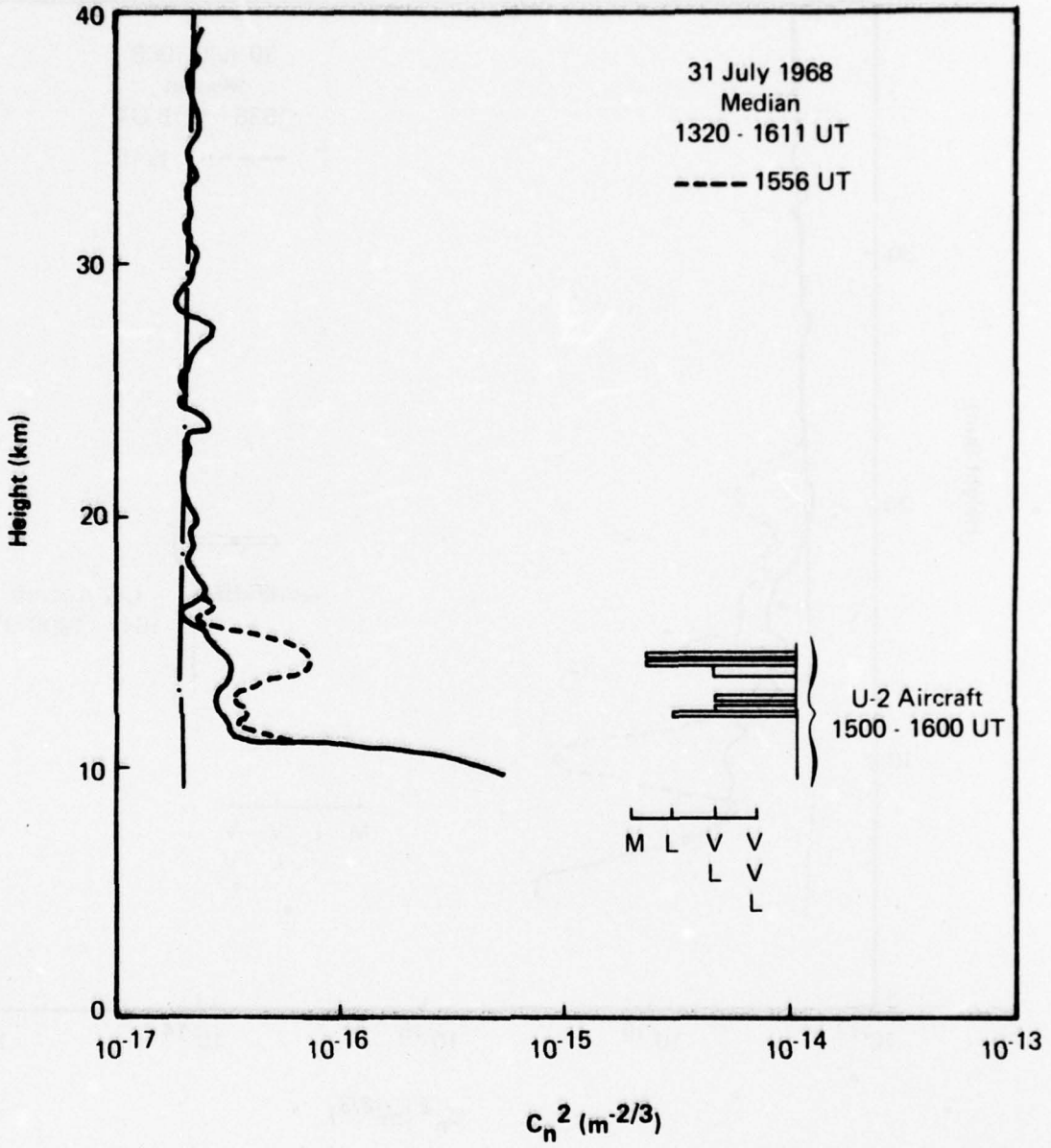
708118


40
30
20
10
0
Height (km)
Noise
29 July 1968
Median
1516 - 1751 UT
10^{-18}
10^{-17}
10^{-16}
10^{-15}
10^{-14}
C_n^2 ($m^{-2/3}$)

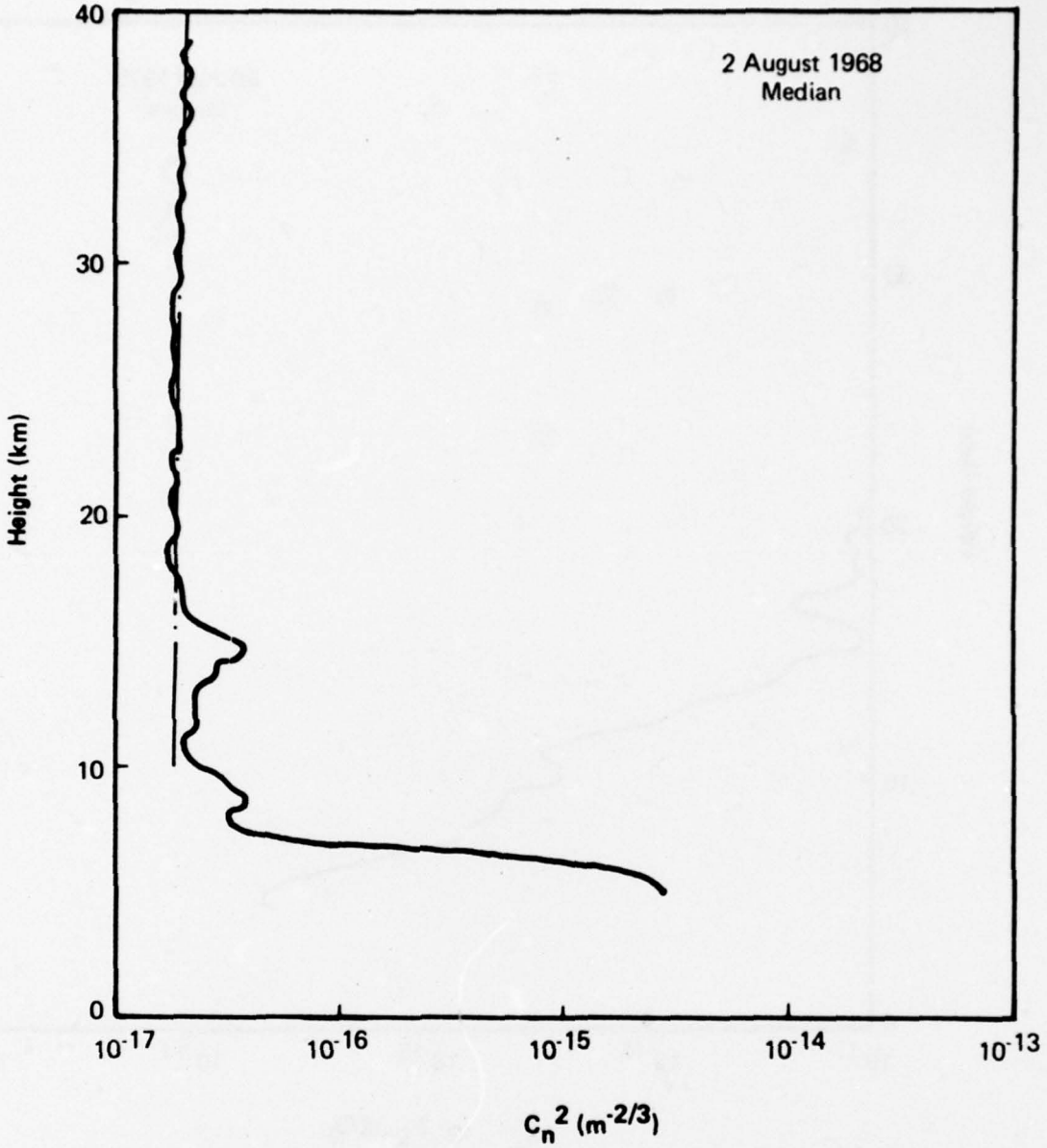
708119


30 July 1968
Median
1536 - 1715 UT
----- 1715
U-2 Aircraft
1647 - 1900 UT
M L V V
L V
L
Height (km)
40
30
20
10
0
10^{-17}
10^{-16}
10^{-15}
10^{-14}
10^{-13}
C_n^2 ($m^{-2/3}$)

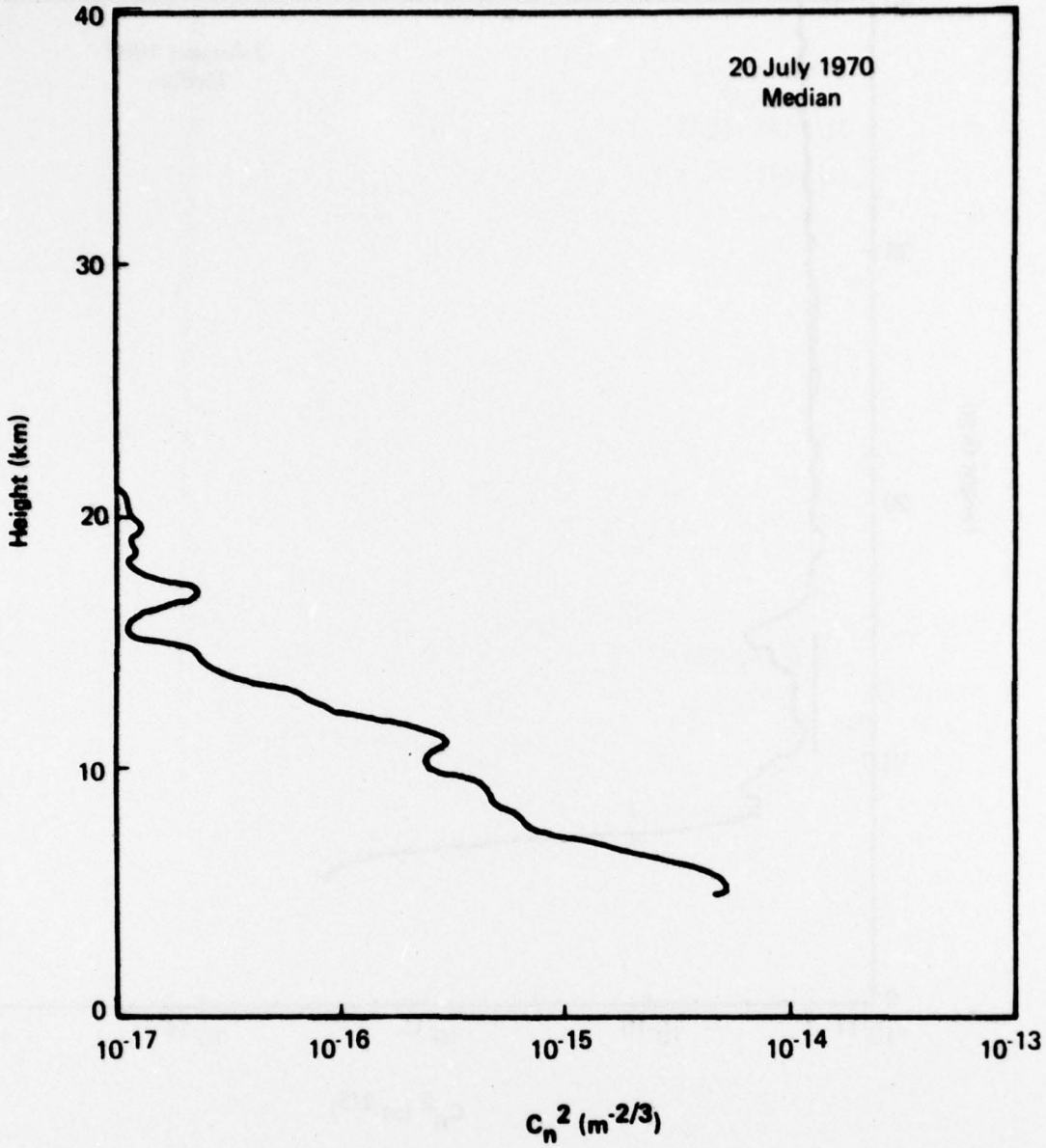
708120


31 July 1968
Median
1320 - 1611 UT
1556 UT
U-2 Aircraft
1500 - 1600 UT
M L V L V V L
Height (km)
40
30
20
10
0
10^{-17}
10^{-16}
10^{-15}
10^{-14}
10^{-13}
C_n^2 ($m^{-2/3}$)

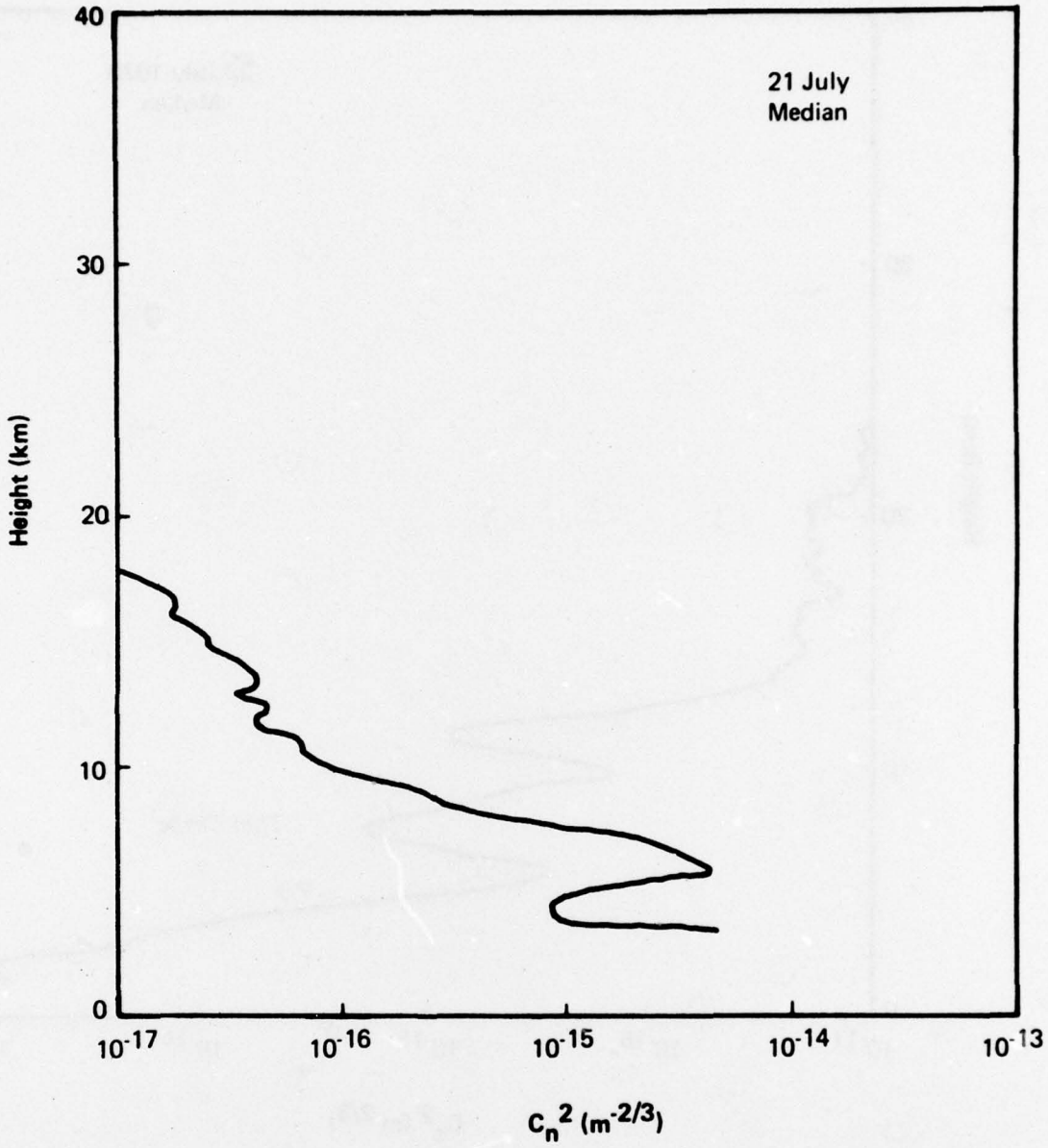
708121


2 August 1968
Median
Height (km)
40
30
20
10
0
10^{-17}
10^{-16}
10^{-15}
10^{-14}
10^{-13}
C_n^2 ($m^{-2/3}$)

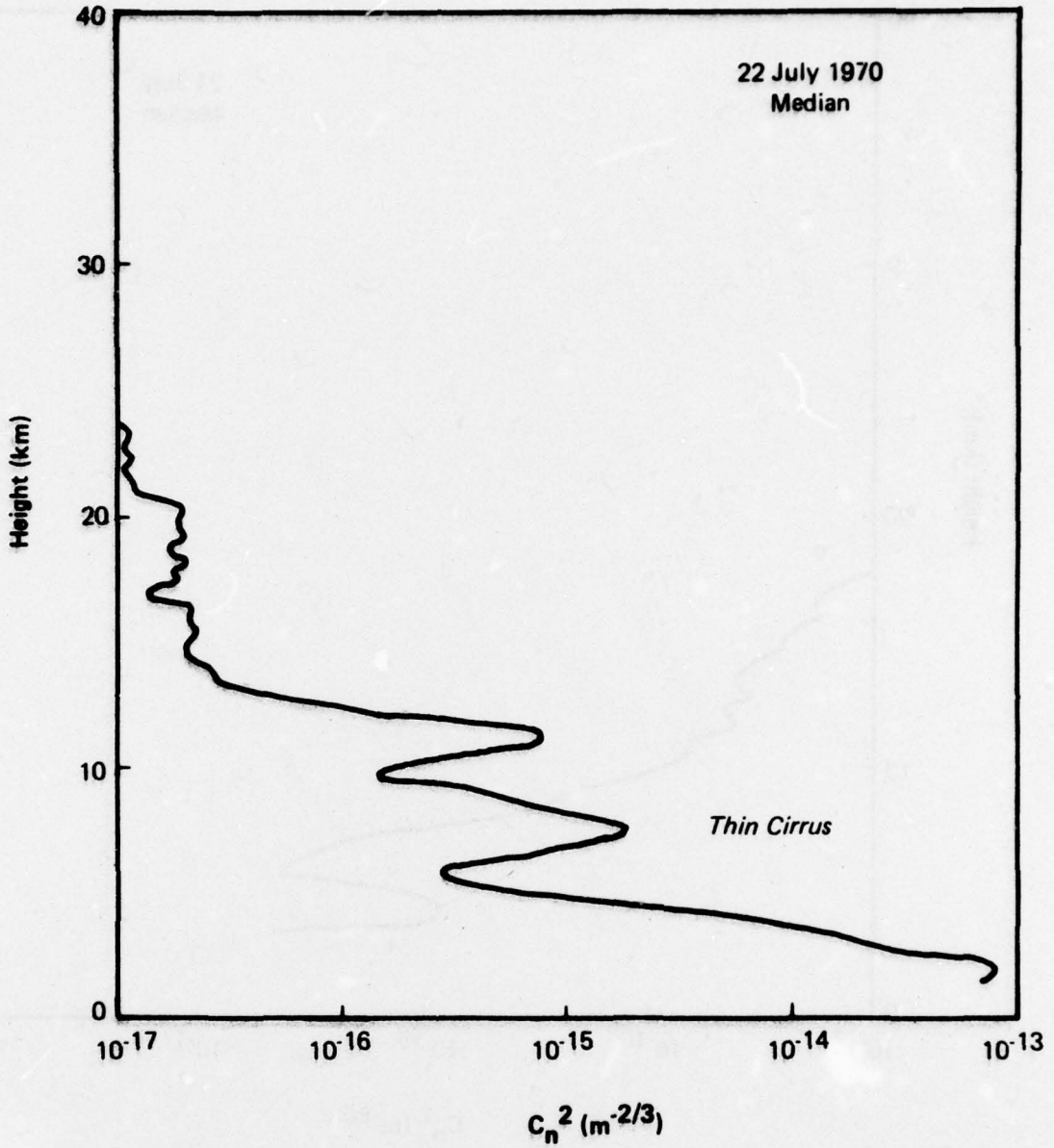
708122


20 July 1970
Median
Height (km)
40
30
20
10
0
10^{-17}
10^{-16}
10^{-15}
10^{-14}
10^{-13}
C_n^2 ($m^{-2/3}$)

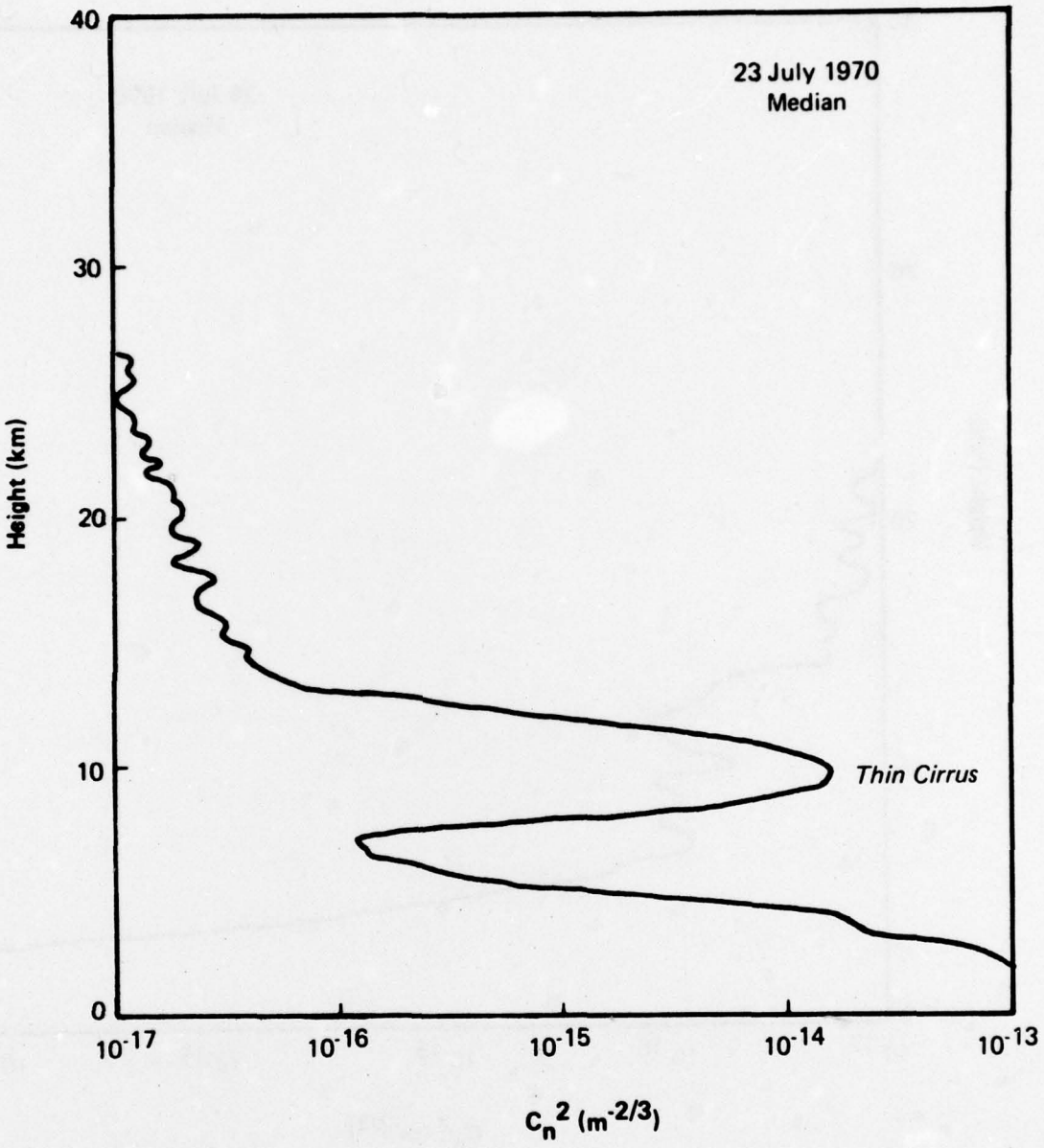
708123


21 July
Median
40
30
20
10
0
Height (km)
10^{-17}
10^{-16}
10^{-15}
10^{-14}
10^{-13}
C_n^2 ($m^{-2/3}$)

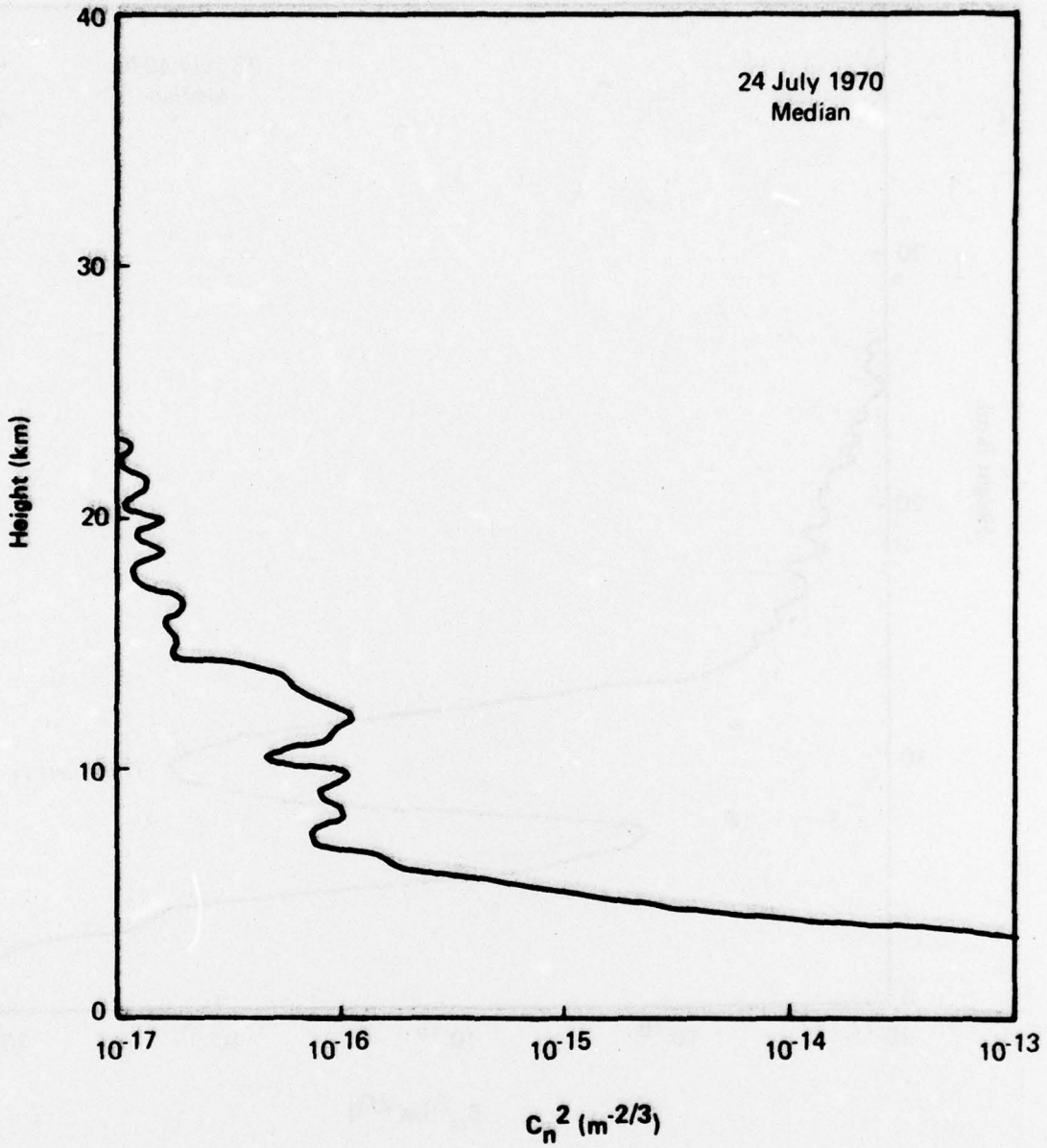
708124


22 July 1970
Median
Thin Cirrus
Height (km)
40
30
20
10
0
10^{-17}
10^{-16}
10^{-15}
10^{-14}
10^{-13}
C_n^2 ($m^{-2/3}$)

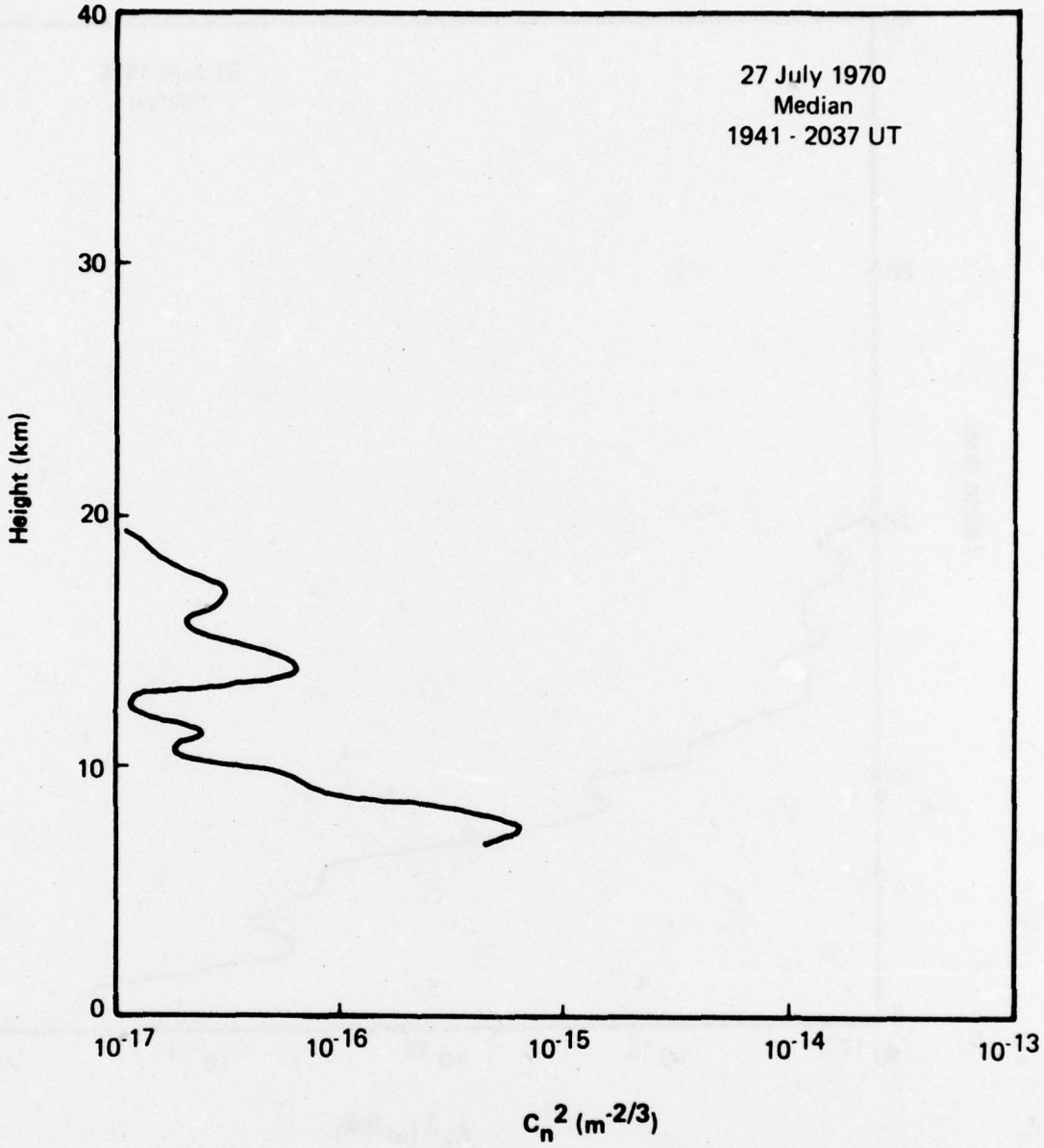
708125


23 July 1970
Median
Thin Cirrus
Height (km)
40
30
20
10
0
10^{-17}
10^{-16}
10^{-15}
10^{-14}
10^{-13}
C_n^2 ($m^{-2/3}$)

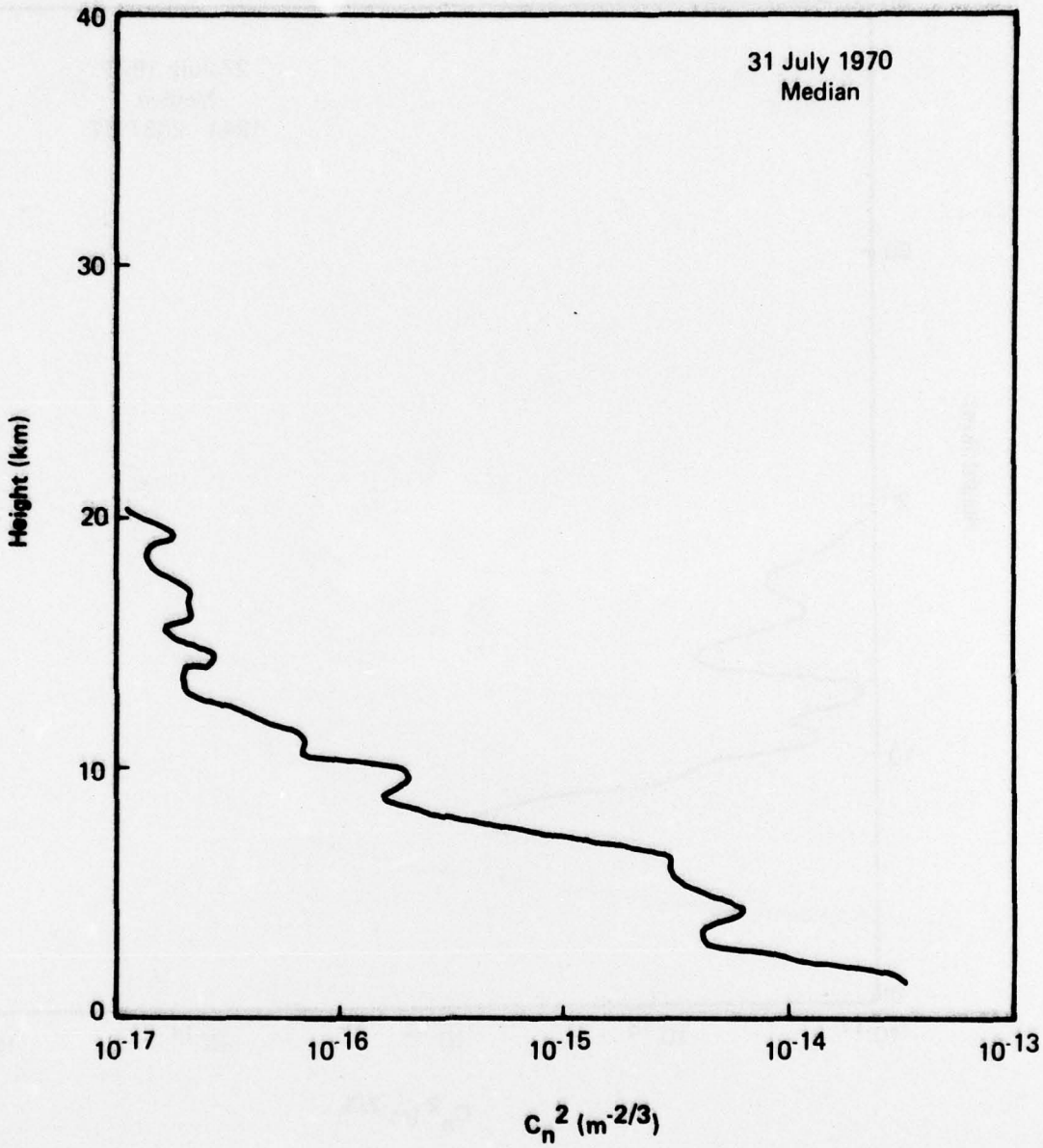
708126


24 July 1970
Median
40
30
20
10
0
Height (km)
10^{-17}
10^{-16}
10^{-15}
10^{-14}
10^{-13}
C_n^2 ($m^{-2/3}$)

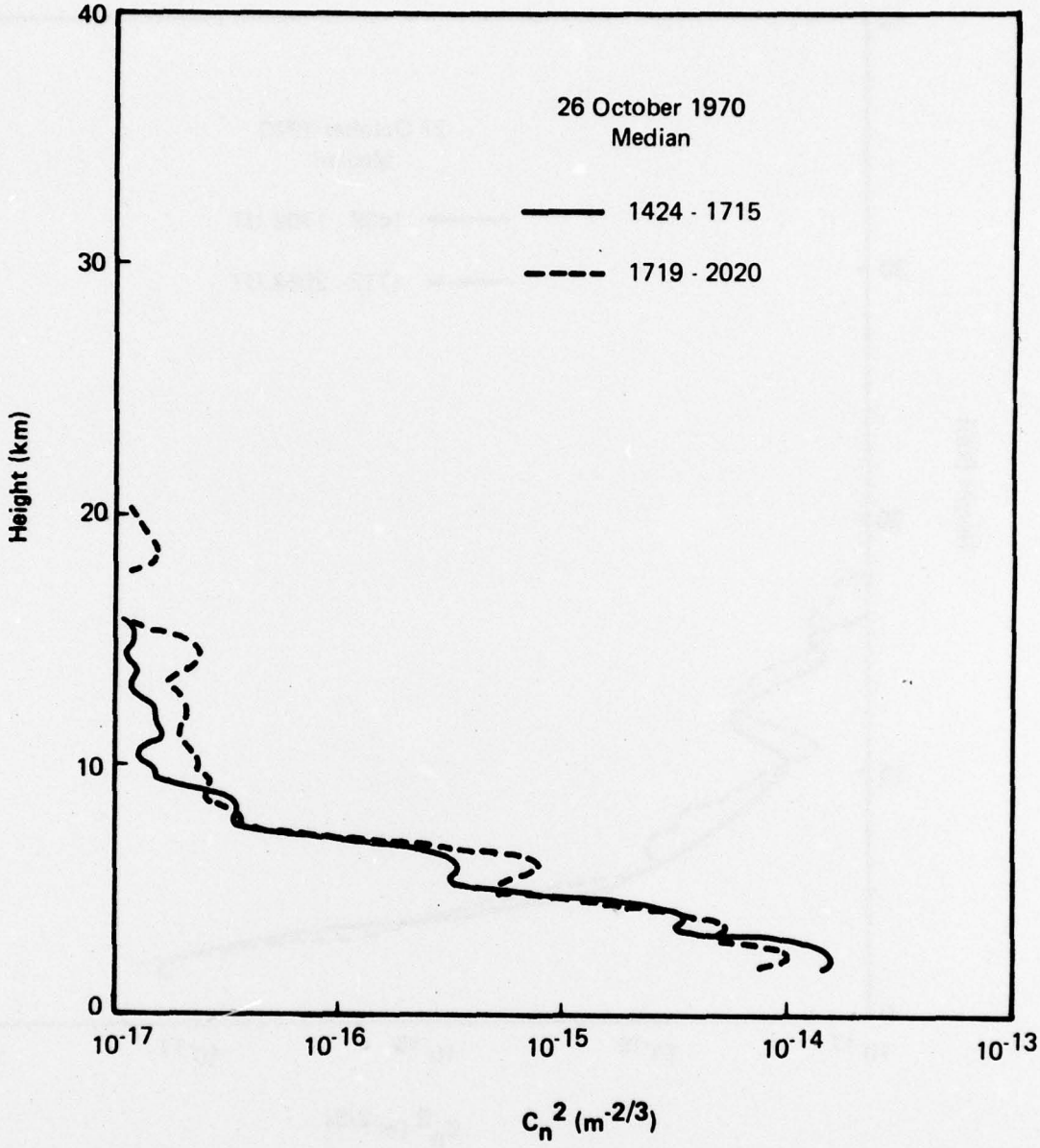
708127


27 July 1970
Median
1941 - 2037 UT
40
30
20
10
0
Height (km)
10^{-17}
10^{-16}
10^{-15}
10^{-14}
10^{-13}
C_n^2 ($m^{-2/3}$)

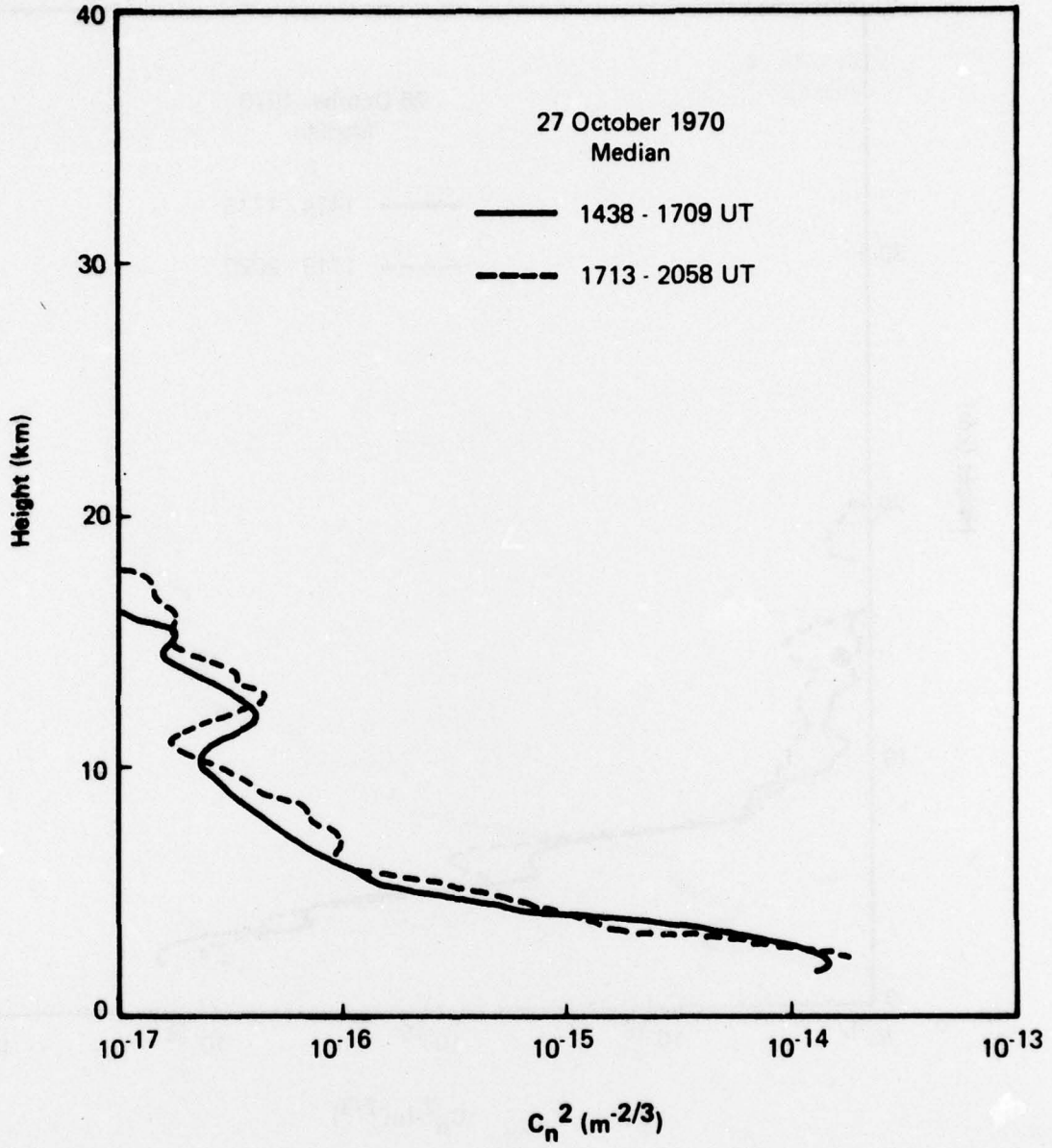
706128


31 July 1970
Median
Height (km)
40
30
20
10
0
10^{-17}
10^{-16}
10^{-15}
10^{-14}
10^{-13}
C_n^2 ($m^{-2/3}$)

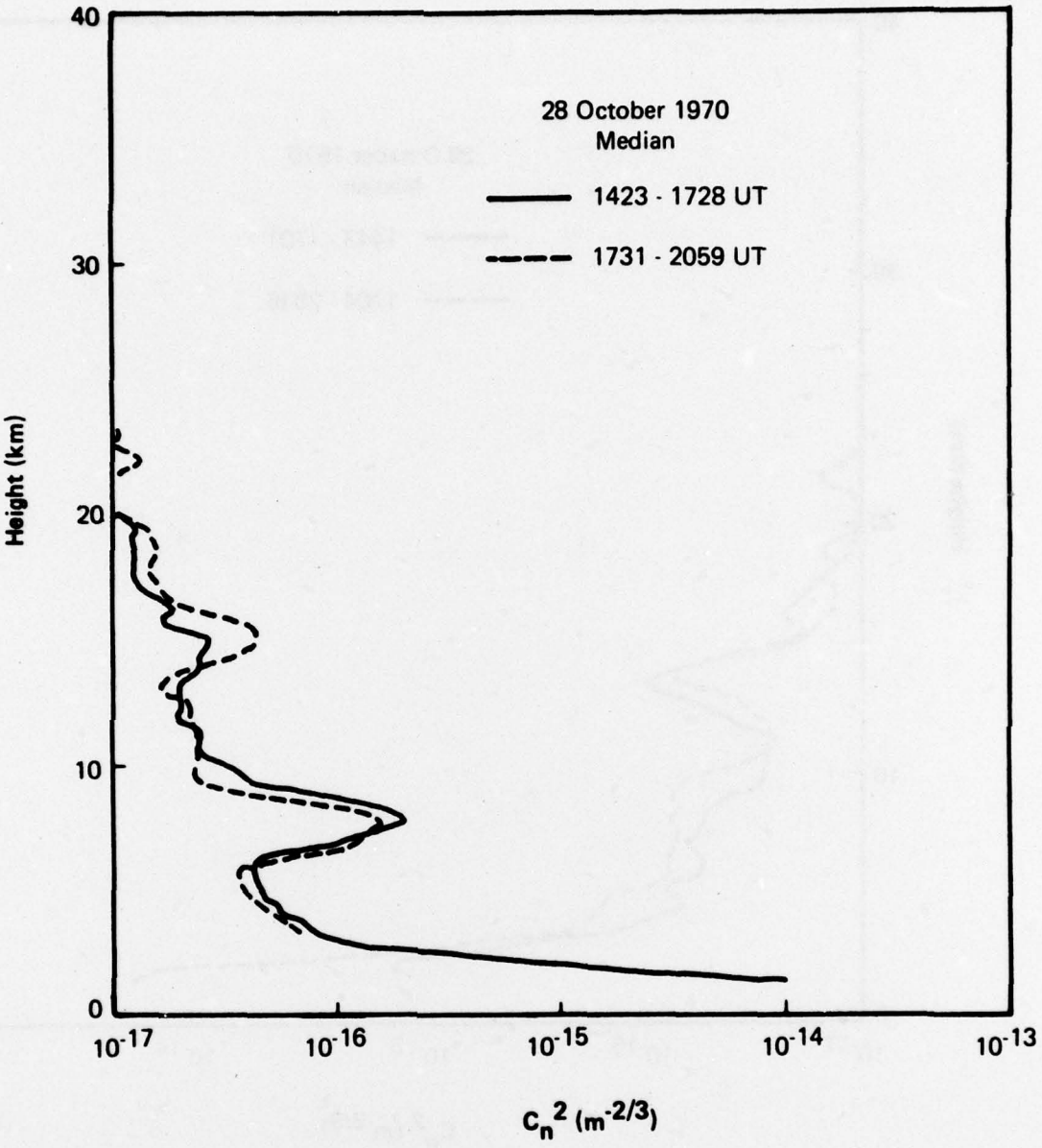
708129


26 October 1970
Median
1424 - 1715
1719 - 2020
Height (km)
40
30
20
10
0
10^{-17}
10^{-16}
10^{-15}
10^{-14}
10^{-13}
C_n^2 ($m^{-2/3}$)

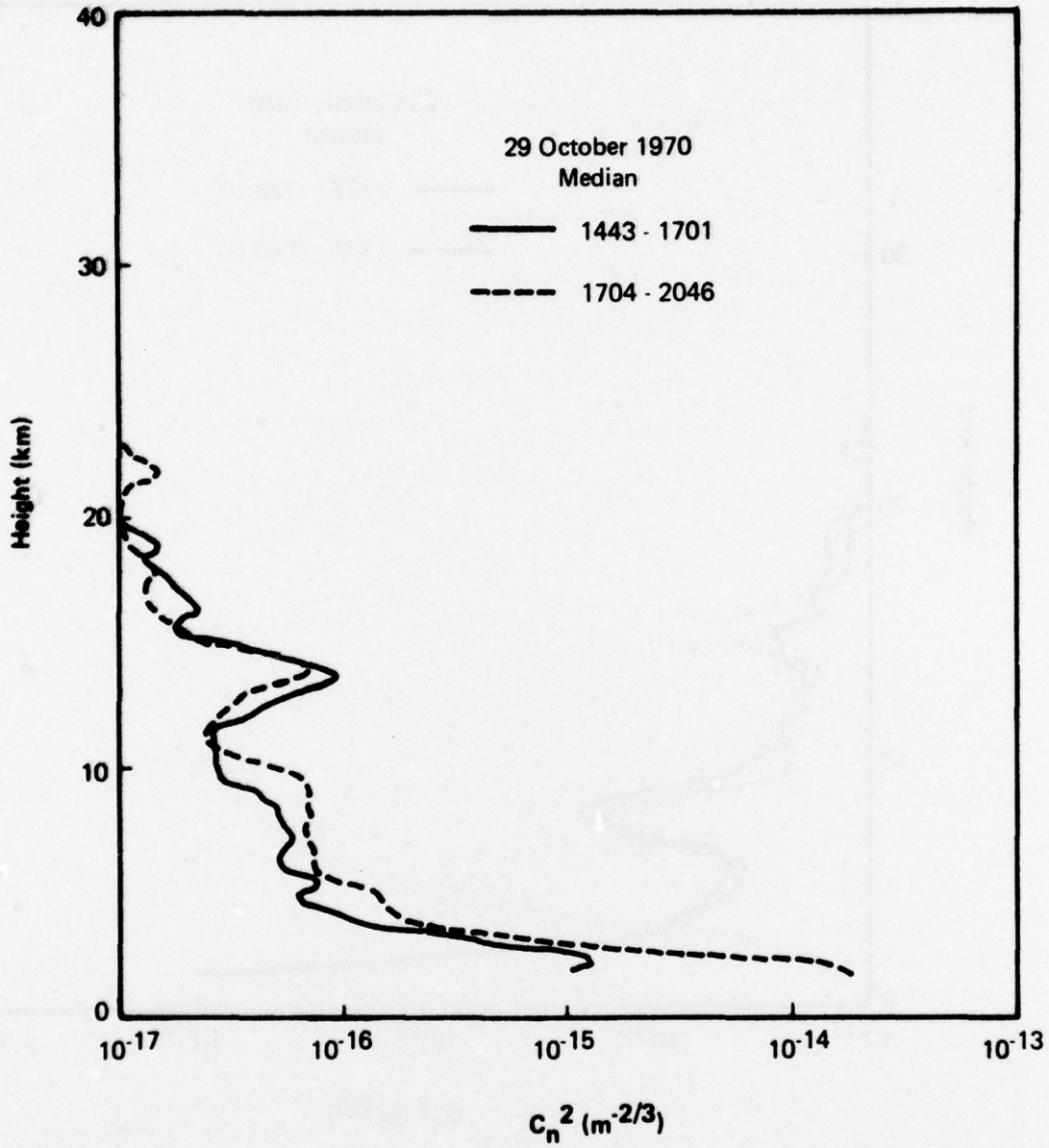
708130


27 October 1970
Median
1438 - 1709 UT
1713 - 2058 UT
Height (km)
40
30
20
10
0
10^{-17}
10^{-16}
10^{-15}
10^{-14}
10^{-13}
C_n^2 ($m^{-2/3}$)

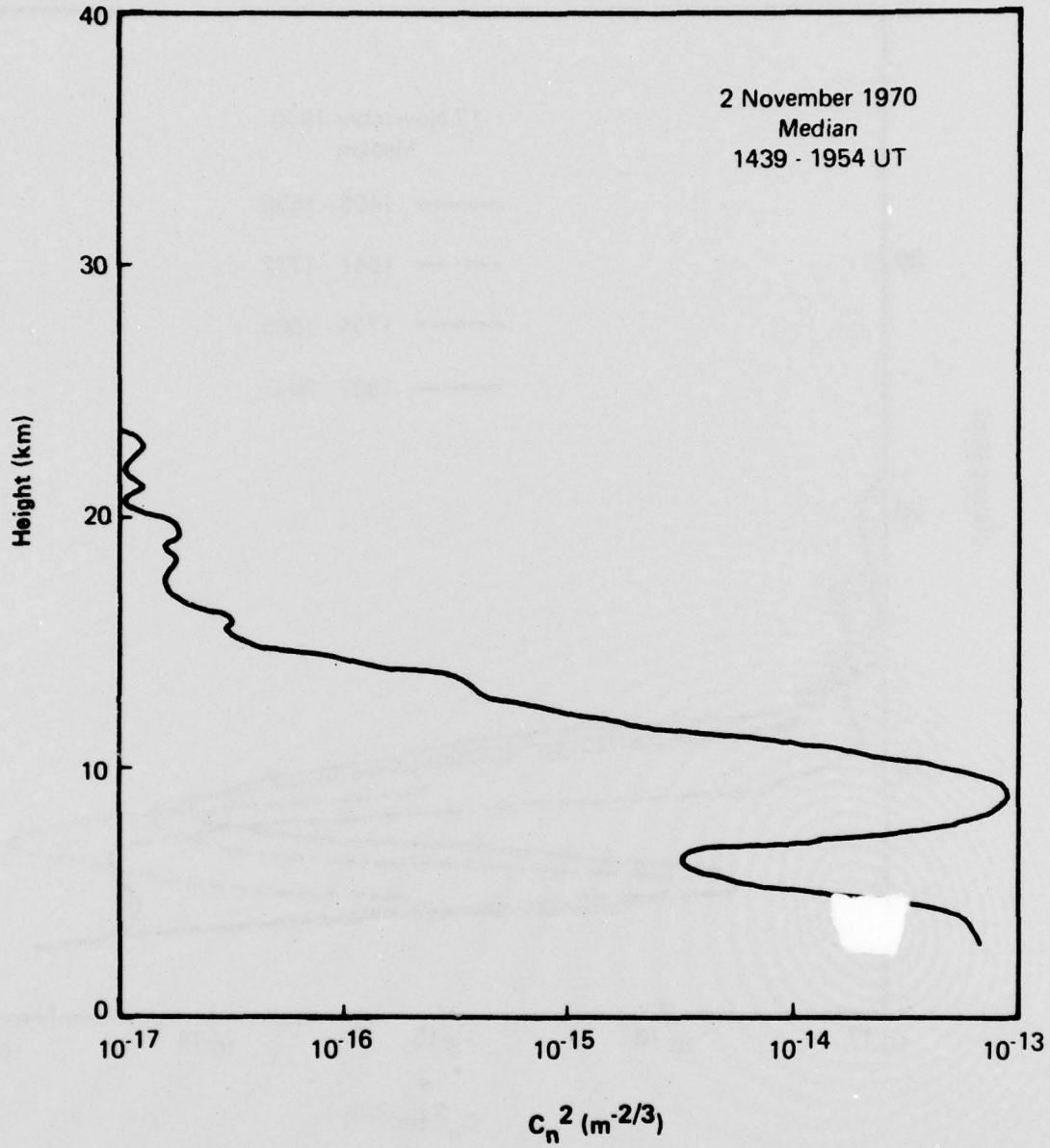
708131


28 October 1970
Median
1423 - 1728 UT
1731 - 2059 UT
Height (km)
40
30
20
10
0
10^{-17}
10^{-16}
10^{-15}
10^{-14}
10^{-13}
C_n^2 ($m^{-2/3}$)

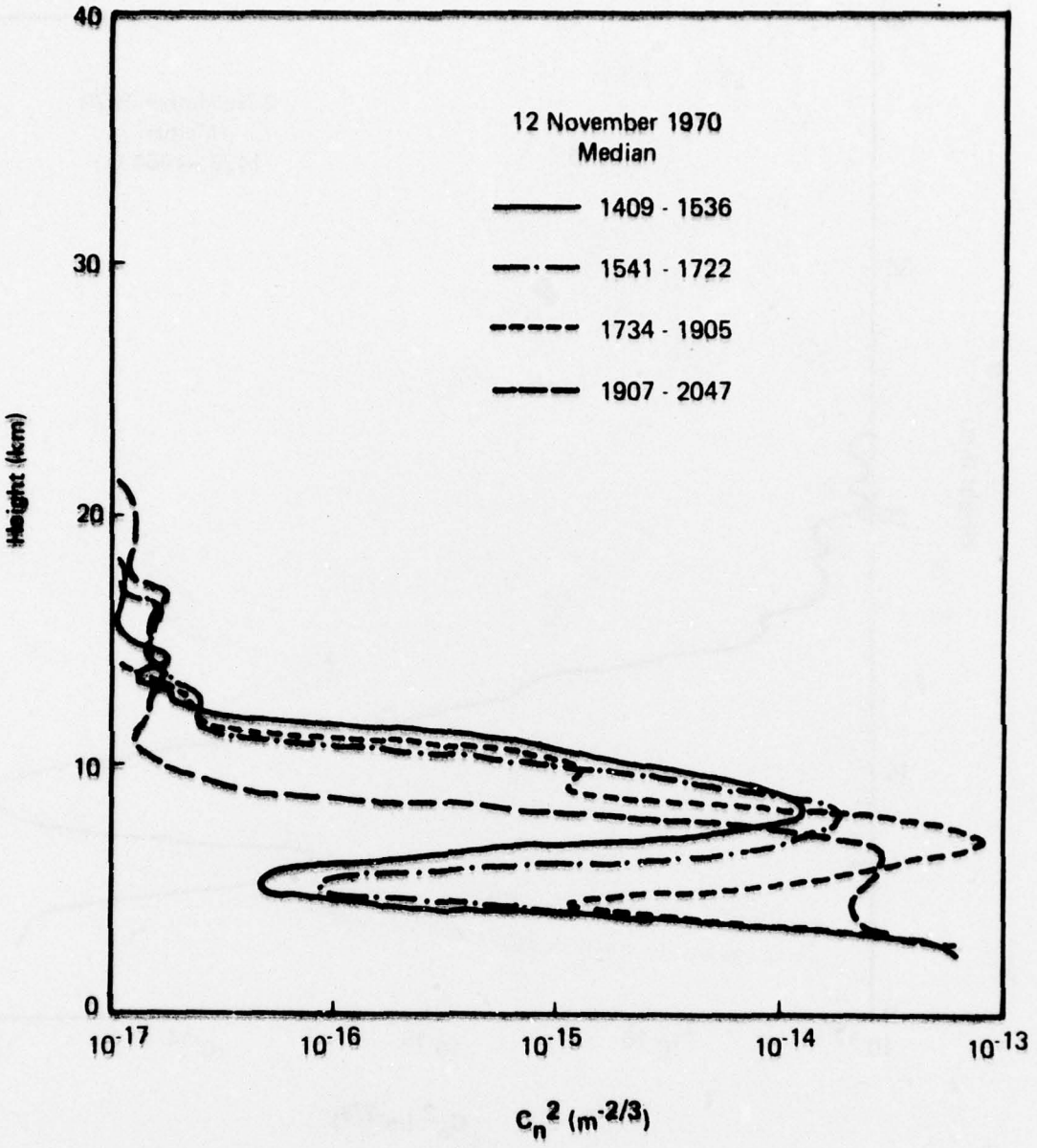
708132


29 October 1970
Median
1443 - 1701
1704 - 2046
Height (km)
40
30
20
10
0
10^{-17}
10^{-16}
10^{-15}
10^{-14}
10^{-13}
C_n^2 ($m^{-2/3}$)

700133


2 November 1970
Median
1439 - 1954 UT
Height (km)
40
30
20
10
0
10^{-17}
10^{-16}
10^{-15}
10^{-14}
10^{-13}
C_n^2 ($m^{-2/3}$)

708134


12 November 1970
Median
1409 - 1536
1541 - 1722
1734 - 1905
1907 - 2047
Height (km)
40
30
20
10
0
10^{-17}
10^{-16}
10^{-15}
10^{-14}
10^{-13}
C_n^2 ($m^{-2/3}$)